

UNIVERSITÄT
BAYREUTH

**Identification of novel
components of the zinc homeostasis mechanism in
*Arabidopsis thaliana***

DISSERTATION

Zur Erlangung des akademischen Grades
Doktor der Naturwissenschaften (Dr. rer. nat.)
der Fakultät Biologie / Chemie / Geowissenschaften
der Universität Bayreuth

vorgelegt von
Blen Beyene Chichaibelu
geboren am 14.04.1979 in Addis Ababa

Bayreuth, August 2013

Die vorliegende Arbeit wurde in der Zeit von Januar 2008 bis August 2013 an der Universität Bayreuth am Lehrstuhl für Pflanzenphysiologie unter der Betreuung von Prof. Dr. Stephan Clemens angefertigt.

Vollständiger Abdruck der von der Fakultät für Biologie, Chemie und Geowissenschaften der Universität Bayreuth genehmigten Dissertation zur Erlangung des akademischen Grades Doktor der Naturwissenschaften (Dr. rer. nat.).

Dissertation eingereicht am: 07. 08. 2013

Zulassung durch die Prüfungskommission: 14.08.2013

Wissenschaftliche Kolloquium fand statt am: 25. 09. 2013

Amtierende Dekanin: Prof. Dr. Beate Lohnert

Datum der Einreichung: 07.08.2013

Promotionskommission:

Prof. Dr. Stephan Clemens (*Erstgutachter*)

Prof. Dr. Olaf Stemmann (*Zweitgutachter*)

Prof. Dr. Gerhard Rambold (*Vorsitz*)

Prof. Dr. Benedikt Westermann

PD. Dr. Werner Borken

Zusammenfassung

Zink ist das zweithäufigste Übergangsmetalle, das in lebenden Systemen Verwendung findet. Es ist hauptsächlich in katalytische Prozesse involviert, hat aber auch in verschiedenen Proteinen eine strukturgebende Funktion. Bei Zink-Defizienz handelt es sich, aufgrund der weitverbreiteten Verwendung in Lebewesen, um eines der häufigsten Mangelerährungsprobleme. Laut aktuellen Schätzungen sind ca. 31% der Weltbevölkerung von Zink-defizienz bedroht. Exponentielles Bevölkerungswachstum und die Verknappung der natürlichen Ressourcen werden dieses Problem höchstwahrscheinlich noch verschärfen. Aus diesem Grund wurde ein genetischer Screen zur Identifizierung molekularer Komponenten des Zinkhomöostase Netzwerkes in pflanzen mit dem Ziel das Verständnis der Zinkhomöostasemechanismen zu verbessern und damit die Forschung im Bereich der Biofortifikation zu unterstützen begonnen. Frühere Untersuchungen haben gezeigt, dass Deregulationen in der Zinkhomöostase oft zu einer verminderten Zinktoleranz in Pflanzen führen. Aus diesem Grund wurden EMS-mutagenisierte Samen (M2-Generation) von *Arabidopsis thaliana* auf ein vermindertes Wurzelwachstum hin selektiert, um neue Mechanismen der Zinkhomöostase zu identifizieren. Die zweite Selektionsrunde, die im Rahmen dieser Arbeit durchgeführt wurde, führte zu Identifizierung von 28 neuen Mutanten. Aufgrund der erhöhten Zinksensitivität wurden diese Mutanten als IZS-Mutanten (für increased zinc sensitivity) bezeichnet. Fünf dieser Mutanten (IZS 377, IZS 389, IZS 390, IZS 394 und IZS 479) wurden im Zuge dieser Arbeit näher charakterisiert. Als einzige dieser fünf Mutanten zeigte IZS 479 eine zinkspezifische Hypersensitivität (keine Hypersensitivität gegenüber anderen getesteten Schwermetallen wie z.B. Cadmium). Weiterführende Untersuchungen konnten zeigen, dass in IZS 479 einen Aminosäureaustausch an Position 293 das Gen MTP1 aufweist. An dieser Stelle wurde Asparaginsäure durch Asparagin ersetzt. Dieser Austausch ist wahrscheinlich der Grund für die beobachtete Zinkhypersensitivität. Darüber hinaus führten detaillierte Untersuchungen an der Mutante IZS 288 (diese Mutante wurde im Zuge der ersten Selektionsrunde identifiziert) zu dem Ergebnis, dass neben der erhöhten Zinksensitivität die Mutation auch noch weitere pleiotrope Effekte bedingt. Zu diesen Effekten zählen Veränderungen in Wurzelarchitektur und Blattmorphologie, sowie eine verfrühte Blühinduktion und eine erhöhte Kältesensitivität. Mittels Kartierung konnte eine variation in einem bisher noch nicht charakterisierten WD40-gen gefunden werden, welches wahrscheinlich Komplexe mit Cullin 4 Ubiquitin E3-Ligasen eingeht. Diese

Komplexe sind für die selektive Degradation von Substratproteinen mittels Proteasomen und vorhergehender Ubiquitinierung verantwortlich. Einzelne putative Orthologe sind in *Homo sapiens*, *D. melanogaster*, *C. elegans*, *X. laevis* und anderen Spezies zu finden. Allerdings gibt es für die meisten dieser orthologen Gene keine funktionelle Daten. Auf Grund dieser Tatsache wurde, drei RNAi-Linien von *Drosophila* untersucht, in denen das orthologe Gen herunterreguliert wurde. Die Ergebnisse dieser Untersuchungen weisen darauf hin, dass dieses Gen wichtig für die Bildung bestimmter Organe und verschiedene Entwicklungsstadien der Fruchtfliege ist. In der Mutante IZS 288 hat der Austausch der Aminosäure 377 von Threonin zu Isoleucin (in einem konservierten Bereich des Proteins) wahrscheinlich eine Veränderung der Proteinstruktur zur Folge, welche eine korrekte Interaktion mit dem Cullin 4 Ubiquitin E3 Ligase Komplex verhindert. Weiterführende Microarray Analysen führten zur Identifizierung von drei potentiellen Substraten (z.B. JAZ8) dieses Komplexes. Es sind aber weitere Experimente nötig, um den Effekt der Punktmutation auf die Struktur des Proteins sowie die Interaktionseigenschaften zu bestätigen. Darüber hinaus müssen auch die potentiellen Substrate noch experimentell bestätigt werden. Neben der Charakterisierung von IZS Mutanten wurden auch andere Mutanten auf ihre Zink sensitivität hin untersucht, die Beeinträchtigungen bei verschiedenen Schritten der Flavonoid biosynthese haben (tt-Mutanten für transparent testa). Diese Mutanten wurden ausgewählt, da frühere Beobachtungen nahelegten, dass Flavonoide eine Rolle bei der Schwermetalltoleranz von Pflanzen spielen. Die beiden Mutanten, die entweder kein Quercitin (tt7) oder überhaupt keine Flavonoide (tt4) synthetisieren konnten, zeigten eine starke Zink-Hypersensitivität. Daraus läßt sich ableiten, dass Quercitin anscheinend effektiver als Kaempferol darin ist, den Effekt von Zinkstress in *Arabidopsis* zu vermindern.

Summary

Zinc is the second most widely used transition metal in living systems. It is mainly involved in catalytic processes; it has also structural role in different proteins. Besides its widespread use in living systems zinc deficiency is one of the prevalent malnutrition challenges. Current estimates suggest that 31% of the world's population is at risk of zinc deficiency. Exponential population growth and natural resources scarcity might aggravate this problem. Therefore, in an initiative to advance the current understanding of the Zn homeostasis mechanism and aid the biofortification research, a forward genetics approach was adopted to identify molecular components of the Zn homeostasis network in plants. Previous observations have indicated that irregularity in zinc homeostasis mechanism often leads to a reduction in zinc tolerance of plants. Hence, EMS mutagenized second generation seeds of *Arabidopsis thaliana* were screened for reduced root growth in the presence of zinc stress (i.e. zinc hypersensitive response) in order to identify new elements of the zinc homeostasis mechanism. On the second round of screening conducted in this project 28 new Increased Zinc Sensitivity (IZS) mutants were identified and five of them (i.e. IZS 377, IZS 389, IZS 390, IZS 394 and IZS 479) were further characterized. Among these five newly characterized IZS mutants, only IZS 497 showed a specific zinc hypersensitivity phenotype (i.e. not hypersensitive to other transition metals tested). In IZS 479 a substitution of the 293rd aspartic acid by asparagine was identified in the MTP1 gene, which could be the reason behind its zinc hypersensitivity phenotype. Furthermore, characterization of IZS 288 (one of the IZS mutants identified in the first round of screening) identified pleiotropic effects of the mutation, such as altered root architecture, changed leaf morphology, early flowering and chilling hypersensitivity, in addition to the zinc hypersensitivity phenotype. Map-based cloning of the mutated gene in IZS 288 lead to the identification of a novel WD-40 gene that is presumed to form a complex with cullin 4 ubiquitin E3 ligases and take part in the selective degradation of substrate proteins via the ubiquitin proteasome pathway. Single putative orthologs of this gene are found in *Homo sapiens*, *D. melanogaster*, *C. elegans*, *X. laevis* etc. However, functional characterization of most of these genes was still missing; hence a phenotypic analysis of three RNAi lines of the putative *Drosophila* ortholog was carried out. Observation in this experiment indicated the potential role of this gene at different organs and developmental stages of *Drosophila*. In IZS 288, the substitution of the 377th threonine by isoleucine (which is

in the conserved region of the protein) might have caused a disruption in the protein structure that led to malfunctioning in the cullin 4 ubiquitin E3 ligases complex. Based on microarray analysis potential substrates (i.e. JAZ8, the TTD-A subunit of the basal transcription factor complex (TFIIH) and three histone families) of this complex were identified. However further experiments will be required to prove the effect of the point mutation on the structure of the protein and its interaction with cullin 4 ubiquitin E3 ligase as well as to verify the potential substrates. Finally, based on prior observation flavonoids were assumed to have a role in heavy metal tolerance of plants; thus, the effect of flavonoids in zinc tolerance of *Arabidopsis thaliana* plants were investigated using five different flavonoids deficient mutants (i.e. transparent testa (tt) mutants). The mutant line that is completely devoid of flavonoids (*tt4*) and the one lacking quercetin (*tt7*) showed strong zinc hypersensitivity. Thus, quercetin appeared to be more effective than kaempferol in shielding the effect of zinc stress in *Arabidopsis*.

Acknowledgment

First, I would like to extend my deepest gratitude to my supervisor Prof. Dr. Stephan Clemens, for giving me the chance to be part of his research team and work on this interesting topic, for his remarkable ideas, guidance and encouragement during the research period and above all for his kindness and understanding that made my stay in the department enjoyable.

I extend my sincere thanks to Dr. Michael Weber, for allowing me to work on one of the mutant lines he has identified and for his supervision and support during lab work. I am also grateful to him for the time he took to discuss experimental procedures and problems and giving important suggestions during the course of the research.

I am grateful to “Bundesministeriums für Bildung und Forschung” for financing this research.

My heartfelt gratitude goes to Ewelina Slowikowska for her important contributions in the confirmation and characterization work of the newly identified IZS mutants, to Dr. Stefan Heidmann and Sina Fischer for their valuable input in the phenotypic characterization of the *Drosophila* RNAi lines, to Ursula Ferrera for her assistance in dealing with university formalities and to Christiane Meinen for her invaluable support in day-to-day activities of the research and her heartily concern about my progress in general.

My sincere appreciation goes to Prof. Dr. Angelika Mustroph, for her esteemed guidance during the analysis of the microarray data and her valuable suggestions. I would like to extend my sincere gratitude to Prof. Dr. Olaf Stemmann for taking interest in this project and for his valuable suggestions and the department of genetics for their good will in sharing their laser confocal microscope.

I am very thankful to all members of the department of plant physiology especially to my lab bench mate Dr. Ulrich Deinlein, for the warm discussions and encouragements as well as for the good working environment.

Finally, I would also like to use this opportunity to express my profound gratitude to my second family Prof. Dr. Harmen Storck, his wife Mrs. Evis Storck and the Lukas community whose care, unlimited kindness and prayers fills me with joy and motivation, to my dad, Dr. Beyene Chichaibelu, for your encouragements since my childhood, you have always appreciated what I have tried to do even when the end result was not the best; to my mom, Yalemshet Wolde Amanuel, for being my mom and my best friend, even in the midst of what seems like a crisis, you always have the right words to say to make me feel better; to my two sisters Birucktawit and Bezawit Beyene, for being there for me when ever I needed you and for making my life complete; to Wubishet Abebe, for being the best study partner and for the arguments and discussions about science and in life. Above all and beyond I am grateful to God the almighty for making this possible and for all his blessings in my life.

This work is dedicated to

To My Dad

You are my hero. Your life path has not been smooth and easy
but you never gave up or lost hope for a brighter tomorrow.

and

To My Mom,

You are the solid rock of support of my life. Your humble, loving and carrying heart
is what gets me out of most of the difficulties in life.

Contents

Zusammenfassung	i
Summary	iii
Acknowledgment	v
1. Introduction	1
1.1 Zinc homeostasis in plants	4
1.1.1 Zinc and its importance	4
1.1.2 Current level of understanding for the Zinc homeostatic mechanism in plants	9
1.1.3 Regulation of the Zn homeostasis mechanism	17
1.1.4 The overall Zn homeostasis mechanism at the organismal level	20
1.1.5 Open questions and missing links in the Zn homeostasis mechanisms	22
1.1.6 Zinc toxicity tolerance in plants	23
1.1.7 Problems related to zinc deficiency	23
1.1.8 Screening for zinc tolerance in EMS mutagenized seeds	25
1.2 Role of flavonoids in heavy metal tolerance	28
1.2.1 Understanding the link between flavonoids and heavy metal ions.....	28
1.2.2 Flavonoid biosynthesis and flavonoid deficient mutants	29
1.2.3 Flavonoids as health promoting factors in human diet.....	31
1.2.4 Flavonoids interaction with heavy metals	32
1.2.5 Screening of flavonoid deficient mutants for heavy metal sensitivity	33
2. Materials and methods	36
2.1 Screening for zinc tolerance in EMS mutagenized seeds	36
2.1.1 Plant materials and growing conditions.....	36
2.1.2 Characterization of 5 newly identified IZS mutants	37
2.1.3 Growth parameters and statistical analysis.....	37
2.2 Mapping and characterization of IZS 288	38
2.2.1 Plant materials and growing conditions.....	38
2.2.2 Heavy metal stress assay.....	38
2.2.3 Physiological parameters and statistical analysis.....	38
2.2.4 Elemental profile determination.....	38
2.2.5 Genetic mapping	39
2.2.6 DNA isolation.....	39
2.2.7 Polymerase chain reaction, gel electrophoresis and sequencing	41
2.2.8 Plasmids, constructs and genetic complementation	42
2.2.9 Genetic transformation	43
2.2.10 Reporter line establishment.....	44
2.2.11 Histochemical GUS staining and Microscopy.....	45
2.2.12 Transcript analysis	45
2.2.13 Drosophila stocks	46
2.3 Screening of flavonoid deficient mutants for heavy metal sensitivity	47

2.3.1	<i>Plant materials and growing conditions</i>	47
2.3.2	<i>Elemental profile determination</i>	47
2.3.3	<i>Growth parameters and statistical analysis</i>	48
3.	Results	49
3.1	The quest for new genes involved in zinc homeostasis	49
3.1.1	<i>New mutants identified in the genetic screen</i>	49
3.1.2	<i>Phenotypic Characterization of Five IZS Mutants</i>	51
3.2	Mapping and characterization of IZS 288	57
3.2.1	<i>Genetic background of IZS 288</i>	57
3.2.2	<i>Observed phenotypes of IZS 288</i>	57
3.2.3	<i>Genetic mapping of IZS 288</i>	78
3.2.4	<i>Functional analysis and subcellular localization of the novel WD40 protein</i>	84
3.2.5	<i>Microarray analysis</i>	89
3.3	Understanding the link between flavonoids and heavy metal ions	111
4.	Discussion and conclusion	117
4.1	The quest for new genes involved in zinc homeostasis	117
4.2	Mapping and characterization of IZS 288	120
4.2.1	<i>Pleiotropic effects of the IZS 288 mutation</i>	120
4.2.2	<i>Chilling hypersensitivity of the IZS 288</i>	124
4.2.3	<i>Zinc hypersensitivity of the IZS 288</i>	127
4.2.4	<i>IZS 288 gene function</i>	129
4.2.5	<i>The IZS 288 mutation</i>	135
4.3	Understanding the link between flavonoids and heavy metal ions	139
4.4	Conclusion	143
5.	Reference	145
Appendix	i
Appendix list-1	<i>i</i>
Appendix list-2	<i>ii</i>
Appendix list-3	<i>vi</i>
Appendix list-4	<i>vii</i>
Appendix list-5	<i>xii</i>
Appendix list-6	<i>xx</i>

1. Introduction

A decade ago the occurrence of the September 11 attack on the United States of America created the eye opener experience regarding imminent danger of terrorism. In the aftermath of this attack the attitude of the general public irremediably changed towards being ill-prepared for this kind of threats, which forced many governments to reconsider their national security policies and to take more elaborate counter terrorism measures. However, in the current state of awareness humanity appears to be oblivious to the looming challenge of feeding an ever increasing world population.

As the world population is estimated to reach 9 billion in 2050, the global demand for food is expected to increase by 60 percent. Therefore, food production will have to increase by 70 percent in order to feed the world population (FAO, WFP and IFAD, 2012). Adding to this challenge, climate change (i.e. changes in temperature and precipitation associated with continued emissions of greenhouse gases) will diminish the agricultural productivity of most sub-Saharan African countries (Schmidhuber and Tubiello, 2007). Furthermore, natural resource (i.e. water, arable land) constraints and competing demands (such as production of biofuels) will restrict the potential of increasing agricultural productivity. On a separate note, the growing per capita income of many countries, especially developing countries leads to an increase in the consumption of animal-source foods (including fish) causing additional pressure on agricultural productivity by raising the demand for animal feed (FAO, WFP and IFAD, 2012).

Adding more layers to the complexity of this challenge, even in a good harvest year where global food production exceeds global food demand, considerable number of the world's population still go hungry. For instance, despite a significant decline in the number of hungry people over the past decade, in 2010-2012 harvest years 12.5 % of the global population (around 870 million people) was chronically undernourished. The vast majority of these people (852 million) are found in developing countries. Furthermore, micronutrient deficiencies (also known as "hidden hunger") are common in over 30 percent of the world's population (FAO, WFP and IFAD, 2012). Particularly, deficiencies in iron, vitamin A, iodine and zinc are the most prevalent (WHO, 2009). Hence, due to uneven food distribution or low purchasing power (poverty), not having enough to eat (malnutrition) or the right kind of

food (low in micronutrient content etc) will remain to be a problem even at times of surplus global food production (Sen, 1982).

Meanwhile, despite the lack of awareness and attitude of the general public, researchers have proposed different approaches for tackling this challenge. Jonathan Foley and his colleagues for example directed their attention on analyzing the shortcomings of the current agricultural practices and deduced strategies that can increase cropping efficiency while reducing the environmental impacts of agriculture (Foley et al., 2011). Conway and Toenniessen (1999) in their part promoted the deployment of plant biotechnology by a strong public-sector agricultural research. In the frontier of combating hidden hunger, food fortification (artificially mixing missing nutrients like vitamin A, iron, zinc or folic acid into a staple food like wheat flour, sugar or cooking oil) has been the popular approach. International NGOs (non-governmental organizations) such as the Helen Keller International (www.hki.org) are providing both “in home fortification” using a cocktail of multiple micronutrients in single-dose sachets that can be added to home-cooked meals as well as large scale food fortification through partnership with private companies producing cooking oil and wheat flour. However, poor farmer communities in rural areas that produce most of their food could not benefit from this approach. A second upcoming strategy was to breed the missing nutrients into staple food crops either through conventional breeding or through genetic engineering (Mayer et al., 2008). This strategy is known as biofortification. In recent years, following the principles of biofortification, HarvestPlus (an international research institute (www.harvestplus.org)) has released a yellow sweet potato variety, which is extremely rich in provitamin A. The efficacy study of the yellow fleshed sweet potato variety among school children in KwaZulu-Natal province of South Africa produced positive outcome by improving the vitamin A stores in liver (van Jaarsveld et al., 2005.). Currently the program is distributing this line to farmers in countries like Uganda and Mozambique and the results of a pilot study indicated >60% rate of adoption among the farms. The introduction of the variety increased the children and mother Vitamin A intake (www.harvestplus.org).

The important steps in biofortification process are identifying crop germplasms with improved micronutrient composition or content and combining these characteristics with locally adapted varieties (i.e. varieties with good agronomic characteristics and high yield in the locality). To achieve this purpose, specific morphological or molecular markers that can

distinguish the genotypes with increased accumulation of micronutrients (such as iron and zinc) in edible parts of a crop need to be identified (Waters and Pedersen, 2009; White and Broadley, 2011). To date, information regarding the β carotene biosynthetic pathway (that were used for bioengineering golden rice (Burkhardt et al., 1997; Ye et al., 2000)) and genes involved in iron homeostasis such as ferritin and nicotianamine (that played vital role in iron biofortification in rice (Goto et al., 1999; Takahashi et al., 2003; Ishimaru et al., 2010)) have been instrumental to the biofortification strategy. However, information regarding zinc homeostasis genes is quite limited and identification and characterization of genes involved in zinc homeostasis in model plants can pave the way for the application of marker-assisted selection in many crop plants (Assunção et al., 2010).

The main aim of the research reported in this thesis was for the advancement of the current understanding of the Zn homeostasis mechanism through the identification of new genes involved in zinc homeostasis mechanism of plants, which could also contribute to zinc biofortification strategies. Additionally, based on prior observation regarding interconnections between secondary metabolites like flavonoids and heavy metals in plants, the role of flavonoids in heavy metal (particularly zinc) tolerance in plants was investigated. The thesis is organized into five parts. It starts with chapter one by describing the rationale behind carrying out this research project and continues to give a comprehensive literature review regarding zinc and zinc homeostatic mechanisms in plants, followed by detailed overview of the current understanding of flavonoids and their interactions with heavy metals. Chapter two, categorized into three sections, describes the materials put to use and implemented methods throughout the course of this project. Chapter three, organized into three subsections, reports the results and findings of the research project. Chapter four discusses the findings stated in chapter three and conveys a summary and conclusion. The last chapter, chapter 5, lists the references cited in the thesis.

1.1 Zinc homeostasis in plants

1.1.1 Zinc and its importance

Zinc (Zn) is a transition metal of atomic number 30 and is the 23rd most abundant element on earth crust (Broadley et al., 2007). The recognition for its importance came in the late 19th century when Raulin discovered its impact on the growth and cell division of *Aspergillus niger* (Sandstead and Klevay, 2000). Since then, the knowledge regarding the role of Zn in different biological systems has intensified.

In living systems Zn is the second most widely used (following iron) transition metal (Clemens, 2010). Particularly, the adult human body contains 2 to 3 g of Zn making it one of the most prevalent trace elements (Berg and Shi, 1996). However, its specific biological role was unknown up until Keilin and Mann (1940) illustrated the detail enzymatic activity of carbonic anhydrase that conveyed the involvement of zinc in its catalytic core. So far, more than 300 Zn containing enzymes have been indentified (Fig. 1.1. and Tab. 1.1) that belong to oxidoreductases, transferases, hydrolases, lyases, isomerases and ligases enzyme families making Zn the only metal ion encountered in each class of enzymes (Vallee and Falchuk, 1993).

In addition to the catalytic role of Zn in enzymes, there are also few enzymes that exploit it for sole structural purpose. Zn ions could form structure-stabilizing cross-links without introducing undesired chemical reactivity (Berg and Shi, 1996). A very good example for such enzymes is aspartate transcarbamoylase of *Escherichia coli*, where the removal of the zinc bound in the regulatory subunits leads to the dissociation of the regulatory subunits from the catalytic subunits leaving the catalytic activity intact (Nelbach et al., 1972).

The first encounter of the structural role of Zn came from the detailed description of the protein transcription factor IIIA (TFIIIA) (Berg and Shi, 1996; Clemens, 2010) which led to the discovery of the “zinc finger” domain. The phrase “zinc finger” stands for a conserved sequence motif in which cysteines (Cys) and/or histidines (His) tetrahedrally coordinate a zinc atom(s) to form a compact structure that interacts with DNA in a sequence-specific manner (Takatsuji, 1998). Proteins containing zinc finger domain are implicated in the regulation of different signal transduction pathways as well as developmental processes and

programmed cell death (Ciftci-Yilmaz and Mittler, 2008). Zinc finger motifs enable proteins to directly bind with DNA and/or RNA, as well as interact with other proteins in order to generate a desired effect within a cell (Broadley et al., 2007). Based on the number and arrangement of the Cys and His residues that bind the Zn ion, zinc finger proteins are categorized into different groups such as the: Cys2-His2, Cys2-Cys2, Cys2-HisCys, Cys2-Cys2-Cys2, and Cys2-His-CysCys2-Cys2. Among them Cys2-His2-type zinc finger proteins are the most abundant in eukaryotes (Klug and Schwabe, 1995; Ciftci-Yilmaz and Mittler, 2008).

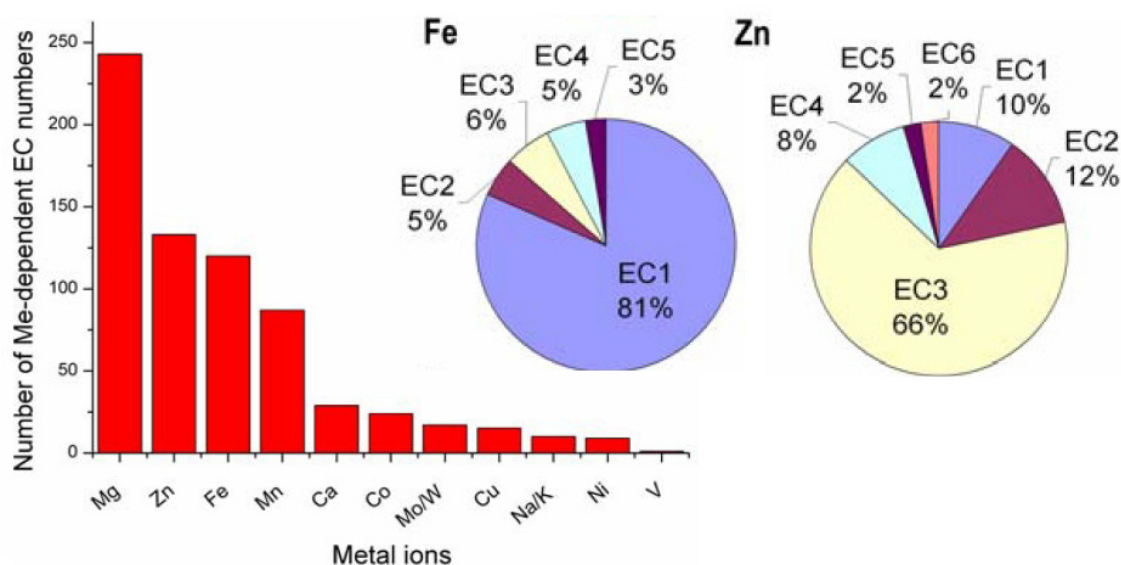


Figure 1.1. The graph represents enzyme classes (EC) that bind a given catalytic metal ion with known structures. The pie charts represent ECs that bind iron (Fe) and Zinc (Zn) ions with known structures. (EC1- oxidoreductases, EC2- transferases, EC3- hydrolases, EC4- lyases, EC5- isomerases, EC6- ligases). The figure is adapted from Andreini et al., (2008).

Table 1.1. The six enzyme classes (EC) and representative zinc-enzymes together with their specified functions. The table is adapted from Vallee and Falchuk (1993).

Enzyme classes (EC)	Enzyme examples	Role
Oxidoreductase (EC I)	Alcohol dehydrogenase	Catalytic & Structural
	Superoxide dismutase	Cocatalytic
Transferases (EC 2)	RNA polymerase	Catalytic
	Reverse transcriptase	Catalytic
Hydrolases (EC 3)	Alkaline phosphatase	Catalytic & Cocatalytic
	Fructose-1,6-bisphosphatase	Cocatalytic
	Aminotripeptidase	Catalytic & Cocatalytic
	Carboxypeptidase	Catalytic
Lyase (EC 4)	Carbonic anhydrase	Catalytic
	Glyoxalase	Catalytic
Isomerases (EC 5)	DNA topoisomerase I	Structural
Ligases (EC 6)	tRNA synthetase	Catalytic
	Pyruvate carboxylase	Catalytic

One can also state a third function of Zn in enzymes. The term a coactive (or cocatalytic) function of zinc stands for those Zn atoms that can enhance or weaken the catalytic function of an enzyme in combination with another active site (which can be another Zn atom or other metals such as Cu and Mg) within the same enzyme, but is not a prerequisite for both enzymatic activity or structural stability (Vallee and Auld, 1992; Vallee and Falchuk, 1993). The best example of such cases is superoxide dismutase that contains Zn and Cu ions in its catalytic core (Tainer et al., 1982).

In general, Zn in its structural role has four coordination numbers (i.e. binding to four amino acid residues which could be either cysteine or histidine and form a stabilizing structure (Fig.1.2)) whereas catalytic Zn is bound to three residues and one water molecule (Matsubara et al., 2003), and in some cases the coordination number may increase from four to five with an additional ligand provided by the substrate or an intermediate (Deerfield II et al., 2001).

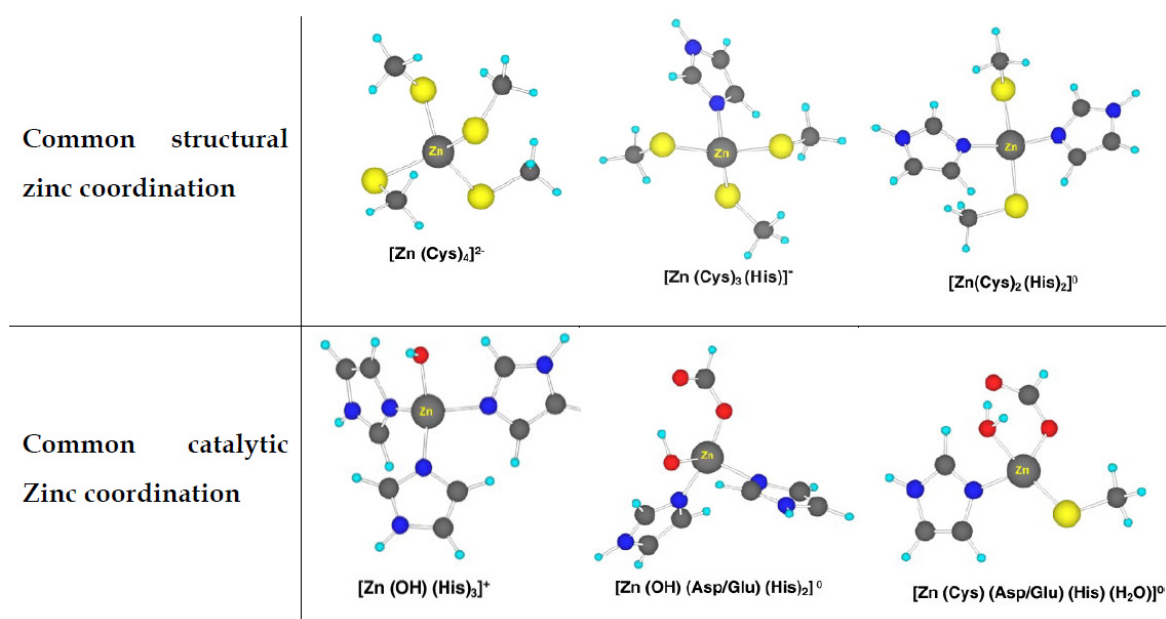


Figure 1.2. Common structural and catalytic Zn-binding sites in proteins. Yellow circles represent cysteine, blue circles histidine and red ones represent water and/or aspartate and glutamate. The figure is adapted from Lee and Lim (2008).

The reasons behind the selection of Zn as the most prominent functional metal are its chemical and physical properties. Zn, under physiological conditions is redox-stable, which is a result of its complete d-shell of electrons (i.e. neither the potential oxidized form, Zn^{3+} , nor the potential reduced form, Zn^+ , is accessible). In aqueous solutions it exists only in one (+2) oxidation state making it safe to be used in the vicinity of DNA. Other redox active transition metals such as copper (Cu) and iron (Fe) have a potential to generate hydroxyl

radicals leading to DNA damage and apoptosis (Barak and Helmke, 1993; Vallee and Falchuk, 1993; Auld, 2001). Secondly, the ligand field stabilization energy of Zn is zero; hence it does not get polarized while binding to ligands allowing it to have more flexible coordination geometry. It can also readily attain a tetrahedral coordination, which makes it more suitable for structural roles than other transition metals (Berg and Shi, 1996; Clemens, 2010).

Additionally, because of its small radius to charge ratio, Zn has pronounced Lewis acid characteristics (i.e. 0.83 \AA , with coordination number of 6) enabling it to react with both soft and strong bases like sulphide and hydroxyl ligands, respectively (Broadley et al., 2007; Clemens, 2010). Furthermore, in relative terms to other divalent transition metals, Zn is kinetically labile permitting fast and free ligand exchange reactions, making it well suited for a catalytic role (Berg and Shi, 1996). In short, the unique combination of the physicochemical nature of zinc allowed it to be one of the most utilized transition metal with multifaceted function in different biological systems.

The sheer-number of predicted Zn interacting proteins within different living systems can be considered as one proof of the multipurpose nature of Zn. Evaluations based on protein family domains (Pfam) and annotations predicted around 2,800 proteins (10% of the proteome) in human and about 2,400 proteins (8% of the proteome) in *Arabidopsis thaliana* to be Zn binding. On average in eukaryotes 9% of the proteome is presumed to be made up of Zn-proteins (Andreini et al., 2006).

Additional facts indicative of the vital role of zinc in living systems are the physiological problems caused by suboptimal zinc availability. In human, limited dietary Zn intake is linked to a wide range of pathological problems, like growth retardation, diarrhea, eye and skin lesions, and delayed sexual maturation (Vinkenborg, 2010). In addition to that, a genetic disorder known by the name *acrodermatitis enteropathica* has been identified, which is caused by a reduction in Zn absorption of the intestine causing dermatological lesions, immune and reproductive dysfunction (Wang et al., 2002; Kury et al., 2002). In plants the most common visible symptoms of Zn deficiency are stunted growth, reduced leaf size and epinasty, hindrance in stem elongation and interveinal chlorosis followed by necrosis (Sharma et al., 1994; Marschner, 1995).

On the other hand, the strong Lewis acids nature of Zn as well as its strong potency in displacing other divalent metal ions from catalytic sites of enzymes plus the increased stability of Zn-ligand complexes have created a high risk for toxicity by elevated concentrations of Zn ions in living systems. As demonstrated by the rank of Zn in the Irving-Williams series (which lists transition metals according to the relative stabilities of complexes they form) Zn is able to displace any metal ion except for Cu and form a stable complex (Fig. 1.3). In plants, Zn concentration is usually maintained at the range of 15-50 μ g per gram of dry weight (Hänsch and Mendel, 2009). In leaves Zn concentration exceeding 300mg per kg of dry weight is reported to cause phytotoxicity. Depending on the susceptibility of the plant species this value can even be lower than 100mg per kg of dry matter (Chaney, 1993). Zn toxicity symptoms in plants include leaf chlorosis, inhibition of root growth, decreased photosynthetic rates and reduced seed sets (Woolhouse, 1983; Ren et al., 1993). For example, in *Phaseolus vulgaris* Zn toxicity caused a reduction in photosynthesis rate by displacing a magnesium(Mg) ion at the water splitting site of photosystem II (van Assche and Clijsters, 1988; Kupper et al., 1996). Similarly, there are reports tying the chlorosis symptoms of zinc toxicity to that of the iron deficiency caused by it (Fukao et al., 2011). On the other hand, in humans toxic effects of high Zn concentrations are demonstrated in cultured lung cells by a decrease in protein and RNA synthesis in dose and exposure time dependent manner (Walther et al., 1995). Furthermore, there are reports of pulmonary damage caused by accidental exposure to zinc fumes (Milliken et al., 1963).

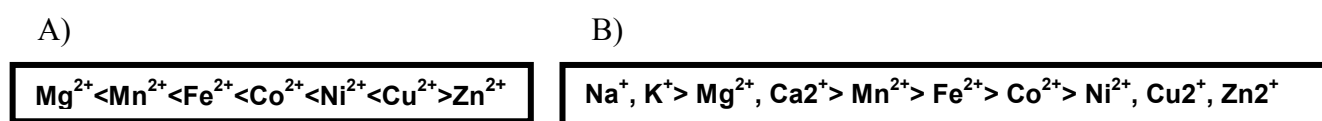


Figure 1.3. A) Irving-Williams series. B) The order for exchange rates of ions from relatively strong binding sites (which is a product of the strength of binding and the activation free energy for release). This figure is adapted from Williams (1982).

The far-reaching functions of Zn plus the requirement for a strict regulation of free cytoplasmic Zn led to the evolution of a sophisticated control and relay system within living systems known as the zinc homeostasis network. In order to maintain Zn within physiological range, cells are fitted with uptake and sequestration mechanisms as well as efflux activities in order to carry the Zn to its desired subcellular location as well as prevent overaccumulation in the cytoplasm. The following subtopic describes the current level of understanding of this complex process.

1.1.2 Current level of understanding for the Zinc homeostatic mechanism in plants

Plants, in addition to being the primary source of energy in the food chain, they are also the main entry point for micronutrients such as Zn into the food chain; thus understanding their homeostasis mechanism for heavy metals like Fe and Zn will aid the fight against micronutrient deficiency. In this section the Zn homeostasis mechanism in plants is discussed focusing on *Arabidopsis thaliana* (given that most of the molecular aspects of the mechanism were revealed using this model plant). However, while describing the universal zinc homeostasis mechanism in plants, metallophyte and their unique nature of hyperaccumulation of metal ions are beyond the scope of this review.

Zinc ion's passive diffusion rate through biological membranes is very limited. Moreover, like with most other metal ions the concentration of Zn in soil is subjected to major fluctuations. Therefore, plants should have a well developed Zn uptake mechanism that will allow them to take up the essential Zn ions into the cytosol (Marschner, 1995; Krämer et al., 2007). However, uptake alone is not enough. For Zn ions to get to particular subcellular destinations (either for ultimate use or further storage) different means of transport are required. These different means of transport that remove Zn ions from the cytosol are collectively referred as the Zn efflux mechanism. Meanwhile, at a given time the level of free Zn ions (liable Zn) within a given cell should be highly regulated. Even if the total amount of Zn in eukaryotic cells can reach up to 100 μM , the intracellular liable zinc concentration is below the nanomolar range (Sinclair and Krämer, 2012). As it has been mentioned previously, free Zn ions can easily form stable complexes with non target ligands or replace other divalent metal ions and cause toxic effects; hence strict regulation intracellular Zn concentration is emplace. In human for example a rise in intracellular liable Zn ion has been shown as a key factor in neuronal death following seizure (Lee et al., 2002). For this purpose plant cells have evolved different molecules with varying Zn binding capacity and function forming the chelation and sequestration mechanism. In short, these three mechanisms (i.e. uptake to the cytosol, chelation and/or sequestration and efflux from the cytosol) jointly form the zinc homeostasis mechanism (Clemens, 2001).

1.1.2.1 Uptake mechanisms

Plants are not able to access the total metal content of a soil; instead they can obtain a limited portion of it. Total metal content of soil can be categorized into different fractions: (1) soluble metals in the soil solution, (2) metal-precipitates, (3) metals sorbed to clays, hydrous oxides

and organic matter and (4) metals within the matrix of soil minerals. Among these subdivisions plants are able to take up free metal ions only from the soluble metal fraction in the soil solution, thus this fraction is known as the bioavailable fraction (Reichman, 2002).

Metal ion acquisition from the bioavailable fraction of soil across plasma membranes engages the use of particular proteins with transmembrane domains. Currently, different protein families with varying number of transmembrane domains have been shown to be involved in metal ion uptake across plasma membrane into the cytosol. Some of these protein families are: the ZRT- IRT- like Protein (ZIP) family, Cation Diffusion Facilitator (CDF) family, P_{1B}-type subfamily of P-type Atpases , the Natural Resistance Associated Macrophage Protein (NRAMP) family, the Yellow-Stripe1-Like (YSL) subfamily of the oligopeptide transporter (OPT) superfamily, the copper transporter (COPT) family, the Ca²⁺-sensitive Cross Complementer 1(CCC1) family and the Iron-Regulated protein (IREG) family (Krämer et al., 2007). Among these known heavy metal ion transporters the ZIP protein family is anticipated to have a major role in the Zn uptake process. Structurally, most of the ZIP proteins are predicted to have eight transmembrane domains having both their amino (N) - and carboxy(C)-terminal ends located on the extracellular side of the membrane. They also have a long cytoplasmic loop between the third and the fourth transmembrane domain, which is rich in histidine and predicted to have metal binding function (Guerinot, 2000; Eide, 2006).

Among the ZIP family proteins the first to be identified was the *Arabidopsis* IRT1 that rescued the growth defect of a *Saccharomyces cerevisiae* strain carrying an iron transport deficient mutation. Thus it was first described as an iron transporter. Later on it was shown that the substrate range of IRT-1 is quite broad including Zn²⁺ Mn²⁺ Cd²⁺ and Co²⁺ (Eide et al., 1996; Korshunova et al., 1999; Clemens, 2006). Subsequently, on the bases of sequence similarity to IRT1, the discovery of ZIP1, ZIP 2, ZIP3 and ZIP4 followed. Since ZIP1 and ZIP3 are expressed in the root system of plants, their function is believed to be in Zn uptake from the soil whereas ZIP4, being expressed in both shoots and roots, is presumed to be involved in the transport of Zn intracellularly (Grotz et al., 1998). Later on, when the genomic sequence of *Arabidopsis* became available the number of predicted ZIP family proteins in *Arabidopsis* genome reached 15. Among these the expression of ZIP5, ZIP9 to ZIP12 as well as IRT3 were shown to be Zn dependent serving as an indicator of their involvement in Zinc homeostasis (Wintz et al., 2003; Krämer et al., 2007). However, the contribution of the individual ZIP

transporters towards Zn uptake is not yet clearly known. A recent work by Milner and colleagues (2013) analyzed metal specificities of 11 ZIP proteins and reported six ZIP genes, namely ZIP1, ZIP2, ZIP3, ZIP7, ZIP11, and ZIP12 were able to complement the *zrt1/zrt2Δ* yeast mutant fully or partially under Zn-limiting conditions. Moreover, the expression level of ZIP1, ZIP2 and ZIP3 in roots was higher than in shoots; hence they could be part of Zn uptake mechanism (Milner et al., 2013).

1.1.2.2 Chelation and Sequestration mechanisms

After entering the cytoplasm metals cannot move simply by random series of binding and dissociation because it would make the movement very slow (i.e. binding can be as fast as $\geq 10^8/s$ but dissociation is very slow $\leq 10^{-2}/s$) (Krämer et al., 2007). On top of that, following the concept of “zinc quota” (i.e. the total Zn content of a cell required for its optimum growth) the average cellular zinc concentration of cells is in the range of 0.1–0.5 mM. However, the metal binding affinities of most metalloproteins is in the nM to pM range. Therefore, cells need to have means of preventing non-specific binding of Zn and directing it to its target proteins without raising the concentration of free zinc in the cell (Eide, 2006). For this purpose cells have metal binding ligands that can buffer the metal ion concentration. Assuming a parallel exist between Cu and Zn transport, there are reports proposing Zn gets delivered to specific proteins by metallochaperones through protein-protein interaction (Huffman and O'Halloran, 2001). However, such ubiquitous metallochaperones that are able to interact with Zn are not yet discovered. On the other hand, based on the absence of indicators for the existence of huge group of genes dedicated to specifically escorting Zn to each particular Zn-proteins as well as the lack of a conserved set of genomic sequences identifying the presence of a few escort metallochaperones serving a family of Zn-proteins, the role of metallochaperones in Zn trafficking could be very limited (Eide, 2006). Meanwhile, directing the focus mainly on plant cells, three ligands that serve in Zn buffers have been identified, namely the two low molecular weight ligands phytochelatins (PCs) and nicotianamine (NA) and the cysteine-rich proteins metallothioneins (MTs) (Cobbett and Goldsbrough, 2002; Weber et al., 2004; Deinlein et al., 2012).

Metallothioneins (MTs) are genetically encoded small molecular weight peptides that are rich in cysteine (Cys) residues with a potential of chelating Cu, Zn, and Cd by forming sulfhydryl ligands (Hara et al., 2010). Based on the arrangement of the Cys residues, which determine

their metal-binding affinity and their functions, MTs are categorized into four groups: Type 1, 2, 3 and 4. Particularly, type 4 MTs (i.e. MT 4a and MT 4b in *Arabidopsis*) have been shown to confer greater Zn tolerance that leads to the accumulation of Zn using the Zn-sensitive yeast mutant $\Delta zrc1\Delta cot1$ (Guo et al., 2008). Moreover, the expression levels of MT 4a and MT 4b were shown to correlate with the amount of Zn stored in seeds and their germination rates in low-Zn conditions (Ren et al., 2011). Additionally, heterologously expressed *Arabidopsis* MT in MT-deficient strains of *Synechococcus* was able to restore Zn tolerance (Robinson et al., 1996; Cobbett and Goldsbrough, 2002). The first plant MT to be discovered was the type 4 MT protein of wheat Ec (Early cysteine-labeled protein). It was purified from wheat embryos as a Zn binding protein. It is presumed that this embryo-specific MT provides means of storing Zn in seeds which is required for proper germination (Kawashima et al., 1992). Similar assumption has been made with regards to MT4a and MT4b of *Arabidopsis* (Ren et al., 2011). Recently, in barley MT3 has been reported to play a house-keeping role in metal homeostasis, while MT4 contributes in Zn storage in developing and mature seeds (Hegelund et al., 2012).

Similarly, phytochelatins are small molecular weight peptides that are rich in cysteines and take part in the detoxification of heavy metals. However, unlike MTs, PCs are enzymatically derived from glutathione. The enzyme that catalyzes the conversion of glutathione into PCs is known as phytochelatin synthase. Using PC-deficient *Arabidopsis* mutant (i.e. *cad1-3*) the involvement of PCs in the detoxification of Cd in plants has long been established. Very recently, the involvement of PCs in the homeostatic mechanism of Zn was clearly demonstrated using *cad1-3* and a second strong allele (*cad1-6*). Both mutants showed pronounced Zn hypersensitivity as well as a significant reduction in root Zn accumulation. Meanwhile, Zn was able to activate PC synthase in almost the same extent as Cd. These observations exemplified the role of PCs in Zn homeostasis, leading to the conclusion of PCs significance for Zn tolerance as well as its task in Zn accumulation (Tennstedt et al., 2009).

On the other hand, nicotianamine (NA) is a non-proteinogenic amino acid synthesized from three molecules of S-adenosyl methionine (SAM) by the enzyme nicotianamine synthase (NAS). NA has a capacity of forming strong complexes with most transition metal ions (Stephan and Scholz, 1993; Callahan et al., 2006) and its first discovered role was in Fe homeostasis (Stephan and Scholz, 1993, Herbik et al., 1999). Four genes that code for NAS are found in the *thaliana* genome. The expression levels of three of them, i.e. NAS1, NAS2 and

NAS3, have been shown to be dependent on the level of available Zn (i.e. they all get induced by Zn deficiency in both roots and shoots) (Wintz et al., 2003). In addition to that, in hyperaccumulating species (*Arabidopsis halleri* and *Thlaspi caerulescens*) the transcript level of several NAS genes as well as SAM synthetase genes were higher than in the non accumulating relative *A. thaliana* (Weber et al., 2004; Talke et al., 2006; Hammond et al., 2006; van de Mortel et al., 2006). Heterologous expression of NAS2 of *A. thaliana* in *Schizosaccharomyces pombe* conferred increased Zn tolerance (Weber et al., 2004). Moreover, the formation of intracellular Zn-NA complexes has been demonstrated using NAS-expressing *S. pombe* cells and synchrotron experiments (Trampczynska et al., 2010). Very recently following the same trend, RNA interference mediated knock down of NAS2 in *A. halleri* resulted in the reduction of root-to-shoot translocation of Zn. Based on all of these observations it is proposed that NA-Zn complexes facilitate the symplastic passage of Zn toward the xylem (Deinlein et al., 2012). However, transporters of NA-Zn complexes are yet to be identified.

In addition to the three ligands discussed above the amino acid histidine (His) has been implicated as Zn-binding ligand in plants. X-ray absorption spectroscopy mediated investigations carried out on *Thlaspi caerulescens* have identified Zn-histidine complexes as being the second most abundant form of Zn-ligand complexes, following the Zn-citrate complex (explained in the next paragraph) (Salt et al., 1999).

Furthermore, organic acids, such as citrate and malate, have been proposed to serve as Zn ligands in plant vacuoles (Haydon and Cobbett, 2007). In this regard, computer based simulation models predicted 90% of the vacuolar Zn content of tobacco (*Nicotiana tabacum*) to be citrate bound (Wang et al., 1992) and the same is true for *Thlaspi caerulescens* (Salt et al., 1999). However, in *Arabidopsis halleri* x-ray absorption spectroscopic analysis identified malate as the most prominent Zn ligand in leaves (Sarret et al., 2002).

One additional groups of ligands implicated in Zn chelation are phytosiderophores (PSs). PSs are synthesized through deamination of NA by nicotianamine amino transferase (NAAT) forming deoxymugineic acid that can undergo hydroxylation to form mugineic acid or through extra hydroxylation many more additional derivatives (Takagi et al., 1984). Even if releasing PSs to facilitate uptake is mainly reported in Fe acquisition process (Schaaf et al.,

2004; Kim and Guerinot, 2007), PSs have been implicated in Zn uptake in maize (von Wirén et al., 1996). Similarly, under Zn and Fe deficient condition different wheat varieties have been reported to release more PSs indicating their involvement in Zn uptake (Cakmak et al., 1994). Specially, Zn efficient genotypes secreted more PSs and showed improved Zn uptake efficiency as well as translocation to shoots than did the sensitive genotypes (Rengel et al., 1998; Guerinot and Eide, 1999). Likewise, in barley and rice, transcript levels of PSs biosynthetic pathway genes were induced under Zn and Fe limited conditions thereby increasing the amount of PSs released. These observations further strengthen the notion of phytosiderophores' involvement in the process of Zn uptake (Suzuki et al., 2006; Schaaf et al., 2004; Suzuki et al., 2008; Sinclair and Krämer, 2012).

1.1.2.3 Efflux mechanisms

After the uptake of a Zn ion into the cytoplasm the next challenge is to deliver it to a destination organelle or plant tissue. Seven protein families are described to transport Zn from the cytoplasm into the lumen of intracellular organelles or across the plasma membrane. Among these the four well known ones are P_{1B}-type subfamily of P-type ATPases, NRAMP and the CDF protein families and the YSL transporter family (Eide, 2006; Palmer and Guerinot, 2009).

The P-type ATPases represent a large family of proteins that pump various charged substrates across biological membranes through the expenditure of ATP. The distinguishing feature of P-type subfamily is the formation of a phosphorylated intermediate during the course of the reaction cycle. Among the P-type ATPase heavy metal ATPases are again sub-grouped into 1B. Heavy metal ATPases (HMA) are predicted to have 8 transmembrane domains with a large cytoplasmic loop between the 6th and 7th transmembrane domain (Mills et al., 2003; Hall and Williams, 2003). The *A. thaliana* genome has 8 HMA genes among which HMA2 and HMA4 are reported to have a vital role in the root to shoot translocation of Zn. Even though neither single mutant showed visible defect, the *hma2hma4* double mutant showed leaf chlorosis, stunted growth and reduced fertility. Moreover, despite elevated Zn content in roots, it accumulated less Zn in shoots. These aberrations of *hma2hma4* could be rescued by supplementing the growth medium with a higher concentration of Zn, which is indicative of impairment in the root-to-shoot translocation of Zn (Hussain et al., 2004). In a different approach, overexpression of HMA4 alone in *Arabidopsis* increased transport of Zn to aerial tissues (Verret et al., 2004). Therefore, it is believed that HMA2 and HMA4 function in

loading of Zn into vascular tissues for long-distance transport (Hussain et al., 2004). It has also been shown that a mutation in HMA1 (protein that localizes to the chloroplast envelope) caused accumulation of Zn ions in the chloroplast and plants carrying inactivating mutation in the HMA1 were sensitive to high concentrations of Zn. Furthermore, expressing HMA1 that lacks the chloroplast-targeting signal (the amine terminus) in *Saccharomyces cerevisiae* caused aggravated Zn sensitivity. These indications imply HMA1 takes part in Zn efflux from the chloroplast (Kim et al., 2009). When it comes to HMA3, not all *Arabidopsis* accessions carrying a functional HMA3 but in *Arabidopsis* accessions carrying functional HMA3 (such as Wassilewskaja (Ws)) a mutated version of it caused hypersensitivity to elevated Zn; whereas overexpression of it has led to increased Zn tolerance. Moreover, the expression level of HMA3 in shoots of two Zn hyperaccumulator species (*Arabidopsis halleri* and *Thlaspi caerulescens*) is comparatively higher than that of *Arabidopsis thaliana* signifying its role in Zn efflux to the vacuole (Morel et al., 2008; Sinclair and Krämer, 2012).

The second protein family associated with Zn efflux mechanism is NRAMP family. The NRAMP have 12 transmembrane domains with consensus transport motif between 8th and the 9th transmembrane domain. Six NRAMP genes have been identified in *Arabidopsis thaliana* among which NRAMP4 is shown to transport Zn (Lanquar et al., 2004). In addition to that, because of the hypersensitivity phenotype observed in the double mutant of *nrmp3nrmp4*, NRAMP3 is also presumed to be involved in the efflux mechanism of zinc homeostasis (Oomen et al., 2009). Besides that, the localization of NRAMP3 and NRAMP4 proteins is in the tonoplast of vascular tissues of roots and shoots that suggests an involvement in long-distance Zn transport (Thomine et al., 2003).

The third category of efflux transporters involved in Zn transport represent the CDF proteins. Most members of this family have six predicted transmembrane domains and both the amino- and the carboxy-terminal ends of the protein are located in the cytoplasm. They also have a histidine-rich domain between the 4th and 5th transmembrane domain that may function as a Zn-binding region (Williams et al., 2000). The *A. thaliana* genome encodes 12 putative CDF genes. The first CDF gene to be shown as Zn efflux transporter was MTP1 (Metal Tolerance Protein 1). MTP1 (formerly named as ZAT1) has tonoplast localization and is constitutively present in both shoots and roots of *A. thaliana* plants. A mutation in this gene caused a strong hypersensitivity to excess Zn as well as lower accumulation of zinc in plant

tissues (Kobae et al., 2004; Desbrosses-Fonrouge et al., 2005). Further investigations have indicated that the characteristic His-rich cytoplasmic loop of MTP1 buffers cytoplasmic Zn and may also serve as sensor because deletion of this loop caused induction of hyperactivity in MTP1 (Kawachi et al., 2009). The second CDF protein to be discovered as Zn efflux transporter was MTP3. The expression pattern of the tonoplast-localized MTP3 is confined to roots and it gets further induced by higher Zn concentration and iron (Fe) limitation. These observations are indicative of the function of MTP3 in sequestration of Zn in root vacuoles especially under elevated Zn and Fe deficient condition (Arrivault et al., 2006).

The fourth transporter family implicated in Zn efflux contains the YSL transporter proteins. YSL proteins belong to the Oligopeptide Transporter (OPT) superfamily. Their function was first observed in monocots where they serve in the uptake of Fe-phytosiderophore complexes. Later on, the *Arabidopsis* genome was shown to carry 8 members of the YSL proteins. Among the eight the transcription level of YSL2 was shown to be responsive of Zn availability whereby it gets repressed by lower availability of Zn. Heterologous expression of *Arabidopsis* YSL2 in yeast has shown its function in the transport of Fe-NA and Cu-NA complexes. Accordingly, YSL2 is assumed to have a role in the transport of various metal-NA complexes including a Zn-NA complex (Schaaf, 2005; Sinclair and Krämer, 2012).

The fifth transporter family that has been identified in plants as Zn efflux transporter is the *Arabidopsis* MHX transporter (Haydon and Cobbett, 2007). The MHX is a proton antiporter transporter that shares sequence similarity to mammalian sodium (Na) and calcium (Ca) exchanger. It has vacuolar localization and it has been implicated in the transport of magnesium (Mg) and Zn (Shaul et al., 1999). The expression pattern of MHX is mainly confined to the vascular cylinder implying its function in the proper partitioning of Zn between different organs of plants. Similar to that of other members of the Zn homeostasis mechanism, MHX showed higher transcript level in *A. halleri* compared to *A. thaliana* which may have important effect in the Zn tolerance of this species (Elbaz et al., 2006).

Another Zn efflux transporter is the zinc-induced facilitator1 (ZIF1). ZIF1 encodes a major facilitator superfamily (MFS) transporter. Having tonoplast localization, it is presumed to be involved in a novel mechanism of Zn sequestration, possibly by transporting Zn ligands or a Zn ligand complex into vacuoles (Haydon and Cobbett, 2007). Latest findings in this regards

have indicated the involvement of ZIF1 in Zn and Fe homeostasis, whereby it contributes to the detoxification of Zn under Fe deficient conditions. It has been shown that overexpression ZIF1 has caused enhanced vacuolar accumulation of NA and Zn which in turn caused Zn and Fe deficiency symptoms that can be corrected by spraying *Arabidopsis* plants with Zn and Fe (Haydon et al., 2012).

In recent years a new member of the Zn efflux transporters named as PCR2 has been reported. The name PCR2 stands for a cysteine-rich protein with only two transmembrane helices localizing in the plasma membrane. When the corresponding cDNA was expressed in yeast PCR2 was able to engage in the efflux of Zn and Cd out of the cytoplasm. The expression of PCR2 is mainly localized in the vascular tissues of the shoot, in the xylem as well as epidermis of the root tip. Furthermore, the *Arabidopsis pcr2* mutant showed higher accumulation of Zn and Fe in roots, as well as sensitivity to both excess and deficient Zn which is a sign of PCR2's involvement in long distance translocation of Zn ions (Song et al., 2010; Sinclair and Krämer, 2012).

1.1.3 Regulation of the Zn homeostasis mechanism

Organisms throughout the course of their lifetime are always exposed to enduring change; they go through various developmental and physiological processes. The surrounding environment also undergoes various climatic as well as seasonal changes. Therefore, living things need to have systems that can accommodate these various ongoing changes. A plant root cell can be mentioned as an example. Based on the developmental stage it is in and nutrient availability in the surrounding, it needs to adjust uptake and utilization of macro and micronutrients. Going back to the main focus of this chapter, Zn homeostasis mechanisms also should be able to entertain the plasticity of demand and supply of a cell. The two main ways of regulating Zn homeostasis mechanism are active Zn flux regulation and transcriptional regulation of genes involved in the process.

Genetic transcription level analysis carried out on *Arabidopsis thaliana* grown under variable zinc concentrations (i.e. deficient, sufficient and excess) have indicated that the expression level of most of the uptake and efflux transporter genes as well as those encoding enzymes for the synthesis of chelating ligands (Tab. 1.2) are dependent on the extent of Zn availability (van de Mortel et al., 2006). Verifying the observed change in transcript abundance, increased

amount of protein levels of MTP3 and IRT1 were measured in *Arabidopsis* under excess Zn concentrations (Fukao et al., 2011).

Further transcription factors regulating the transcription rate of genes involved in the zinc homeostasis mechanism have been identified. Two basic-region leucine zipper (bZIP) transcription factors (bZIP19 and bZIP23) have been identified as a result of the positive interaction they have manifested with the promoter regions of ZIP4 gene in a yeast-one-hybrid screening. Similar to that of ZIP4 the expression levels of bZIP19 and bZIP23 were higher under Zn deficiency and the double mutant *bZIP19bZIP23* showed a strong hypersensitivity towards zinc-deficiency, whereas the single mutant *bZIP19* showed a mild but visible effect indicating their role in controlling the zinc deficiency response of *Arabidopsis thaliana*. Further investigations on the palindrome (RTGTCGACAY) discovered in the promoter region of ZIP4 led to the establishment of the *cis* element called Zinc Deficiency Response Element (ZDRE) which is also present in the promoters of six (i.e. ZIP1, ZIP3, ZIP5, ZIP9, ZIP12, and IRT3) other alleged Zn transporter encoding genes. Additionally, microarray analysis carried out on *bZIP19bZIP23*, the double mutant in comparison to the wild type, increased the number of genes anticipated to be under the regulation of these two transcription factors. Among the genes picked up by the microarray analysis are two of the NA synthase genes (NAS2 and NAS4) that provides further support to the central role of bZIP19/23 transcription factors in the regulation of Zn homeostasis under zinc deficient conditions (Assunçãoa et al., 2009).

Table 1.2. List of genes up-regulated (expression differences of ≥ 3 fold and P value of < 0.05) under zinc deficient ($0\mu\text{M}$) and surplus Zn ($25\mu\text{M}$) when compared to optimal zinc availability ($2\mu\text{M}$). This table is adapted from van de Mortel et al., (2006).

<i>Up regulated genes</i>	<i>Zn deficient medium</i>			<i>Zn surplus medium</i>
CDF genes	MTP2			MTP3 MTP8
NRMP genes				NRAMP4
YSL genes	YSL2 YSL3			
ZIP genes	IRT3			IRT1
	ZIP1	ZIP2	ZIP3	IRT2
	ZIP4	ZIP5	ZIP9	ZIP8
	ZIP10	ZIP11	ZIP12	
Zn binding ligand related	NAS2			NAS1
	NAS4			SAM1

The second approach of regulating Zn homeostasis process is through posttranscriptional modification of the uptake and efflux transporters depending on the intracellular Zn status. In yeast the presence of such regulation methods has been reported, where high concentration of Zn induces the removal of the uptake transporter ZRT1 from the plasma membrane through ubiquitination mediated endocytosis and subsequent degradation in the vacuole (Gitan and Eide, 2000). Similarly, in human and mouse the Zn availability dependent regulation of the localization of the uptake transporter ZIP4 has been reported, in which Zn deficiency increased the ZIP4 protein levels at the plasma membrane and resulted in increased Zn uptake, whereas higher Zn concentration stimulated the rapid endocytosis of the transporter in order to limit the amount of Zn uptake (Kim et al., 2004). However, the parallel regulatory process in plants has not yet been identified. Nevertheless, the report regarding monoubiquitin-dependent trafficking of the uptake transporter IRT1 can be mentioned as the first evidence for the presence of posttranslational regulation in plants. Even if iron availability is not serving as signal, the observation reveals the requirement for constant turnover of IRT1 between the plasma membrane and the vacuole in order to control the localization of IRT1, ensure proper iron uptake and prevent metal toxicity (Barberon et al., 2011).

However, for both transcriptional and posttranscriptional regulations of Zn homeostasis mechanism to work properly plant cells need to have means of detecting extracellular and intracellular Zn levels. Unlike in *S. cerevisiae* where a Zn-sensing transcription factor (ZAP1) is identified, in plants a Zn sensing mechanism is not yet discovered (Clemens, 2010).

When discussing about the regulatory mechanism of Zn homeostasis, one thing that should not be forgotten is its interdependence with other macro and micronutrient availability and acquisition processes. This interdependency could be due to shared network components like transporters and chelators or due to physiological changes that impact the concentration of multiple elements in plants (Baxter, 2010). Zn uptake and levels in plants have been linked to phosphate (P), Magnesium (Mg) and Fe concentration and uptake of plants. With regards to the interaction of Zn and P, the first observation was made when Zn limited condition lead to reduced accumulation of phosphate (P) in plants (Cakmak and Marschner, 1986). Later on after the identification P uptake transporters, it has been shown that in barley roots at lower Zn availability the transcript levels of high affinity P transporters were highly induced that

led to the accumulation of more P. Normally, the activity of high affinity P transporter is dependent on the P status of the plant. However under Zn deficiency, this regulatory mechanism seems to be overridden (Huang et al., 2000). When it comes to influence of Fe and Mg on Zn concentrations in plants, both metal ions share uptake transporters with Zn (IRT1 and HMX1, respectively) and the availability of each has an impact on the uptake and accumulation of the other metal (Emery et al., 2012). Accordingly, the accumulation of Zn in plants under Fe deficiency has been correlated to increased IRT1 protein level. Similarly, exposure to excess Zn causes physiological Fe deficiency. By the same token, the transcriptional response of Zn efflux transporters like MTP3, HMA3 and ZIF1 to excess Zn and limited Fe availability are identical showing the interconnection of the two homeostasis processes (Sinclair and Krämer, 2012).

1.1.4 The overall Zn homeostasis mechanism at the organismal level

Plants have shown their potential in influencing the solubility and speciation of metals in the rhizosphere by exuding chelators and manipulating rhizosphere pH (Fan et al., 1997). Nevertheless, the activity of such mechanisms in manipulating the availability of Zn has not been recorded yet.

Once Zn is taken up across the plasma membrane of root epidermal cells (possibly through ZIPs and ITRs) it can either be kept within the root system by being sequestered (by MTPs and ZIF1) into vacuoles (i.e. root vacuoles are the main storage site of surplus Zn and they contribute greatly towards basal Zn tolerance (Sinclair and Krämer, 2012)), or it can be moved through symplastic passage via plasmodesmata to the pericycle to be loaded into the xylem (via HMA2 and HMA4). After being loaded into the apoplastic route of xylem, Zn is transported like most other transition metals by mass flow of water created by the transpiration stream and root pressure (Welch, 1995; Curie et al., 2008). Within the xylem, pH (which is in the range of 5.4 to 6.5) and redox potential are important for regulating the solubility and speciation of metals (Welch, 1995). Zn is assumed to be transported as ligand complex (possibly bind to citric / malic acid or NA) that prevents unspecific uptake and retention by neighboring cells (Palmgren et al., 2008). Similarly, remobilization of Zn from senescing leaves and translocation to sink tissues such as seeds takes place via long distance transport within the phloem. Generally, transport in phloem occurs via the hydrostatic pressure gradient created as a result of loading of sucrose into the phloem from

photosynthetically active leaves and unloading of sucrose into the sink tissues such as meristematic zones of shoot and root tips. Phloem unlike xylem is composed of alive and metabolically active cells. Thus it has the potential to make the phloem sap more responsive to changes in the internal plant environment (Welch, 1995). Here again, since phloem has higher pH (≥ 8) and carries large amount of solutes that can bind Zn, the requirement for Zn chelation is strong (Sinclair and Krämer, 2012). The phloem mobility of Zn is considered to be dependent on the level of Zn within individual plant as well as the species of the plant. In a split-root experiment, it has been shown that during inadequate Zn supply, the phloem transport of Zn is lacking. However, in the presence of adequate Zn supply its phloem transport also increases (Welch et al., 1999). Representative picture of the Zn homeostasis mechanism in plants is depicted in figure 1.4.

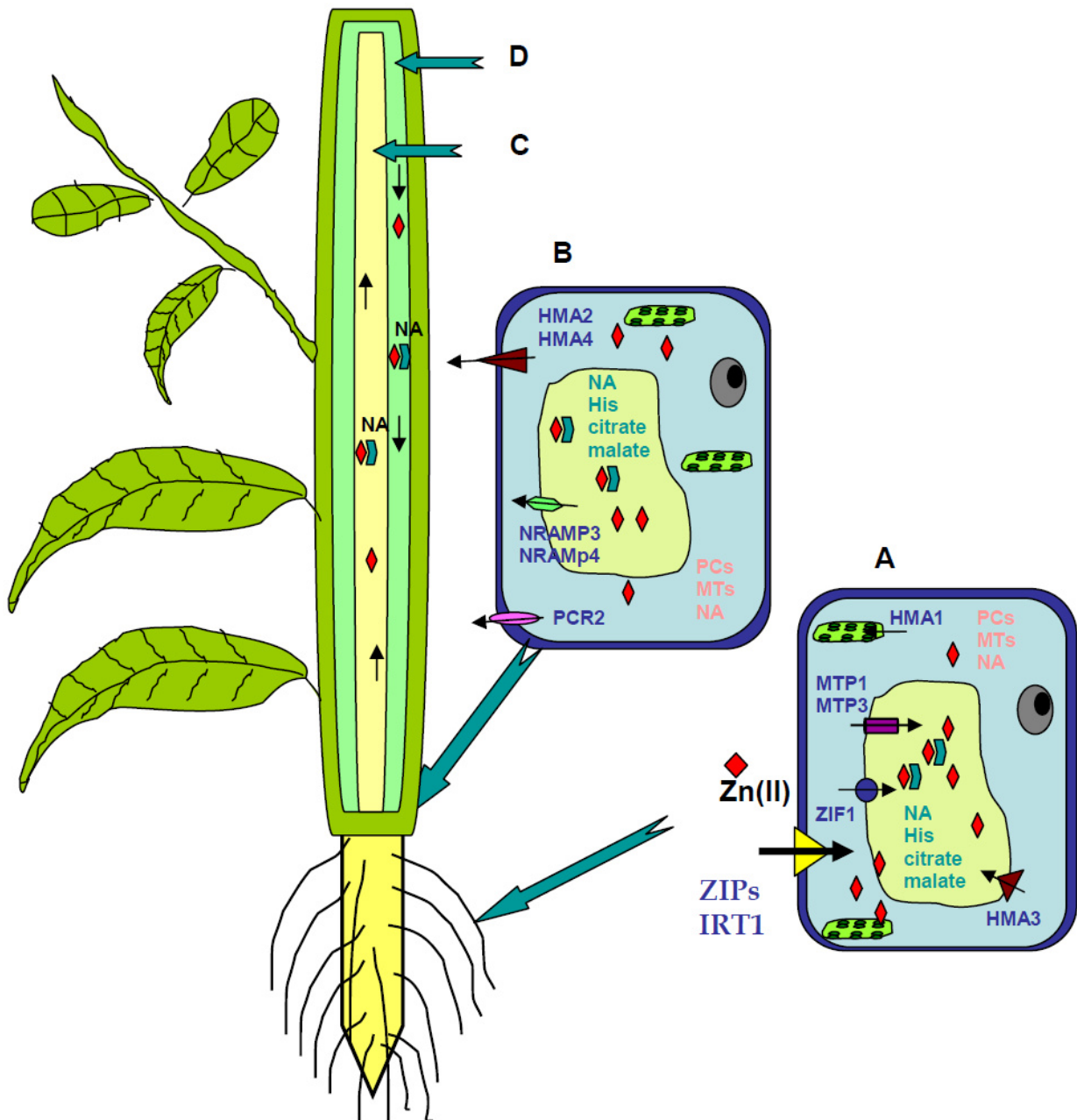


Figure 1.4. Model representation of Zn transport within a plant. A) represents epidermal root and B) pericycle cells, C) represents xylem and shows the apoplastic Zn movement  represent Zn-ligand complex whereas  stands for free Zn D) stands for the symplastic Zn translocation in the phloem.

1.1.5 Open questions and missing links in the Zn homeostasis mechanisms

So far, one important open question in the Zn homeostasis mechanism in plants is that no sensors for Zn status have been identified. Multiple responses to excess or lack of Zn in plant cells have been observed but a particular Zn sensing apparatus is yet to be discovered. The second important missing link in the Zn homeostasis mechanism is the interaction between transporters (i.e. both uptake and efflux) and chelators (Clemens, 2010). The understanding about “how do the different components of the Zn homeostasis mechanisms interact and

regulate each other and fit to the overall plant ionomics” is still a work in progress (Baxter, 2010). In recent years, the detailed knowledge about single components (i.e. transporters, chelators etc.) of the Zn homeostasis mechanisms has advanced considerably. However, a clear picture of the overall Zn homeostasis mechanism is yet to be achieved.

1.1.6 Zinc toxicity tolerance in plants

Plants have evolved different schemes to maintain the concentration of heavy metals like Zn within a physiological limit. During exposure to toxic concentration of metal ions first they use mechanisms like: (1) limiting the amount of ions taken-up either by releasing chelating agents that would hinder their uptake or by binding ions at the cell wall and cell membrane and preventing their entry (e.g. cell wall and cell membrane of moss *Pohlia drummondii* functions as barrier to excluded harmful doses of zinc from reaching the protoplast (Lang and Wernitznig, 2011)), (2) sequestering them into special compartments in order to isolate them from sensitive organelles (e.g. excess Zn induces the transcript level of MTP3 in order to increase the Zn efflux into the vacuole (van de Mortel et al., 2006)) or (3) increasing the rate of root to shoot translocation (e.g. HMA2 and HMA4 confer tolerance through Zn translocation from roots to shoots (Clemens, 2010)). When these mechanisms are exhausted, plants activate secondary line of defense that involves the oxidative stress defense mechanism and synthesis of stress-related signaling molecules like heat shock proteins, hormones (e.g. toxic level of Zn leads to increased production of ethylene (Maksymiec, 2007)) and reactive oxygen species (Clemens, 2001; Manara, 2012). However, detailed understanding of how these systems function in dealing with toxic level of Zn is still unclear (Clemens, 2010).

1.1.7 Problems related to zinc deficiency

Zn deficiency is among the factors reducing the productivity of the agricultural sector. Zn availability in the soil is mainly influenced by three things: pH, organic matter content and water availability. At higher pH Zn gets more easily adsorbed to the clay minerals of the soil or it precipitates as a phosphate or carbonate. Similarly, shortage of water hampers the solubility of Zn slowing down the diffusion process through which it reaches the root surface (Broadley et al., 2007; Clemens, 2010). Therefore, arable lands with high pH (>7) and semiarid environments are predisposed to suffer from Zn deficiency. In areas like Australia, China, India and Turkey, where calcareous soil with higher pH is prevalent, Zn deficiency is a critical

problem (Broadley et al., 2007). Especially in cereals like wheat and rice major grain-yield reduction has been observed as a result of Zn deficiency (Cakmak et al., 1996; Sudhalakshmi et al., 2007). In the paddy cropping system of rice the flooding phase has made matters worse, because the low redox potential causes Zn to precipitate as zinc sulphide, zinc carbonate or zinc oxy-hydroxides (Rose et al., 2013).

Besides the yield reduction, cereal grains produced under Zn deficiency have poor nutritional qualities due to lower levels of Zn in seeds (Cakmak et al., 1996; Sinclair and Krämer, 2012). Correspondingly, in populations where the diet is mainly comprised of cereals the prevalence of Zn deficiency is also very high. Despite lack of reliable biomarkers for Zn deficiency, the WHO estimates 31% of the world's population to be at risk of Zn deficiency (Sinclair and Krämer, 2012). In human the bioavailability of Zn is mainly dependent on the quantity of zinc ingested, but the amount of dietary factors (such as inositol hexa-/penta-phosphate commonly known as phytate) can also affect its bioavailability by impairing its absorption (Hambidge et al., 2010). Therefore, in the developing world where diets constitute less animal product (that have more dietary Zn content), the severity of Zn deficiency could be extremely high (Fig. 1.5). Inadequate Zn supply in human diet can lead to growth retardation, eye and skin lesions, impotence and delayed sexual maturation (Vinkenborg, 2010). Particularly, in infants Zn deficiency has been linked with the prevalence and severity of infectious diseases like pneumonia and diarrhea where Zn supplements reduced the morbidity rate caused by diarrhea (Bouis, 2003).

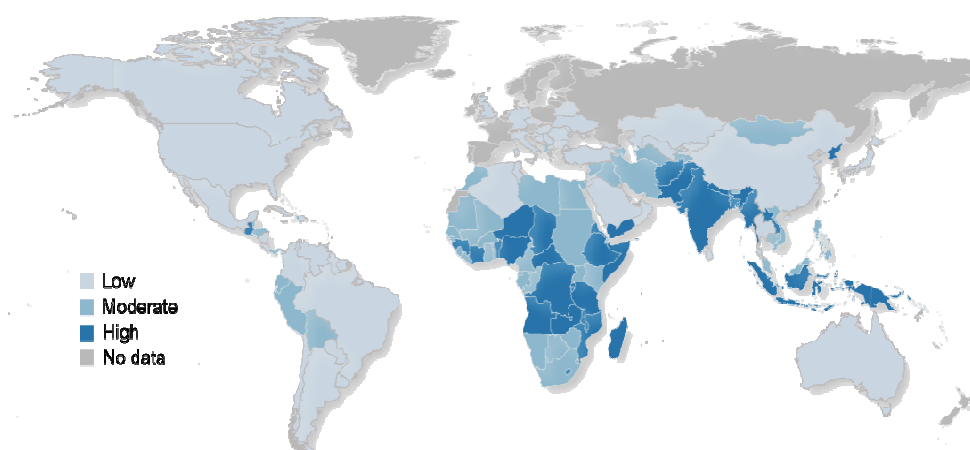


Figure 1.5. Global prevalence of zinc deficiency.

The prevalence of Zn deficiency in a population is inferred from the percentage of children under 5 years of age with low height-for-age ratio (which is indicative of growth stunting).The significance of Zn deficiency prevalence towards public health is classified as low ($\leq 20.0\%$), moderate ($>20\% - 40\%$), or high ($\geq 40\%$)

Source: World Health Organization, Global Health Observatory Database: <http://apps.who.int/ghodata/>

In the past few years, this problem has gained lots of attention and various approaches have been designed in order to alleviate zinc deficiency in the developing world. One of such programs working on the area is the zinc and nutrition initiative of the International Zinc Association (IZA) that works to ensure the survival, growth and development of children through Zn supplementation (www.zinc.org). The other approach in tackling this problem is utilization of Zn efficient varieties and Zn fertilizers in order to maximize yield as well as obtain cereal grains with better Zn accumulation. With this regard there are joint ventures such as HarvestPlus (www.harvestplus.org) that are working to breed staple crop genotypes that load high amounts of bioavailable micronutrients (such as Zn) in their seeds. Identifying different crop genotypes with higher Zn accumulation by screening different varieties would be a cumbersome job and very time consuming. On the other hand, most of the identified components of the Zn homeostasis mechanism contribute to basal Zn tolerance of plants. As it has been mentioned in previous subtopics malfunctioning of parts of the uptake, chelation or efflux mechanisms of the Zn homeostasis mechanism leads to growth inhibition of plants during the presence of excess Zn (Weber et al., 2013; Krämer and Clemens, 2005). For example, mutants like *mtp1* (loss of function mutant of Zn efflux transporter) and *cad1-3* (phytochelatin deficient line) show Zn hypersensitivity signifying the role of MTP1 and Phytochelatins in Zn tolerance (Kawachi et al., 2009; Tennstedt et al., 2009). However, as discussed in the previous subtopics, comprehensive understanding of the Zn homeostasis mechanism is still lacking. Hence, screening for Zn hypersensitivity mutants could be one suitable approach to identify novel components of Zn homeostasis mechanisms that can lead to Zn tolerance and at the same time be useful for the biofortification strategy.

1.1.8 Screening for zinc tolerance in EMS mutagenized seeds

Genetic studies set up to identify the function of a gene have been a favored method in deciphering complex biosynthetic pathways as well as homeostasis mechanisms. In such studies, the classic approach is to look for mutant phenotypes. If the impact of a mutation in a particular gene is known then it would be possible to infer the activity of the gene in its native state. The first step in this kind of processes is inflicting genetic lesions (which is referred to as mutagenesis). The choice of mutagens used in order to inflict genetic lesions is dependent on the type of mutant desired. For mutants with large deletions of pieces of chromosome or chromosomal re-arrangement that can be mapped with ease are induced by physical mutagens such as X-rays, γ -rays, electrons and ion beams (Magori et al., 2010).

Whereas, chemical mutagens such as ethyl methane sulfonate (EMS) and diethyl sulfate (DES) are better suited for creating mutations restricted to individual genes (Kim et al., 2006). There are also insertional mutations that are produced either through T-DNA or transposon integration into the genome. Based on the integration site, insertion mutations can be loss of function mutants (i.e. when the insertion is within the coding region) or mutants with compromised intron splicing or gene expression patterns (Stracke et al., 2010).

One way of conducting genetic studies is the classical method, where first a particular mutant phenotype is identified and later on it is mapped to the gene that is affected by the mutation. This kind of method is known as forward genetics. Within the arm of forward genetics there is a practice referred as saturation genetics or saturation mutagenesis in which large numbers of mutations are inflicted on one area of a genome or in one biological function expecting to identify all the genes in that area, or affecting that particular function. Meanwhile, in the last decade, the number of organisms whose genome has been sequenced increased that lead to a new technique in the identification of the function of a gene. Whole genome sequencing initiatives have created new challenges where all the genes in an organism are known but very little is revealed about their function. In this era a new approach of genetic studies has crystallized, where a particular gene with a predicted function is mutated and the resulting phenotype is noted. This way of identifying the function of a gene is referred as reverse genetics.

The mutagen selected to be used in this particular project is the chemical mutagen ethyl methane sulfonate (EMS). Its effect originates from its alkylating nature that can induce chemical modification of nucleotides mostly guanine (G) residues. Strong alkylation of guanine forms O⁶-ethylguanine that pairs with thymine (T) instead of cytosine (C). Subsequent DNA repair processes then might replace the G/T pair with A (adenine)/T pair. Hence, 99% of the time EMS induces C-to-T changes resulting in C/G to T/A substitutions (Kim et al., 2006) and the frequency of EMS-induced stop codon and missense mutations in *Arabidopsis* has been deduced to be around 5% and 65%, respectively (McCallum et al., 2000). Two most important advantages of EMS mutagenesis are:

- there is no real bias in the distribution of mutations caused by EMS throughout the genome creating a potential for generating mutants of genes located near the telomere and centromere regions,

- Secondly, like all other chemical mutagens EMS can induce weak nonlethal alleles that are useful in the understanding of the function of essential genes where total disruption of the gene is lethal.

In addition to that, chemical mutagens including EMS are shown to have better efficiency and frequency in achieving saturation mutagenesis. Furthermore, by using EMS mutagenesis chromosomal rearrangements (common feature of insertion mutagens like T-DNA and transposable elements) and inversions and deletion of chromosomes (common effect of irradiation mutagenesis) can be evaded (Kim et al., 2006).

In this project a forward genetic approach has been implemented where second generation (M2) EMS mutagenized *Arabidopsis thaliana* Colombia-0 ecotype seeds were screened for increased Zn sensitivity manifested in terms of reduced root length in the presence of Zn. Identifying mutants with increased Zn hypersensitivity signifies the disruption of the basic Zn tolerance mechanism of plants that involves regulation of transport, sequestration and translocation processes. Hence, genetic and functional characterization of such mutants could lead to the identification of pathways that contribute to improved efficiency of root to shoot translocation and Zn loading of grains. Concomitantly, such knowledge could serve as a molecular tool for biofortification strategy.

1.2 Role of flavonoids in heavy metal tolerance

1.2.1 Understanding the link between flavonoids and heavy metal ions

Plants, being sessile organisms, have evolved various mechanisms of dealing with the adverse effects of the environment they live in. Secondary metabolites like flavonoids are part of such mechanisms involved in the defense responses of plants to biotic factors like pathogens and herbivores attack (Koes et al., 1994; Lin and Weng, 2006) as well as abiotic stresses like ultraviolet (UV) light and low temperature (Winkel-Shirley, 2002; Sharma et al., 2007).

Flavonoids represent a diverse set of polyphenolic compounds that are part of the plant secondary metabolism. The main structure of flavonoids (Fig. 1.6) is made up of two hydroxyl substituted aromatic rings (A and B) joined by three carbon chains that form an oxygenated heterocyclic ring (C) (Nijveldt et al., 2001; Marais et al., 2006; Tsimogiannis et al., 2007). Flavonoids, with an estimated 10,000 different members, have a widespread occurrence in the plant kingdom (Dixon and Pasinetti, 2010). Some common flavonoids and their edible plant sources are listed in table 1.3.

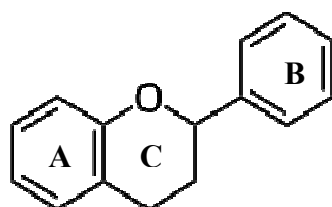


Figure 1.6. General structure of flavonoids

Table 1.3. Common flavonoids and their edible plant sources

Name	Flavonoid subgroup	Plant source
Catechin	Flavanol	Grape, Tea
Epicatechin		
Hesperidin	Flavanones	Citrus plants
Naringenin		
Apigenin	Flavones	Parsley
Luteolin		
Daidzein	Isoflavones	Legumes (e.g. soybean)
Glycitein		
Kaempferol	Flavonols	Lettuce
Quercetin		
Cyanidin	Anthocyanidins	Berries
Malvidin		

Adapted from Koornneef et al. (1982)

1.2.2 Flavonoid biosynthesis and flavonoid deficient mutants

One of the well characterized biosynthetic pathways in plants is the phenylpropanoid pathway. Especially the branch pathway leading to the synthesis of flavonoids has been thoroughly analyzed (Winkel-Shirley et al., 1995).

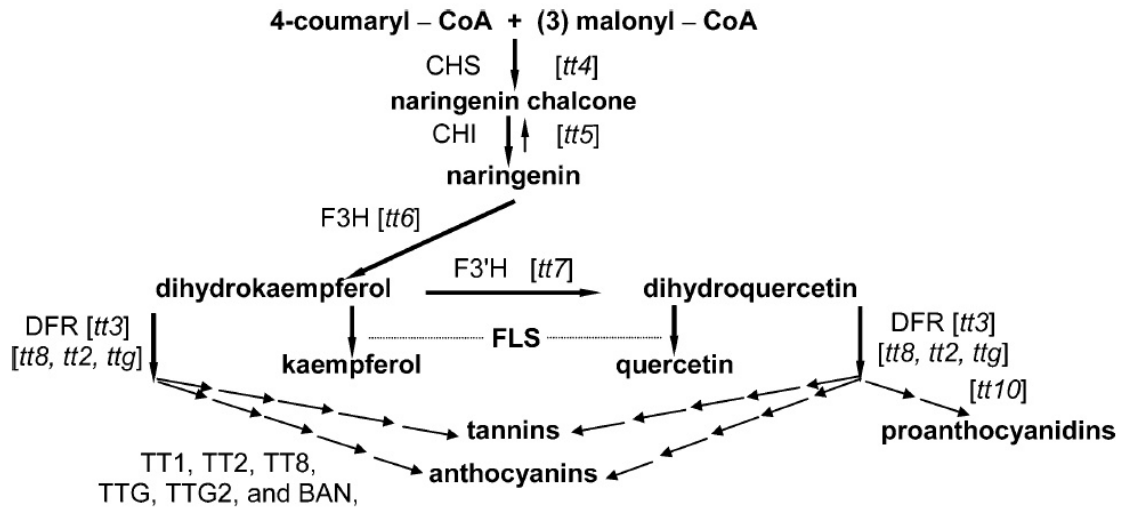


Figure 1.7. The flavonoid biosynthesis pathway in *Arabidopsis*. This figure is adapted from Buer and Djordjevic (2009).

Flavonoid synthesis (Fig. 1.7) starts with condensation of one molecule of 4-coumaroyl-CoA and three molecules of malonyl-CoA yielding naringenin chalcone through the enzymatic activity of chalcone synthase (CHS). Coumaroyl-CoA, one of the precursors of the flavonoid biosynthesis, is synthesised from phenylalanine by three enzymatic steps, collectively known as the general phenylpropanoid pathway. The name general phenylpropanoid pathway was coined because the structures involved at this stage are phenylpropane-based and this step is a common step to the biosynthesis of a variety of compounds such as lignin, coumarins, stilbenes and flavonoids. The second precursor, malonyl-CoA, is synthesized by carboxylation of acetyl-CoA, a central intermediate in the Krebs tricarboxylic acid cycle. The second step in the biosynthesis of flavonoids is that of the enzyme chalcone flavanone isomerase (CHI) that isomerizes the naringenin chalcone (NC) to naringenin (a flavanone). From these central intermediates the pathway diverges into several side branches, each yielding a different class of flavonoids (Koes et al., 1994).

In *Arabidopsis thaliana*, different mutant lines carrying defective genes in various steps of the flavonoid biosynthesis pathway have been identified. The loci are collectively called transparent testa (*tt*) because of the lighter seed coat phenotype produced as a result of the reduction or absence of pigments in the seed coat (testa). Flavonoid-deficient mutants (Tab.

1.4) provide useful tools for studying the roles of flavonoids in plant growth and development (Koornneef et al., 1982; Koornneef, 1990; Winkel-Shirley et al., 1995). These mutants could be grouped into two subclasses (Fig. 1.8.): those with yellow seeds (testa lacking color completely showing the yellow color of the cotyledon) including *tt1*, *tt2*, *tt3*, *tt4*, *tt5* and *tt8* and those with pale brown seeds comprising *tt6*, *tt7*, *tt10* and *ttg2* (Winkel-Shirley et al., 1995).

Table 1.4. List of *transparent testa* mutants of *Arabidopsis* and the genes affected by the mutation

Line	Enzyme lesion
<i>tt1</i>	WIP zinc finger protein
<i>tt2</i>	MYB domain protein
<i>tt3</i>	Dihydroflavonol 4-reductase (DFR)
<i>tt4</i>	Chalcone synthase (CHS)
<i>tt5</i>	Chalcone isomerase (CHI)
<i>tt6</i>	Flavonone 3-hydroxylase (F3H)
<i>fls1</i>	Flavonol synthase
<i>tt7</i>	Flavonoid 3'-hydroxylase (F3'H)
<i>tt8</i>	bHLH domain protein
<i>tt10</i>	Polyphenol oxidase
<i>ttg1</i>	WD40 repeat protein
<i>ttg2</i>	WRKY Transcription Factor

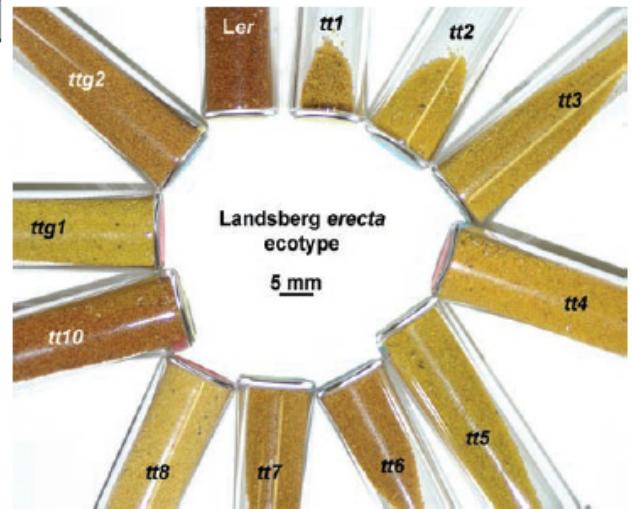


Figure 1.8. Seed color of common transparent testa mutants compared with the wild type. The figure is adapted from Buer et al., (2010).

Chalcone synthase (CHS) is encoded by single gene in *Arabidopsis*. Therefore, CHS knockout plants (i.e. *tt4*) are deficient in flavonoids (Saslowsky et al., 2000). The rest of the *tt* mutants, depending on the type of the affected enzyme, accumulate different intermediate compounds and flavonoids (i.e. *tt5* accumulates NC; *tt7* accumulates an excess amount of kaempferol, whereas, excess amounts of quercetin and kaempferol are accumulated in *tt3* (Peer et al., 2001)).

The flavonoid biosynthesis pathway is partly regulated by TT2 (a MYB transcription factor), TT8 (a bHLH transcription factor) and TTG1 (a WD40 repeat gene), which form a complex in order to induce BANYLUS expression that leads to the formation of anthocyanins. TT1 (a WIP family zinc finger transcription factor) and TTG2 (a WRKY type transcription factor) act downstream of TTG1 (Buer and Djordjevic, 2009). In addition to these processes

isoflavonoids that are only present in leguminous plants are synthesized through enzymatic activity of chalcone reductase (CHR) and isoflavone synthase (IFS) (Buer et al., 2010).

1.2.3 Flavonoids as health promoting factors in human diet

The isolation of the first flavonoid from oranges in 1930 sparked an interest in identifying new flavonoids and their activities. Furthermore, the discovery of the French paradox (i.e. the low cardiovascular mortality rate observed in Mediterranean populations in association with red wine consumption and a high saturated fat intake) created tremendous momentum in the fields of research dealing with flavonoids and their impact on human health (Nijveldt et al., 2001). The most important effect of flavonoids on human health arises from their oxygen-derived free radicals scavenging potential. *In-vitro* experimental systems also showed that flavonoids possess anti-inflammatory, anti-allergic, anti-viral, and anti-carcinogenic properties (Middleton, 1998).

Free radicals and reactive oxygen species which are produced during normal oxygen metabolism or induced by exogenous damage are constant sources of threat for different body cells and tissues (de Groot, 1994). One mechanism by which free radicals interfere with the normal functioning of the body seems to be lipid peroxidation that causes cellular membrane damage. Consequently, the membrane damage leads to a shift in the net charge of the cell that alters the osmotic pressure leading to swelling and eventually cell death. Free radicals can attract various inflammatory mediators, contributing to a general inflammatory response and tissue damage (Nijveldt et al., 2001). As a protection from reactive oxygen species, organisms have enzymatic mechanisms like superoxide dismutase (that catalyzes the dismutation of the superoxide radical into hydrogen peroxide and oxygen), peroxidase (that facilitates the conversion of hydrogen peroxide to water using different electron donors) and catalase (that enzymatically converts hydrogen peroxide into water and oxygen molecule) as well as compounds like glutathione, ascorbic acid, and tocopherol that scavenge them (Dunand et al., 2007; Yurekl and Porgali, 2006). However, during injury and illness the endogenous protection mechanism becomes abnormally overstretched. In such cases flavonoids can have an additive effect to the endogenous system (Nijveldt et al., 2001). Most common flavonoids can scavenge superoxides; whereas other flavonoids can scavenge the highly reactive oxygen derived radical called peroxynitrite. Peroxynitrite is formed as a result of the released nitric oxide (destined to maintain the dilation of blood vessels during injury)

reacting with free radicals. Interestingly, flavonoids like silibin can also directly scavenge nitric oxide molecules. Whereas, flavonoids like quercetin provide similar effects by regulating the synthesis of nitric oxide (van Acker et al., 1995). The other mechanism by which flavonoids influence the level of free radical ions within a cell is by chelating heavy metal ions like iron and copper, which are potential causatives for the accumulation of free radicals. Quercetin in particular is known for its iron-chelating and iron-stabilizing properties (Ferrali et al., 1997).

Another interesting effect of flavonoids on enzyme systems is the inhibition of the metabolism of arachidonic acid. This feature gives flavonoids anti-inflammatory and anti-thrombogenic properties. The release of arachidonic acid is a starting point for a general inflammatory response (Ferrandiz and Alcaraz, 1991).

In a separate direction of research, isoflavonoids have been indicated to have a role in the prevention of cancer, particularly of hormone-dependent cancers such as breast and prostate cancer (Wiseman, 2006). In support of this notion, breast and prostate cancer are much less prevalent in countries where soybean-containing foods (having the highest isoflavone content) are widely consumed. However, the risk of encountering these diseases increases in emigrant population from these same countries, like in the case of emigrant population from Far Eastern countries like Japan living in the United States of America. These changes have been mostly attributed to changes in diet, in particular the switch to a low-soy Western diet (Shimizu et al., 1991). Lower incidence of heart disease has also been reported in populations consuming large amounts of soy products (Sirtori and Lovati, 2001). Similarly, soy isoflavones have been reported to improve cardiovascular risk factors in pre-pubertal rhesus monkeys (Anthony et al., 1996).

As a result of their strong antioxidant and metal chelating potential, flavonoids appear to be effective in reducing the risk of cancer and preventing cardiovascular disease. Overall, several of these flavonoids appear to be effective chemo-preventive agents.

1.2.4 *Flavonoids interaction with heavy metals*

As mentioned previously, flavonoids particularly quercetin have the ability to chelate metal ions which is believed to be related to their strong antioxidant nature. Excess metal ions such

as iron and copper have a potential to create free hydroxyl radicals through the Fenton reaction. Flavonoids can scavenge Fe^{3+} through the formation of phenoxyradicals by transferring charge from their deprotonated hydroxyl group (Ren et al., 2008). A strong evidence for the formation of flavonoid-metal complexes in vivo comes from morin (a pentahydroxyflavone) that forms a complex with aluminum and is routinely used to stain for aluminum in the root apoplast (Gunse et al., 2000). Catechin also forms stable aluminum complexes; consequently, green tea that contains high levels of catechin tolerates as well as accumulates high tissue levels of aluminum (Kidd et al., 2001).

Additionally, according to Lachman et al. (2005) young barley plants grown on hydroponic solution treated with different cadmium concentration showed a significant reduction in the amount of free flavonoids. The strongest reduction in free flavonoid content was observed in the root that also accumulated the highest cadmium concentration in dose dependent manner implying the young barley plants are using flavonoid-metal complex to alleviate the heavy metal stress.

Furthermore, there is experimental evidence showing flavonoid metal complexes having significantly higher radical scavenging potencies than those of bare flavonoids. For example, the data from Kostyuk et al. (2001) demonstrated that complexes formed between metal ions and flavonoids like rutin, dihydroquercetin, and epicatechins are considerably more potent than parent flavonoids in protecting red blood cells against asbestos-induced injury.

1.2.5 Screening of flavonoid deficient mutants for heavy metal sensitivity

In recent years, the quest for understanding the direct interaction of flavonoids with heavy metals has intensified. A number of in-vitro experiments demonstrating complexation mechanisms as well as structural elucidations of flavonoid metal ion complexes have been reported. For instance, Ren et al. (2008) and Lekka et al. (2009) compared different chelating sites and identified the most likely site of complexation for Fe^{3+} and Cu^{2+} , respectively, as well as demonstrated its dependence on pH. Similarly, the chemical structures of different flower pigments that hold metal ions in their core structure have been identified, e.g. Al^{3+} in hydrangea (Yoshida et al., 2003), Fe^{3+} in tulips (Shoji et al., 2007), Fe^{3+} and Mg^{2+} in Himalayan poppy (Yoshida et al., 2006) and Fe^{3+} , Mg^{2+} and Ca^{2+} in cornflower (Shiono et al., 2005). Moreover, Kostyuk et al. (2004) for the first time experimentally demonstrated flavonoids

bound to metal ions were much less subjected to oxidation compared with those of free compounds and formulated the suggestion that flavonoid metal complexes may exhibit superoxide dismuting activity. Likewise, de Souza and de Giovani (2004) investigated antioxidant activities of metal ion complexes with the flavonoids quercetin, rutin, galangin and catechin and found that complexed flavonoids showed higher antioxidant activity, which could be due to the acquisition of additional superoxide dismutating centers.

However, most of the investigations carried out in this area of researches were *in-vitro* experiments. Hence, similar sets of experiments must be conducted in a living system in order to investigate whether the effects observed *in-vitro* cause detectable phenotypes in plants.

Transparent testa mutant lines (previously described under the topic of flavonoid biosynthesis) are mutant lines carrying defective genes in various steps of flavonoid biosynthesis. Based on the enzymatic step disrupted by the mutated gene *tt* mutants accumulate either precursors or a range of flavonoids (Tab. 1.5). These lines have been instrumental in studying the function of flavonoids in a plant system. For example, in the process of proving the role of flavonoids in UVB protection *in vivo*, *tt4*, *tt5* and *tt7* were used (Li et al., 1993). Similarly, in experiments conducted to elucidate the negative impact of flavonoids on auxin transport, two different alleles of *tt4* mutants were used (Brown et al., 2001).

Table 1.5. List of *tt* mutants and major flavonoids that accumulate at their root tips

<i>Line</i>	<i>Enzyme Mutated</i>	<i>Flavonoid Accumulated</i>
tt3	DFR	kaempferol, Quercetin
tt4	CHS	None detected
tt5	CHI	Naringenin chalcone
tt6	F3H	Naringenin
tt7	F3'H	kaempferol

Adapted from Koornneef et al. (1982)

Therefore, part of this project was carried out with the aim of investigating the role of heavy metal ions and the complexes they form with flavonoids on health-promoting biological activities (antioxidant and free radical scavenging potential) of flavonoids. For this purpose

five flavonoid deficient mutant lines of *Arabidopsis thaliana* were analyzed for possible phenotypes in relation to heavy metal ion concentration.

Based on the knowledge from literature, the presumed research hypotheses were:

Since flavonoid deficient mutants are unable to form flavonoid-metal complexes they would be predisposed to suffer from oxidative stress.

In accordance to the type of precursors and flavonoids that they accumulate, the five transparent testa mutants would behave differently towards tolerance of heavy metal stress.

2. Materials and methods

2.1 Screening for zinc tolerance in EMS mutagenized seeds

2.1.1 Plant materials and growing conditions

EMS mutagenized M2 seeds of *Arabidopsis thaliana* Columbia ecotype (Col-0) provided by Lehle seeds (M2E-02-05 Lehle seeds) were used. Seeds were surface sterilized by incubating them in chlorine gas within a desiccator jar under a fume hood for duration of 45 minutes (chloride gas was generated by mixing 10 ml sodium hypochlorite (12%) and 5 ml 35% HCl). Then seeds were inoculated onto rectangular agar (1% Type A, Sigma) plates that contain, 1% Sucrose and 1/10-strength Hoagland medium (appendix list-1) without microelements, buffered with MES buffer (0.01%) at a final pH of 5.7 and with 50 μ M ZnSO₄ added. After stratification for 2 days at 4°C, the agar plates were moved to light room under long day condition (16-h light/8-h dark) and vertically placed and incubated for one week.

After the one week growing period those seedlings with roots shorter than half of the average root length (Fig. 2.1a) were picked up and transferred onto control plates (i.e. without Zn treatment) and laid in such a way that the starting root length could be differentiated (Fig. 2.1b). After additional 10 days, those seedlings that showed root growth recovery (that showed root growth comparable to the control seedlings on the plate) were identified as putative mutants and transferred to soil filled pots and left to produce seeds. These putative mutants were named with a combination of numbers and the abbreviation IZS that stands for **I**ncreased **Z**inc **S**ensitivity (e.g. IZS 479).

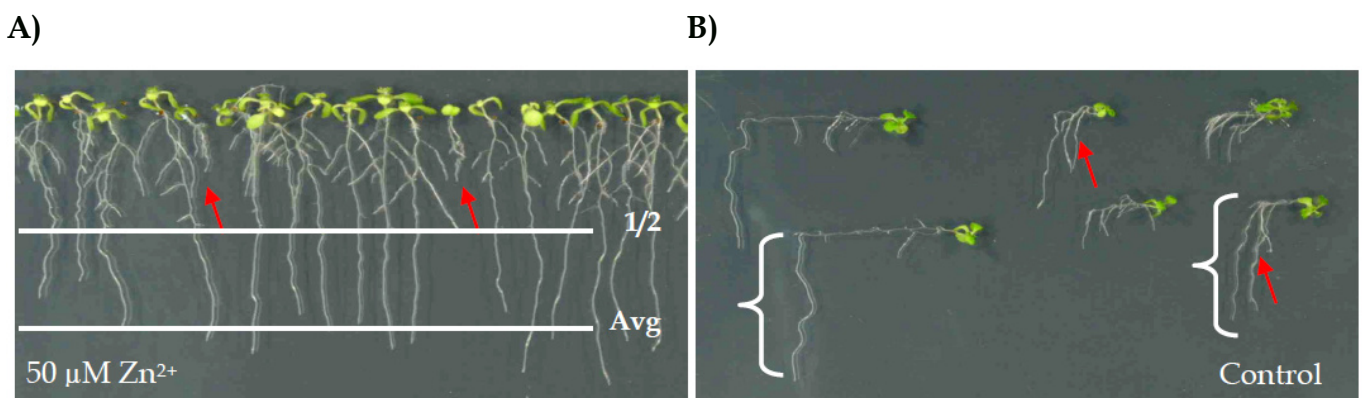


Figure 2.1. Genetic screen for increased zinc sensitivity. A) Stands for the first step of the genetic screen where seedlings with root length shorter than half the length of the average root length on the plate are indicated with red arrow. B) Represents the second step of the screen where seedlings picked from plate together with seedlings with normal root length are placed on control plate horizontally. Then those seedlings that showed root growth in the horizontal plane at the same extent to that of the control seedlings (indicated by red arrow) are picked as putative IZS mutants. This picture is adapted from Weber et al., 2013.

Then as a confirmation step seeds of putative IZS mutants are grown again on vertical agar plates that contain 50 μ M ZnSO₄ (similar to the one used in the first step of the screen) and those lines that showed root growth reduction consistently including in this step are designated as IZS mutants.

2.1.2 Characterization of 5 newly identified IZS mutants

Second generation seeds of five newly identified mutants namely IZS 377, IZS 389, IZS 390 IZS 394 and IZS 479 were assayed for cadmium, copper, manganese, zinc and sodium chloride tolerance and compared to the response of the wild type Col-0 towards these stress causative agents. Seeds were surface sterilized through incubation in chlorine gas in a similar way as mentioned in section 2.1.1. Then seeds were inoculated onto rectangular agar (1% Type A, Sigma) plates that contain 1% Sucrose and 1/10-strength Hoagland medium (appendix list-1) without microelements and buffered with MES buffer (0.01%) having a final pH of 5.7. For plates with heavy metal stress Cd and Cu were added to the medium as chloride salts whereas, Zn and Mn were added as sulfate salt. The different ion concentrations applied to the agar plates are given in table 2.1. After stratification for 2 days at 4°C, the agar plates were moved to light room under long day condition (16-h light/8-h dark) and incubated vertically for up to three weeks.

2.1.3 Growth parameters and statistical analysis

Each conducted experiment consisted of three biological replicates. Root length was measured manually using a standard ruler. For each individual treatment a total of 30 seedlings were measured. For all the data collected one way analyses of variance was performed using R statistical package version 2.14.2 and means were separated using a Tukey tests at 0.05 significance level.

Table 2.1. Final concentrations of metal ions applied at different tolerance testes

<i>Heavy metal ions</i>	<i>Different applied concentrations</i>
CdCl ₂	0.5 μ M, 1.5 μ M, 3 μ M, 5 μ M
ZnSO ₄	20 μ M, 40 μ M, 60 μ M, 80 μ M
CuCl ₂	2 μ M, 4 μ M, 6 μ M, 8 μ M,
MnSO ₄	400 μ M, 550 μ M
NaCl	15mM, 30mM

2.2 Mapping and characterization of IZS 288

2.2.1 *Plant materials and growing conditions*

Two independent backcross lines of IZS 288 (namely E1-1 and E2-5) and wild type Col-0 seeds were surface sterilized and cultivated using procedures stated under section 2.1.1. For elemental profiling analysis and metal accumulation plants were grown hydroponically as described by Weber et al., (2004) in growth chambers (Percival Scientific) with light and temperature regime of 16 h light ($110 \mu\text{E m}^{-2}\text{s}^{-1}$) at 23°C (day) and 8 h dark at 18°C (night).

2.2.2 *Heavy metal stress assay*

The concentrations used in the heavy metal stress assays were $2\mu\text{M Cd}^{2+}$, $10\mu\text{M Cu}^{2+}$, $6\mu\text{M Ni}^{2+}$, $5\mu\text{M Co}^{2+}$, $450\mu\text{M Mn}^{2+}$, $300\mu\text{M Fe}^{2+}$. In addition to those stated here, concentration series were tested for Zn and Mn. The different concentrations used in these experiments are mentioned under the result section.

2.2.3 *Physiological parameters and statistical analysis*

Root length, cotyledon size and petiole length were measured manually using a standard ruler. Daily root growth rate was determined by demarcating the daily root length increment of seedlings. Hypocotyl length of dark grown seedlings was determined using image processing software called ImageJ version 1.43u (<http://rsb.info.nih.gov/ij>). Unless stated otherwise each conducted experiment consisted of three biological replicates. For each individual treatment of the heavy metal stress assays a total of 30 seedlings were measured. For the determination of average cotyledon size 50 individual plants from each group were measured. On all the data collected one way analyses of variance was performed using R statistical package 2.14.2 version and means were separated using a Tukey tests at 0.05 significance level.

2.2.4 *Elemental profile determination*

For elemental profile analysis, *Arabidopsis* plants grown hydroponically on 1/10-strength Hoagland medium (appendix list-1) as well as soil grown plants were used. Leaves were harvested and up until they were lyophilized they were stored under -20°C. Roots after being rinsed with Millipore water and blotted dry, were desorbed for 10 min each in ice-cold solutions of 0.1M CaCl_2 and 10mM EDTA , and finally washed again with Millipore water and

blotted dry using layers of paper towels. The lyophilized plant materials (both roots and shoots) and seeds were digested in a microwave (START 1500 of the company MLS) using 4 mL HNO₃ (65% V/V) and 2 mL (30% V/V) hydrogen peroxide. Then elemental profile was determined using ICP-OES on an iCAP 6000 Series spectrometer (from Thermo-Fisher).

2.2.5 Genetic mapping

IZS 288 was mapped using three types of PCR based molecular markers, one that detect simple sequence-length polymorphisms commonly known as SSLPs (simple sequence length polymorphism) markers (Bell and Ecker, 1994), a second type that detects restriction fragment-length polymorphisms called CAPS (cleaved amplified polymorphic sequences) markers (Konieczny and Ausubel, 1993) and a third type that detect single nucleotide polymorphisms in short known as SNPs, which exploit the natural differences between Colombia (Col-0) and Landsberg erecta (Ler-0) ecotypes (Tab. 2.2). Mapping populations were constructed by outcrossing IZS 288 (Col-0 background) with the ecotype Landsberg erecta (Ler-0) and the F1 progeny were allowed to self-pollinate then the rustling F2 progeny were screened for Zn tolerance and those seedlings that showed Zn hypersensitivity phenotype similar to that of IZS 288 were selected to construct the mapping population. Genomic DNA from each individual plant of the mapping population was isolated as described in the 2.2.6 section and used as a template for the PCR- based mapping. Recombination events were scored for each molecular marker employed and the genomic window with the lowest recombination frequency was identified on the lower arm of Chromosome two. To narrow the map position of IZS 288 novel markers (CAPS markers and Tetra-primer ARMS-PCR (Ye et. al., 2001) and triple primers that lack the PCR product for Colombia) that detect single nucleotide variations between Col-0 and Ler-0 were utilized (Tab. 2.3). Finally, 14 candidate genes within the genetic window were sequenced and the sequences were compared to the published *Arabidopsis* genomic sequences (<http://www.arabidopsis.org/>), which lead to the identification of a point mutation in a single gene.

2.2.6 DNA isolation

Genomic DNA isolation from the mapping population was carried out following a fast and economical procedure referred as the quick prep method. Two or three leaves were harvested

and put in liquid nitrogen and stored away at -80°C. When the genomic DNA is required, a sample was finely grinded and 500µl extraction buffer (200 mM Tris-HCl (pH 7.5), 250 mM NaCl, 25 mM EDTA and 0.5 % (w/v) SDS) was added to it. Then, after mixing it very well, it was centrifuged for 5 minutes at a maximum speed (Eppendorf 5424) and 300µl of the supernatant was transferred into new tube. Then to the supernatant 300µl isopropanol was added and gently mixed followed by centrifugation for 10 minutes at maximum speed. Then after the supernatant was removed the pellet was washed by 500µl of 70% ethanol (without re-suspending it again) and centrifuged for 5 minutes. Following that the pellet was air dried for 30 minutes in a fume hood. Finally, it was re-suspended in 30µl Millipore water and incubated for 5 minutes at 50°C and then cooled down on ice for 1 minute and centrifuged for another minute at maximum speed. Genomic DNA that was stored at 4°C did maintain its quality for up to 8 to 10 weeks.

Table 2.2. Commercially available PCR-based markers used in the chromosome mapping of IZS 288. Positions of markers on chromosomes are given in mega base pairs (Mbp).

<i>Primer Name</i>	<i>Type</i>	<i>Position</i>		<i>Band Size</i>		<i>Restriction enzyme</i>
		<i>Chromosome</i>	<i>Locus</i>	<i>Col</i>	<i>Ler</i>	
NF21M12	SSLP	1	3.2	200	150	
NF21J9	SSLP	1	8.65	189	<189	
CIW 12	SSLP	1	9.6	128	115	
So 392	SSLP	1	10.86	142	156	
CIW1	SSLP	1	18.37	159	135	
NF19K23	SSLP	1	22.8	200	180	
CIW3	SSLP	2	6.40	230	200	
Thy1	CAPs	2	7.08	2 bands	3 bands	RSAI
PLS2	SSLP	2	8.36	155	>155	
PLS 3	SSLP	2	8.99	175	>175	
PLS 6	SSLP	2	9.27	189	<189	
NGA 361	SSLP	2	13.7	114	120	
NGA 168	SSLP	2	16.2	151	135	
NGA 172	SSLP	3	0.79	162	136	
NGA 162	SSLP	3	4.6	107	89	
CIW 11	SSLP	3	9.7	179	230	
GAPAB	SSLP	3	9.8	142	150	
F14G16	SSLP	4	4.19	220	221	
CIW 7	SSLP	4	11.52	130	123	
NGA 1107	SSLP	4	18,10	150	140	
CA 72	SSLP	5	4.2	124	110	
NGA 76	SSLP	5	10.4	220	260	
So 191	SSLP	5	15.2	148	156	

Clean and super quality genomic DNA for sequencing and other purpose was isolated using potassium acetate and phenol method. In this procedure on grinded leaf samples 1ml extraction buffer (100 mM Tris-HCl (pH 8), 50 mM EDTA (pH 8), 500 mM NaCl, 1.5 % SDS, 0.5 % β -Mercaptoethanol) was added and incubated for 10 minutes at 65°C and then 300 μ l „5 M“ K-Acetate (60 ml 5M K-Acetate, 11.5 ml acetic acid (pH 5.2) and 28.5 ml Millipore water) was added and incubated for about an hour on ice. After centrifugation for 10 minutes at maximum speed the supernatant was taken and 800 μ l PCI was added to it. After mixing it very well it was centrifuged for 5 minutes at maximum speed. Following that the pellet was washed by 500 μ l of 70% ethanol and air dried. Finally, it was re-suspended by 25 μ l Millipore water.

Table 2.3. Newly designed tetra-arm PCR- markers, triple primers (that lack Col product from the tetra arm primer PCR marker) and derived caps markers. Positions of markers on chromosomes are given in mega base pairs (Mbp). Size of PCR products are given in base pairs.

Primer Name	Type	Position (Mbp)	Band Size			Restriction enzyme	
			Col (bp)	Ler (bp)	Internal control		
PERL0337738(Per1738)	Tetra primer	7.34	238	394	590		
PERL0341953 (Per1953)	Tetra primer	7.82	400	295	674		
SGCSNP8909(SNP909)	Tetra primer	7.91	221	297	477		
PERL0343403(Per103)	Tetra primer	7.99	455	351	767		
PERL0347907(Per1907)	Tetra primer	8.59	459	276	690		
PERL0349100(Per1100)	Tetra primer	8.70	334	197	484		
PERL0349143(Per1143)	Triple primer	8.718		357	525		
SGCSNP8965(SNP965)	Triple primer	8.75		302	518		
PERL0349339(Per1339)	Triple primer	8.77		202	425		
BKN000004331(BNK331)	Triple primer	8.79		191	451		
PERL0349577(Per19577)	Triple primer	8.820		204	360		
PERL0349785(Per1785)	Tetra primer	8.841	310	203	527		
PERL0349811(Per19811)	Triple primer	8.846		242	383		
PERL0350617(Per1617)	Tetra primer	8.98	430	216	603		
SGCSNP8985(SNP985)	Tetra primer	9	193	258	407		
PERL0351797(per11797)	Tetra primer	9.17	281	145	381		
MASC02909(Mas909)	dCAPs	8.768	111	61	172	28	TaiI(MaeII)
PERL0349457(per1457)	dCAPs	8.796	406	122	528	319	RsaI
PERL0349222(per1222)	dCAPs	8.742	135	328	518	77	RsaI

2.2.7 Polymerase chain reaction, gel electrophoresis and sequencing

Polymerase chain reaction (PCR) for mapping purpose was set in two reaction volumes. SLLP and tetra-primer markers had 11 μ l reaction volumes and CAPS markers had 51 μ l reaction volumes. The compositions of the PCR reactions are stated in table 2.4. The reactions were carried out in MJ mini 48-well personal thermal cycler and Icyler version 3.021 (from

BIO-RAD). PCR products were separated using 3% Nusieve-Agar (from BIOZYM SCIENTIFIC). Sequence of novel markers and their annealing temperatures are included in appendix list 2. Sequencing of candidate genes were carried out by amplifying fragments of the gene (~700 base pairs long) with overlaps in both 3' and 5' ends. The sequencing reactions were performed in a commercial sequencing lab (AGOWA).

Table 2.4. Composition of PCR reactions carried out using Tetra primers and CAPs markers

<i>Tetra Arms-PCR (11µl rxn mix)</i>		<i>CAPs marker PCR (51µl rxn mix)</i>	
10x Taq-buffer with MgCl ₂	1.1µl	10x Taq-buffer with MgCl ₂	5.2µl
dNTPS (20mM)	0.11 µl	dNTPS (20mM)	1 µl
Primer MIX (20µM inner primers & 2µM outer primers)	2.1 µl	Primer Fw	1 µl
Taq polymerase	0.21 µl	Primer Rev	1 µl
Millipore water	6.48 µl	Taq polymerase	1µl
Template DNA	1µl	Millipore water	40.8 µl
		Template DNA	1µl

2.2.8 Plasmids, constructs and genetic complementation

PCR amplification of genes for sequencing and cloning purpose were carried out using the Phusion polymerase (from INVITROGEN) that has lesser degree of errors as a result of its proof reading ability. The reaction mix had a volume of 50µl and its composition is given in table 2.5.

In order to check for functional complementation, genomic construct consisting of the promoter region (2000 base pairs up stream of the start codon) the 5' UTR region (500base pairs down stream the stop codon) as well as exons and introns of the coding region was introduced into IZS 288 using the TOPO® cloning Kit (from INVITROGEN). Similarly, a second construct carrying only the coding sequence under the promoter of cauliflower mosaic virus (35S) was also introduced into IZS 288. In the constructs used for testing the hypothesis of loss of phosphorylation site single alanine and serine substitutions of the 377th threonine were introduced individually into the gene by oligonucleotide-directed mutagenesis (Kunkel, 1985), and the introduced mutations were confirmed by DNA sequencing. For the *Xenopus* WDR70 construct coding sequence of the gene was introduced into plasmid carrying a 35S promoter. Plasmids used in these procedures are given in table 2.6.

Table 2.5. Composition of Cloning PCR reactions using Phusion polymerase.

<i>Cloning PCR (50µl rxn mix)</i>	
5x HF buffer(10 µl
dNTPS (20mM)	1 µl
Primer Fw	1 µl
Primer Rev	1 µl
Phusion polymerase	0.5 µl
Millipore water	35.5 µl
Template DNA	1µl

2.2.9 Genetic transformation

Plasmids carrying different constructs were first introduced into chemically induced *E. coli* (DHB 10 strain) competent cells. The procedure used for transforming competent *E. coli* cells was as follows. 2µl of the ligation reaction mix (composed of the designed construct and the destination vector) was added to properly thaw competent cells and after gradually mixing it was left on ice for 30 minutes. Then cells were exposed to heat shock by incubating them at 42°C for 1 minute followed by rapid cooling by placing them on ice. Then 1ml sterile LB medium (Appendix list 3) was added to them and further incubated in a shaker with adjusted temperature of 37°C and 180 revolutions per minute. Following that the cells were centrifuged (Eppendorf 5424) at 5000 revolutions per minute for 5 minutes. Finally, for re-suspension 60µl of sterile LB medium was added to the pellet and plated on LB agar plates that carry specific antibiotic as a selection marker (depending on the type of plasmid used) and placed in 37°C incubator for overnight. The next day a number of single colonies were picked (using sterile pipette tips) and transferred into fresh LB agar plates with the selection marker (by scratching the surface of the agar plate) and at the same time the tips were used to inoculate 2ml liquid LB medium with the specific selection marker and incubated overnight in 37°C shaker. Then plasmid DNA was isolated from the overnight liquid culture using the Wizard® Plus Mini-prep DNA Purification kit (from PROMEGA) and used to identify positive clones by performing colony PCR and/or restriction enzyme digestion.

Later on a plasmid carrying the right construct was transformed into chemically induced *Agrobacterium tumefaciens* (DV3101) competent cells. The method used for transforming the competent *Agrobacterium tumefaciens* was as follows. 1 µg of a plasmid DNA carrying the right construct was introduced into properly thaw competent cells. In parallel as a negative

control 4µl of sterile water was also introduced into another tube of competent *Agrobacterium tumefaciens* cells. Following appropriate mixing, cells were let to instantly freeze by drooping them in liquid nitrogen. Then heat shock was introduced by incubating the cells on a heat bock with adjusted temperature of 37°C for duration of 5 minutes. Then 1ml YEP (Appendix list-3) media was added to it and incubated for 3 hours and 30 minutes on a shaker with adjusted temperature of 28°C. Finally, the culture was centrifuged at 5000 revolutions per minute for 10 minutes and the pellet was re-suspended by 100µl YEP medium and plated on LB agar plates treated with the appropriate selection marker and placed in 28°C incubator for two days.

Finally, the *Agrobacterium tumefaciens* colony carrying the specific plasmid was introduced into IZS 288 plants by the floral dip method (Clough and Bent, 1998). First generations of floral dip treated plants were screened for transformants using specific screening marker based on the specification of the plasmid utilized (i.e. the herbicide BASTA or hygromycin). Later on the second generation of the positive transformants were used in different experimental set ups.

Table 2.6. List of plasmids together with their specifications, selection markers and sources.

<i>Plasmid Name</i>	<i>Characteristics</i>	<i>Selection markers</i>	<i>Source</i>
pCR8/GW/TOPO®	entry vector	Spectinomycin	Invitrogen
pMDC123	Complementation vector, Phosphorylation site test	Kanamycin, Basta	Curtis and Grossniklaus (2003)
pMDC83	2X35S, GFP N-terminal tag	Kanamycin, Hygromycin	Curtis and Grossniklaus (2003)
pMDC43	2X35S, GFP C-terminal tag	Kanamycin, Hygromycin	Curtis and Grossniklaus (2003)

2.2.10 Reporter line establishment

The auxin response reporter DR5::GUS (Ulmasov et al., 1997) and the cell cycle reporter cycB1::GUS (Colon-Carmona et al., 1999) were crossed into IZS 288 background and the F2 generations were used for the respective analysis.

2.2.11 Histochemical GUS staining and Microscopy

3-5 days after germination seedlings of DR5::GUS and cycB1::GUS lines in both IZS 288 and Col-0 backgrounds were histochemical stained and examined under light microscope (Leica Microscope DM1000) pictures were taken with Leica DFC 420 digital microscope camera. The staining procedure included incubation of seedlings for three hours at 37°C in staining solution composed of 20mM X-glucuronidase, 100mM NaHPO₄ (pH 7), 0.05% Triton X-100 and 5mM each of K₄[Fe(CN)₆].3H₂O and K₃[Fe(CN)₆] . Followed by destaining step where samples were overnight incubated in 70% ethanol. Root tips were also investigated using propidium iodide (PI) staining and confocal microscope (Leica SP5 laser scanning microscope) at excitation wavelength 488 nm. The PI staining procedure utilized a propidium iodide working solution of 1µg/ml in PBS buffer. Whole plant seedlings were incubated in the PI staining solution for 10 minutes followed by two rounds of washing with Millipore water. Finally, root tips were mounted under coverslip. Protein localization study using the GFP tagged 35S:Atg20330 line was also performed using Leica SP5 laser scanning microscope.

2.2.12 Transcript analysis

For transcript level identification by microarray analysis and real-time (RT-PCR), RNA was extracted from IZS 288 and WT roots with Trizol (Invitrogen Life Technologies). For the microarray analysis the hybridization to Affymetrix ATH1 chips was performed at the Affymetrix service provider and core facility KFB center of excellence for fluorescent bioanalytics (Regensburg, Germany). Following the requirement of the service center 250 ng of purified (using RNeasy Mini columns (Qiagen)) RNA from both genotypes (IZS 288 and WT) and stress condition (chilling stressed and unstressed samples) were sent. The center uses Agilent 2100 bioanalyzer (Agilent Technologies) for analyzing the fragment length of the cRNA and hybridization is achieved by 16h incubation at 45°C in a rotating chamber. For washing and staining the hybridized ATH1 chips an Affymetrix Fluidics Station FS450 was used, and the fluorescent signals were measured using an Affymetrix Gene Chip Scanner 3000. CEL files from the Affymetrix microarray hybridization were processed using the R program and Bioconductor packages (Gentleman et al., 2004). The robust multichip average normalization was performed using the default settings of the corresponding R function (Irizarry et al., 2003). To estimate the amount of expressed mRNAs, the present call information of the nonparametric Wilcoxon signed rank test (PMA values) was computed

with the “affy” package (Gautier et al., 2004). Hybridization data from three biological replicates were generated for both genotypes and stress conditions. Analysis of differentially expressed genes was performed with the LIMMA package using the robust multichip average normalized expression values (Smyth, 2004). P values were corrected for multiple testing and adjusted to a 5% false discovery rate (Benjamini and Hochberg, 1995). The confidence threshold for up or down regulated genes was set to an adjusted P value of <0.05.

For the RT-PCR, the synthesis of cDNA was carried out using an Invitrogen SuperScript II kit and reaction mix composition is given in table 2.7. SYBR Green (Eurogentec) was used to monitor cDNA amplification. RT-PCR was set up in 96-well plates in a Bio-Rad iCycler with a MyiQ real-time PCR detection system. For data analysis the system uses iQ5 optical system software version 2.0. Relative expression values were calculated by using the difference in cycle threshold (CT) value of the target gene and a reference gene, namely EF1a. Primers for the RT-PCR were designed using the Primer3 software (<http://primer3.sourceforge.net/>). List of RT-PCR primers and their sequences are given in appendix list-2.

Table 2.7. Composition of RT-PCR reactions.

<i>RT- PCR rxn mix</i>	
SYBR Green mix	10 μ l
Primer mix (Fw & Rev 1 μ M)	5 μ l
cDNA (1:50 dilution)	5 μ l

2.2.13 *Drosophila* stocks

Three independent RNAi lines each containing an inducible UAS-RNAi construct against the IZS 288 homolog gene in *Drosophila* (CG5543) were obtained from the Vienna *Drosophila* RNAi center (<http://stockcenter.vdrc.at>). Lines VDCR_27454 and VDCR_106320 were viable transgenic lines; hence the acquired flies were homozygous RNAi lines. However, since the insertion in VDCR_41441 was lethal, this line was kept over a balancer (i.e. TM3, Sb). For the expression of UAS-transgenes, females from all three lines were crossed with males of 5 different GAL4 driver lines (i.e. *ey-GAL4*, *gmr-GAL4*, *sev-GAL4*, *da-GAL4* and *MS 1096-GAL4*) obtained from Dr. Stefan Heidmann Lab. The crosses were setup in two replicates and the results from the first cross were confirmed by setting up a second separate cross. Depending

on the type of GAL4 driver in use phenotypes of the RNAi effects were observed at different developmental stages and organs.

2.3 Screening of flavonoid deficient mutants for heavy metal sensitivity

2.3.1 Plant materials and growing conditions

For the metal tolerance as well as deficiency test assays, seeds of *Arabidopsis thaliana* Landsberg erecta ecotype (Ler-0) and five *transparent testa* mutant lines (Tab. 2.8) were used. Seed sterilization and plant growth on agar plates were performed according to the methods described in section 2.1.1. In the case of the iron deficiency test, 1/10 of Hoagland medium was prepared without including the iron source. For plates with heavy metal stress Cd and Cu were added to the medium as chloride salts whereas Zn was added as sulfate salt. The different ion concentrations applied to the agar plates and or hydroponic medium are given in table 2.8. For the analysis of elemental profiles and metal accumulation, plants were grown hydroponically as described by Weber et al., (2004) in growth chambers (Percival Scientific) with light and temperature regime of 16 h light ($110 \mu\text{E m}^{-2}\text{s}^{-1}$) at 23°C (day) and 8 h dark at 18°C (night) and 8 h dark.

Table 2.8. List of seed stock used in the experiments

<i>Lines</i>	<i>Seed source</i>
<i>Ler-0</i>	Nottingham Arabidopsis Stock Centre(NASC, Nottingham, UK)
<i>tt3(N84)</i>	Nottingham Arabidopsis Stock Centre(NASC, Nottingham, UK)
<i>tt4</i>	Kindly provided by Prof. Bernd Weisshaar (Bielefeld)
<i>tt5</i>	Kindly provided by Prof. Bernd Weisshaar (Bielefeld)
<i>tt6 (N87)</i>	Nottingham Arabidopsis Stock Centre(NASC, Nottingham, UK)
<i>tt7 (N88)</i>	Nottingham Arabidopsis Stock Centre(NASC, Nottingham, UK)

* All five *tt* mutants are in Landsberg erecta ecotype background (Ler-0)

2.3.2 Elemental profile determination

For elemental analysis, *A. thaliana* plants grown hydroponically on 1/10-strength Hoagland medium were treated with different Cu concentration (Tab. 2.9) for one week. The hydroponic experiment was carried out only under Cu stress, since *tt7* uniquely showed Cu

phenotype and the hydroponic experiment was designed as a follow up experiment on this observation. After 7 days roots and leaves of treated and control plants were harvested. Both shoot and root samples were prepared for ICP-OES analysis following the procedure stated in section 2.2.4.

Table 2.9. Final concentration of heavy metal ions applied at different experiments

<i>Heavy metal ions</i>	<i>Different applied concentrations</i>
CdCl₂	0.5 μ M, 1.5 μ M, 3 μ M, 5 μ M
ZnSO₄	- 40 μ M, 70 μ M, 100 μ M
CuCl₂	- 2 μ M (hydroponic), 4 μ M, 6 μ M, 8 μ M, 12 μ M (agar plate)

2.3.3 Growth parameters and statistical analysis

Growth parameters and statistical analysis used in these experiments were similar to those described in section 2.2.3.

3. Results

3.1 The quest for new genes involved in zinc homeostasis

3.1.1 *New mutants identified in the genetic screen*

The Zn tolerance genetic screen implemented in this project is part of a continuous effort laid out in the lab of Prof. Dr. Stephan Clemens to identify new genes involved in the Zn homeostasis process. The first round of genetic screen conducted gave rise to 6 IZS mutants namely IZS 101, IZS 129, IZS 130, IZS 133, IZS 171 and IZS 288, which belong to different complementation groups. These six mutants are also newly named as OZS 1-6. OZS stands for overly Zn sensitive (Weber et al, 2013). In order to increase the number of the Zn hypertensive mutant library a second round genetic screen was conducted. The seed collection, used for this project, represent 32,448 M1 plants and so far in the two round genetic screens 22,000 M2 seeds have been screened that covers around 3000 M1 seeds. Therefore, the genetic screen is far from getting saturated.

The genetic screen for increased Zn sensitivity is composed of two major steps. The first step filters out seedlings with compromised root growth on agar plates treated with Zn. However, at this stage the selected seedlings are not exclusively Zn hypersensitive, rather the group contains all seedlings with short roots but the reason for their compromised root growth can be late germination, general root growth defect or miniature sized stature. Therefore, the second step is introduced to sift through this group and retain only those with Zn hypersensitivity. This is attained by comparing the extent of root growth recovery of seedlings picked at the first step of the screen on control agar plates (i.e. without the Zn treatment). Then, those seedlings with the highest root growth recovery are picked as putative IZS mutants. The rationale behind this step is that seedlings, which had shorter root length for reasons other than Zn hypersensitivity, will not be able to recover on the second step because the only change introduced at this stage is the absence of Zn from the plates. Therefore, the seedlings that exhibited root growth recovery at the second step are only those seedlings that were not able to grow fully on the first plate due to the presence of Zn and their increased sensitivity towards it.

In this second round genetic screen 8,800 EMS mutagenized Col-0 seeds were screened for increased Zn sensitivity phenotype and 255 putative IZS mutants were identified. Among

Results

these 255 putative IZS mutants, the confirmation step has selected 28 IZS mutants (Fig.3.1, Tab.3.1). Within these 28 IZS mutants 14 exhibited pleiotropic effects (particularly shorter root length under optimal growing conditions) (Fig.3.2).

Table 3.1. List of newly identified IZS mutants

	<i>Normal rooted</i>	<i>Short rooted</i>
1	IZS 377	IZS 366
2	IZS 381	IZS 371
3	IZS 389	IZS 386
4	IZS 394	IZS 388
5	IZS 404	IZS 390
6	IZS 416	IZS 391
7	IZS 436	IZS 395
8	IZS 460	IZS 455
9	IZS 479	IZS 461
10	IZS 505	IZS 462
11	IZS 507	IZS 464
12	IZS 511	IZS 474
13	IZS 512	IZS 508
14	IZS 607	IZS 615

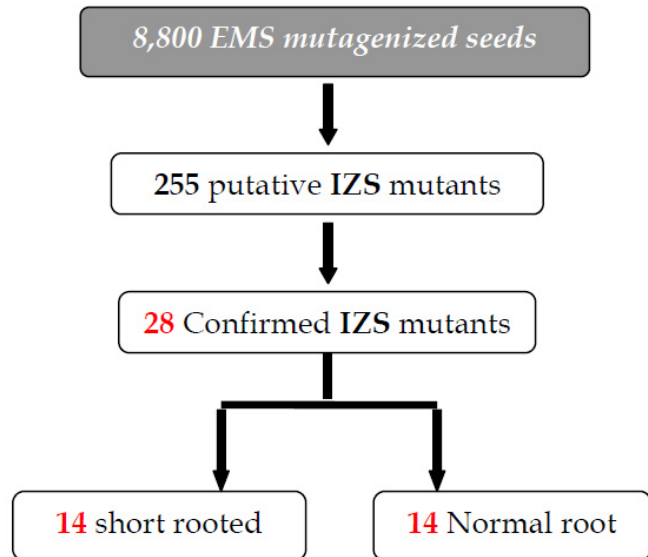
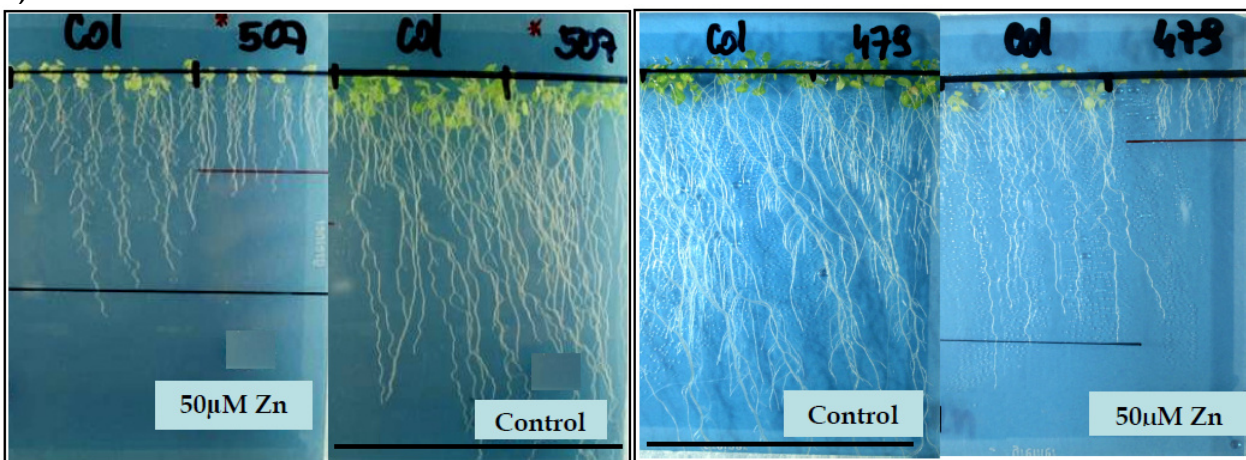


Figure 3.1. Figurative illustration of the results of the second round screen of the M2 seeds of EMS mutagenized *Arabidopsis thaliana* seeds.

A)



B)

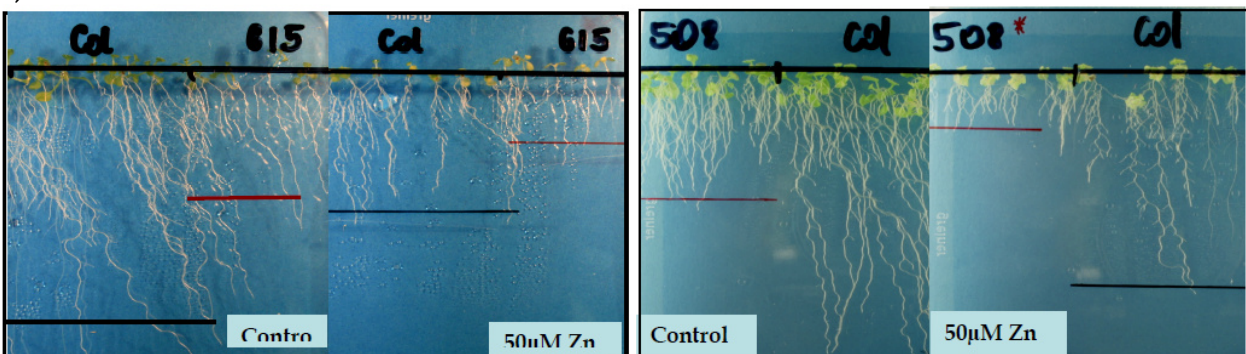


Figure 3.2. Representative pictures of newly identified mutants. A) IZS 479 and IZS 507 represent those with normal root length whereas B) IZS 615 and IZS 508 represent those with reduced root growth even under optimal growing conditions.

3.1.2 Phenotypic Characterization of Five IZS Mutants

Deciphering the function of genes involved in different biological processes such as the Zn homeostasis mechanism is quite complex because a single gene may have different functions depending on circumstances such as the presence or absence of other gene products (Gillis and Pavlidis, 2011). Especially during characterization of phenotypes caused by mutations there is a condition referred to as pleiotropy that explains the ability of a gene to influence multiple phenotypic traits like in the case of mutants of AUX/IAA gene that exhibit different pleiotropic phenotypes related to auxin response (Rogg et al., 2001). Multifunctionality of a gene is also reported in iron homeostasis mechanism, where the iron uptake transporter IRT1 under iron deficient condition is reported to transport other metal ions like Zn and Cd (Barberon et al., 2011). Hence, phenotypic characterization were conducted on the newly identified IZS mutants whereby the specificity of the increased Zn sensitivity phenotype is tested in comparison to other metal ions and salt as a representative for other abiotic stresses.

The phenotypic characterization of five of the newly identified IZSs revealed that each mutant line has a unique combination of response to various metal ions. Some are sensitive to a wide range of metal ions while others are explicitly sensitive to a particular metal ion (Tab.3.2). Furthermore, the sensitivity response of the IZS mutants to the stress caused by the various metal ions tested was not uniform. Some of them were hypersensitive to lower concentrations of metal ions but these effects got diminished with the increasing concentration, whereas others did not exhibit hypersensitivity response up until exposure to higher concentrations.

Table 3.2. Summary of phenotypes of the five newly identified IZS mutants

	Zn^{2+}	Cd^{2+}	Cu^{2+}	Mn^{2+}	$NaCl$
<i>IZS 377</i>	+	+	+/-	-	-
<i>IZS 389</i>	+	+	+	-	-
* <i>IZS 390</i>	+	+	+	-	-
<i>IZS 394</i>	+	+	+	+	+
<i>IZS 479</i>	+	+/-	-	-	-

* Reduced root growth under control condition

+ Sensitive - Not sensitive

Results

IZS 377 (Fig 3.3) in particular was hypersensitive to cadmium (Cd) and Zn in a dose dependent manner. It also showed a hypersensitivity response to higher concentrations of copper chloride (namely at 6 μ M and 8 μ M concentrations). However, no apparent difference to the wild-type was observed in its response to different concentration of manganese sulfate and sodium chloride.

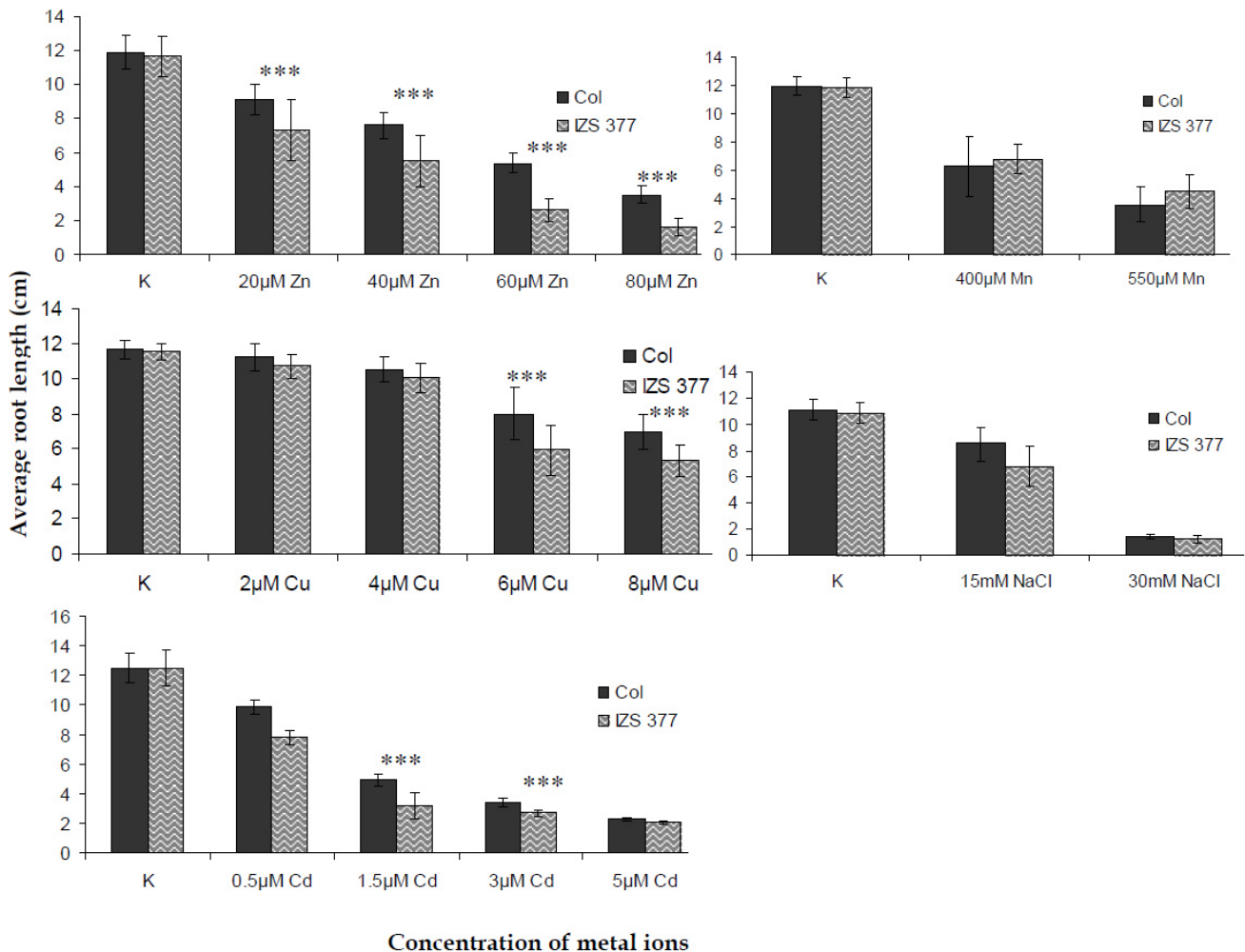


Figure 3.3. IZS 377 showed significantly stronger sensitivity towards Zn, Cd and higher concentration of Cu than wild type Col-0. (‘***’ for 0.001, ‘**’ for 0.01 and ‘*’ for 0.05 significance level)

Similarly, IZS 389, showed hypersensitivity to Cd and Zn (Fig. 3.4). The peculiar character of IZS 389 that differentiates it from IZS 377 is its hypersensitivity response to copper even at lower concentrations (i.e. 2 μ M and 4 μ M) which might be an indication for stronger impact of the mutation on copper related physiological process.

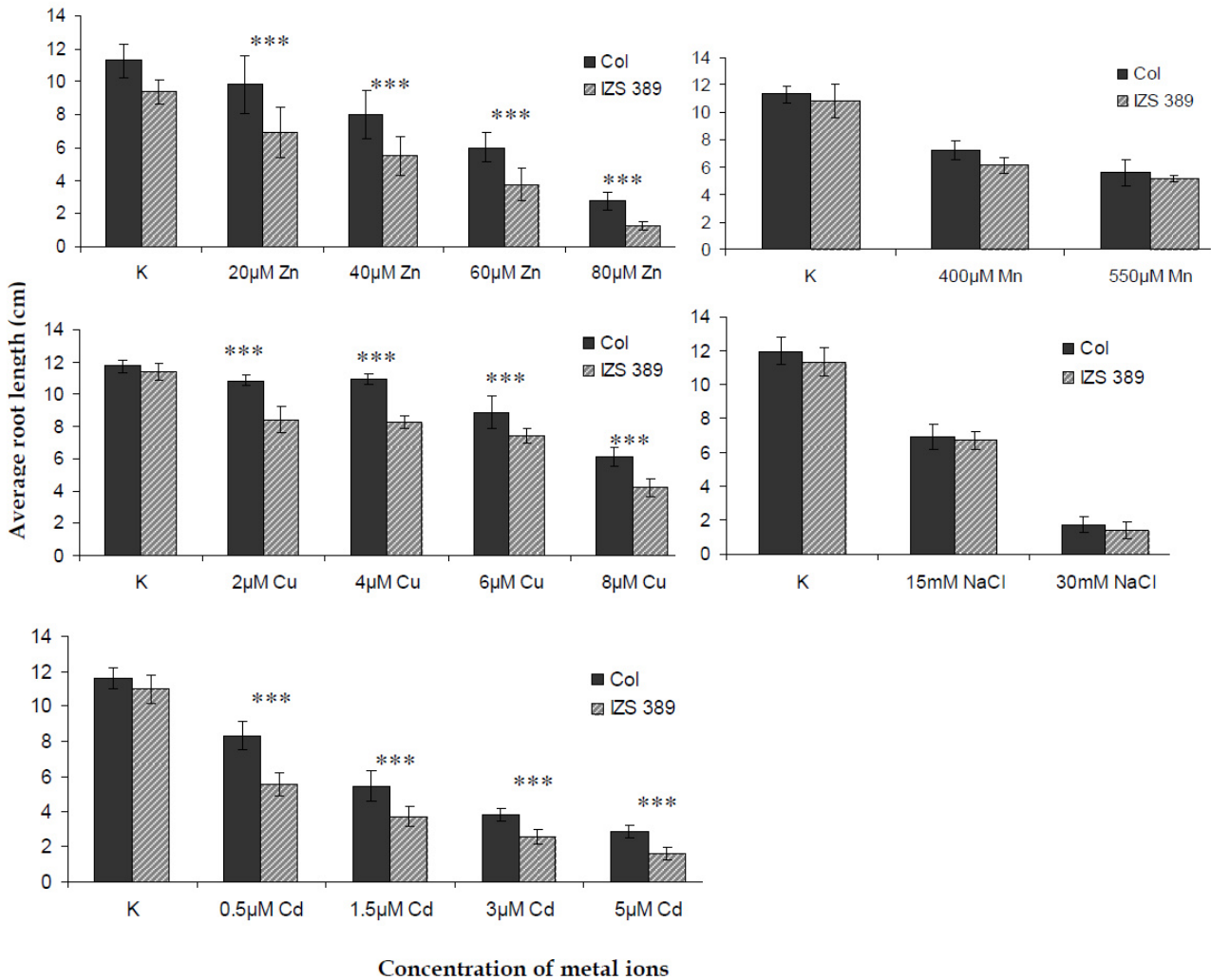


Figure 3.4. IZS 389 showed significantly stronger hypersensitivity towards Zn, Cd and Cu than wild type Col-0 (*** for 0.001, ** for 0.01 and * for 0.05 significance level).

Likewise, IZS 394 showed dose dependent hypersensitivity to Cd, Cu and Zn (Fig. 3.5). However, uniquely IZS 394 showed hypersensitivity to Mn at both concentrations tested (i.e. 400µM and 550µM) and to sodium chloride at lower concentration (15mM). In addition to that IZS 394, in comparison to the other four IZS, exhibited the largest percentage of root growth reduction (namely 81%, 94% and 84%) under 8µM CuCl₂, 5µM CdCl₂ and 550µM MnSO₄, respectively.

Results

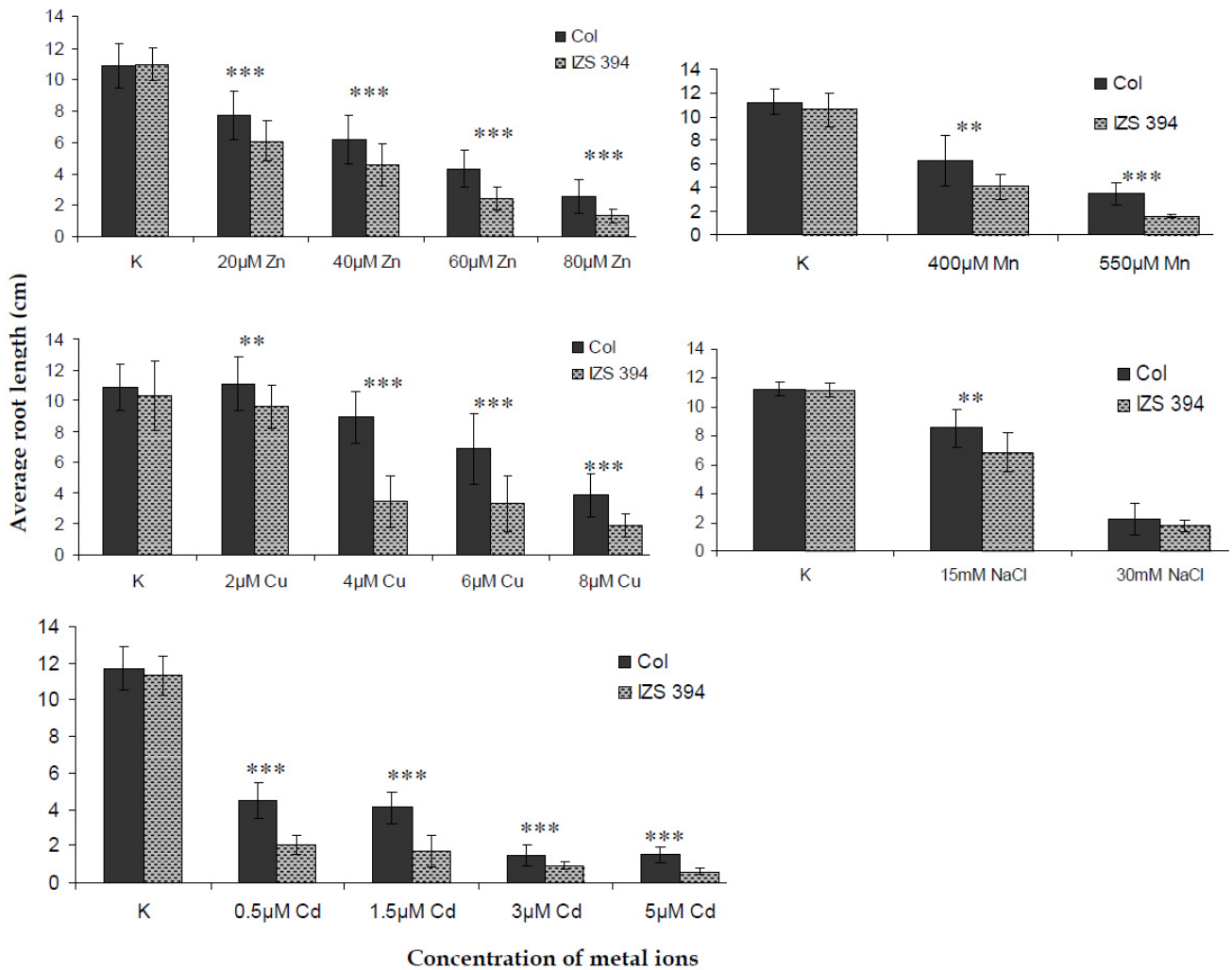


Figure 3.5. IZS 394 showed significantly stronger hypersensitivity towards all four metal ions tested (i.e. Zn, Cd, Cu and Mn) and to lower concentration of salt than wild type Col-0. (‘***’ for 0.001, ‘**’ for 0.01 and ‘*’ for 0.05 significance level).

When it comes to IZS 390 (short rooted even under optimal growing condition) the stress effects observed are as strong as the other three mutant lines. The strongest root growth inhibition (87%) was caused by 80 μM of ZnSO₄. However, at moderate concentrations of Cu, Cd and Mn a significant difference of hypersensitivity has also been observed (Fig. 3.6).

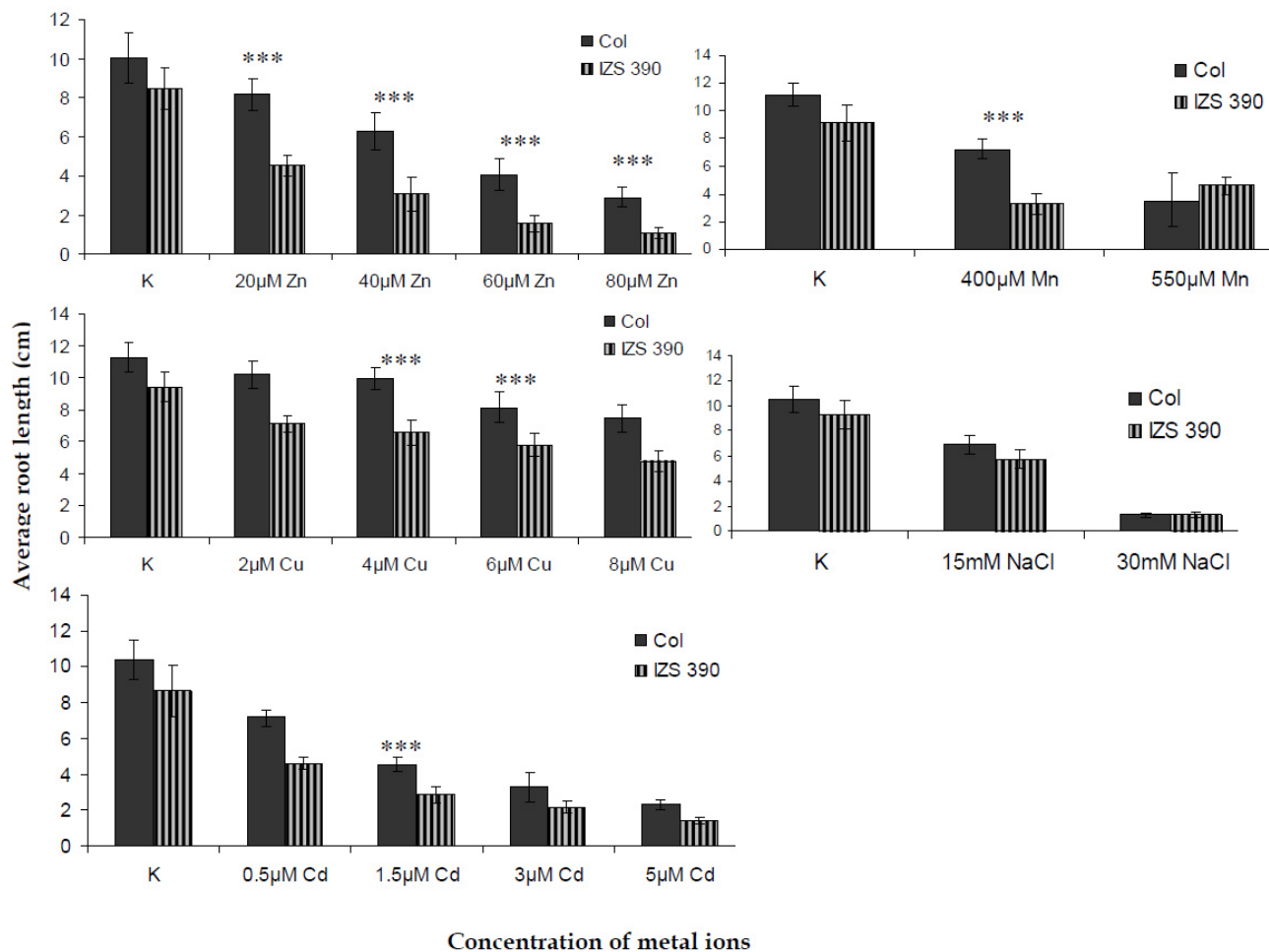


Figure 3.6. IZS 390 in addition to the Zn hypersensitivity, it showed significant root growth reduction under moderate concentration of Cd, Cu and Mn. (**** for 0.001, *** for 0.01 and ** for 0.05 significance level).

Meanwhile, IZS 479 distinctively showed root growth hindrance only in the presence of Zn in the agar plates (Fig. 3.7). Furthermore, it showed the highest percentage of root growth reduction (98%) at 80 μM of ZnSO₄. Therefore, among the five IZS mutants phenotypically characterized the only mutant with an exclusive Zn hypersensitivity phenotype was IZS 479. It also showed a significant root growth reduction at low concentration of cadmium (0.5 μM Cd²⁺). The unique characteristic of IZS 479 bare greater resemblance to that of a well documented mutant phenotype of MTP1, which is CDF transporter family protein that has been shown to be involved in Zn transport. Therefore, it is likely for the mutated gene in IZS 479 to be MTP1. Consequently, sequencing the MTP1 (At2g46800) gene in IZS 479 revealed a point mutation at the 877th base pair where guanine (G) is substituted with adenine (A) that lead to the replacement of the 293rd amino acid, which was aspartic acid (D), with asparagine (N). The multiple sequence alignment of homologues genes obtained from KEGG (Kanehisa and Goto, 2000) identifies this particular amino acid to be conserved across different species. Similarly, the 3D model of AtMTP1 generated through homology modeling based on the

Results

crystal structure of *Escherichia coli* MTP1 (EcYiiP) showed the location of the mutated amino acid to be at the start of the sixthth transmembrane domain of MTP1 (Fig. 4.1) (Kawachi et al., 2012).

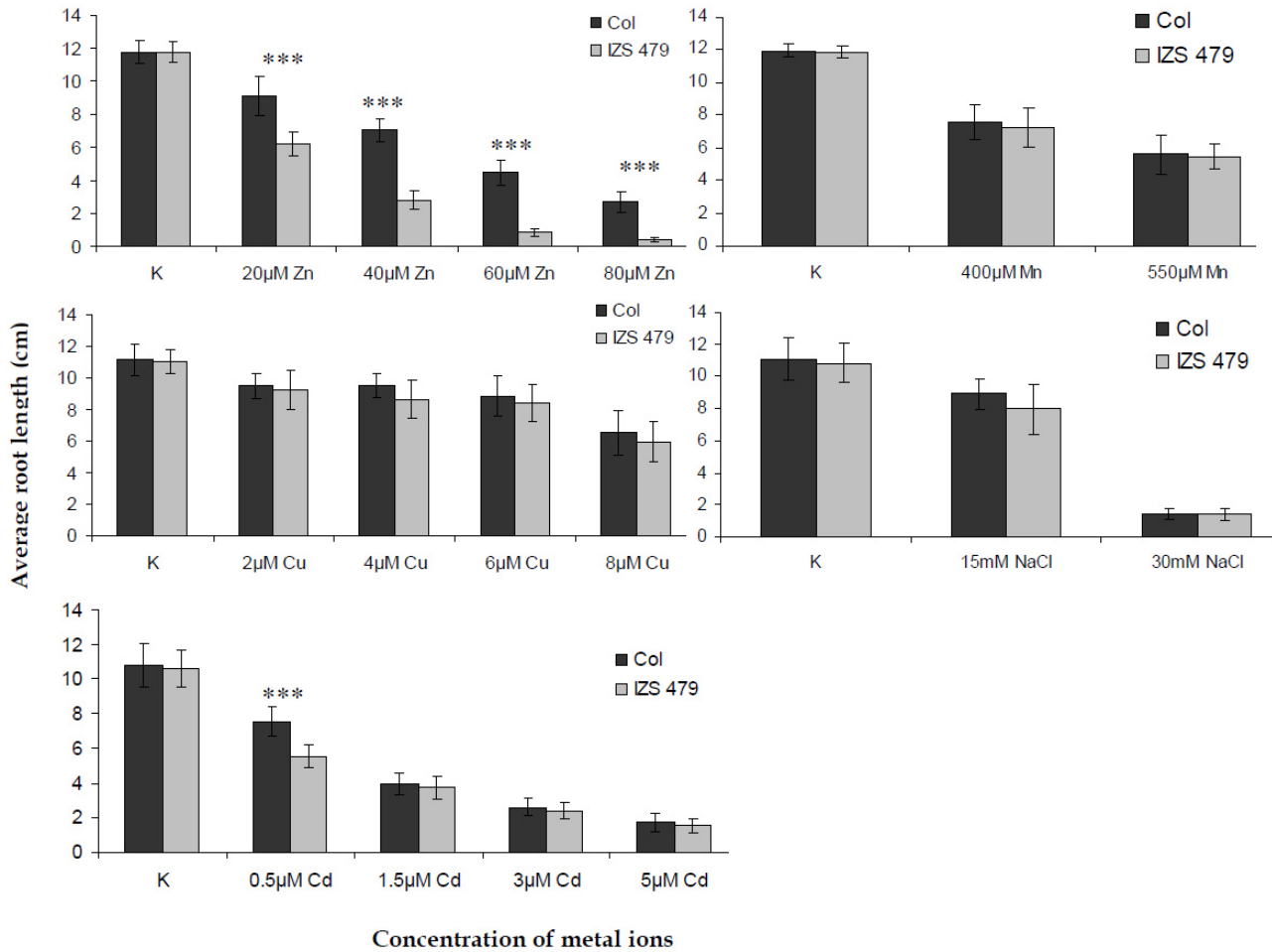


Figure 3.7. IZS 479 showed specific hypersensitivity towards Zn and to limited extent to lower concentration of cadmium. (‘***’ for 0.001, ‘**’ for 0.01 and ‘*’ for 0.05 significance level)

3.2 Mapping and characterization of IZS 288

3.2.1 Genetic background of IZS 288

The first step of the characterization work on IZS 288 was identifying the number of mutated genes that resulted in the Zn hypersensitivity phenotype. The allelic segregation observed in the second generation (F2) progenies of different backcross lines of IZS 288 were all above 0.0625. If the Zn hypersensitivity phenotype was the effect of two genes the allelic segregation ratio would have been 1/16 (Tab. 3.3). Therefore, the mutation under consideration seems to be a single gene mutation. Meanwhile, all the F1 (first generation) progenies of the backcross lines behaved similar to the wild-type, hence the mutated gene is believed to be inherited as a recessive trait.

Table 3.3 Allelic segregation of different backcross lines of IZS 288

<i>Backcross line</i>	<i>Wild-type like</i>	<i>IZS 288 like</i>	<i>Segregation ratio</i>
C3	39	32	0.45
C4	24	53	0.31
E3	28	68	0.29
E4	31	58	0.53

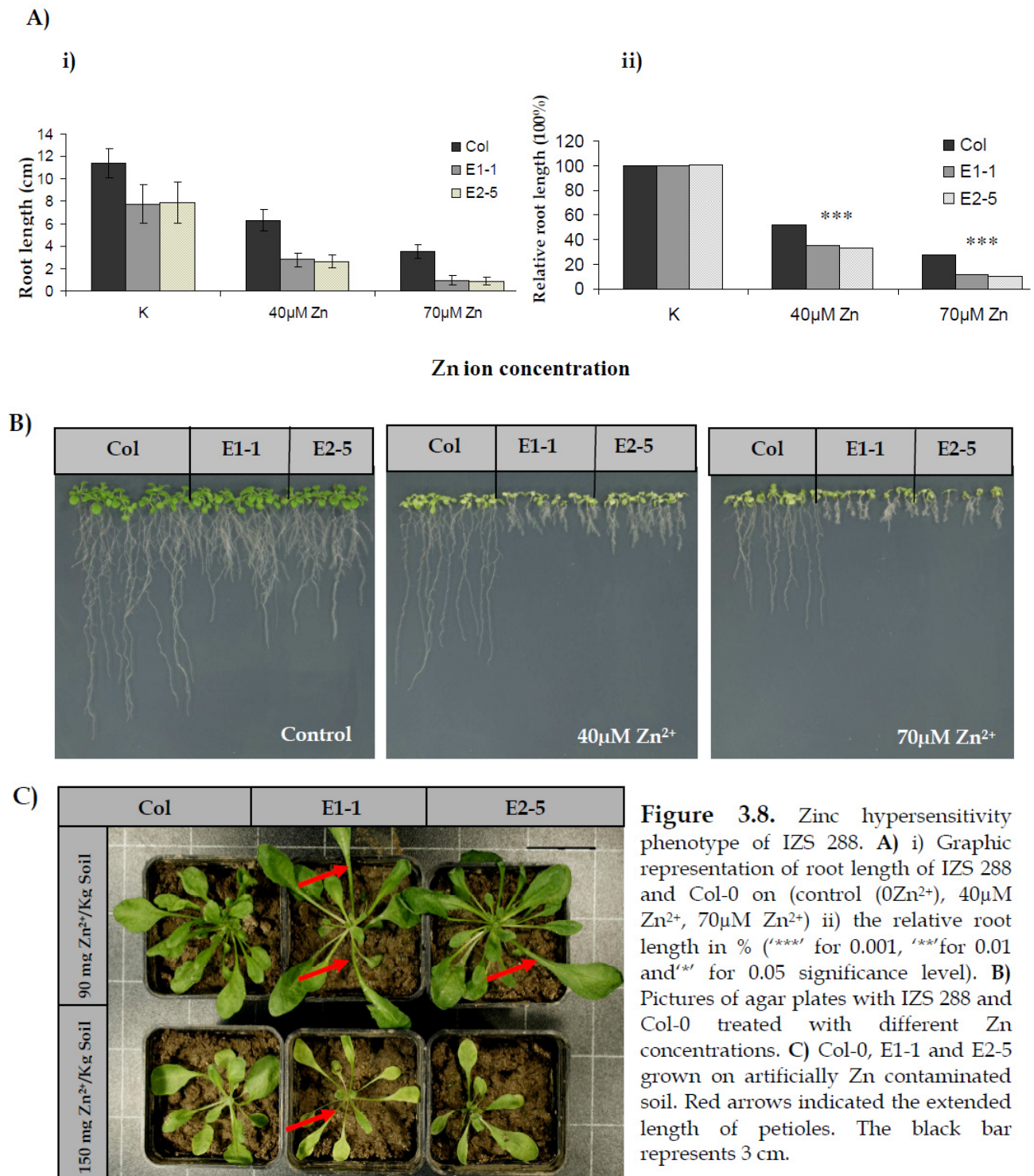
Since IZS 288 is isolated from EMS mutagenized seeds its genome carries a large number of background mutations in addition to the mutation causing the Zn hypersensitivity. In order to clean up the unwanted mutations a series of backcrossing with the wild-type is required. However, instead of the time-intensive clean up work, the alternative approach of excluding the impact of unwanted mutations is to use two independent backcross lines and verify each observation using these two independent backcross lines. Accordingly, in all the traits taken into consideration the two independent back cross lines of IZS 288 (i.e. E1-1 and E2-5) showed similar behaviors verifying the very small effects from unwanted background mutations.

3.2.2 Observed phenotypes of IZS 288

The Zn tolerance assay conducted on vertical agar plates treated with different Zn concentrations (Fig.3.8) confirmed the dose dependent Zn hypersensitivity of IZS 288, where the highest concentration tested (70 μ M Zn²⁺) caused almost 90% root length reduction in IZS 288 while the wild-type only lost 73% of its root length. Likewise, the Zn tolerance test

Results

conducted on artificially contaminated soil also showed similar outcome, where the Zn hypersensitivity phenotype of IZS 288 was manifested in the form of leaf size reduction and loss of chlorophyll content resulting in leaf yellowing. Surprisingly, under the experimental set up of the artificially contaminated soil IZS 288 showed an additional phenotype, where under both optimal as well as excess Zn availability the petiole length of IZS 288 appeared to be longer than the wild-type. To further investigate this phenotype the average petiole length of five fully developed leaves of IZS 288 and Col-0 grown on non contaminated soil were measured.



Results

The results confirmed that the average petiole length of IZS 288 was significantly longer than that of Col-0. Previous reports have indicated a link between the trait of developing extra long petioles and shade avoidance mechanism of plants; therefore the difference in petiole length of IZS 288 and Col-0 were tested under low light availability. When IZS 288 and Col-0 plants were cultivated under low light intensity (i.e. in the range of 10-16 $\mu\text{E m}^{-2}\text{s}^{-1}$) IZS 288 showed more pronounced increment in petiole length. During the cultivation under optimal light intensity (i.e. 110-90 $\mu\text{E m}^{-2}\text{s}^{-1}$) depending on the position in the growth chamber) the average petiole length of the wild-type measured only 84% of the petiole length of IZS 288, meanwhile during shading this variation got even wider where the petiole length of Col-0 covered only 70% of the petiole length of IZS 288 (Fig 3.9).

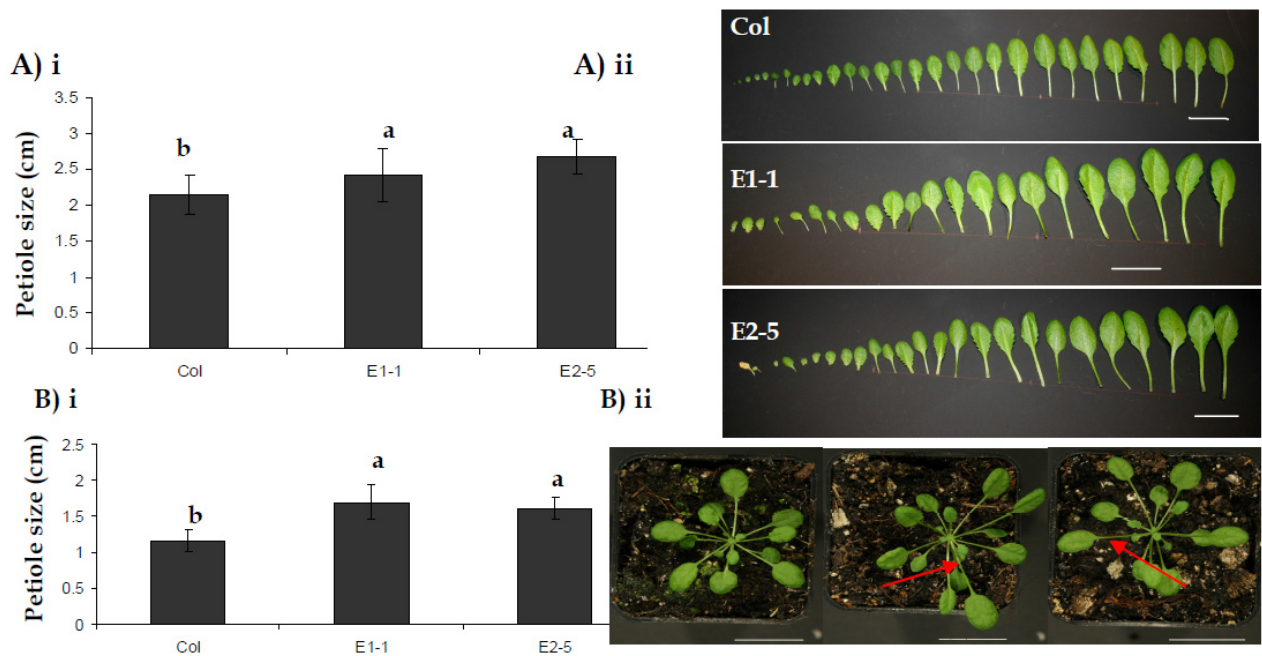


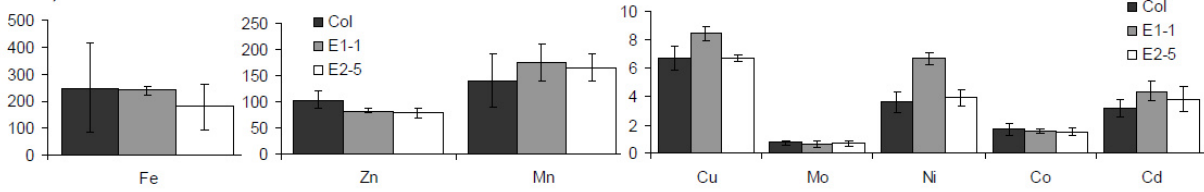
Figure 3.9. A) i Petiole length of five mature leaves of Col-0 and the two backcross lines of IZS 288. Different letters represent significantly different petiole length. A) ii Pictures of all the leaves in the rosette of Col-0 and E1-1 and E2-5. B) i Petiole length of five mature leaves of Col-0 and the two backcross lines of IZS 288 under dim light condition. B) ii Pictures of whole plants cultivated under dim light. The white bars represent 2 cm.

In order to determine whether the observed Zn hypersensitivity is accompanied by alteration in metal ion content of IZS 288, the elemental profile of roots and shoots cultivated on both hydroponic system and soil substrate were determined using inductively coupled plasma-optical emission spectroscopy (ICP-OES). The comparison of the elemental profiles of IZS 288 and WT conveyed the absence of significant difference among the two genotypes in both cultivating systems (Fig. 3.10-12). Similarly, preliminary analysis conducted on seeds also showed parallel result except for manganese and calcium contents where it seems that IZS 288 accumulated more than Col-0, but more elaborate analysis must be conducted in larger

Results

sample sets before making a concrete conclusion. In short, despite the hypersensitivity response to Zn stress, under optimal growing condition IZS 288 did not show a significant variation in the amount of both micro and macronutrient contents of different organs.

A) i



A) ii

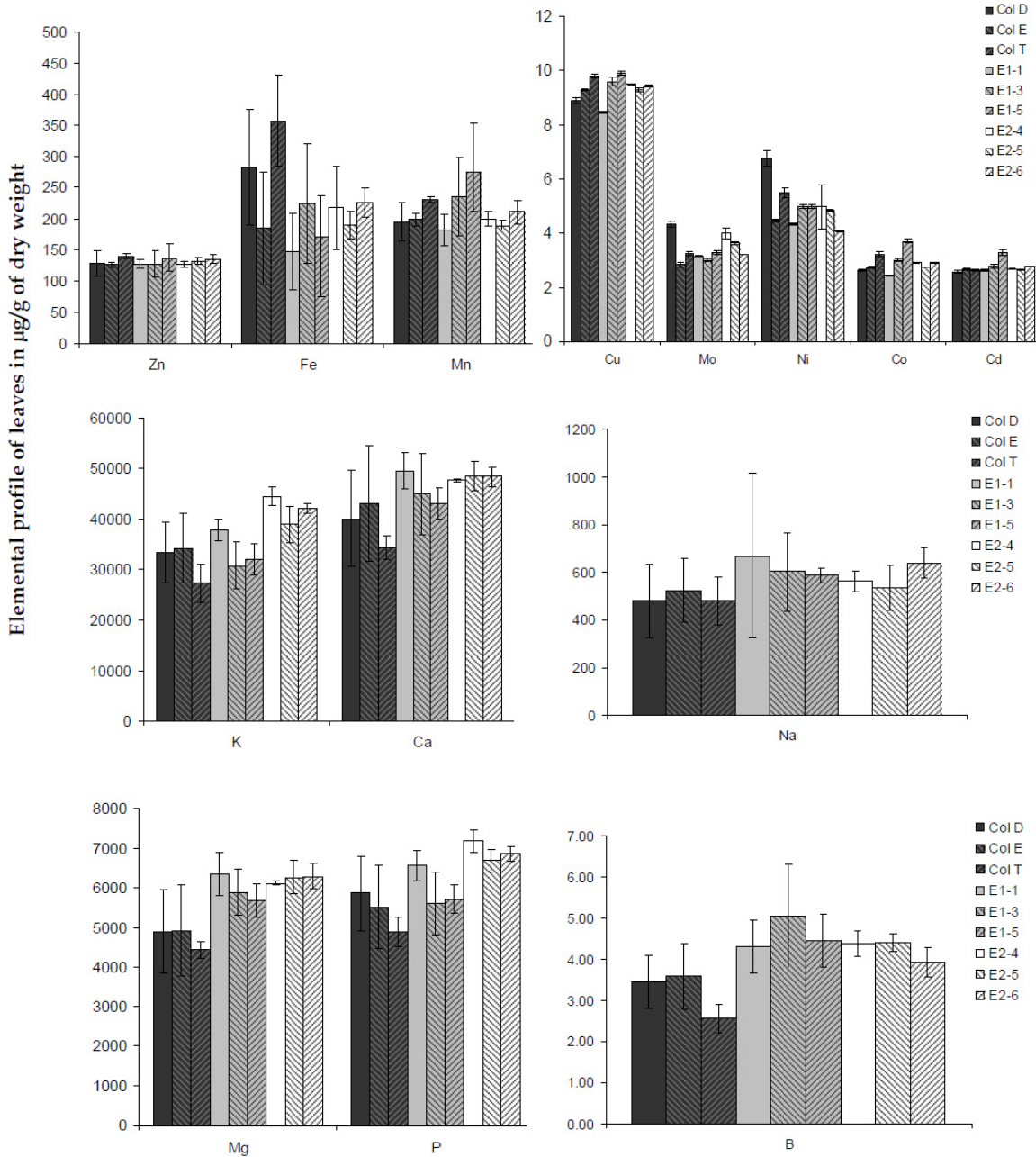


Figure 3.10. Elemental profile of leaves of A) i Col-0 and two backcross lines of IZS 288 (E1-1 and E2-5) that were cultivated hydroponic system and A) ii three different lines of Col-0 (namely Col D, Col E and Col T) and three different lines of the two backcross lines of IZS 288 (namely E1-1, E1-3, E1-5 and E2-4, E2-5, E2-6) on soil substrate.

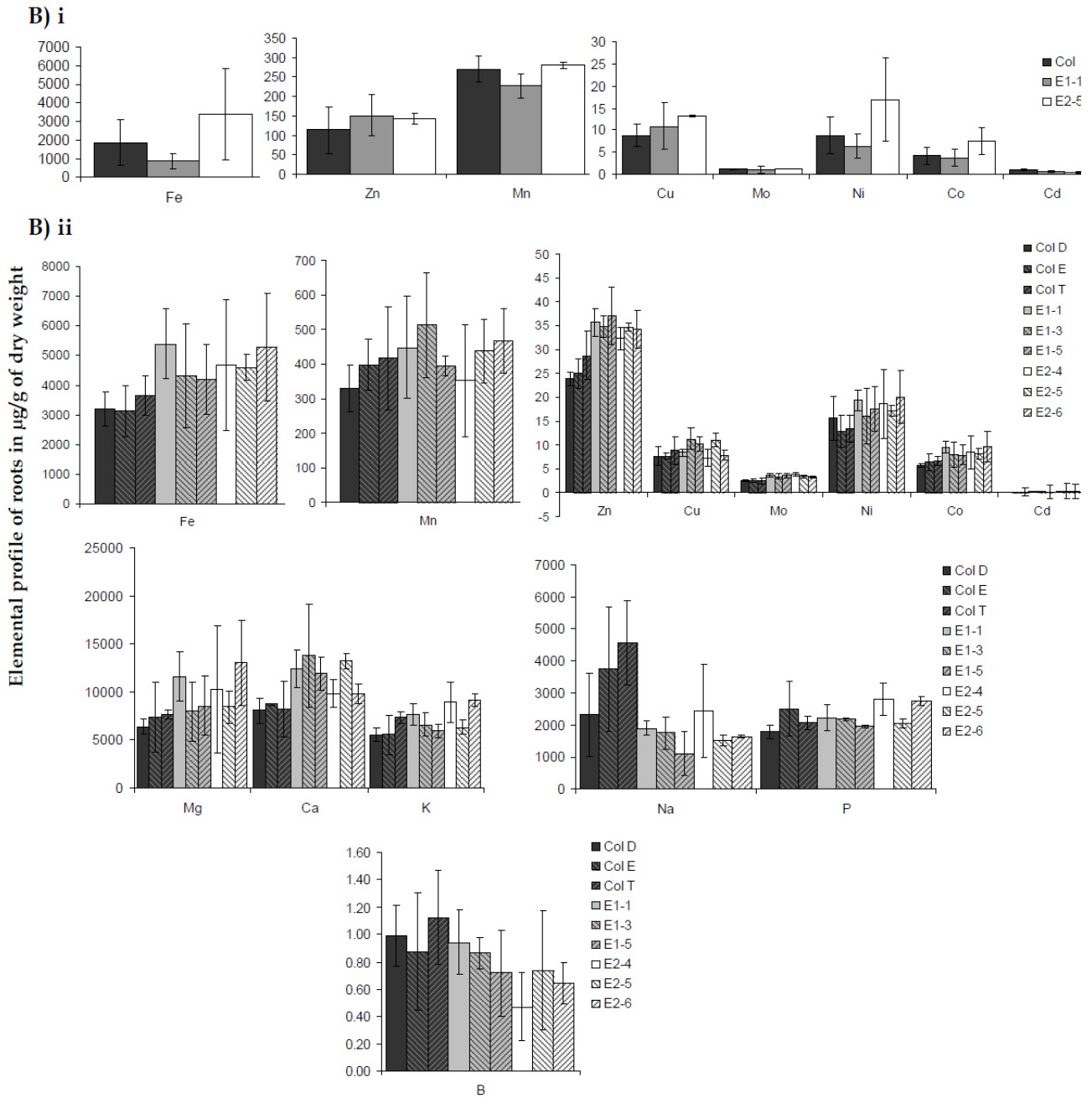


Figure 3.11. Elemental profile of roots of **B) i** Col-0 and two backcross lines of IZS 288 (E1-1 and E2-5) that were cultivated in hydroponic system and **B)ii** three different lines of Col-0 (namely Col D, Col E and Col T) and three different lines of the two backcross lines of IZS 288 (namely E1-1, E1-3, E1-5 and E2-4, E2-5, E2-6) on soil substrate.

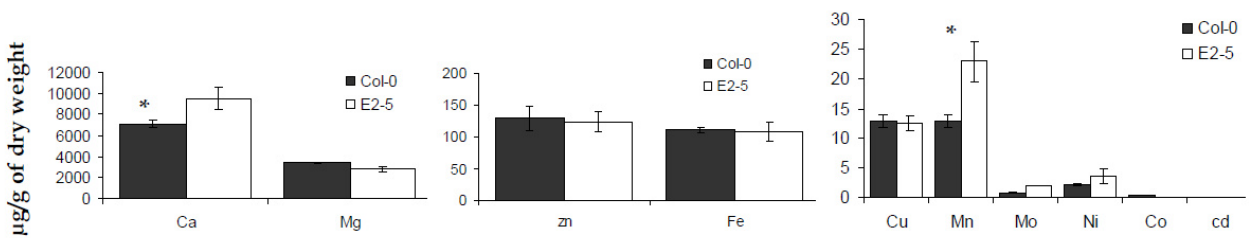


Figure 3.12. Preliminary results of elemental profile of seeds Col-0 and E2-5, where IZS 288 seemed to have more Mn and Ca. (* * 0.01 significance level).

Results

Moreover, the tolerance test conducted using Cu, Ni, Co, Mn, Cd, Fe and sodium chloride proved the specificity of the Zn hypersensitivity phenotype of IZS 288. Astonishingly, IZS 288 showed significantly higher level of tolerance towards cobalt, manganese, cadmium and iron than the wild-type Col-0 (Fig 3.13).

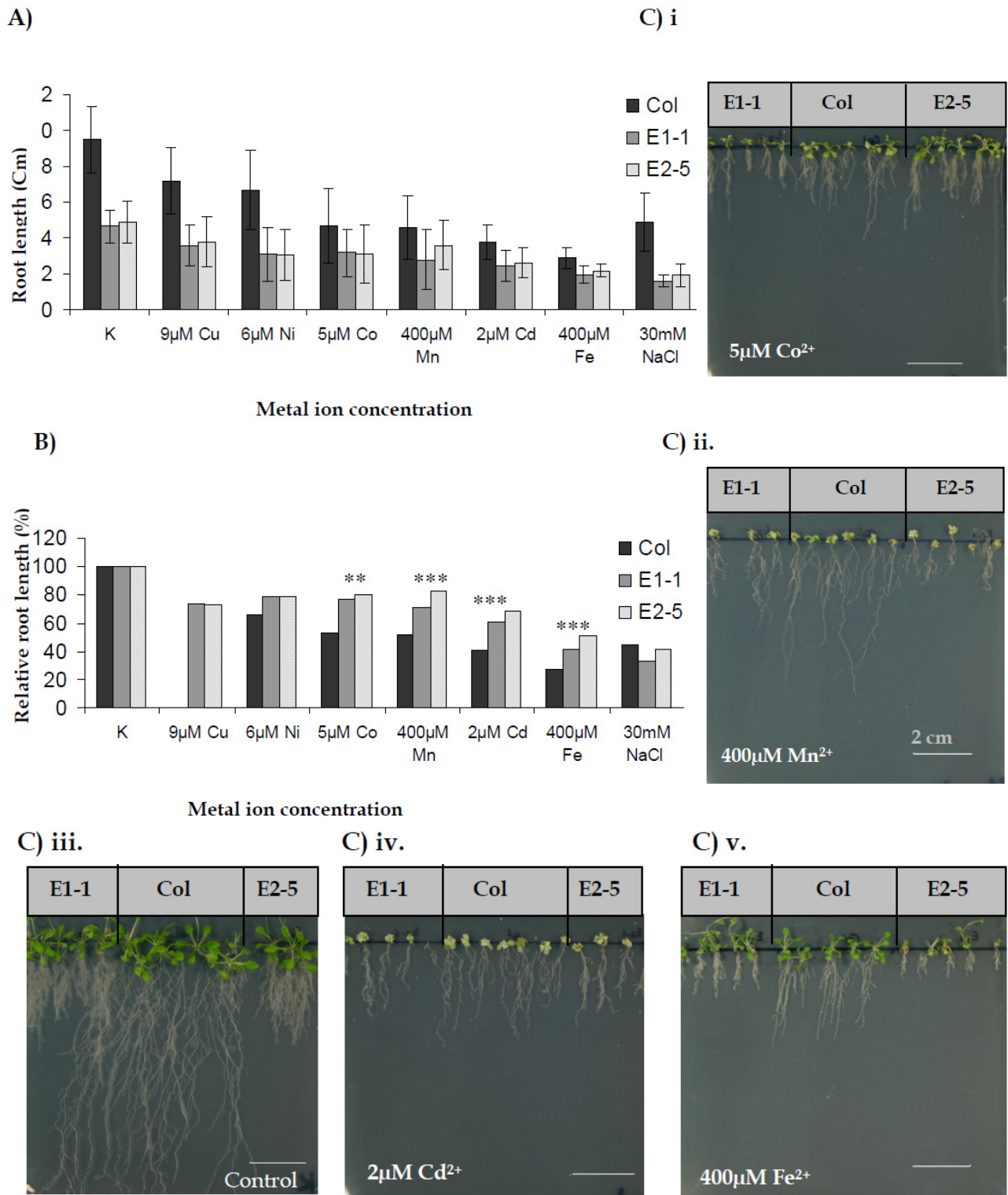


Figure 3.13. Root growth assay of IZS 288 in comparison to wild-type Col-0 on plates with different metal ion concentrations. A) Shows average root length of IZS 288 and Col-0 grown on plates treated with $9\mu\text{M Cu}^{2+}$, $6\mu\text{M Ni}^{2+}$, $5\mu\text{M Co}^{2+}$, $400\mu\text{M Mn}^{2+}$, $2\mu\text{M Cd}^{2+}$, $400\mu\text{M Fe}^{2+}$, 30mM NaCl . B) Relative root length of IZS 288 and Col-0 in % (**** for 0.001, *** for 0.01 and ** for 0.05 significance level). C) picture of a plate containing i) $5\mu\text{M Co}^{2+}$, ii) $400\mu\text{M Mn}^{2+}$, iii) Non treated, iv) $2\mu\text{M Cd}^{2+}$ and v) $400\mu\text{M Fe}^{2+}$. The bars represent 2 cm.

Results

On the other hand, the abiotic stress tolerance test has led to the discovery of strong chilling sensitivity in IZS 288. When seeds of the two backcross lines of IZS 288 and Col-0 were set to germinate under chilling temperature (4°C), the seedlings of IZS 288 stopped growing completely after the onset of cotyledons. Likewise, when seedlings of IZS 288 and wild-type were transferred to chilling temperature on the fourth day after germination, the seedlings of IZS 288 suspended their growth at the stage they were in before they were moved to the chilling environment (Fig. 3.14).

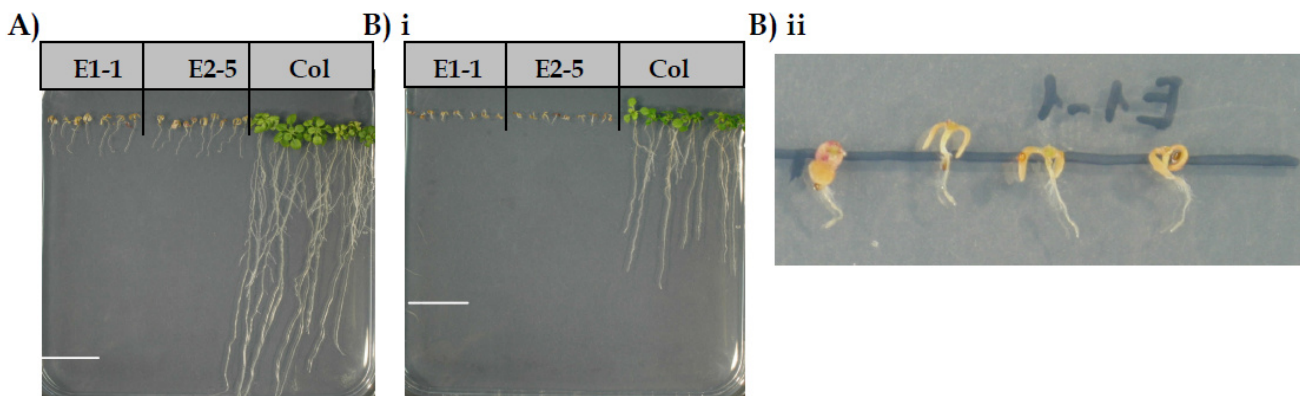


Figure 3.14. A) Picture of seedlings of IZS 288 and Col-0 transferred to 4°C and cultivated for six weeks, B) i Pictures of seedlings of both IZS 288 and Col-0 that were germinated in a cold room with ambient temperature of 4°C, B) ii close up picture of IZS 288 seedlings germinated under chilling condition. Development stops at cotyledon stage.

However, despite the prominent chilling hypersensitivity observed in IZS 288, chilling stress did not cause lethality. Recovery experiments conducted on seedlings that stayed in the cold room with the ambient temperature of 4°C for different durations (i.e. 1, 2, 4 and 8 weeks) showed full recuperation after one week of being moved back to optimal growing condition (Fig. 3.15). Furthermore, the chilling hypersensitivity of IZS 288 manifested in the form of growth arrest was observed only during cultivation under 4°C, when seedlings were placed in a growth chamber with an ambient temperature of 12°C instead, they were able to sustain growth. Nonetheless, the chilling hypersensitivity of IZS 288 could not be overcome by acclimatization process. When the seedlings that were cultivated at 12°C got transferred to 4°C, the IZS 288 seedlings were still unable to sustain growth (Fig. 3.16).

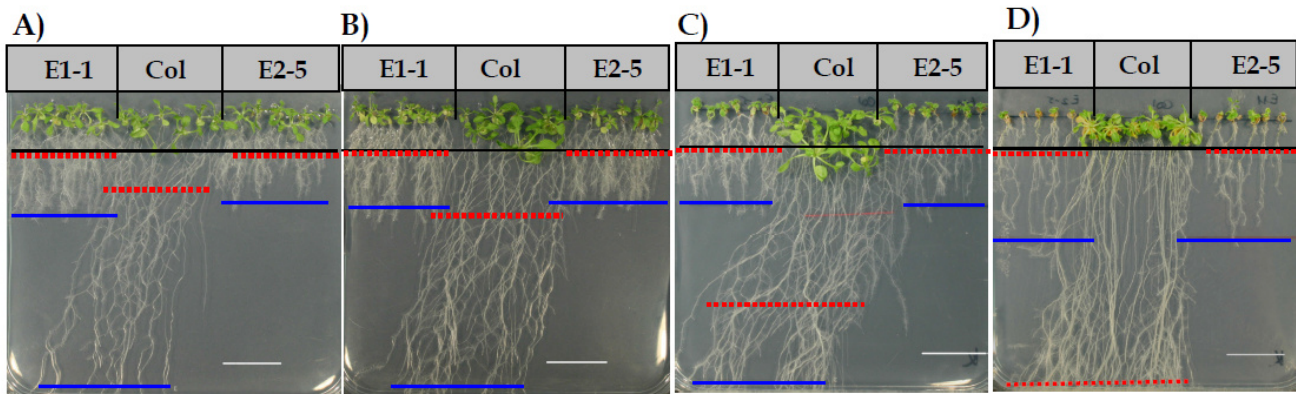


Figure 3.15. Pictures of recovery experiments **A)** after one week **B)** after two weeks **C)** four weeks and **D)** after eight weeks stay in 4°C they were moved to optimal growing condition and cultivated for one week, black bars represent the root length of seedlings at the time they were placed in the cold room, the red broken line represents the root growth under chilling condition, blue bars represents the root growth recovery under optimal growing condition. Picture of seedlings of IZS 288 and Col-0 transferred to 4°C and cultivated for six weeks.

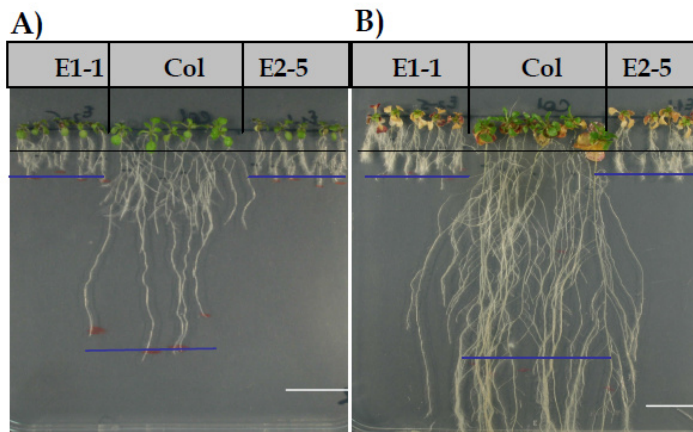


Figure 3.16. Pictures of seedlings **A)** cultivated under 12°C for one week, the black line indicates the original root length before being moved to 12°C, blue line indicates the root growth under 12°C **B)** after being transferred to 4°C and incubated for 4 weeks, Only Col-0 plants were able to sustain growth at 4°C.

Meanwhile, in order to rule out the possibility of nutritional deficiency or any other factors introduced by the growing media, the influence of the lack of micronutrients (since the agar plates are made up of 1/10 Hoagland media without micronutrients) and increased sugar concentrations (up to 2%) on the root length of IZS 288 were tested. The supplementation of micronutrients to the growing medium and the increment in sugar concentration resulted in a moderate root length improvement in both wild-type and IZS 288. However, the observed level of increment of the root length of IZS 288 was insignificant when compared to the average root length of the wild-type (Col-0) (Fig. 3.17). Therefore, the short root phenotype of IZS 288 seems to be a developmental defect observed in different growing media irrespective of their composition.

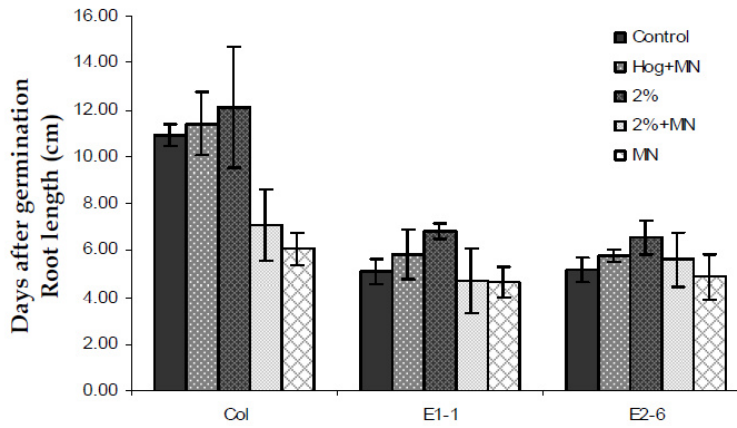


Figure 3.17. Root length of IZS 288 and Col-0 on **Control**=1/10 Hoagland without micronutrients (MN) **Hog+MN**=1/10 Hoagland +micronutrients, **2%** = 2% sugar added to 1/10 Hoagland media, **2%+MN**=1/10 Hoagland + MN+ 2% sugar, **MN**= micronutrients only.

To further elucidate the short root phenotype of IZS 288, the root growth rates of IZS 288 was deduced under optimal growing condition as well as under Zinc stress ($50\mu\text{M Zn}^{2+}$). Under optimal growing condition the daily root growth rate of IZS 288 was comparable to that of Col-0 up until the 4th day after germination. Beyond the 4th day after germination IZS 288 maintained a very slow root growth rate. This root growth rate reduction of IZS 288 in optimal growing condition has the same magnitude as the reduction of Col-0 root growth rate under Zn stress condition. In addition to that, under Zn stress the root growth rate reduction of IZS 288 was quite tremendous (Fig. 3.18). In short, IZS 288 maintained average root growth rate up until the 4th day after germination, but afterwards the root growth rate dropped considerably leading to a significant decrease in the average length of the primary root. Thus, the short root phenotype of IZS 288 did not occur as a result of root growth cessation rather it is due to a reduction in root growth rate that started after the 4th day of germination.

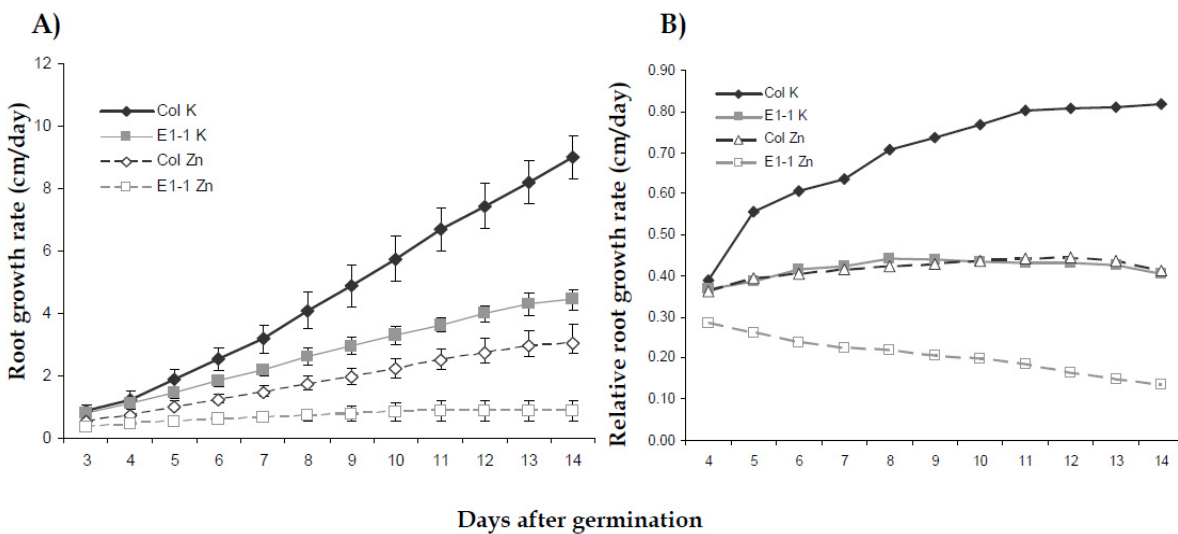


Figure 3.18. A) Root growth rate of IZS 288 and Col-0 per day under optimal growing and zinc stress conditions. **B)** Relative root growth rate per day of IZS 288 and Col-0.

Results

Going further into the details of the short root phenotype, observation of the root tips of IZS 288 under light microscope revealed a reduction in the size of the elongation zone. Furthermore, under Zn stress ($50\mu\text{M Zn}^{2+}$) the meristematic zone of IZS 288 was also smaller than that of Col-0 (Fig. 3.19). A closer inspection of propidium iodide stained root tips of IZS 288 under the confocal microscope uncovered defects in the root tip organization. Particularly, the cells at lateral side of the root cap (lateral root cap cells) contained too many smaller sized cells instead of larger sized differentiating cells (Fig. 3.20 A-C). Moreover, the short root phenotype of IZS 288 correlated with a reduced rate of cell division in the meristem, as indicated by the cyclin B1 marker (i.e. CycB1;1::GUS). Especially, in the presences of Zn stress the number of mitotically active cells dropped significantly in the meristem of IZS 288 (Fig. 3.20 D-I).

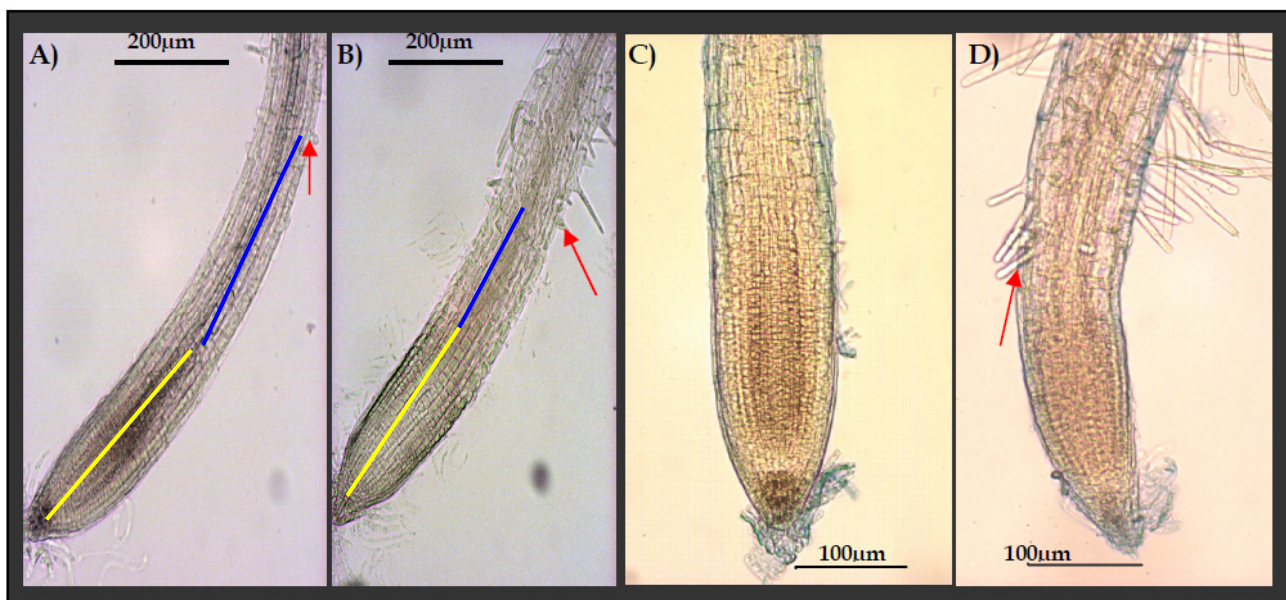


Figure 3.19. Root tip of A) Col-0 and B) IZS 288 grown on control plates. Yellow line represents the meristematic zone and blue line stands for the elongation zone. C) Col-0 and D) IZS 288 grown on $50\mu\text{M Zn}^{2+}$ -treated plates. Arrows indicate root hairs that signify the beginning of the zone of maturation.

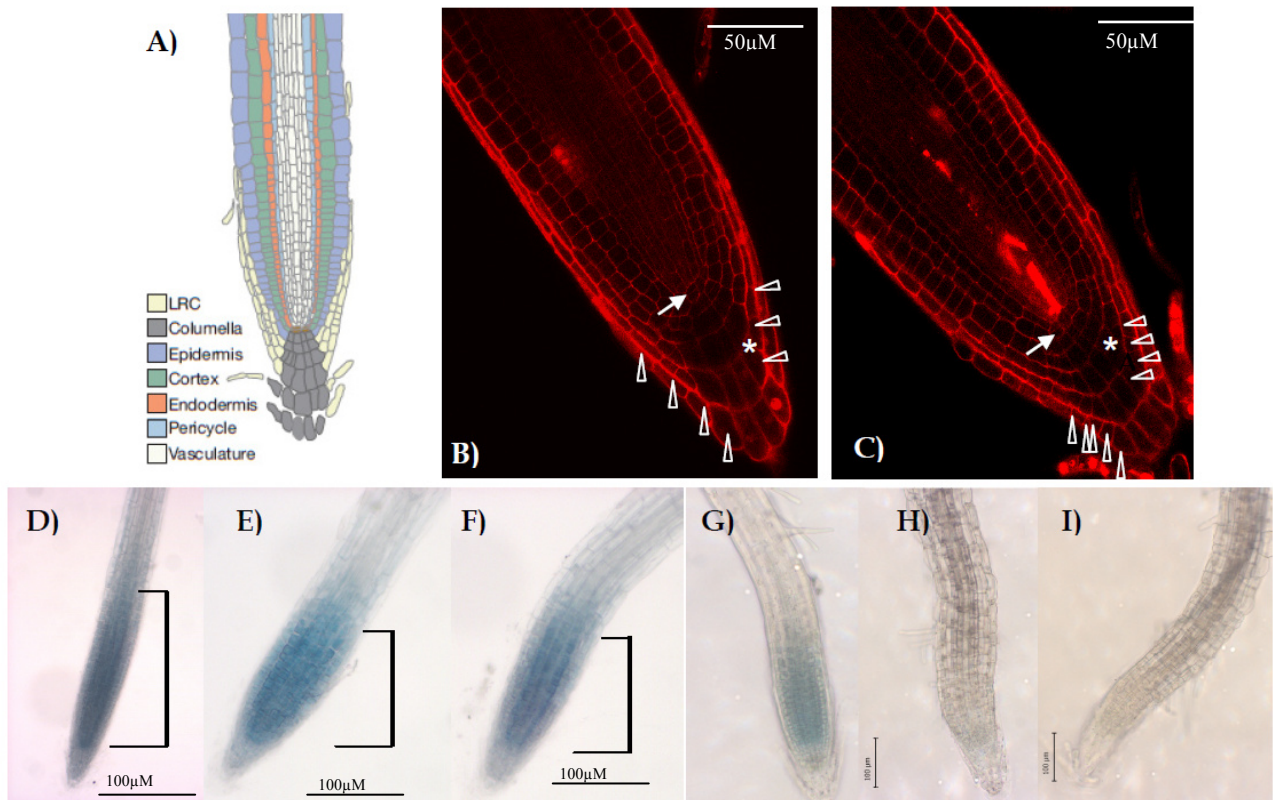


Figure 3.20. **A)** Schematic representation of the *Arabidopsis* root tip. Adapted from Swarup et al., (2005). **B)** Root tip of Col-0, **C)** IZS 288, white arrow indicates the quiescent center (QC), arrow heads show cells in lateral root cap and the star symbol stands for dividing cells. Root tip of **D)** Col-0 **E)** E1-1 and **F)** E2-5 cultivated without Zn stress; **G)** Col-0 **H)** E1-1 and **I)** E2-5 grown in the presence of 50 μ M Zn²⁺ visualized by CycB1;1::GUS staining.

The other morphological alteration observed on the root architecture of IZS 288 was the increased number of lateral root formation. Particularly, the numbers of secondary and tertiary lateral roots were significantly higher than that of the wild-type (Fig. 3.21). However, Zn stress seems to reverse this effect, whereby the number of secondary lateral roots increased in the wild-type but decreased in IZS 288. The observed lower number of secondary lateral roots in IZS 288 could be due to the considerable reduction of root length caused by the Zn stress.

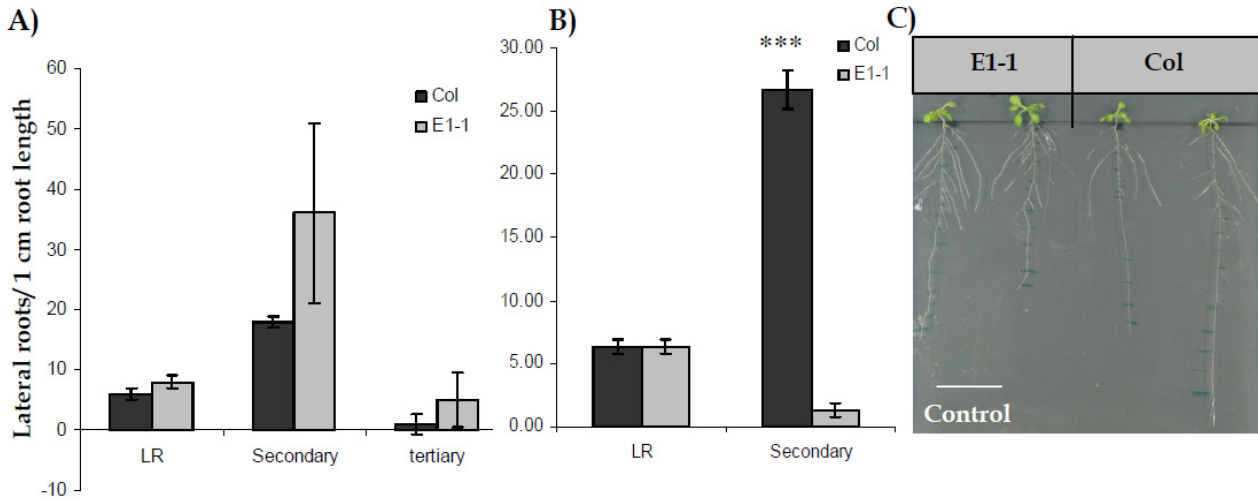


Figure 3.21. A) Number of lateral roots (i.e. primary secondary and tertiary) of IZS 288 and Col-0 per the first 1 cm of root length grown under optimal growing condition. B) Number of lateral roots of IZS 288 and Col-0 grown on 50µM Zn²⁺ treated plates. (*** for 0.001 significance level). C) Picture of agar plate showing the difference in root architecture of E1-1 and col-0

Following up the observed influence of Zn on the incidence of lateral roots, IZS 288 and Col-0 were exposed to mild Zn stress (i.e. 1µM, 5µM and 10µM) and lateral roots of 15 day old seedlings were counted. Moreover, in order to take into count the effect of sugar on the development of root architecture, sugarless agar plates treated with the same level of mild Zn stress were also tested. Under optimal growing condition as well as during the presence of 1µM Zn²⁺ the ratio of lateral roots to overall root length of IZS 288 was significantly higher than that of wild-type. However, as the concentration of Zn ion present in the agar plate increased the difference between IZS 288 and the wild-type Col-0 disappeared (Fig. 3.22 A). On the other hand, the absence of sugar in the growing media caused greater variability in-between seedlings of the same genotype treated with the same concentration of Zn ion. Therefore, in the experimental set up where sugar was absent from the agar plates, no apparent difference was observed between IZS 288 and Col-0 (Fig. 3.22 B).

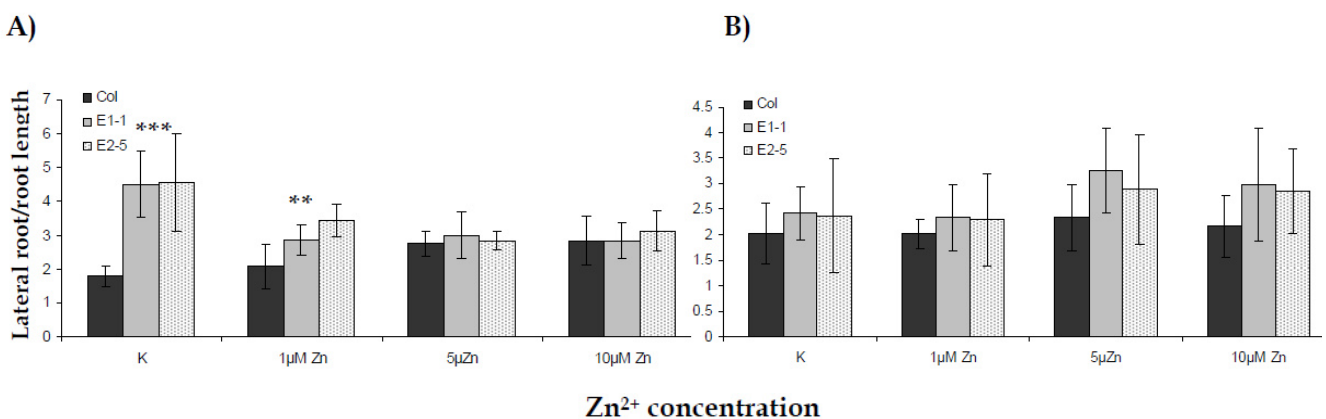


Figure 3.22. The comparison of the ratio of lateral roots to root length of the wild-type Col-0 and two back cross lines of IZS 288 A) on agar plates that contain sugar and different concentration of Zn ions. B) on agar plates without sugar. (**** for 0.001, *** for 0.01 and ** for 0.05 significance level).

Results

In the meantime, to see the effect of mild Zn stress on both genotypes, the ratio of lateral root to root length of each genotype was compared across different Zn concentrations. The wild-type showed a significant increase in the number of lateral roots per unit root length across the different Zn concentrations. On the contrary, in the case of IZS 288 the highest ratio of lateral root per unit root length was observed at optimal growing condition and it got reduced by the presence of Zn ion (Fig.3.23). Here also the absence of sugar from the growing media caused huge variability among seedlings within the same treatment that masked the effect of Zn ion on lateral root numbers of both genotypes.

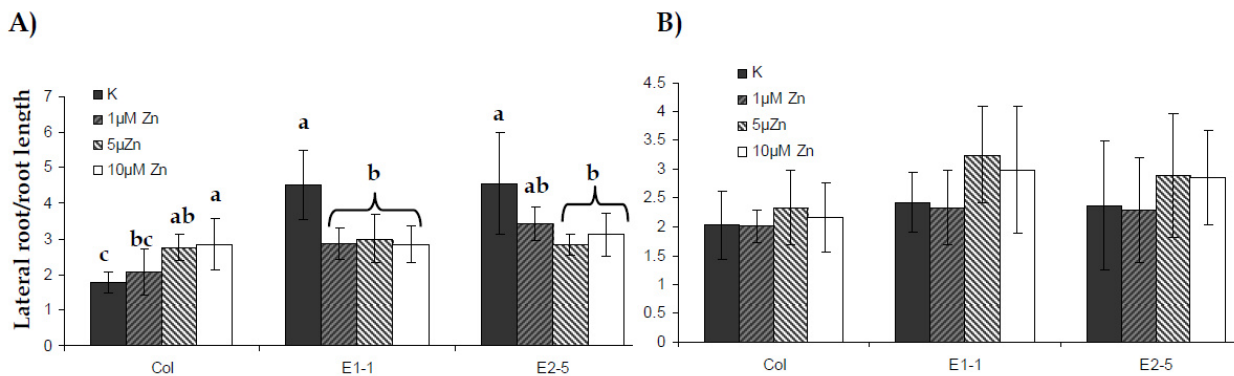


Figure 3.23. The ratio of lateral roots to root length of the wild-type Col-0 and two back cross lines of IZS 288 compared across different Zn ion concentrations A) on agar plates that contain sugar B) Grown on agar plates without sugar. Different letters represent significantly different means.

Furthermore, in the comparison of IZS 288 to that of the wild-type secondary lateral roots were considered as one additional parameter. Here also under optimal growing condition IZS 288 appeared to have significantly higher number of secondary lateral roots than Col-0. This difference was still visible even when sugar was absent from the growing media. Similar to that of the number of lateral roots per unit root length, the total number of secondary lateral roots of IZS 288 also got reduced by the presence of Zn in the growing media (Fig. 3.24).

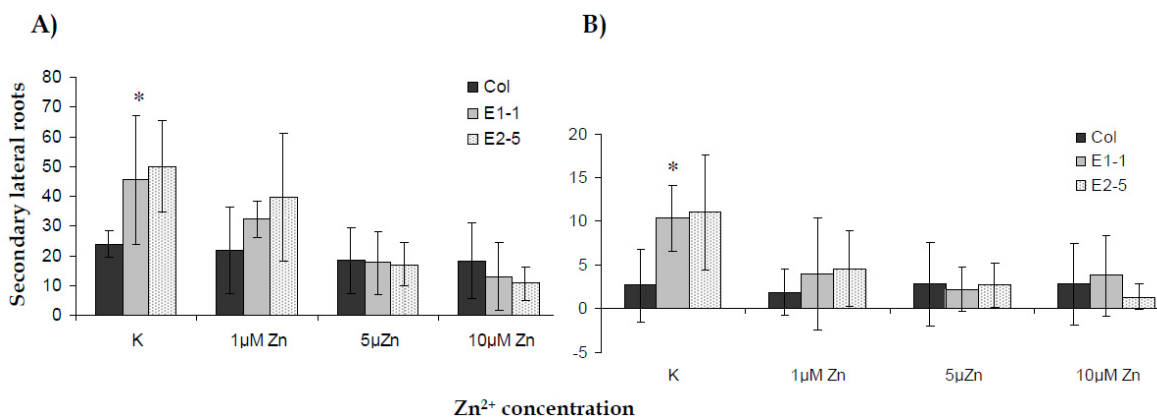


Figure 3.24. Comparison of number of secondary lateral roots of the wild-type Col-0 and two back cross lines of IZS 288 in the presence of different Zn ion concentration A) grown on agar plates that contain sugar B) grown on agar plates without sugar. (**** for 0.001, *** for 0.01 and ** for 0.05 significance level).

Results

The root architectural alteration of IZS 288 caused by Zn stress was more severe in hydroponically grown plants. During prolonged Zn stress (20 μ M Zn for a duration of three weeks) the occurrence of lateral roots in IZS 288 increased considerably, yet they did not presume the normal developmental progress of lateral roots rather they appeared to have a root nodule like structure (Fig 3.25).

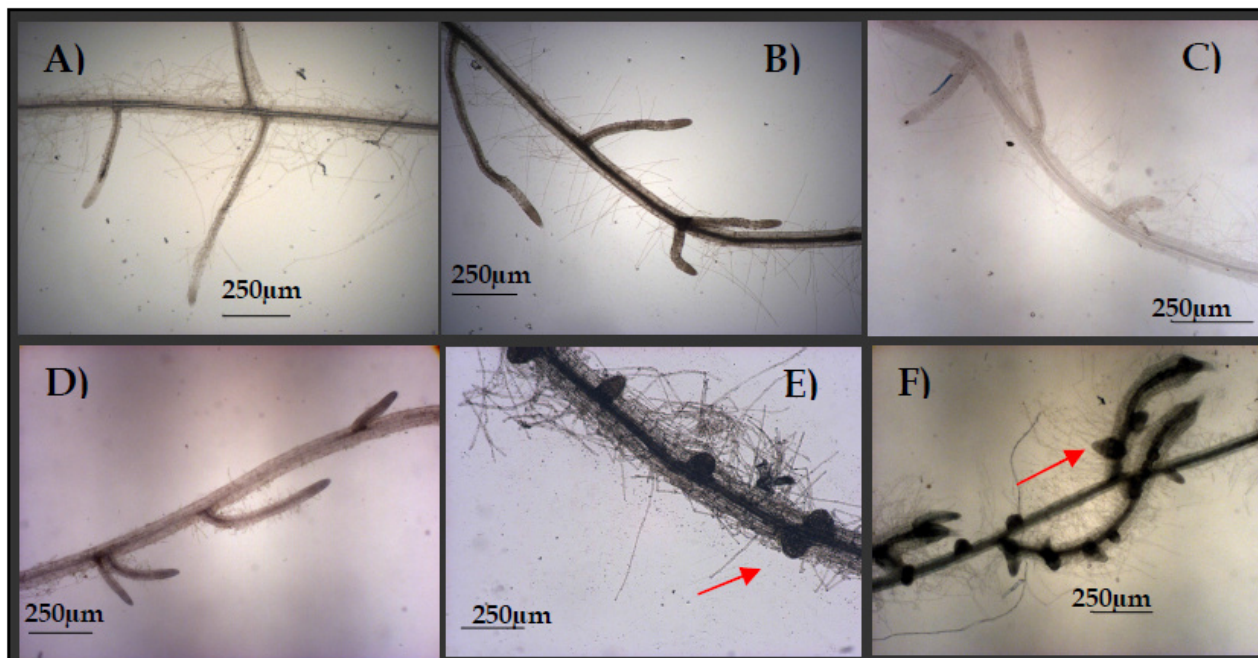


Figure 3.25. Lateral roots of A) Col-0, B) E1-1 and C) E2-5 hydroponically grown under optimal growing condition. Whereas D) Col-0, E) E1-1 and F) E2-5 hydroponically grown seedlings exposed to 20 μ M Zn for three weeks consecutively. Arrows indicate root nodule like out growth of lateral roots.

The distinctive root architectural alterations plus the morphological defects of the leaves of IZS 288 ignited an interest on the involvement of plant hormones on the observed phenotypes of IZS 288. Hence, the level of tolerance of IZS 288 towards different kinds of plant hormones was tested. In these tests IZS 288 showed increased tolerance towards different kinds of auxin applied exogenously (i.e. indole-3-acetic acid (IAA), 1-naphthalene acetic acid (NAA), synthetic auxin (2, 4-D) and Indole-3-butyric acid (IBA)) (Fig. 3.26). Additionally, IZS 288 showed dissimilar response towards known auxin inhibitors. The response towards the auxin transport inhibitor *N*-(1-naphthyl) thalamic acid (NPA) was quite similar to that of the wild-type, where the development of lateral roots was blocked and the primary root tips grew in circular forms and showed moderate level of root length reduction. However, the response of IZS 288 towards the anti-auxin *p*-chloro-phenoxy-iso-butyric acid (PCIB) and 2,3,5-triiodobenzoic acid (TIBA) was different from that of the wild-type, where the reduction of the primary root length in IZS 288 was lesser than Col-0 and seemed to have more lateral roots than the wild-type. Meanwhile, possible variation in the auxin response

Results

maxima of IZS 288 was investigated using the auxin response marker DR5::GUS. The present results did not give any indication for the presence of an alteration in the auxin response maxima of IZS 288 (Fig. 3.27). However, a thorough investigation needs to be carried out, like the effect of exogenous auxin and auxin inhibitors on DR5::GUS activity, before ruling out the impact of the mutation of IZS 288 on auxin response maxima.

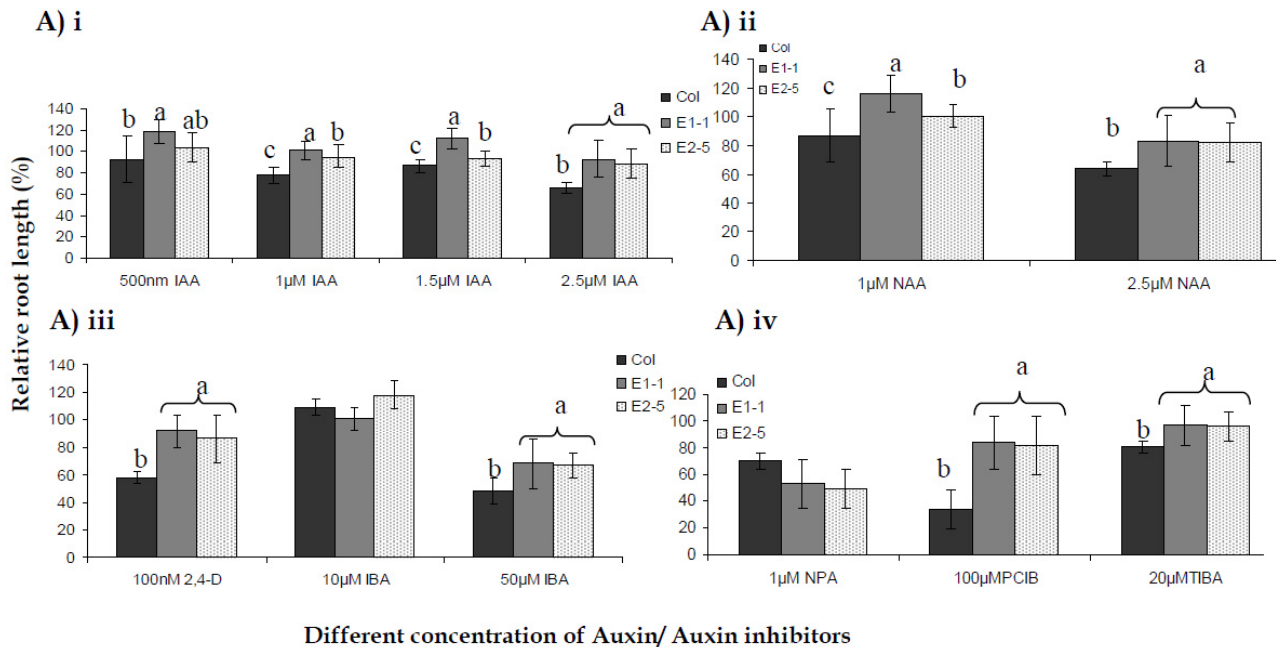


Figure 3.26. Relative root length of IZS 288 and Col-0 in the presence of **A) i** different IAA concentrations, **A) ii** different NAA concentrations **A) iii** 2,4-D and two IBA concentrations, **A) vi** three auxin inhibitors (i.e. NPA, PCIB, TIBA). Letters represent significant difference at average relative root length.

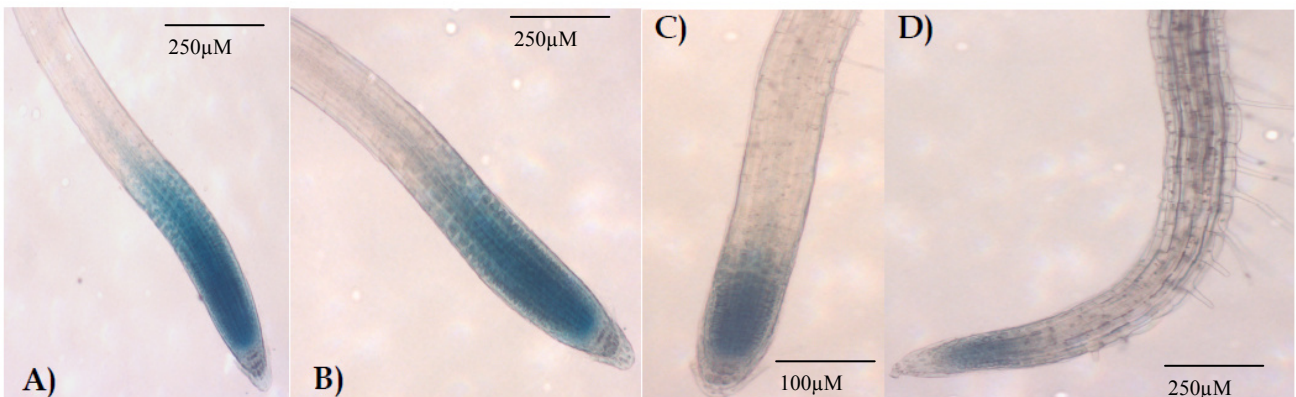
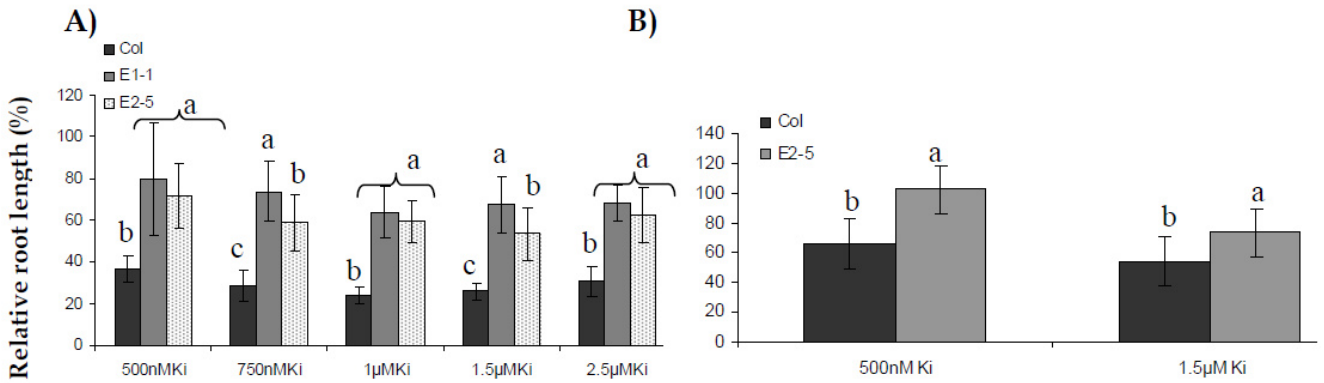


Figure 3.27. Auxin response maxima visualized by DR5::GUS of **A) Col-0, B) IZS 288** under optimal growing condition, **C) Col-0** and **D) IZS** in the presence of Zn stress.

Similarly, the tolerance test conducted using series of kinetin concentrations revealed the tolerance response of IZS 288 towards exogenous cytokinins (Fig. 3.28 A). Especially when IZS 288 seeds were directly sown on agar plates treated with different concentration of kinetin the root architecture resembled that of the wild-type (Fig. 3.28 B). Furthermore, the inhibitory effect of abscisic acid (ABA) on the root growth of IZS 288 was smaller than the

Results

wild-type, but the effect of ABA on the germination rate (considering the emergence of radicle as the onset of germination) of IZS 288 and Col-0 seemed to be more or less similar. In contrast, the tested concentrations of gibberellic acid (GA) did not cause any apparent effect on the root length of IZS 288 as well as Col-0 (Fig. 3.29).



Different concentrations of Kinetin

Figure 3.28. Relative root length of IZS 288 and Col-0 in the presence of different concentrations of kinetin, **A)** seedlings transferred to agar plates containing different concentration of Kinetin after the fourth day of germination **B)** seeds of IZS 288 and Col-0 directly sown on agar plates treated with 500nM and 1.5µM kinetin. Letters represent significant difference at average relative root length.

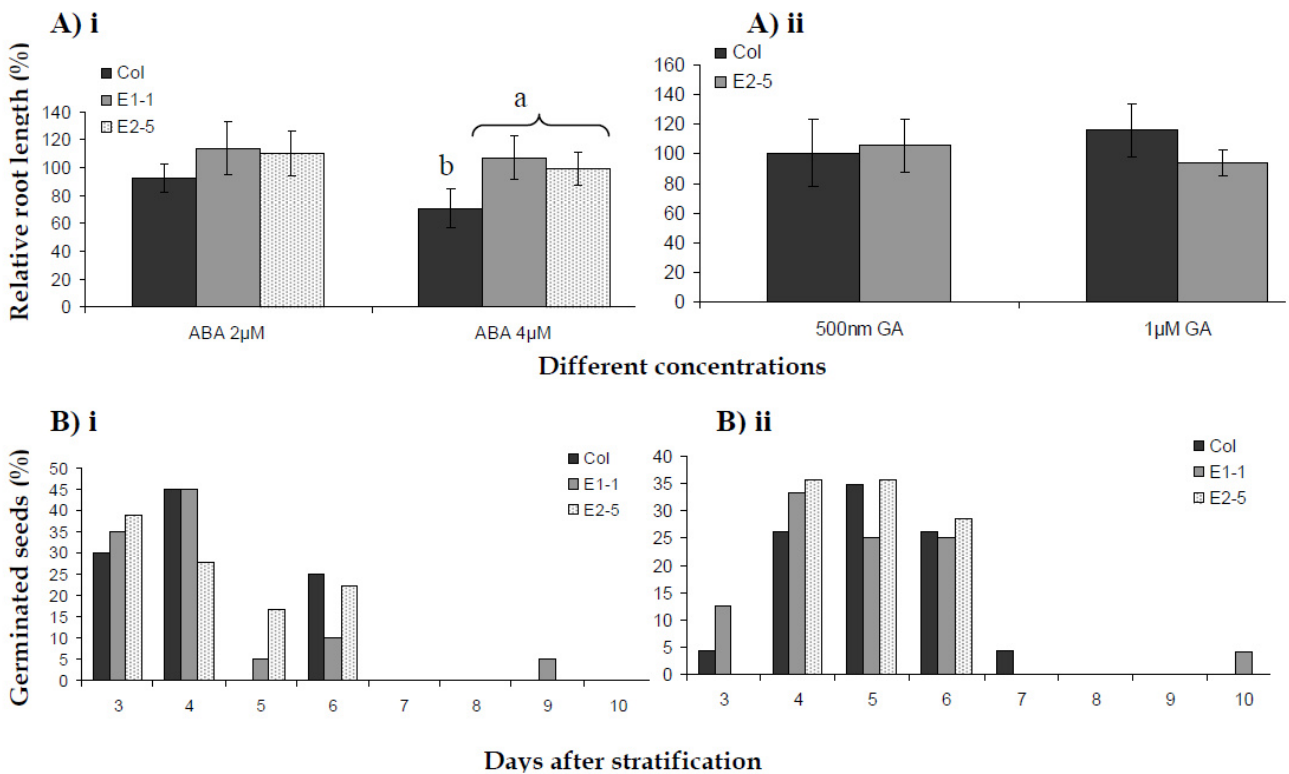


Figure 3.29. Relative root length of IZS 288 and Col-0 directly grown on agar plates containing **A) i** 2µM and 4µM ABA, **A) ii** 500nM and 1µM GA, **B) i** germination rate of Col-0 and IZS 288 on plates containing 2µM ABA and **B) ii** 4µM ABA.

In short, IZS 288 was only hypertensive towards Zn and chilling stress. In contrast, it showed enhanced tolerance towards heavy metals Cd, Co, Mn and Fe. Similarly, it showed better root

growth than the WT in the presence of different forms of auxin and auxin inhibitors, kinetin as well as ABA. These phenotypic responses of IZS 288 are summarized in table 3.4.

Table 3.4 Summary of phenotypic responses of IZS 288 towards abiotic stress and phytohormones. (-) represents hypersensitivity, (+) represents tolerance.

<i>Type of stress</i>		<i>IZS 288</i>	
<i>Abiotic stress</i>	Chilling	-	
	Salt (NaCl)	-	
<i>Heavy metals</i>	Cadmium	+	
	Cobalt	+	
	Copper		
	Iron	+	
	Manganese	+	
	Nickel		
	Zinc	-	
<i>Phytohormones</i>	Auxin	IAA	+
		NAA	+
		2,4-D	+
		IBA	+
	Auxin inhibitors	NPA	
		PCIB	+
		TIBA	+
	Kinetin		+
	Absciscic acid (ABA)	root growth germination	+
	Gibberellic acid (GA)		

Previous observations of mutants with defects in auxin response revealed the presence of additional phenotypes such as alteration in cotyledon size, hypocotyl and root hair length. Hence, the cotyledon size, hypocotyl and root hair lengths of IZS 288 were compared and contrasted with that of the wild-type that led to the finding of three additional phenotypes of IZS 288. The cotyledons and dark grown hypocotyls of IZS 288 were significantly smaller than that of Col-0 but root hairs were considerably longer in IZS 288 than in Col-0 (Fig. 3.30).

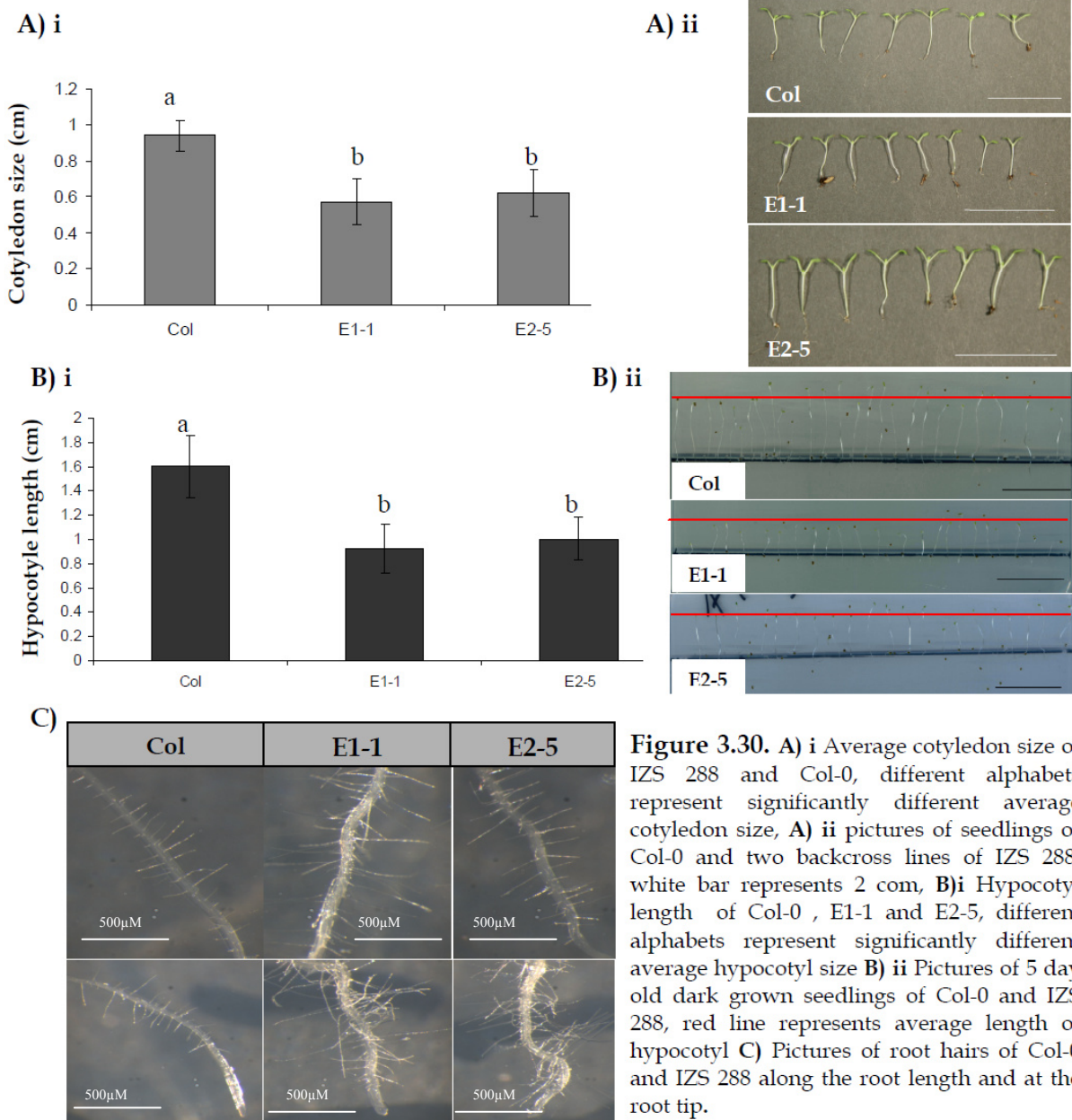


Figure 3.30. A) i Average cotyledon size of IZS 288 and Col-0, different alphabets represent significantly different average cotyledon size, A) ii pictures of seedlings of Col-0 and two backcross lines of IZS 288, white bar represents 2 cm, B) i Hypocotyl length of Col-0, E1-1 and E2-5, different alphabets represent significantly different average hypocotyl size B) ii Pictures of 5 day old dark grown seedlings of Col-0 and IZS 288, red line represents average length of hypocotyl C) Pictures of root hairs of Col-0 and IZS 288 along the root length and at the root tip.

Earlier, leaf morphological aberration of IZS 288 in regards to petiole length has been mentioned. In addition to that, leaves of IZS 288 seemed to have shape defects, where their tips appeared to be more oval than round. The depth of the leaf coloration also varied between Col-0 and IZS 288, where Col-0 leaves appeared to be bright green; whereas the leaves of IZS 288 had grayish green appearance and accumulated more anthocyanins at their lower side (Fig. 3.31). Moreover, they appeared to have more trichomes than Col-0. The distribution of stomata in the lower side of IZS 288 leaves also looked as if they aggregate in close proximity to each other than in Col-0. The venation of IZS 288 cotyledons also seemed to show irregularities. However, since there were disparities among plants within the same

genotype, it is very difficult to make a concrete and quantitative statement about these phenotypes (Fig. 3.32).

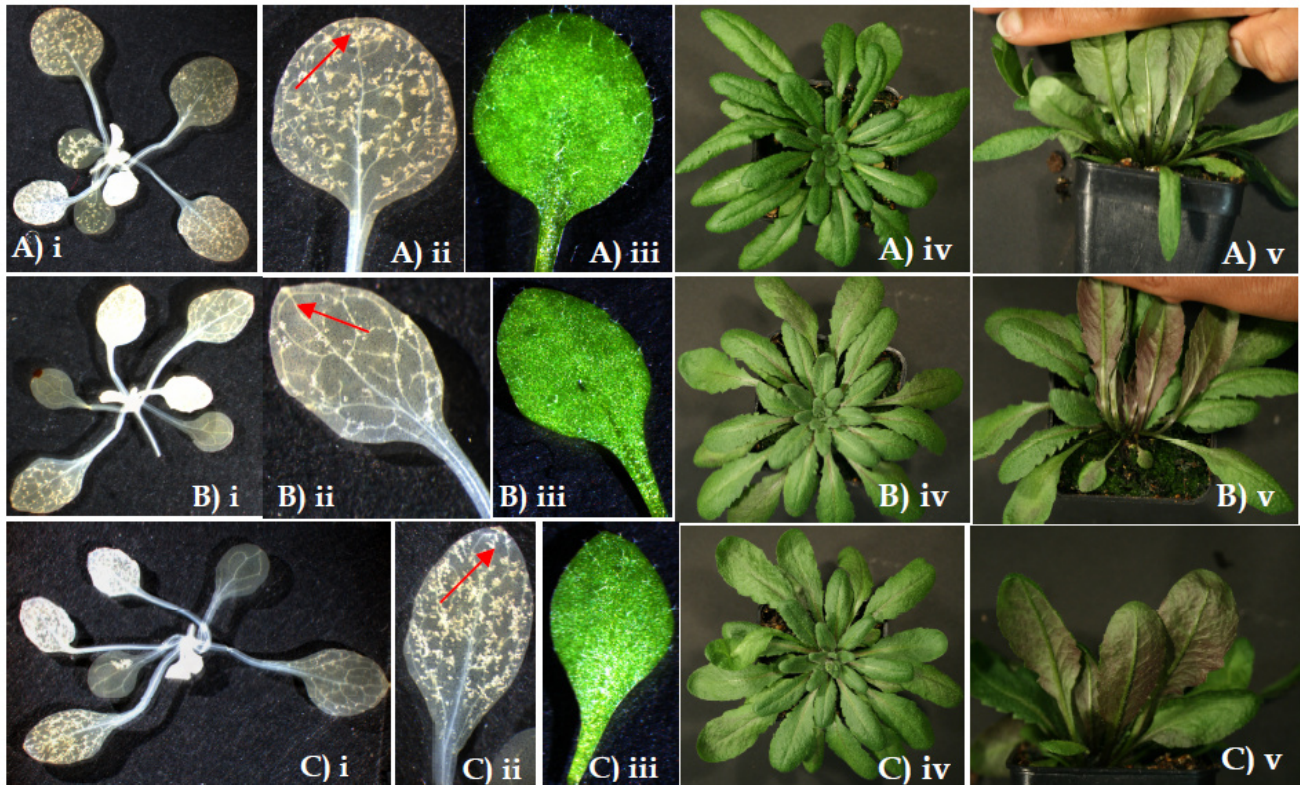


Figure 3.31. Pictures of **A) i** rosette of Col-0, **A) ii** and **A) iii** single leaves of Col-0 having more round and symmetrical shape, **A) iv** fully grown rosette of Col-0 showing bright green color and **A) v** back side of leaves of Col-0 lacking anthocyanin accumulation. **B) i** rosette of E1-1, **B) ii** and **B) iii** single leaves of E1-1 having more oval shapes, **B) iv** fully grown rosette of E1-1 showing grayish green color and **B) v** back side of leaves of E1-1 showing anthocyanin accumulation. **C) i** roseate of E2-5, **C)ii** and **C) iii** singles leaves of E2-5 showing oval shapes. Red arrows indicate the difference in shape, **C) iv** fully grown rosette of E2-5 showing grayish green color and **C) v** lower side of leaves of E2-5 showing anthocyanins accumulation.

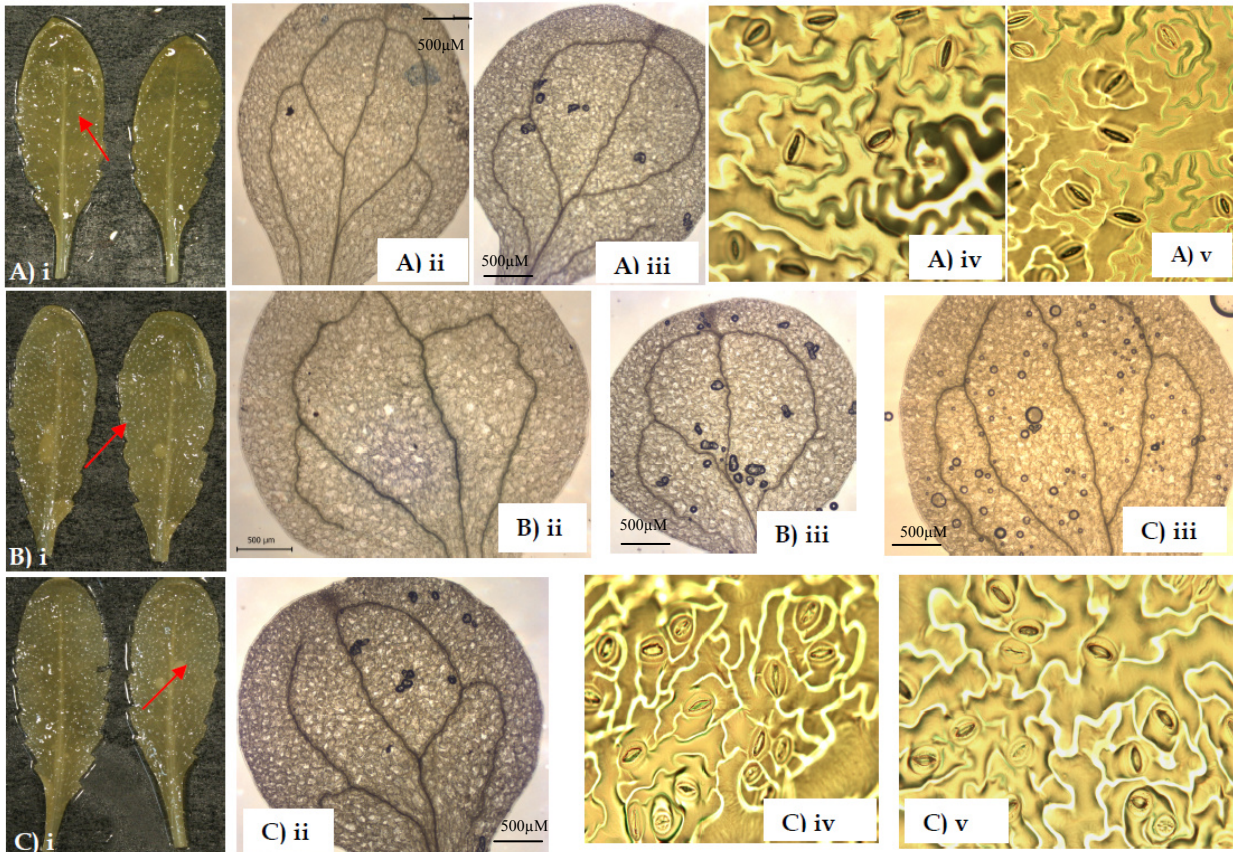


Figure 3.32. A) i Pictures of two leaves of Col-0 cleared with ethanol having fewer trichomes, here red arrows indicate trichomes. A) ii and A) iii showing close up view of venation in cotyledons of Col-0 leaves where the leaf veins are formed symmetrically around the mid rib, A) iv and A) v Col-0 lower leaf impression showing evenly distributed stomata. B) i Pictures of two E1-1 leaves cleared with ethanol showing large number of trichomes, B) ii and B) iii showing close up view of venation in cotyledons of E1-1 where the leaf veins are formed asymmetrically around the mid rib. C) i Pictures of two leaves of E2-5 cleared with ethanol showing increased number of trichomes, C)ii and C)iii close up view of venation in cotyledons of E2-5 where the leaf veins are not formed symmetrically around the mid rib, C) iv and C) v lower leaf impression of E2-5 where stomata seems to aggregate in close proximity.

On the other hand, under short day condition (8D/16N) the onset of flowers in IZS 288 started earlier than the wild-type. It appeared as if the vegetative stage of IZS 288 was cut short in order to transit to the reproductive stage and for this transition IZS 288 did not require the classical long day condition (Fig. 3.33).

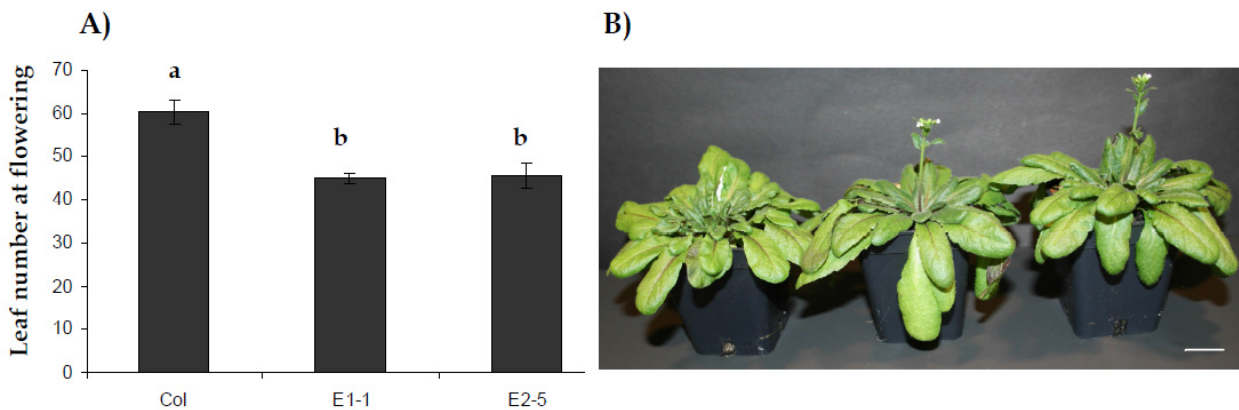


Figure 3.33. A) Number of leaves at the time of flowering in Col-0 and IZS 288 under short day condition, B) Pictures of Col-0 and IZS 288 that have already sated flowers, white bar represent 3 cm.

Results

In the aim of establishing a connection for the defects in auxin response of IZS 288 and its hypersensitivity towards Zn and chilling, Col-0 and IZS 288 seeds were cultivated on agar plates treated with a combination of Zn and auxin (2, 4-D) or Zn and NPA (the auxin transport inhibitor) and placed under optimal temperature (23°C) or under chilling temperature (4°C). Based on the growth response of Col-0 towards Zn stress under chilling condition and in the presence or absence of auxin, chilling temperature (4°C) appeared to have amplified the Zn toxicity, whereas auxin down played the negative effect of Zn stress. However, NPA did not have a significant impact on Zn stress under both temperatures regimes (Fig. 3.34). Moreover, Zn tolerance test conducted on well established auxin response mutants (i.e. *aux-1*, *tir1-1* and *eir1*), chilling hypersensitive mutants (i.e. *hos1*, *sar1* and *sar3*), ABA insensitive mutant (*aba-1*) and *sinat2* (a mutant with a defect in the ring ubiquitin ligase) identified Zn hypersensitivity phenotype in *aux-1* which is an auxin influx transporter. This observation further strengthened the interconnection between Zn and auxin signaling (Tab. 3.5 and Fig 3.35).

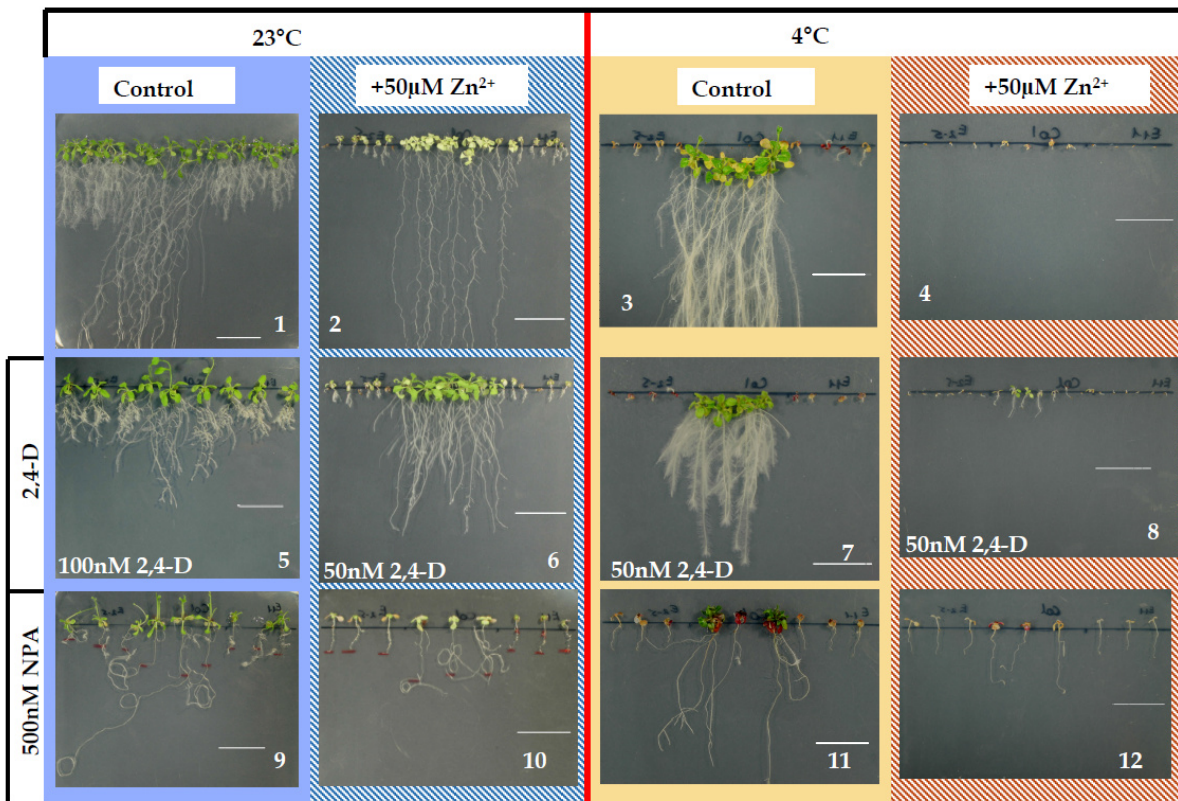


Figure 3.34. Systematically arranged pictures of agar plates with different treatments, as the number progress from left to right the stress effects got intensified. Particularly **picture 4** depicts the strongest effect on both Col-0 and IZS 288 caused by the combination of Zn and chilling temperature. **Picture 8** shows the minimizing effect of auxin on the combined stress effect of Zn and 4°C. **Pictures 9-12** show the NPA effect. On the NPA experimental set up seedlings were transferred to agar plates with treatments after 4th day of germination and under all conditions tested NPA did not have a significant impact on Zn stress. NPA has been reported to promote root looping (Buer et al., 2003), here also as it can be seen on **picture 9** and **10** WT roots were forming loops which is caused by the disruption of proper auxin signaling.

Table 3.5 List of known mutants tested for Zn hypersensitivity

Name	Description of the mutated gene	Zn hypersensitive
aux-1	an auxin influx carrier	Yes
eir1(PIN2)	an auxin efflux carrier	No
tir1-1	an auxin receptor that mediates auxin-regulated transcription	No
sar1	putative nucleoporin (NUP160)	No
aba-1	Encodes gene involved in the biosynthesis of abscisic acid (ABA)	No
sar3	putative nucleoporin (NUP96)	No
hos1	E3 ubiquitin ligase	No
sinat2	Encodes a RING finger domain	No

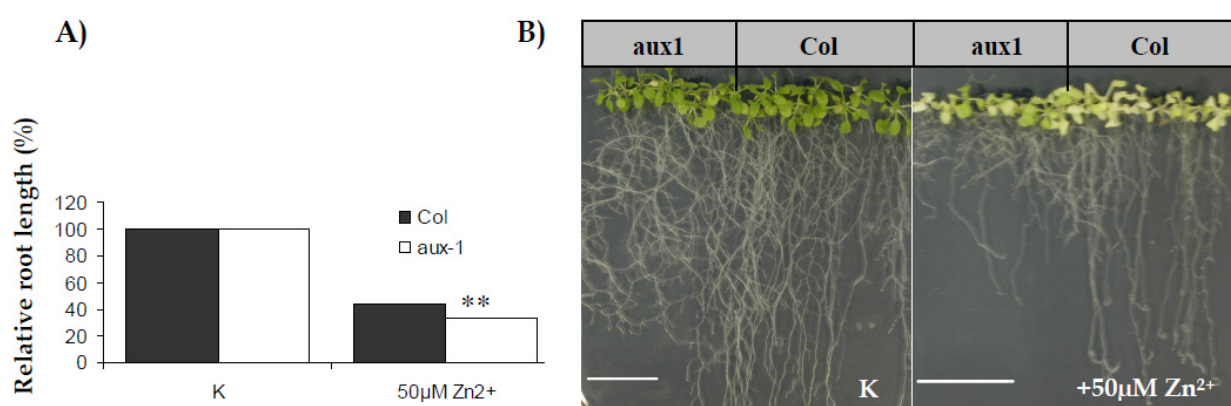


Figure 3.35. A) Relative root length of aux-1 in the presence of Zn stress. B) Pictures of agar plates with and without Zn on which Col and aux-1 seedlings are growing- white bars represent 2 cm. Gravitropic response of aux-1 is greatly compromised

3.2.3 Genetic mapping of IZS 288

To isolate the IZS 288 gene, a map-based cloning strategy was implemented. Following the principle of linkage mapping (i.e. the closer a gene and a molecular marker are located to one another on a chromosome, the greater the chance that they will be inherited together as a unit) the genetic locus of IZS 288 was identified by means of scoring recombination events in the mapping population. The mapping population was derived through crossing IZS 288 with that of the Ler-0 ecotype. Since IZS 288 has Col background, the number of recombination events is equivalent to the number of times the Ler-0 ecotype is found on a chromosome. This means, as the recombination frequency scored by a molecular marker gets smaller and smaller the closer it gets towards the location of the mutated gene. Accordingly, after analyzing 907 individual F₂ plants the mutation was found to map on chromosome two between the CAPS marker Thy1 and the SSLP marker NGA361. Subsequent fine mapping using novel SNP markers further narrowed the genomic window of the mutation into 44.918

Kbp, which lay between the per1339 markers (located at 8,775,325bp) and per19577 (located at 8,820,243bp) within a contig of two bacterial artificial chromosome (BAC) clones (F11A3 and T13C7). 14 candidate genes located in this region were sequenced using genomic DNA of IZS 288 plants as a template. Subsequent sequence analysis revealed a single nucleotide substitution (G^{1156} to A^{1156}) in the coding sequence of the AT2G20330 gene. This substitution resulted in the replacement of a conserved amino acid namely threonine at position 377 (T^{377}) by an isoleucine (I^{377}) residue (Fig.3.36).

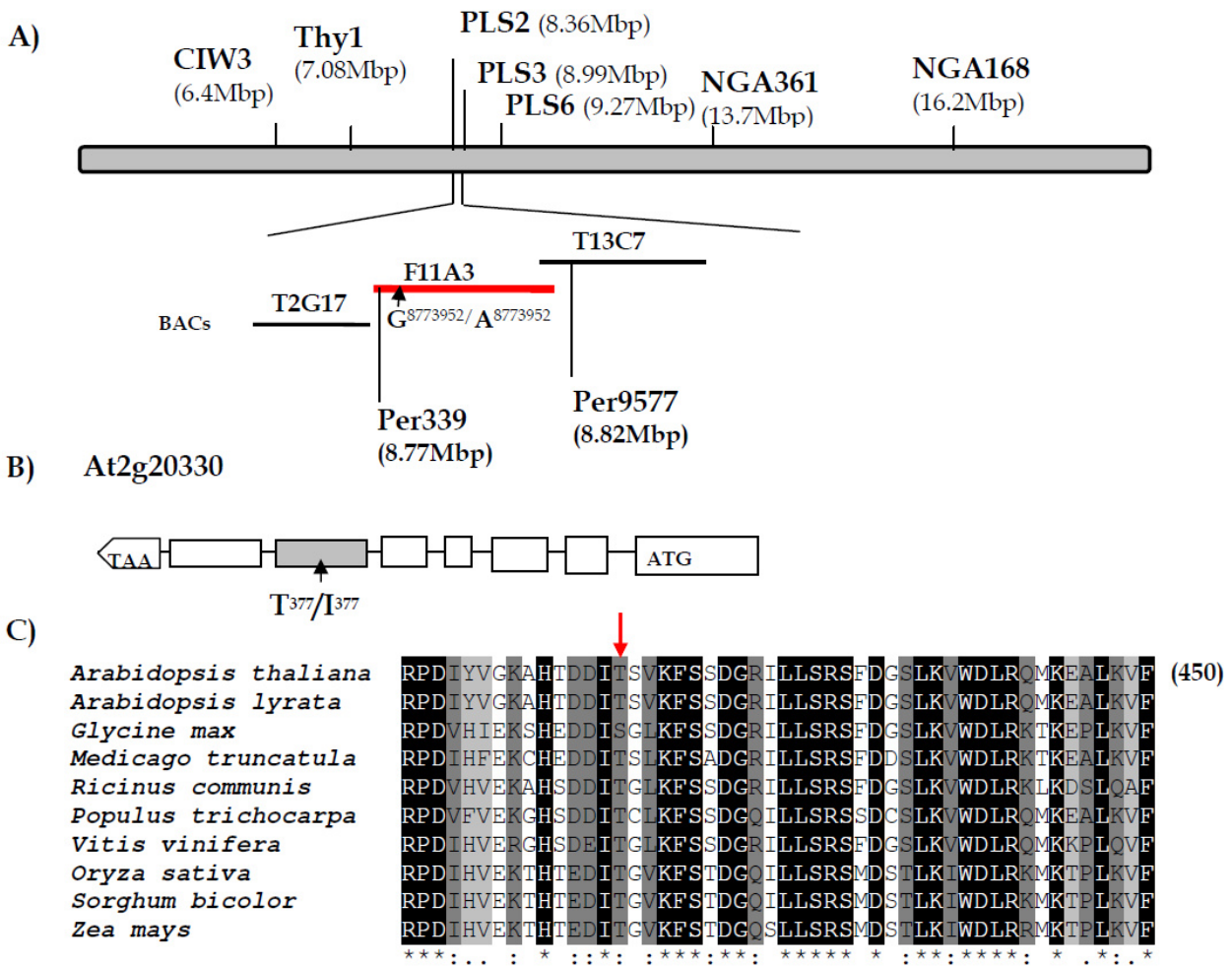


Figure 3.36. Positional cloning of IZS 288. **A)** Genetic mapping of IZS 288 using commercially available PCR-based markers. Genetic region where the mutation is located is represented by a contig of three BAC clones (T2G17, F11A3 and T20). Numbers in brackets represent location of a marker on the chromosome. **B)** Diagrammatic representation of the gene At2g20330 which is composed of 8 exons. Exons and introns are represented by filled boxes and lines, respectively. IZS 288 carries missense mutation in the sixth exon where it led to the substitution of the 377th amino acid (threonine) by isoleucine. **C)** Multiple sequence alignment of the closest 10 homologous genes of At2g20330 (At2g20330, ARALYDRAFT_900383, Gmx_100815380, MTR_7g098900, RCOM_0541360, POPTR_573381, Vvi_9819, osa_4348832, SORBI_01g019930 and zma_100280725), red arrow indicates the amino acid that is mutated in IZS 288.

Results

Furthermore, to ascertain the Zn hypersensitivity of IZS 288 resulted from the mutation of At2g20330, a complementation experiment was set up on IZS 288 using the WT At2g20330 gene under the control of its own promoter as well as the coding sequence of At2g20330 under the control of the cauliflower mosaic virus promoter (35S:At2g20330). Both constructs were able to restore WT phenotypes in IZS 288. This confirmed that the IZS 288 phenotypes were caused by the mutation in the At2g20330 gene (Fig.3.37).

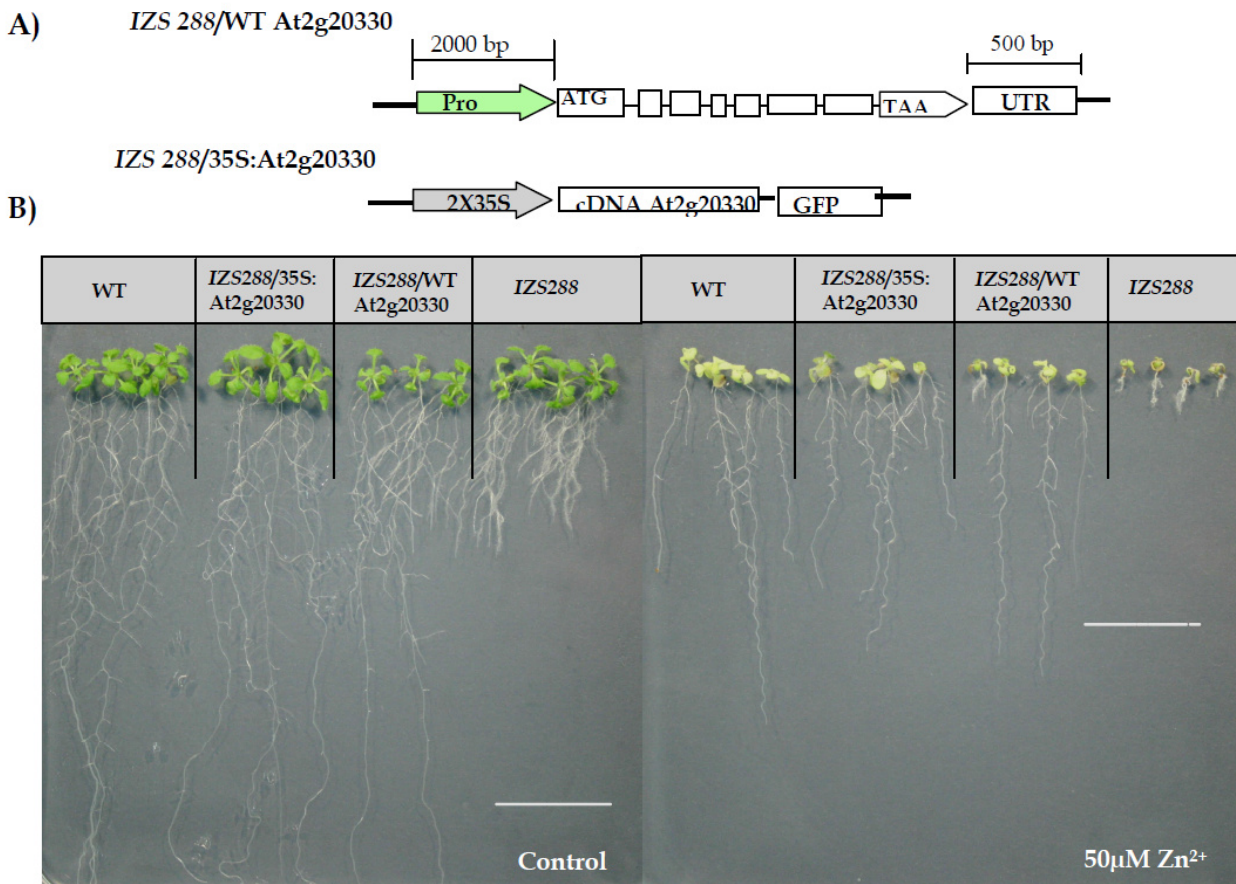


Figure 3.37. Complementation test using genomic fragment and cDNA of At2g20330 under 35S promoter. **A)** Diagram of constructs used for the complementation assay. Exons and introns are represented by filled boxes and lines, respectively. **B)** Pictures of agar plates with and without Zn on which WT, IZS 288 and the two transgenic lines carrying the complementation constructs are growing. As it can be seen both the short root phenotype as well as the Zn hypersensitivity was restored. White bars represent 2cm.

In order to identify additional mutant alleles for the At2g20330 gene, three different T-DNA insertion lines (namely SALK_140479, SALK_038590 and SALK_065643) were obtained from the SALK T-DNA insertion collection (Alonso et al., 2003). The reported T-DNA insertion site in the SALK_140479 line was in the first exon of the gene (i.e. 10 bp downstream of the start codon); whereas in lines SALK_065643 and SALK_038590 it was in the promoter (i.e. 213bp upstream of the start codon) and 3' untranslated region of the gene (i.e. 296 bp down stream

of the stop codon), respectively (Fig. 3.38). Homozygous T-DNA insertion mutants were sought-after through PCR screening using a combination of gene specific primers and a T-DNA left border-specific primers. The gene specific primers were designed in such a way that the forward and reverse primers flanked the T-DNA insertion site, thus a PCR product was formed only when there is no T-DNA insertion. In homozygous T-DNA insertion lines a PCR product is detected using the reverse gene specific primer and a left border T-DNA primer. Heterozygous lines (i.e. insertion in one of the pair chromosomes) would form both the WT PCR product and T-DNA insertion PCR product. On the first round of PCR screening carried out on 10 plants taken from each SALK lines no homozygous T-DNA insertion lines were detected (Fig. 3.39a). Assuming homozygous mutations in the *At2g20330* gene might lead to embryo lethality; siliques from 3 individual plants from each SALK line were examined for aberrant embryo development. Since in *Arabidopsis* embryos within a single silique develop approximately at the same rate, individual embryos with aberrant development can be easily scored (Errampalli et al., 1991), however in case of all three SALK lines under investigation no such aberrant embryo development was observed (data is not included here). Subsequently, extensive screening was carried out on additional 30 individuals of the SALK_140479 line (given that SALK_140479 line has the T-DNA insertion in the first exon of *At2g20330*, it is more likely to show stronger effect) and also a second gene specific primer pair obtained using the SALK institutes T-DNA primer design tool (<http://signal.salk.edu/tdnaprimers.2.html>) was included in the analysis. However, contradicting results were attained; where the analysis using the first pair of gene specific primers did not detect any homozygous lines, the second gene specific primer pair identified 7 individual plants as homozygous lines (Fig. 3.39 b).

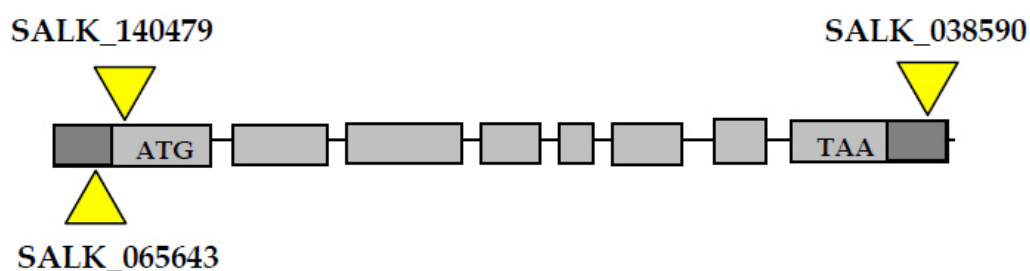
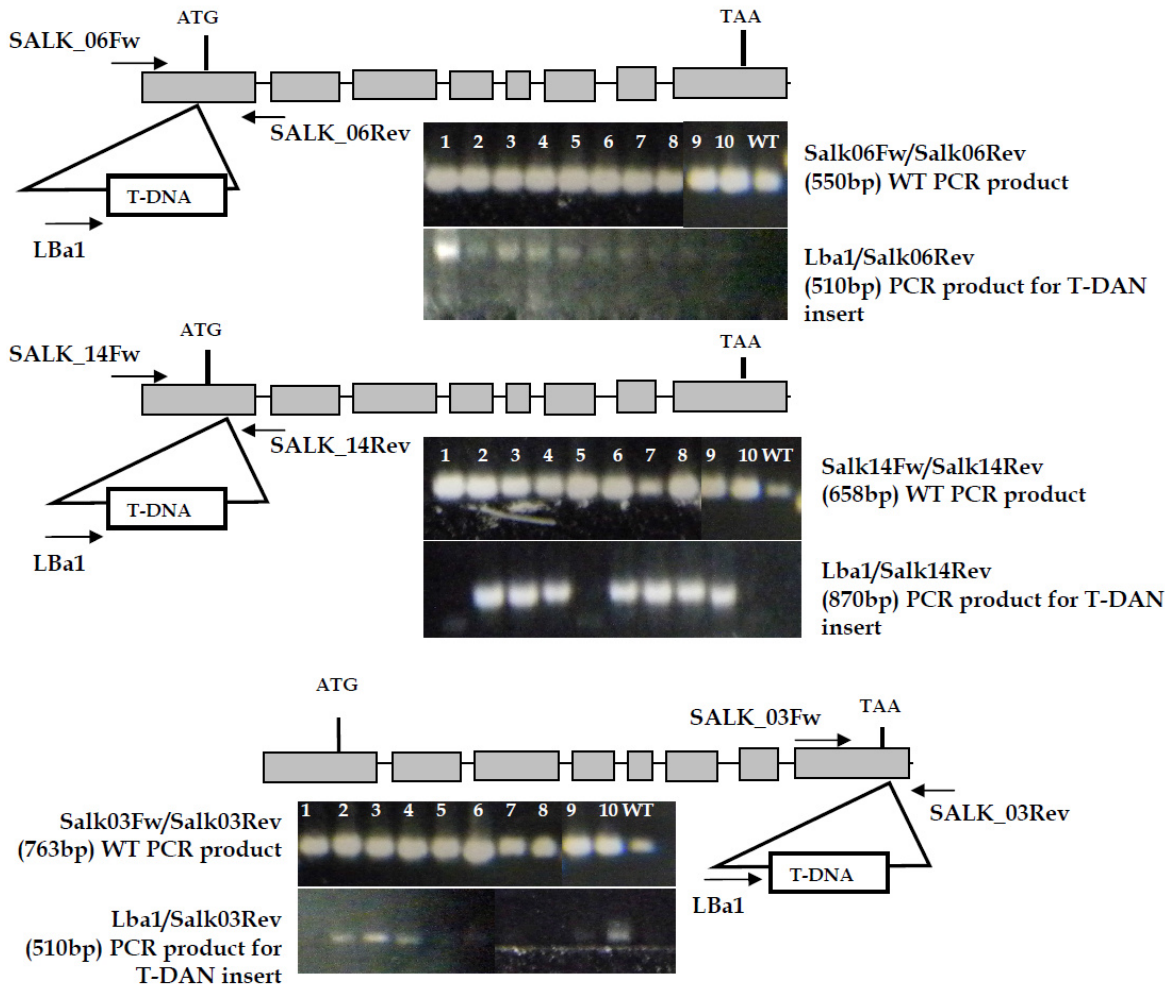


Figure 3.38. A) Schematic structure of *At2g20330* gene and inserted T-DNA. Exons and introns are represented by filled boxes and lines, respectively. T-DNA insert is not drawn to scale. The T-DNA insertion site in the SALK_065643 line is in the promoter region (i.e. 213bp upstream of the start codon), in SALK_140479 line it is in the first exon (i.e. 10bp down stream of the start codon) and in SALK_038590 line it is in the UTR region (i.e. 296 bp down stream of the stop codon).

A)



B)

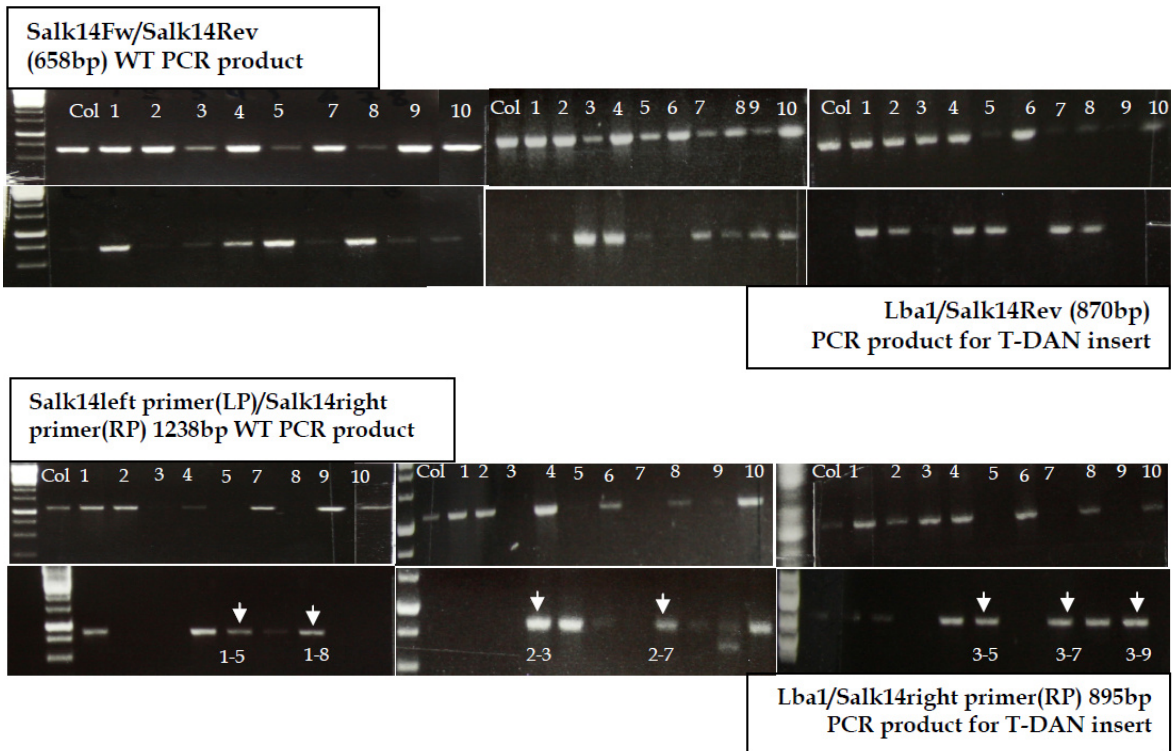


Figure 3.39. A) Picture representation of gene specific primers for each T-DNA insertion lines and gel picture of PCR screening on 10 individuals of each lines. B) Gel pictures of PCR screening on additional 30 individuals of SALK_140479 line. White arrows indicate putative homozygous lines identified by the second primer pare in test.

Results

In order to detect the effect of the T-DNA insertion on the integrity of the genomic sequence surrounding the insertion site, the transcript abundance of At2g20330 in four putative homozygous lines was quantified using quantitative real time PCR (qRT-PCR). Despite the fact that, within the genomic sequence the T-DNA insertion site and the binding site of the RT-PCR primers were further apart, no apparent difference in transcript level was observed among the WT and the four putatively homozygous lines (Fig. 3.40 a).

In a different approach, all three T-DNA insertion lines were crossed with one of the IZS 288 backcross lines (i.e. E1-1) and the first generation seeds were observed for possible phenotypes. In SALK_140479 and SALK_038590 lines, 33% (7 out of 21 individuals) and 43% (6 out of 14 individuals) of the F1 progenies respectively failed to germinate. These observations further supported the notion that complete knockout of the WD40 gene can cause embryo lethality. However, the ratio of non-germinated to germinating F1 seeds failed to accurately demonstrate Mendel's Law of Segregation (Fig. 3.40 b).

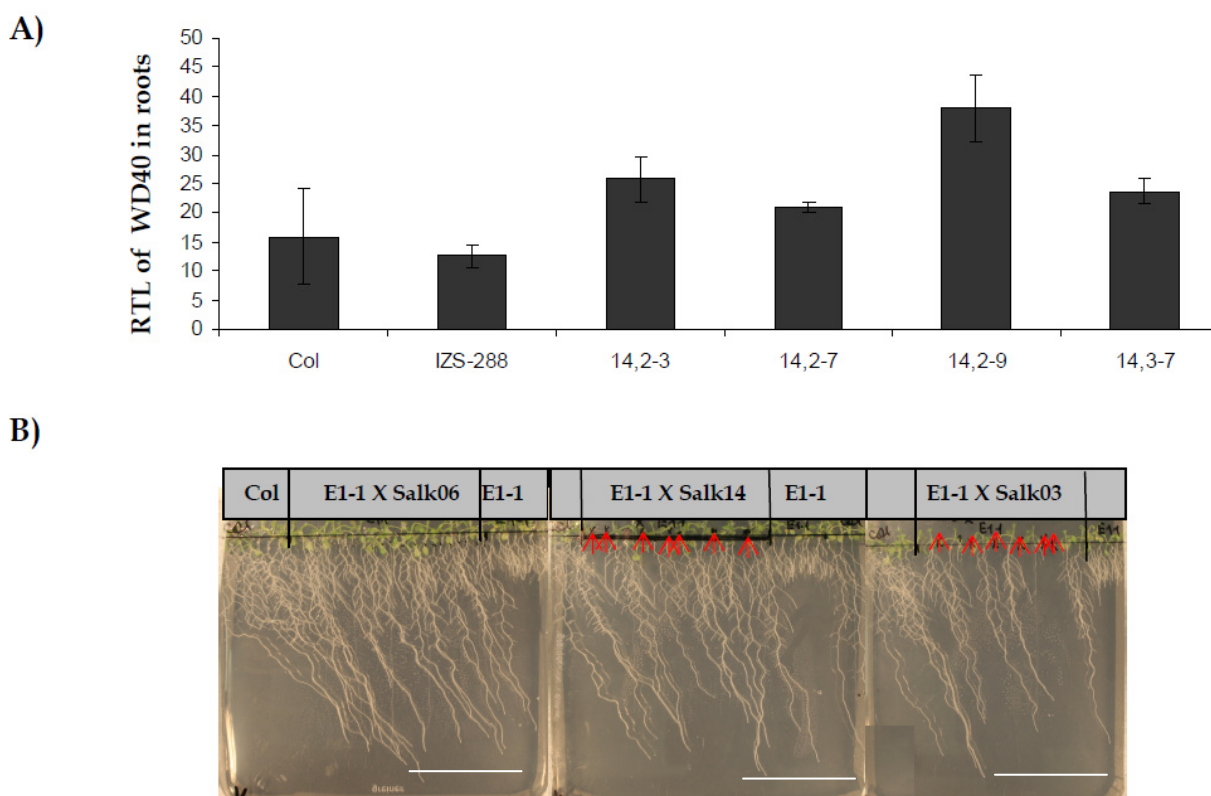


Fig 3.40. A) Relative transcript levels (RTL) of the WD40 gene in roots of WT, IZS 288 and three putative homozygous T-DNA insertion lines (i.e. Salk14 2-3, 2-7 and 3-7) and one heterozygous line (2-9). RTL values are arithmetic means of three independent experiments and bars represent standard deviation. **B)** Pictures of agar plates with first generation progenies of a cross between E1-1 and three independent T-DNA insertion lines. Red arrows indicate seeds that failed to germinate. The ratio of non-germinated seeds in Salk14 line was 7/21 and in Salk03 line it was 6/14. However in Salk06 line no such effect was observed. White bars represent 2cm.

3.2.4 Functional analysis and subcellular localization of the novel WD40 protein

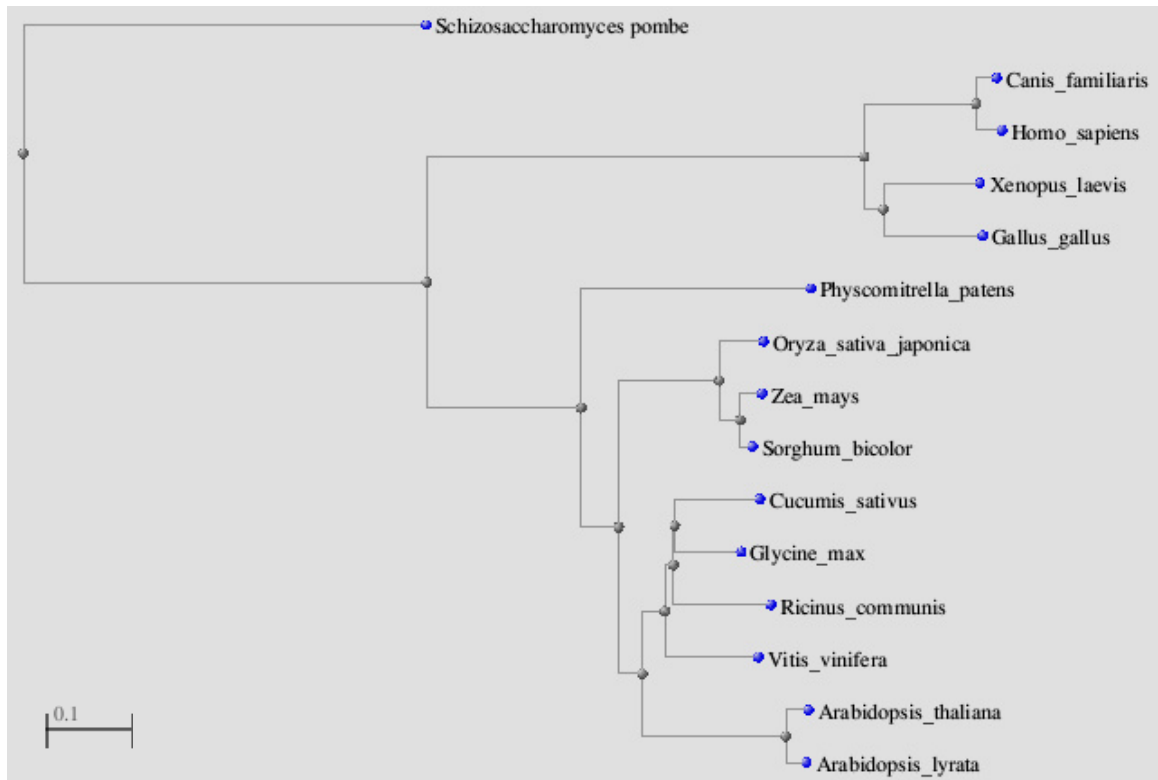
The At2g20330 gene is a member of WD40 protein family. WD-40 repeat (also known as beta-transducin repeat) proteins got their name from ~40 amino acid motifs that often terminate in a tryptophan (W) - aspartic acid (D) dipeptide. WD40 repeats usually assume a 7-8 bladed beta-propeller fold. The WD40 protein family is a large protein family found in all eukaryotes. Members are implicated in a variety of functions ranging from signal transduction and transcription regulation to cell cycle control and apoptosis. Repeated WD40 motifs act as a site for protein-protein interaction, and proteins containing WD40 repeats are known to serve as platforms for the assembly of protein complexes or mediators of transient interplay among other proteins (<http://www.ebi.ac.uk/interpro/>).

The homologs of At2g20330 are found in a range of organisms from yeast (*Schizosaccharomyces pombe*) to plants and human (Fig.3.41). Moreover, there is a single orthologous gene per species and no paralogs within a species can be detected (Penkett et al., 2006). However, in *Arabidopsis thaliana* as well as in most other species the function of this gene is not yet described. Among the very few that have been functionally characterized is the homologous gene in *Caenorhabditis elegans* known as gastrulation defective (*gad-1*), which is required maternally for gastrulation initiation during early embryogenesis (Knight and Wood, 1998). Since information regarding At2g20330 and putative orthologs was quite limited, it was useful to determine functionality of the gene in other model eukaryotic organisms. For this purpose three RNAi (RNA-mediated gene interference) lines, namely VDCR_27457, VDCR_106320 and VDCR_41441 carrying constructs that target the *Drosophila melanogaster* homolog (CG5543), were obtained from the Vienna *Drosophila* RNAi center (<http://stockcenter.vdrc.at>). The genome-wide library of *Drosophila melanogaster* RNAi transgenes carry short gene fragments cloned as inverted repeats expressed using the binary GAL4/UAS system enabling the conditional inactivation of gene function in specific tissues of the intact organism (Dietzl et al., 2007). Progenies of crosses set up between the three RNAi lines and five different GAL4 driver lines kindly provided by Dr. Stefan Heidmann showed different RNAi phenotypes. Among the five driver lines three drivers activate the expression of a hairpin RNA (hpRNAs) in the eye (i.e. *eyeless-GAL4* (*ey-GAL4*), *glass multiple reporter-GAL4* (*gmr-GAL4*) and *sevenless-Gal4* (*sev-GAL4*)), one driver has a wing directed expression (i.e. *MS 1096-GAL4*) and the last driver has ubiquitous expression (i.e. *daughterless-GAL4* (*da-GAL4*)). Two of the UAS-RNAi transgenes (VDCR_27454 and VDCR_106320) when

Results

expressed under the control of the *da-GAL4* driver caused a lethal phenotype, whereas when expressed under the control of the *ey-GAL4* driver resulted in a “missing eye” phenotype. In the case of *MS 1096-GAL4* driver that has “X” linked expression showed strong wing deformity in all hatched female flies. In the third UAS-RNAi line (VDCR_41441) sterile female flies were hatched when expressed under the control of the *da-GAL4*, but no visible phenotype was detected when the hairpin RNA was activated by the *ey-GAL4* driver and *MS 1096-GAL4*. Meanwhile, the remaining two GAL4 drivers (*sev-GAL4* and *gmr-GAL4*) did not create any visible phenotypes in all three RNAi lines (Tab. 3.6). In short the knock-down of the CG5543 gene (a homolog of the *Arabidopsis* At2g20330 gene) led to lethal or semi-lethal (sterile progeny) phenotype when expressed under the control of a driver with ubiquitous expression.

A)



B)

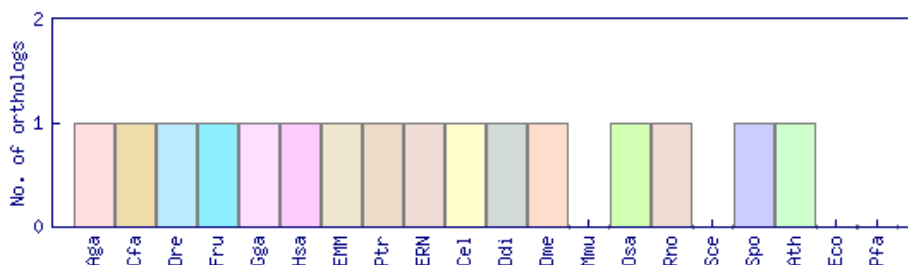
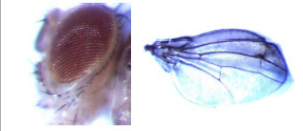
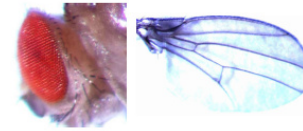
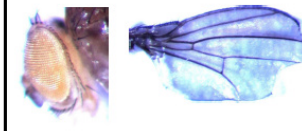
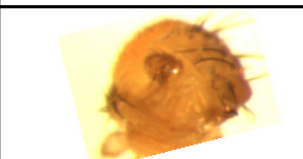
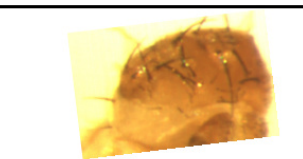
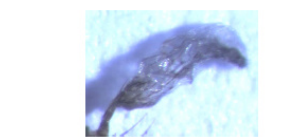


Figure 3.41. A) Phylogenetic tree showing AT2G20330 and 14 putative orthologs. Multiple protein sequence alignment was created using COBALT (Papadopoulos and Agarwala, 2007). B) Phylogenetic pattern representing different orthologs of AT2G20330. In each genome no paralogs were detected. Orthologous proteins were retrieved using YOGY (Penkett et al., 2006).

Table 3.6 Three RNAi lines in *Drosophila melanogaster* expressed under the control of five different drivers. The first row represents the characteristic feature of the parental lines. The third row, in case of the first two lines, shows a missing eye on a detached head. The fifth row carries pictures of severely deformed wings from female files.

	<i>RNAi lines</i>		
	VDRRC 27454	VDRRC 106320	VDRRC 41441
<i>Parents</i>			
<i>da-GAL4</i>	Lethal	Lethal	Sterile progeny
<i>ey-GAL4</i>			WT
<i>sev-GAL4</i>	WT	WT	WT
<i>gmr-GAL4</i>	WT	WT	WT
<i>MS1096-GAL4</i> (<i>X-linked</i>)	 (Only in female)	 (Only in female)	WT

Beyond the established structural homologs of At2g20330, an experiment was conducted to identify a possible functional homology using the *Xenopus laevis* WDR70 gene (i.e. putative orthologous gene). Inferred from EST profiles the WDR70 gene in *Xenopus* shows higher level of expression in the testis and at early embryonic development (i.e. at gastrula stage) (<http://www.xenbase.org>). Similarly, in *Arabidopsis* AT2G20330 shows higher level of expression in mature pollen grains and imbibed seeds (<https://www.genevestigator.com>). Therefore, an attempt was made to rescue the mutant phenotype of IZS 288 using the *Xenopus* WDR70. A construct (i.e. 35S:XlaWDR70) was created using the coding sequence of *Xenopus* WDR70 (kindly provided by Prof. Dr. Olaf Stemmann) under the control of the cauliflower mosaic virus promoter. However transgenic plants carrying this construct did not show rescuing of the mutant phenotype of IZS 288 (Fig. 3.42).

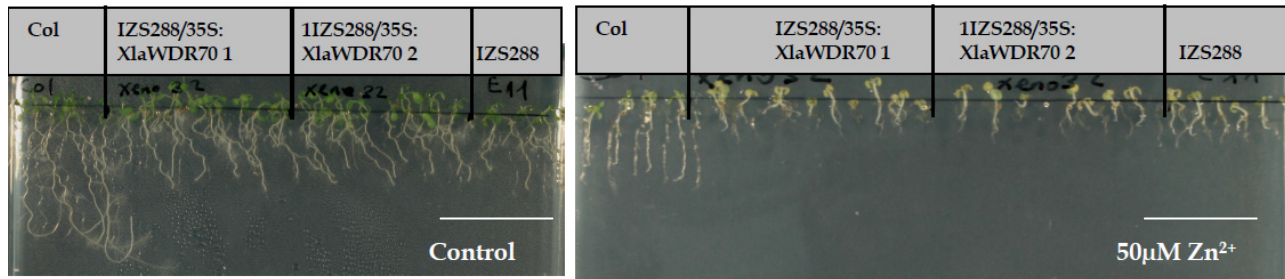


Figure 3.42. Pictures of agar plates, with and without Zn treatment, on which transgenic lines (in IZS 288 background) carrying a construct containing cDNA XlaWDR70 under the control of 35S promoter and the WT Colombia as well as IZS 288 were growing. White bars represent 2cm.

One distinctive feature about the missense mutation that occurred in IZS 288 (i.e. the 377th threonine was replaced by isoleucine) was that the replaced threonine belongs to a group of amino acids predicted as phosphorylation sites in the protein (<http://phosphat.mpimp-golm.mpg.de/>). Therefore, the observed phenotypes of IZS 288 could have been caused by disruption in the phosphorylation state of the protein caused by loss of a particular phosphorylation site. In order to test this hypothesis, two point mutations were introduced into the genomic sequence of At2g20330 that created two alternative constructs. In the first construct where the 377th threonine is substituted by serine (T377S) the protein is presumed to maintain its phosphorylation site. In the second construct where alanine is substituted for the 377th threonine (T377A), the protein is believed to keep its overall structure intact but lose the ability to be phosphorylated at this particular site. This construct serves as a negative control for the hypothesis that proposes disruption of the phosphorylation state of the protein as a reason for the phenotypes of IZS 288. Homozygous transgenic lines (in IZS 288 background) carrying either one of the two constructs were tested for phenotypic rescue. However, both constructs were able to rescue the short root and Zn hypersensitivity phenotypes of IZS 288 (Fig. 3.43). Therefore, it is less likely that the effects of the IZS 288 mutation are due to loss of a phosphorylation site.

Results

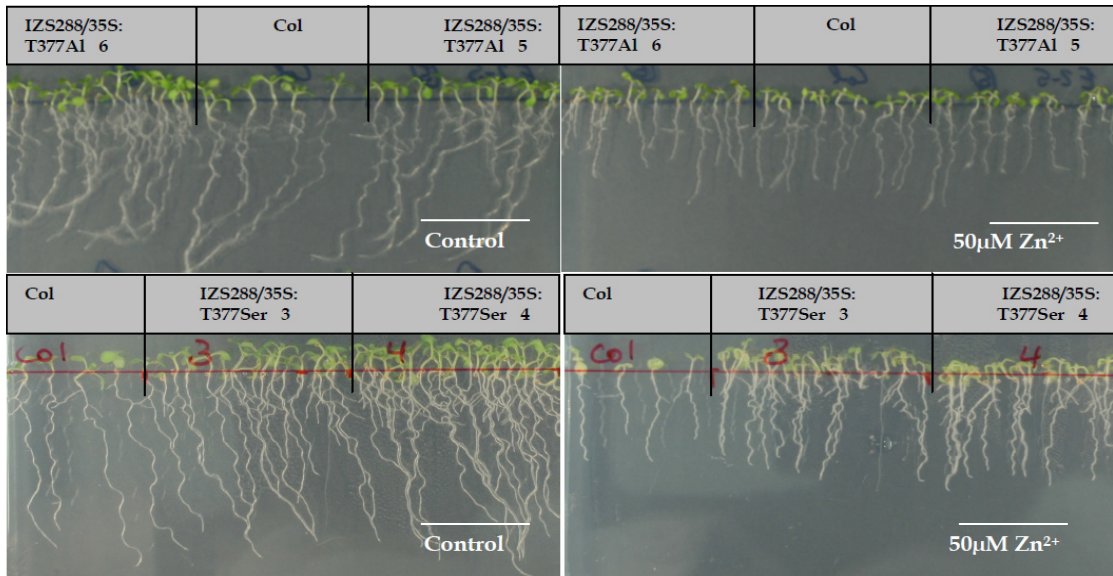


Figure 3.43. Picture of agar plate with and without Zn treatment on which transgenic lines (in IZS 288 background) carrying a construct made of cDNA At2g20330 with T377Ala and T377Ser substitutions under the control of 35S promoter and the wild type Col were growing. White bars represent 2cm.

Meanwhile, the localization of the IZS 288 protein was investigated using a transgenic line that was used in the complementation assay (i.e. 35S:At2g20330 in IZS 288 background). In this transgenic line the cDNA of At2g20330 was expressed under the promoter of the cauliflower mosaic virus (35S), and had green fluorescent protein (GFP) fused in frame to its C terminus. The detected GFP signal colocalized with that of the DAPI signal coming from the nucleus. Therefore, based on this observation subcellular localization IZS 288 protein is in the nucleus (Fig.3.44).

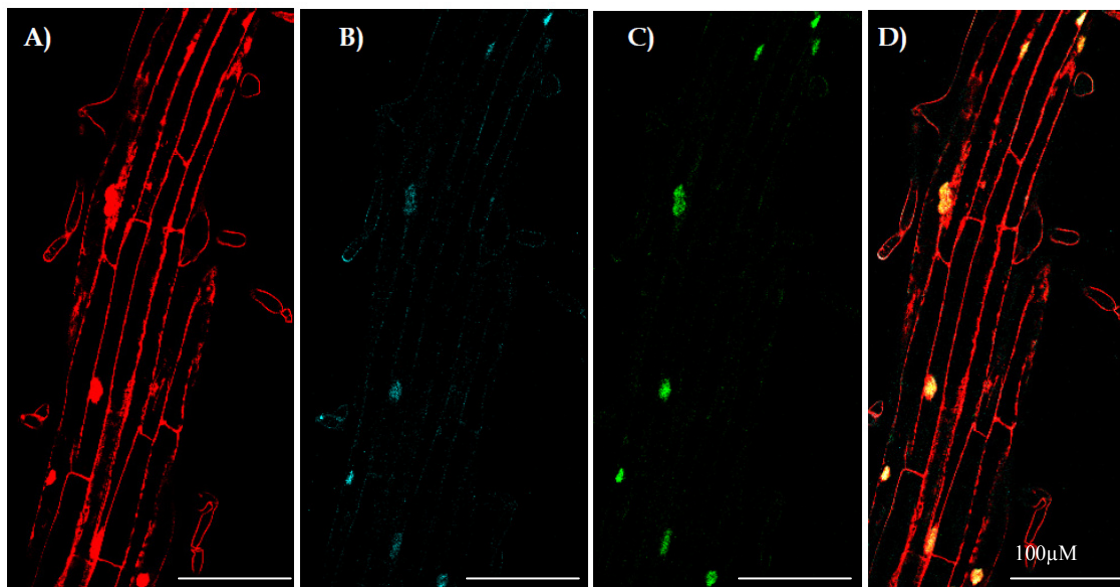


Figure 3.44. Root cells under confocal microscope A) Propidium iodide staining of root tissue, B) DAPI staining of the same root tissue shown in panel A, C) At2G20330-GFP signal of the same root tissue shown in panel A, D) Merged image of panels A, B, and C. Note that the GFP signal colocalizes with the DAPI signal in the nucleus.

3.2.5 Microarray analysis

To determine the effect of the IZS 288 mutation on global gene expression, a microarray experiment was carried out on hydroponically grown 4-week-old roots of IZS 288 and wild-type plants. In parallel, a group of plants were exposed to chilling stress (4°) for 24 hours in order to compare the transcript levels of the two genotypes under chilling stress.

The comparative transcriptome of the two genotypes under optimal growing condition identified 183 genes that showed statistically significant alteration of transcript levels i.e. exceeding a 2-fold difference threshold and adjusted P-value cutoff of 0.05. Among these differentially expressed genes the three most up-regulated genes in IZS 288 were: starch biosynthesis gene QUA-QUINE (QQS) (AT3G30720), ankyrin repeat-containing protein (AT5G50140) and CC-NBS-LRR class disease resistance protein (At5g43730); whereas the three most down-regulated genes were thioredoxin H8 (AT1G69880), RPM1-interacting protein 4 (RIN4) (AT3G48450) and Core-2/I-branching beta-1,6-N-acetylglucosaminyltransferase family protein (AT1G10880). For further investigation these differentially expressed genes were clustered into 5 groups using K-mean clustering algorithm and the resulting gene lists were analyzed for significantly enriched GO terms using Gene Ontology Enrichment Analysis Software Toolkit (GOEAST) (Zheng and Wang, 2008) and with adjusted p value (false discovery rate (FDR) cut off 0.05.

In addition to the expression difference between the two genotypes at optimal growing condition, peculiar character of the genes included in the first cluster was they showed chilling stress induced expression only in WT roots. These genes are mainly involved in three biological processes: *oxidation-reduction process*, *sulfur assimilation* and *triterpenoid metabolic process*. The second cluster consisted of genes that are constitutively active in WT but not in IZS 288. *Oxidation-reduction process* was the only biological process enriched in this group. The third cluster contained genes that showed chilling stress induced expression only in IZS 288 roots. This group included genes that take part in *responses to wounding*, *chitin*, and *jasmonic acid stimulus*. Two cold acclimation genes ZAT12 (AT5G59820) and LTI30 (AT3G50970), were also found in this group. The unique feature of the genes in the fourth cluster was that they showed lower level of transcript abundance in WT at optimal growing conditions. The main biological process represented in this group is *innate immune response* and the molecular function of *transmembrane signaling receptor activity*. The fifth cluster is

made up of genes that were constitutively active only in IZS 288 at optimal growth condition. Genes included in this group are mainly involved in *programmed cell death (apoptotic) process*. Additionally, in this group five (i.e. AT5G43040, AT3G46800, AT5G02350, AT5G02360, AT4G02540) Zn binding, cysteine/histidine-rich C1 domain-containing proteins were included that perform protein-disulfide reductase activity (Fig. 3.45 and Tab. 3.7).

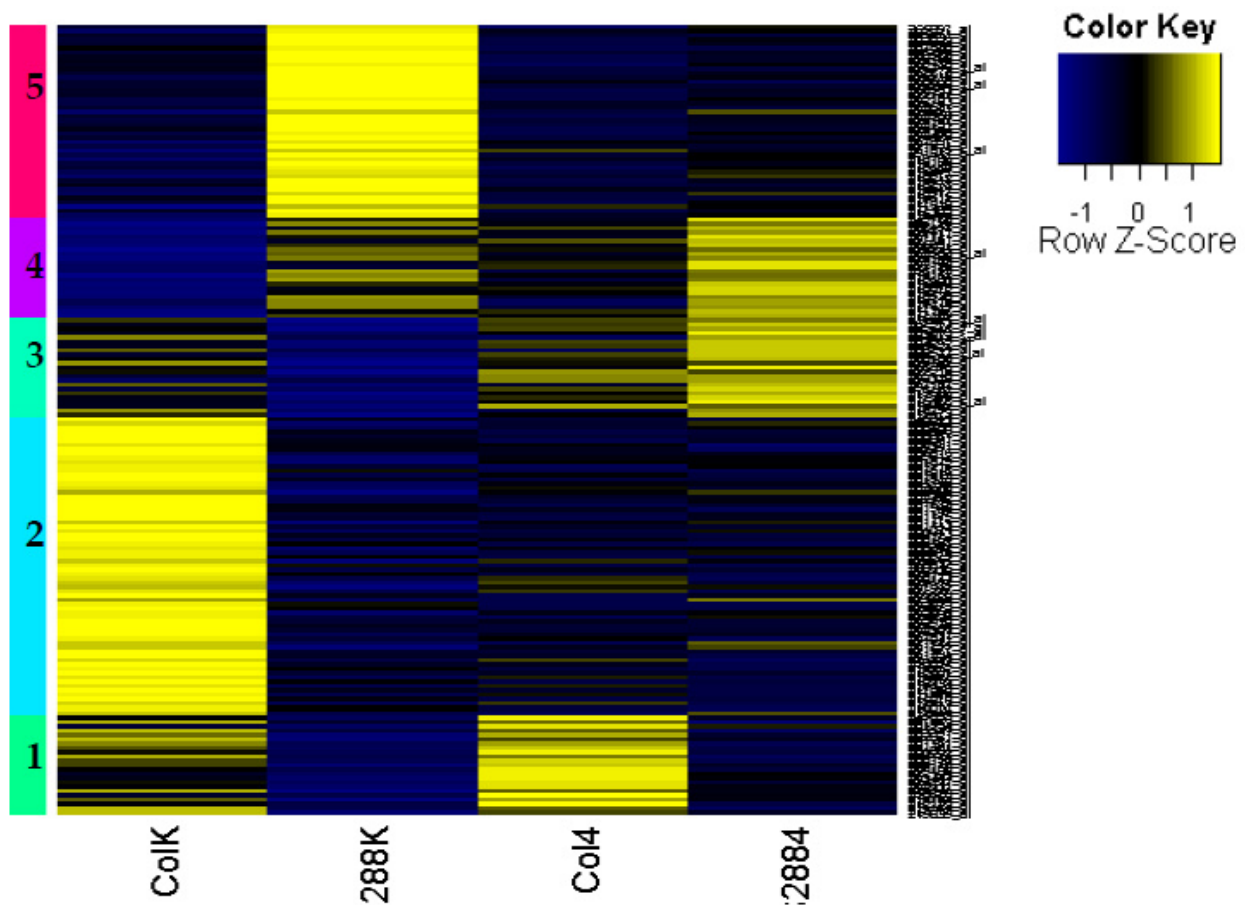


Figure 3.45. Heat map of scaled expression values of 183 genes that are differential expressed in IZS 288 roots at optimal growing condition compared to WT roots and clustered into five groups by K-mean algorithm using the Pearson correlation coefficient as the distance metrics. The average of three unlogged expression values for each genotype and stress condition were used (i.e. ColK represents the average transcript level of three replicates of WT at optimal growing condition, whereas Col4 represents the average transcript level after 24 hour chilling (4°) stress. The same is true for 288K and 2884).

Results

Table 3.7. Highly enriched gene ontology terms in 183 genes that were differential expressed in IZS 288 roots at optimal growing condition and clustered into five groups by K-mean algorithm using the Pearson correlation coefficient as a distance metrics. The enrichment analysis was carried out using the Gene Ontology Enrichment Analysis Software Toolkit (GOEAST) (Zheng and Wang, 2008). The header 'level' represents the longest path connecting back to the root of the GO hierarchical tree and adjusted p value or false discovery rate (FDR) was calculated using Benjamini Yekutieli (2001) method. Cluster -1 is made up of genes that showed cold induced expression only in WT, Cluster-2 contains genes that are constitutively active in WT but not in IZS 288, Cluster-3 contains genes that showed chilling stress induced expression only in IZS 288, Cluster-4 contains genes that showed lower level of transcript abundance in WT at optimal growing conditions and Cluster-5 is composed of genes that were constitutively active only in IZS 288.

<i>Cluster-1 (23 genes)</i>	<i>Level</i>	<i>No. Genes associated to GO-ID</i>	<i>No. genes in common</i>	<i>p value</i>
sulfur amino acid biosynthetic process	9	50	3	0.00613
AT2G26400 acireductone dioxygenase 3 ARD3				
AT4G21990 5'-adenylylsulfate reductase 3 APR3				
AT2G17640 serine acetyltransferase 2, ATSRAT3;1				
oxidation-reduction process	3	1315	7	0.03181
AT2G26400 acireductone dioxygenase 3 ARD3				
AT5G48000 cytochrome P450, family 708, subfamily A				
AT4G21990 5'-adenylylsulfate reductase 3 APR3				
AT1G52790 oxidoreductase, 2OG-Fe(II) oxygenase family protein				
AT1G52820 putative 2-oxoglutarate-dependent dioxygenase				
AT1G80320 oxidoreductase, 2OG-Fe(II) oxygenase family protein				
AT2G42250 cytochrome P450, family 712, subfamily A				
triterpenoid metabolic process	7	15	2	0.02084
AT5G48000 cytochrome P450, family 708, subfamily A				
AT3G45130 lanosterol synthase ,1LAS1				
sulfate assimilation	4	14	2	0.02084
AT4G21990 5'-adenylylsulfate reductase 3 APR3				
AT2G17640 serine acetyltransferase 2, ATSRAT3;1				
Cluster-2 (63 genes)				
oxidation-reduction process	3	1315	14	0.03069
AT1G28480 Glutaredoxin-C9				
AT1G60730 NAD(P)-linked oxidoreductase-like protein				
AT1G14540 Peroxidase 4				
AT1G14290 sphingoid base hydroxylase 2				
AT3G21720 Isocitrate lyase				
AT3G46480 iron ion binding / oxidoreductase protein				
AT1G24470 beta-ketoacyl reductase 2				
AT4G37370 cytochrome P450, family 81, subfamily D				
AT1G09090 Respiratory burst oxidase homolog protein B				
AT5G06900 cytochrome P450, family 93, subfamily D				
AT1G60750 auxin-induced atb2-like protein				
AT1G09420 Glucose-6-phosphate 1-dehydrogenase 4 (G6PD4)				
AT3G14660 cytochrome P450, family 72, subfamily A				
AT1G14550 Peroxidase 5				
Cluster-3 (23 genes)				
response to hormone stimulus	4	944	6	0.02958
AT2G40340 Dehydration-responsive element-binding 2C, DREB 2C				
AT2G47520 Ethylene-responsive transcription factor ERF071				
AT5G37260 CIRCADIAN 1, REVEILLE 2 transcription factor				
AT3G15500 NAC domain-containing protein 55, NAC3				
AT3G23250 myb domain protein 15				
AT3G50970 Dehydrin Xero 2, LTI30				

Results

response to wounding	3	145	3	0.03851
AT5G59820	C2H2-type zinc finger protein, RHL41, ZAT12			
AT5G20230	blue copper protein, BCB, SAG14			
AT1G80840	putative WRKY transcription factor 40			
cold acclimation	5	22	2	0.02946
AT5G59820	C2H2-type zinc finger protein, RHL41, ZAT12			
AT3G50970	Dehydrin Xero 2, LTI30			
response to chitin	5	120	3	0.02946
AT5G59820	C2H2-type zinc finger protein, RHL41, ZAT12			
AT5G20230	blue copper protein, BCB, SAG14			
AT1G80840	putative WRKY transcription factor 40			
response to organic nitrogen	3	992	7	0.0305
AT5G59820	C2H2-type zinc finger protein, RHL41, ZAT12			
AT5G20230	blue copper protein, BCB, SAG14			
AT1G80840	putative WRKY transcription factor 40			
response to jasmonic acid stimulus	5	154	3	0.04322
AT5G37260	CIRCADIAN 1, REVEILLE 2 transcription factor			
AT3G23250	myb domain protein 15			
AT3G15500	NAC domain-containing protein 55, NAC3			
Cluster-4 (23 genes)				
transmembrane signaling receptor activity	4	187	4	0.00883
AT5G45080	PHLOEM PROTEIN 2-LIKE A6, AtPP2-A6			
AT5G45070	PHLOEM PROTEIN 2-LIKE A8, AtPP2-A8			
AT5G51630	TIR-NBS-LRR class disease resistance protein			
AT5G45090	PHLOEM PROTEIN 2-LIKE A7, AtPP2-A7			
innate immune response	4	280	4	0.03137
AT5G45080	PHLOEM PROTEIN 2-LIKE A6, AtPP2-A6			
AT5G45070	PHLOEM PROTEIN 2-LIKE A8, AtPP2-A8			
AT5G51630	TIR-NBS-LRR class disease resistance protein			
AT5G45090	PHLOEM PROTEIN 2-LIKE A7, AtPP2-A7			
Cluster-5 (45 genes)				
apoptotic process	5	165	5	0.00601
AT5G43730	CC-NBS-LRR class disease resistance protein			
AT5G46520	TIR-NBS-LRR class disease resistance protein			
AT3G44400	TIR-NBS-LRR class disease resistance protein			
AT3G46730	Putative disease resistance RPP13-like protein 3			
AT1G15890	CC-NBS-LRR class disease resistance protein			

The second set of differentially expressed genes was identified based on comparative transcriptome of the two genotypes after being exposed to chilling stress. After chilling stress 180 genes showed statistically significant (≥ 2 -fold difference threshold and adjusted P-value cutoff of 0.05) variation of transcript level between the two genotypes. The list of genes showing the highest level of increases in IZS 288 include uridine diphosphate glycosyltransferase 74E2 (AT1G05680), sulphotransferase 12 (At2g03760) and MATE efflux family protein (AT2G04050), whereas the list of down-regulated genes with the highest fold difference include methionine sulfoxide reductase B5 (AT4G04830), sulfate transporter 1.1 (AT4G08620) and thalianol hydroxylase/cytochrome 450 708A2 (AT5G48000).

Results

After K-mean clustering of the 180 genes into five groups GO term enrichment analysis was carried out for each cluster. The first cluster consisted of genes that showed transcriptional repression due to chilling stress only in WT roots. However, statically significant enrichment of GO terms was not observed in this cluster group. The second cluster included genes that were constitutively active in both genotypes but transcriptionally repressed in IZS 288 after chilling stress. *RNA polyadenylation* was the only biological process enriched in this group. The third cluster contained genes that are constitutively up-regulated under both optimal and chilling stress condition in WT, but due to chilling stress showed transcriptional repression in IZS 288. In this group also no apparent enrichment of GO terms of biological process was observed. The fourth cluster was made up of genes that showed chilling stress induced transcriptional activation only in IZS 288. Some of the biological processes enriched in this group are *regulation of transcription (DNA-dependent)*, *regulation of cellular biosynthetic process*, particularly *regulation of RNA biosynthetic process*, and *response to ethylene stimulus*. The fifth cluster is composed of genes that showed transcriptional induction due to chilling stress in WT roots only. Genes included in this group are implicated in biological processes such as *sulfur transport*, *root development*, *cellular lipid metabolic process* and *cysteine biosynthetic process* (Fig. 3.46 and Tab. 3.8).

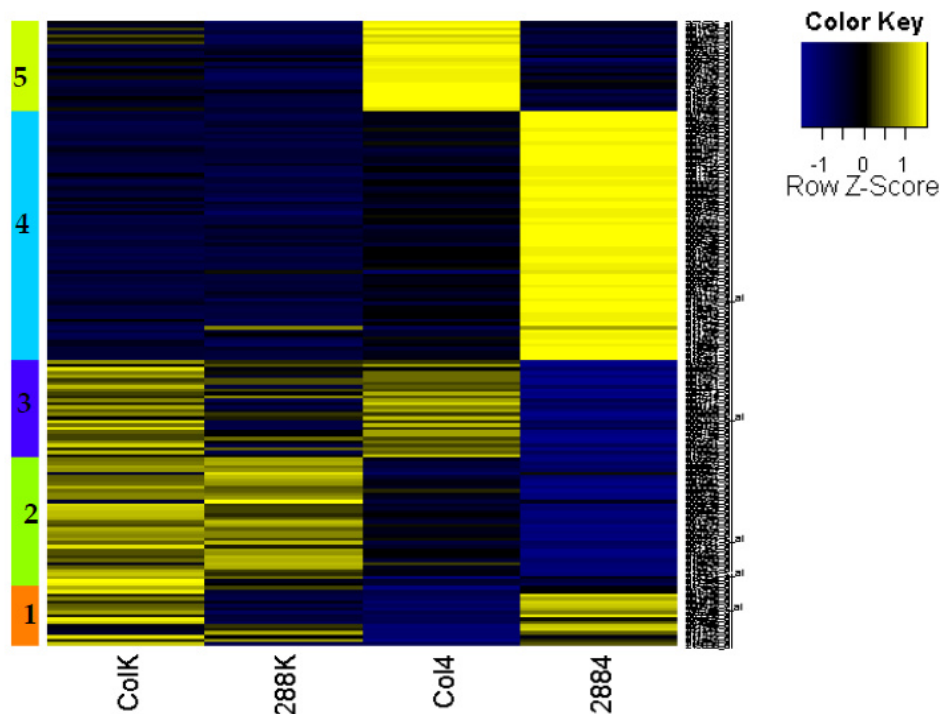


Figure 3.46. Heat map of scaled expression values of 180 genes that are differentially expressed in IZS 288 roots after 24 hours of chilling stress compared to WT roots after chilling stress and clustered into five groups by K-mean algorithm using the Pearson correlation coefficient as the distance metrics. The average of three unlogged expression values for each genotype and stress condition were used (i.e. ColK represents the average transcript level of three replicates of WT at optimal growing condition, whereas Col4 stands for the average transcript level after 24 hour chilling (4°) stress. The same is true for 288K and 2884).

Results

Table 3.8. Highly enriched gene ontology terms in 180 genes that were differential expressed in IZS 288 roots after chilling stress and clustered into five groups by K-mean algorithm using the Pearson correlation coefficient as a distance metrics. The enrichment analysis was carried out using the Gene Ontology Enrichment Analysis Software Toolkit (GOEAST) (Zheng and Wang, 2008). The header 'level' represents the longest path connecting back to the root of the GO hierarchical tree and adjusted p value or false discovery rate (FDR) was calculated using Benjamini Yekutieli (2001) method. Cluster -1 is made up of genes that showed transcriptional repression due to chilling stress only in WT roots, Cluster-2 contains genes that are constitutively active in both genotypes but transcriptionally repressed in IZS 288 after chilling stress, Cluster-3 contains genes that are constitutively up-regulated under both optimal and chilling stress condition in WT, but showed transcriptional repression in IZS 288 under chilling stress, Cluster-4 contains genes that showed chilling stress induced transcriptional activation only in IZS 288 and Cluster-5 is composed of genes that showed transcriptional induction due to chilling stress in WT roots only.

	No. Genes associated Level to GO-ID	No. genes in common	p value	
Cluster-1 (17 genes)				
No GO Terms were found significantly enriched				
Cluster-2 (37 genes)				
RNA polyadenylation	9	7	2	0.03926
AT4G32850 nuclear poly(a) polymerase, nPAP				
AT2G25850 poly(A) polymerase 2, PAPS2				
Cluster-3 (28 genes)				
No GO Terms were found significantly enriched				
Cluster-4 (72 genes)				
regulation of transcription, DNA-dependent	8	940	12	0.01008
AT1G59530 basic leucine-zipper 4				
AT3G22830 Heat stress transcription factor A-6b, AT-HSFA6B				
AT4G05100 myb domain protein 74, MYB74				
AT5G49520 Probable WRKY transcription factor 48				
AT1G44830 Ethylene-responsive transcription factor ERF014				
At4g17780 putative F-box protein				
At4g17785 Transcription factor MYB39				
AT4G25490 Dehydration-responsive element-binding 1B, CBF1				
AT4G31800 WRKY transcription factor 18				
AT3G23250 myb domain protein 15, MYB15				
AT2G23760 BEL1-like homeodomain protein 4, BLH4				
AT1G21910 Ethylene-responsive transcription factor ERF012				
AT4G28140 Ethylene-responsive transcription factor ERF054				
regulation of cellular biosynthetic process	5	1025	12	0.01226
AT1G59530 basic leucine-zipper 4				
AT3G22830 Heat stress transcription factor A-6b, AT-HSFA6B				
AT4G05100 myb domain protein 74, MYB74				
AT5G49520 Probable WRKY transcription factor 48				
AT1G44830 Ethylene-responsive transcription factor ERF014				
At4g17780 putative F-box protein				
At4g17785 Transcription factor MYB39				
AT4G25490 Dehydration-responsive element-binding 1B, CBF1				
AT4G31800 WRKY transcription factor 18				
AT3G23250 myb domain protein 15, MYB15				
AT2G23760 BEL1-like homeodomain protein 4, BLH4				
AT1G21910 Ethylene-responsive transcription factor ERF012				
AT4G28140 Ethylene-responsive transcription factor ERF054				
regulation of RNA biosynthetic process	7	940	12	0.01008
AT1G59530 basic leucine-zipper 4				
AT3G22830 Heat stress transcription factor A-6b, AT-HSFA6B				
AT4G05100 myb domain protein 74, MYB74				
AT5G49520 Probable WRKY transcription factor 48				
AT1G44830 Ethylene-responsive transcription factor ERF014				
At4g17780 putative F-box protein				
At4g17785 Transcription factor MYB39				
AT4G25490 Dehydration-responsive element-binding 1B, CBF1				
AT4G31800 WRKY transcription factor 18				
AT3G23250 myb domain protein 15, MYB15				
AT2G23760 BEL1-like homeodomain protein 4, BLH4				

Results

AT1G21910	Ethylene-responsive transcription factor ERF012				
AT4G28140	Ethylene-responsive transcription factor ERF054				
response to chitin		5	120	5	0.01008
AT5G49520	putative WRKY transcription factor 48				
AT4G31800	WRKY transcription factor 18				
AT4G28140	ethylene-responsive transcription factor ERF054				
	zinc finger AN1 domain-containing stress-associated				
AT3G28210	protein 12				
AT3G23250	myb domain protein 15				
response to ethylene stimulus		5	235	6	0.01434
AT1G68765	inflorescence deficient in abscission, IDA				
AT4G05100	myb domain protein 74, MYB74				
AT1G44830	Ethylene-responsive transcription factor ERF014				
AT3G23250	myb domain protein 15, MYB 15				
AT1G21910	Ethylene-responsive transcription factor ERF012				
AT4G28140	Ethylene-responsive transcription factor ERF054				
floral organ abscission		9	13	2	0.01434
AT3G25655	protein IDA-LIKE 1				
AT1G68765	protein IDA				
Cluster-5 (26 genes)					
sulfate transport		8	14	3	5.7E-05
AT5G13550	sulfate transporter 4.1, SULTR4;1				
AT1G23090	putative sulfate transporter 3.3, AST91				
AT4G08620	sulfate transporter 1.1, SULTR1;1				
inorganic anion transport		7	55	4	5.7E-05
AT3G26570	inorganic phosphate transporter 2-1, PHT2;1				
AT5G13550	sulfate transporter 4.1, SULTR4;1				
AT1G23090	putative sulfate transporter 3.3, AST91				
AT4G08620	sulfate transporter 1.1, SULTR1;1				
root development		6	215	3	0.04909
AT5G47990	Cytochrome P450 708A2, THALIAN-DIOL DESATURASE				
AT5G48010	Thalianol synthase, thalianol synthase 1				
AT5G48000	Cytochrome P450 705A5, THALIANOL HYDROXYLASE				
oxidation-reduction process		3	1315	8	0.00356
AT5G47990	Cytochrome P450 708A2, THALIAN-DIOL DESATURASE				
AT5G48000	Cytochrome P450 705A5, THALIANOL HYDROXYLASE				
AT4G21990	5'-adenylylsulfate reductase 3 APR3				
AT4G04610	5'-adenylylsulfate reductase 1, APR1				
AT1G62180	5'-adenylylsulfate reductase 2, APR2				
AT1G52790	oxidoreductase, 2OG-Fe(II) oxygenase family protein				
	2-oxoglutarate (2OG) and Fe(II)-dependent oxygenase-like				
AT1G80320	protein				
AT2G42250	cytochrome P450, family 712, subfamily A,				
cellular lipid metabolic process		3	751	5	0.00706
AT5G47990	Cytochrome P450 708A2, THALIAN-DIOL DESATURASE				
AT5G48010	Thalianol synthase, thalianol synthase 1				
AT5G48000	Cytochrome P450 705A5, THALIANOL HYDROXYLASE				
	S-adenosyl-L-methionine-dependent methyltransferase-like				
AT5G38020	protein				
At3g45130	Lanosterol synthase, LAS1				
tricyclic triterpenoid metabolic process		8	5	3	2.6E-06
AT5G47990	Cytochrome P450 708A2, THALIAN-DIOL DESATURASE				
AT5G48000	Cytochrome P450 705A5, THALIANOL HYDROXYLASE				
AT5G48010	Thalianol synthase, thalianol synthase 1				
triterpenoid biosynthetic process		8	12	2	0.00377
AT5G48010	Thalianol synthase, thalianol synthase 1				
At3g45130	Lanosterol synthase, LAS1				
pentacyclic triterpenoid biosynthetic process		9	10	2	0.00293
AT5G48010	Thalianol synthase, thalianol synthase 1				
At3g45130	Lanosterol synthase, LAS1				
carboxylic acid biosynthetic process		7	476	5	0.00016
	S-adenosyl-L-methionine-dependent methyltransferase-like				
AT5G38020	protein				
AT3G55120	chalcone--flavonone isomerase 1				
AT4G21990	5'-adenylylsulfate reductase 3				
AT4G04610	5'-adenylylsulfate reductase 1				
AT1G62180	5'-adenylylsulfate reductase 2				

Results

cellular amino acid biosynthetic process	8	232	4	0.00706
AT3G55120 chalcone--flavonone isomerase 1				
AT4G21990 5'-adenylylsulfate reductase 3				
AT4G04610 5'-adenylylsulfate reductase 1				
AT1G62180 5'-adenylylsulfate reductase 2				
sulfate assimilation	4	14	3	0.00573
AT4G21990 5'-adenylylsulfate reductase 3				
AT4G04610 5'-adenylylsulfate reductase 1				
AT1G62180 5'-adenylylsulfate reductase 2				
serine family amino acid biosynthetic process	9	29	3	0.0004
AT4G21990 5'-adenylylsulfate reductase 3				
AT4G04610 5'-adenylylsulfate reductase 1				
AT1G62180 5'-adenylylsulfate reductase 2				
cysteine biosynthetic process	10	21	3	0.00016
AT4G21990 5'-adenylylsulfate reductase 3 APR3				
AT4G04610 5'-adenylylsulfate reductase 1, APR1				
AT1G62180 5'-adenylylsulfate reductase 2, APR2				

The third sets of differentially expressed genes were identified through a comparison of the individual transcriptional responses of WT and IZS 288 roots to chilling stress. Chilling stress induced a two fold or more change in the transcript abundance of 1992 and 2560 genes in WT and IZS 288 roots, respectively. As shown in the Venn diagram of Fig. 3.47 the degree of overlap between the chilling response of WT and IZS 288 roots was huge i.e. only 29% and 45% percent of the transcriptional responses to chilling are unique to WT and IZS 288 roots, respectively. Meanwhile, the comparison of these unique gene lists (i.e. 1142 genes differentially expressed only in IZS 288K/IZS 288^{4°} and 574 genes differentially expressed only in ColK/Col4[°]) with that of previously determined lists (i.e. 183 genes differentially expressed in the WT versus IZS 288 comparison at optimal condition (ColK/IZS 288K) and the 180 genes identified after chilling stress (ColK^{4°}/IZS 288^{4°}) identified very little overlaps. Therefore, not to overlook the details of the variation in chilling response between the two genotypes, further investigations were carried out on these data sets aiming to uncover the causes for the chilling hypersensitivity phenotype of IZS 288.

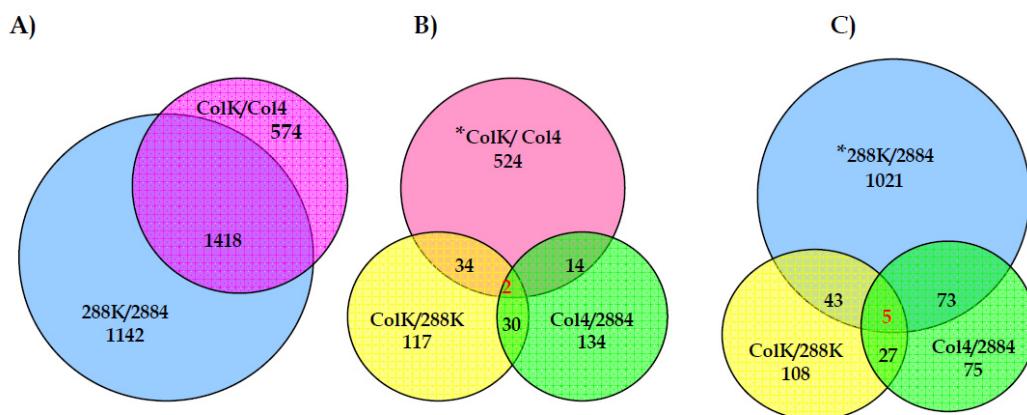


Figure 3.47. A) Venn diagram showing overlap between chilling responsive genes in WT roots (1992) and in IZS 288 roots (2560). B) Overlap between **exclusive** chilling responsive genes in WT roots (574) and differentially expressed genes of IZS 288 at optimal growing condition (183) and after chilling stress (180). C) Overlap between **exclusive** chilling responsive genes in IZS 288 roots (1142) and differentially expressed genes of IZS 288 at optimal growing condition (183) and after chilling stress (180).

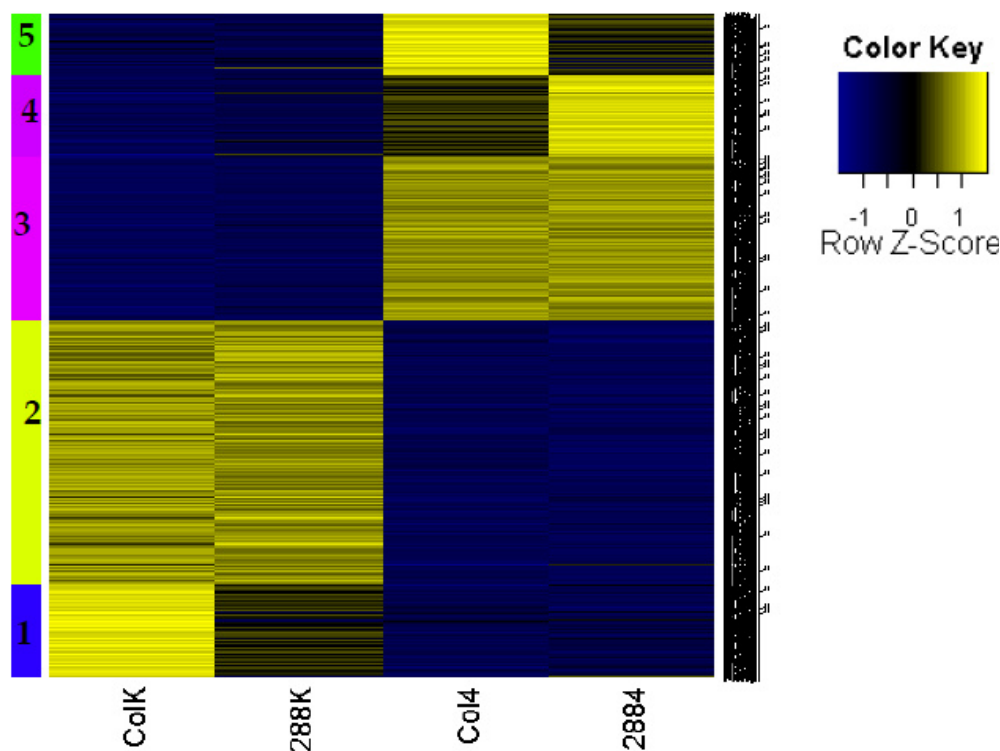


Figure 3.48. Heat map of scaled expression values of 1992 genes that are chilling responsive in WT roots after 24 hours of chilling stress and clustered into five groups by K-mean algorithm using the Pearson correlation coefficient as the distance metrics. The average of three unlogged expression values for each genotype and steers condition were used (i.e. ColK represents the average transcript level of three replicates of WT at optimal growing condition, whereas Col4 stands for the average transcript level after 24 hour chilling (4°) stress. The same is true for 288K and 2884).

Following the same methods of analysis first the 1992 of genes that showed transcriptional response in WT were clustered into 5 groups and each cluster was investigated for GO term enrichments. The first cluster consisted of genes that showed similar response to chilling stress in both genotypes but at optimal growing conditions they were constitutively up-regulated only in WT. Genes included in this category were involved in *response to heat* and *response to reactive oxygen species*. The second cluster of genes showed similar chilling induced transcriptional repression in both WT and IZS 288 roots. *Photosynthesis* and *light harvesting* were the main biological processes represented by this group. The third cluster consisted of genes that showed chilling stress induced expression in both genotypes. Standard biological process implicated in cold response process such as *cold acclimation*, *response to water deprivation* and *phenylpropanoid biosynthetic process* were found in this group. The fourth cluster is composed of genes that showed strong induction of expression as a result of chilling stress only in IZS 288 roots. The biological process enriched in this group included *carbohydrate biosynthetic process*, *trehalose biosynthetic process* and most importantly *response to*

Results

cold, *water deprivation* and *abscisic acid stimulus* are also implicated in this group. Well established cold responsive genes of *Arabidopsis* genome like C-repeat-dehydration responsive element (DRE) Binding Factors 1B/ CBF1 (AT4G25490), CBF2 (AT4G25470), Cold Regulated protein 15 A/ COR15A (AT2G42540), COR15B (AT2G42530) and COR27 (AT5G42900) were among this group showing higher transcript level in IZS 288 than in WT roots after chilling stress. The fifth cluster is made up of genes that showed strong induction of expression as a result of chilling stress only in WT roots. Genes included in this group were involved in metabolic process of *tryptophan*, *phenylpropanoids*, *triterpenoids*, *flavonoids* and *lignins*. Other biological processes enriched in this group were *response to temperature stimulus*, *defense response by callose deposition in cell wall* and *auxin transport* (Fig. 3.48 and Appendix. list-4).

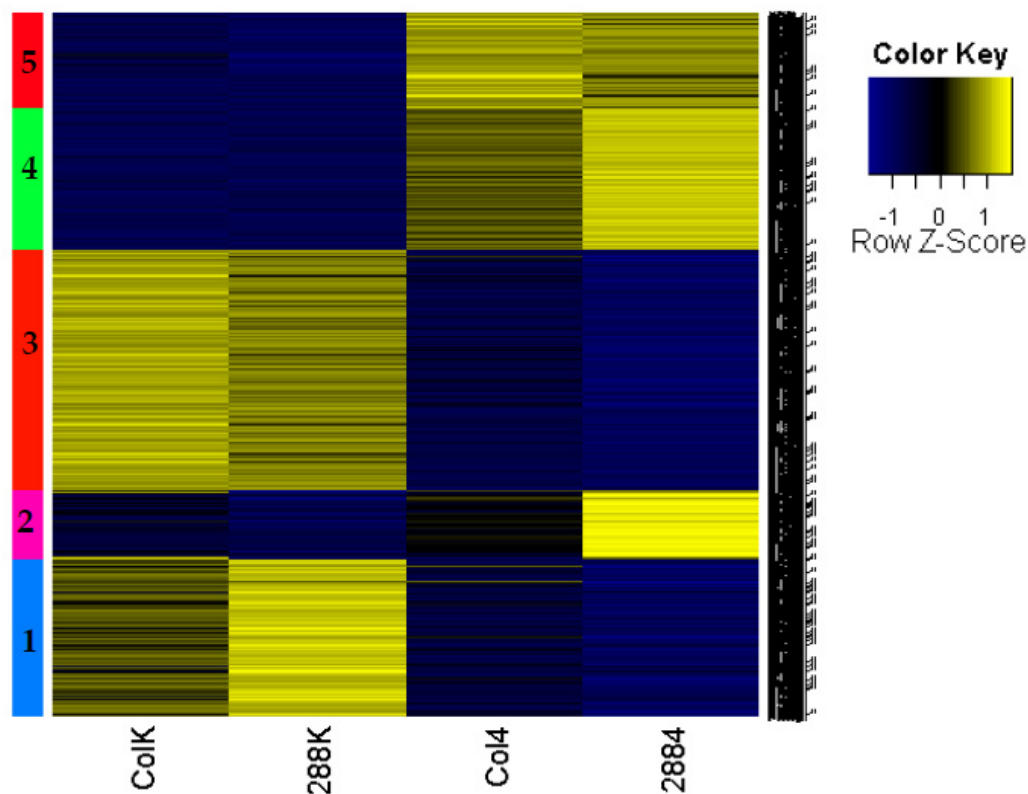


Figure 3.49. Heat map of scaled expression values of 2560 genes that are chilling responsive in IZS 288 roots after 24 hours of chilling stress and clustered into five groups by K-mean algorithm using the Pearson correlation coefficient as the distance metrics. The average of three unlogged expression values for each genotype and steers condition were used (i.e. ColK represents the average transcript level of three replicates of WT at optimal growing condition, whereas Col4 stands for the average transcript level after 24 hour chilling (4°) stress. The same is true for 288K and 2884).

Meanwhile, clustering and further analysis of the 2560 genes that showed transcriptional response to chilling stress in IZS 288 was also carried out into 5 groups (Fig. 3.49 and

Appendix. list-5), but since two groups showed the most striking transcriptional variation the focus was directed only in these two groups. The first group (i.e. cluster 2 on Fig. 3.49) showed strong induction of expression only in IZS 288 as a result of chilling stress. This group of genes showed similar expression pattern to that of the fourth cluster of genes described earlier during the analysis of chilling response in WT roots. However, in this particular cluster additional genes involved in *transcriptional regulation* and *RNA biosynthesis process* have been identified. Most importantly, 10 cold response genes (i.e. AT2G38470, AT3G22370, AT3G50260, AT5G59820, AT5G50720, AT3G49530, AT4G03430, AT4G34150, AT5G43760, and AT2G40140) were also found in this group. Whereas, the second group (i.e. cluster 5 on Fig. 3.49) of genes showed stronger induction of transcript levels after chilling stress in WT roots than in IZS 288. They were also known to be involved in *cold response* and *acclimation*. Some of these genes were KIN1 (AT5G15960), Low Temperature Induced 30/LIT30 (AT3G50970), Early Response to Dehydration 10/ ERD10 (AT1G20450) and putative low temperature and salt responsive protein (At4g30650).

3.2.5.1 Differentially expressed and chilling responsive genes in IZS 288

The comparative analysis of the root transcriptome of WT and IZS 288 in both optimal growing condition and after chilling stress generated a large list of genes taking part in a broad spectrum of biological processes. This list included genes that are described in cold response and cold acclimation process of plants. Since IZS 288 is predisposed to chilling sensitivity, looking further into these differentially expressed cold response and cold acclimation genes could lead to understand the underlying cause of the chilling hypersensitive phenotype of IZS 288. The overall analysis identified 13 cold acclimation genes and 55 cold responsive genes as differentially expressed between WT and IZS 288. Within the cold acclimation genes strong expressional variation was observed in the transcript values of the ZAT 12 gene. Under optimum condition the transcript level of ZAT12 in IZS 288 roots was lower than that of WT but after chilling stress higher transcript level was observed in IZS 288 roots. In contrast, genes like cold regulated 413 plasma membrane 1/COR431-PM1 (AT2G15970), cold regulated 314 thylakoid membrane 2/COR314-TM2 (AT1G29395) and Early Response to Dehydration 10/ ERD10 (AT1G20450) were showing comparable amount of transcript levels in both genotypes before being exposed to chilling stress, but after chilling stress their expression level in IZS 288 was lower than that of the WT (Fig. 3.50).

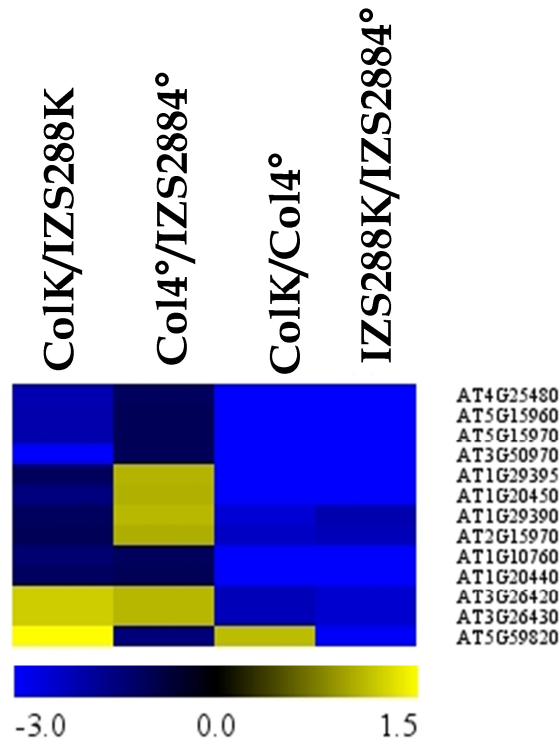


Figure 3.50. Heat map of 13 cold acclimation genes that are differentially expressed in IZS 288 roots. Unlogged fold changes between WT (Col) and IZS 288 at optimal (K) and after chilling stress (4°) conditions are shown. ColK/IZS288 represents the fold difference in transcript level between WT and IZS 288 at optimal growing condition, whereas Col4°/IZS2884° stands for the fold difference in average transcript level after 24 hours chilling (4°) stress. ColK/Col4° shows fold changes in WT roots as a result of chilling stress and IZS288K/IZS2884° shows the fold changes in IZS 288 as a result of chilling stress.

Furthermore, among the 55 differentially expressed cold response genes identified so-far **Low Temperature Induced / LIT30** (AT3G50970), **LIT78** (AT5G52310), **Galactinol Synthase 3/ GoIS3** (AT1G09350), **C-repeat-dehydration responsive element (DRE) Binding Factors 3 / CBF3/DREB1A** (AT4G25480), **stress-induced protein KIN1** (AT5G15960) & **KIN2** (AT5G15970) and **putative low temperature and salt responsive protein** (AT4G30650) showed moderate up-regulation in IZS 288 roots at optimal growing condition, however, after chilling stress the accumulation of their transcript levels was lower than what is in WT roots. On the other hand, **Cold-Regulated protein 15B /COR15B** (AT2G42530), **COR27** (AT5G42900), **CBF1** (AT4G25490), **Salt Tolerance Zinc finger STZ/ZAT10** (AT1G27730) and **pre-mRNA-processing factor 6/SAT1** (AT4G03430) showed the highest level of transcript level in IZS 288 after chilling stress (Fig. 3.51). On the contrary, ethylene-responsive transcription factors **RAP2-1** (AT1G46768) and **RAP2-6** (AT1G43160), **inducer of CBF expression 1/ICE1** (AT3G26744) and **outer plastid envelope protein 16-1/OEP16-1**

(AT2G28900) showed similar transcript level in both genotypes at optimal growing condition but got strongly induced in WT roots after chilling stress (Fig. 3.51).

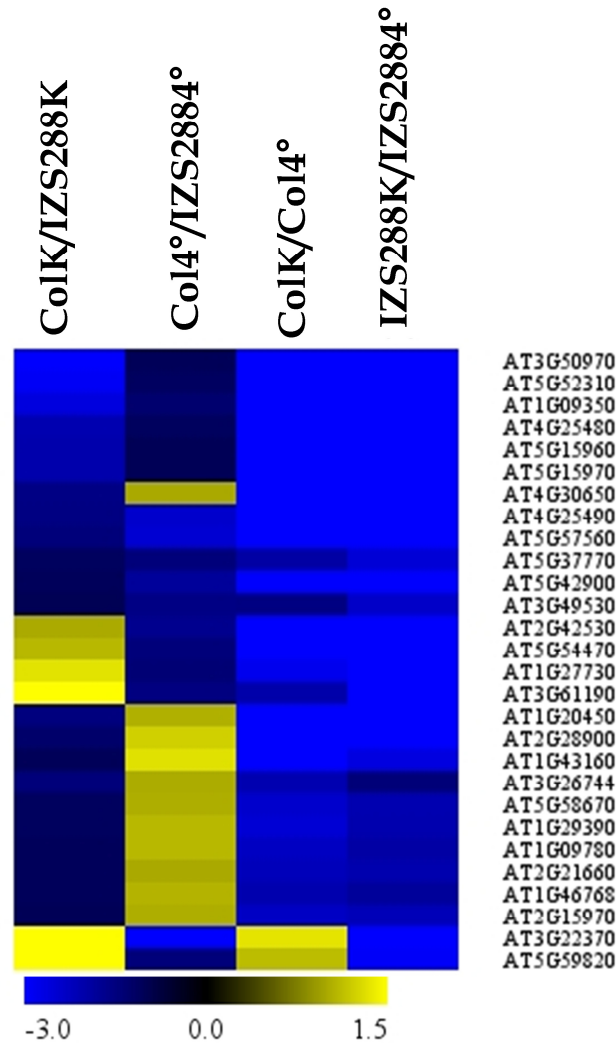


Figure 3.51. Heat map of 28 cold responsive genes that are differentially expressed in IZS 288 roots. Unlogged fold changes between WT (Col) and IZS 288 at optimal (K) and after chilling stress (4°) conditions are shown. ColK/IZS288 represents the fold difference in transcript level between WT and IZS 288 at optimal growing condition, whereas Col4°/IZS2884° stands for the fold difference in average transcript level after 24 hours chilling (4°) stress. ColK/Col4° shows fold changes in WT roots as a result of chilling stress and IZS288K/IZS2884° shows the fold changes in IZS 288 as a result of chilling stress.

3.2.5.2 Differentially expressed and Zn homeostasis related genes in IZS 288

One of the interesting observations made about the IZS 288 transcriptome was that a number of sulfur metabolic genes were showing different expression pattern than what they usually show in WT roots. This discrepancy was observed under both optimal growing conditions as well as after chilling stress. Sulfate adenylyltransferase /APS4 (AT5G43780) and molybdate transporter 1/ MOT1 (AT2G25680) showed twofold up-regulations in IZS 288 with and

Results

without chilling stress, whereas sulfate transporter 1.1 /SULTR1.1 (AT4G08620), serine acetyltransferase /SAT-106 (AT2G17640), 5'-adenylylsulfate reductase 3/APR3 (AT4G21990) showed lower transcript level in IZS 288 under both conditions. On the other hand, bifunctional 3'(2'),5'-bisphosphate nucleotidase and inositol polyphosphate 1-phosphatase/SAL1 (AT5G63980), tryptophan N-hydroxylase/ CYP79B2 (AT4G39950) and putative 2-oxoacid dependent dioxygenase (AT2G25450) showed induction by chilling stress in WT roots but in case of IZS 288 roots no similar response was observed. Uniquely, at optimal growing condition the roots of IZS 288 showed significantly lower transcript level of 1-aminocyclopropane-1-carboxylate synthase 7/ACS7 (AT4G26200), however, after chilling stress higher level of transcript abundance was observed in IZS 288 roots (Fig. 3.52).

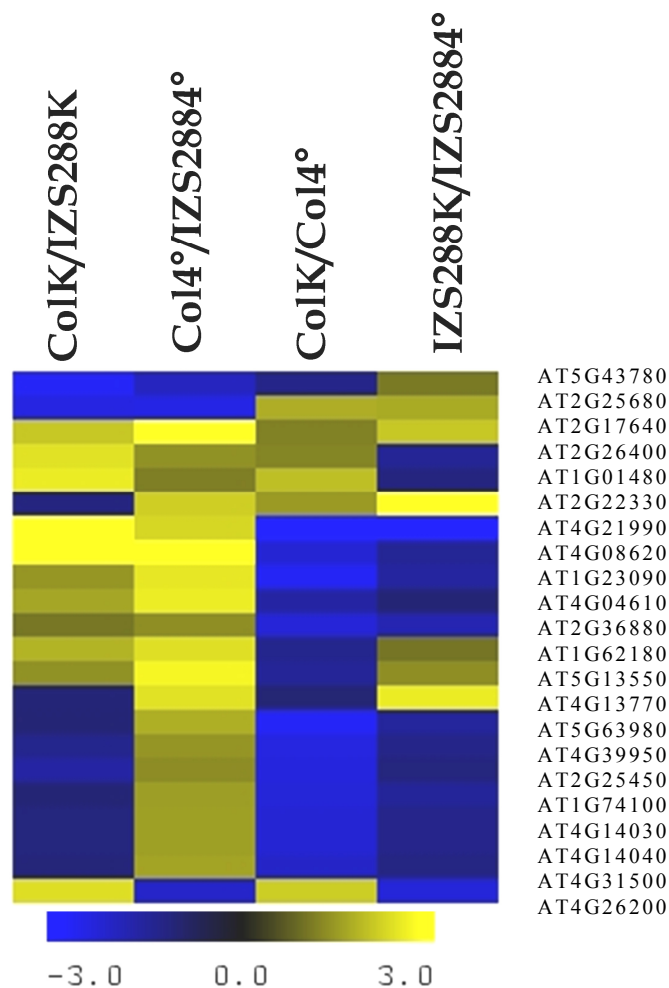


Figure 3.52. Heat map of 22 genes involved in sulfur transport and sulfur assimilation process, which are differential expressed in IZS 288 roots. Unlogged fold changes between WT (Col) and IZS 288 at optimal (K) and after chilling stress (4°) conditions are shown. ColK/IZS288 represents the fold difference in transcript level between WT and IZS 288 at optimal growing condition, whereas Col4°/IZS2884° stands for the fold difference in average transcript level after 24 hours chilling (4°) stress. ColK/Col4° shows fold changes in WT roots as a result of chilling stress and IZS288K/IZS2884° shows the fold changes in IZS 288 as a result of chilling stress.

In an attempt to explain the Zn hypersensitivity phenotype of IZS 288 a comparison was made between the differentially expressed genes of IZS 288 (i.e. 69 genes were up-regulated and 114 genes were down-regulated) and three previously reported zinc-responsive sets of genes. The first set of Zn responsive genes were identified through exposure to excess ($30\ \mu\text{M}$ ZnSO_4) Zn concentration (Talke et. al., 2006); the second set included genes responding to both excess concentration ($25\ \mu\text{M}$ ZnSO_4) and Zn deficient condition (van de Mortel et. al., 2006) and the third set was identified using iTRAQ (isobaric tags for relative and absolute quantification)-based quantitative proteomics approach conducted on *Arabidopsis* roots grown on Murashige and Skoog (MS) medium supplemented with $300\ \mu\text{M}$ ZnSO_4 (Fukao et. al., 2011). Considerable number of overlaps was observed between the differentially regulated genes of IZS 288 and the first two data sets (Tab. 3.9). Particularly, MTPA1 (AT3G61940) and NAS4 (AT1G56430), which are among well established Zn deficiency responsive genes, were significantly down-regulated in IZS 288. Interestingly, BHLH039 (AT3G56980), a transcription factor implicated in iron homeostasis, which gets induced by excess Zn concentration, was also down-regulated in IZS 288. The same is true for R2R3 MYB transcription factor/ MYB 15 (AT3G23250) and jasmonate-zim-domain protein 8 /JAZ8 (AT1G30135). On the other hand, 1-aminocyclopropane-1-carboxylate synthase 2/ ACS2 (AT1G01480) and ethylene-responsive transcription factor ERF071 (AT2G47520) that gets repressed by Zn deficiency were down-regulated in IZS 288. However, only LIT 30 (AT3G50970) was found in both the third Zn responsive data set (Fukao et al., 2011) and in the differentially expressed genes of IZS 288. In both data sets LIT30 showed strong induction.

Results

Table 3.9. Overlap between the 183 genes that were differential expressed in IZS 288 roots at optimal growing condition and three previously reported Zn responsive genes sets. Blue color represents down-regulation whereas yellow color stands for up-regulation of genes.

Gene ID	Gene Symbol	Description:	IZS 288	Talke et.al.,2006	van de Mortel et. al., 2006	
				Zn 30µM	Zn 0	Zn 25µM
AT2G15960		hypothetical protein				
AT1G72800		RNA-binding (RRM/RBD/RNP motifs) family protein				
AT4G31020		esterase/lipase domain-containing protein				
AT2G40340	DREB2C	dehydration-responsive element-binding protein 2C				
AT1G09090	RBOHB	Respiratory burst oxidase-B				
AT2G38870		serine protease inhibitor, potato inhibitor I-type protein				
AT2G47520	HRE2	ethylene-responsive transcription factor ERF071				
AT1G75830	LCR67	defensin-like protein 13				
AT2G21640		hypothetical protein				
AT5G51440		heat shock protein 23.5				
AT1G01480	ACS2	1-aminocyclopropane-1-carboxylate synthase 2				
AT1G60730		NAD(P)-linked oxidoreductase-like protein				
AT3G48450	RIN4	RPM1-interacting protein 4 (RIN4)				
AT3G49160		pyruvate kinase				
AT5G45020		putative glutathione S-transferase				
AT1G24420		HXXXD-type acyl-transferase-like protein				
AT1G52820		putative 2-oxoglutarate-dependent dioxygenase				
AT1G56430	NAS4	nicotianamine synthase				
AT3G61940	MTPA1	metal tolerance protein A1				
AT3G45130	LAS1	lanosterol synthase 1				
AT2G42250	CYP712A1	cytochrome P450, family 712, subfamily A, polypeptide 1				
AT5G06900	CYP93D1	cytochrome P450, family 93, subfamily D, polypeptide 1				
AT1G52790		oxidoreductase, 2OG-Fe(II) oxygenase family protein				
AT1G80320		2-oxoglutarate (2OG) and Fe(II)-dependent oxygenase-like protein				
AT5G05250		hypothetical protein				
AT4G16370	OPT3	oligopeptide transporter				
AT3G56980	BHLH039	transcription factor ORG3				
AT5G45080	PP2-A6	protein PHLOEM protein 2-LIKE A6				
AT1G14540		peroxidase 4				
AT1G69920	GSTU12	glutathione S-transferase TAU 12				
AT1G14550		peroxidase 5				
AT2G26400	ARD3	1,2-dihydroxy-3-keto-5-methylthiopentene dioxygenase 1				
AT3G23250	MYB15	myb domain protein 15				
AT2G26530	AR781	hypothetical protein				
AT2G30670		tropine dehydrogenase				
AT2G26560	PLA2A	phospholipase A 2A				
AT1G28480	GRX480	glutaredoxin-C9				
AT3G55790		hypothetical protein				
AT1G30135	JAZ8	protein TIFY 5A				
AT1G09080	BIP3	Hsp70 protein BiP chaperone BIP-L				
AT1G26380		FAD-binding and BBE domain-containing protein				

Additionally, using the plant gene set enrichment analysis toolkit /PlantGSEA (Yi et. al., 2013) ranking of associations between the differentially expressed genes of IZS 288 and 20,290 gene sets that are available in the PlantGSEA platform was performed. Important associations were observed between the differentially expressed genes of IZS 288 and gene sets representing response to nutrient availability, phytohormones biosynthesis and their mediated signaling pathways, response to abiotic stress like cold and hypoxia and long day photoperiodism (Tab. 3.10).

Table 3.10. Overlap between the differential expressed genes in IZS 288 roots and different gene sets hosted on the 'PlantGSEA' platform ([www. http://structuralbiology.cau.edu.cn/PlantGSEA/](http://structuralbiology.cau.edu.cn/PlantGSEA/)). The header title 'category' represents sources of data sets i.e. 'LIT' for literature and GO term categories 'BP' for biological process and 'CC' for cellular component. False discovery rate (FDR) was calculated using Benjamini Yekutieli (2001) method.

	Description & No. Genes in gene set ()	NO. Genes in			
		Category	Overlap (k)	p value	FDR
Down-regulated in IZS 288	Downregulated Se-reponsive genes in root tissue (896)	LIT	36	2.19E-22	1.01E-18
	Upregulated Se-reponsive genes in root tissue (555)	LIT	28	1.36E-20	3.12E-17
	Significant up-regulation in 72hrs in response to iron-deprivation (528)	LIT	24	5.34E-17	6.13E-14
	repressed genes of arsenic-treated <i>Arabidopsis thaliana</i> Columbia (90)	LIT	6	2.13E-06	0.000218
	Upregulated genes early in response to treatment at 4 degree in CAMTA3 (AT2G22300) mutant (30)	LIT	6	2.52E-09	4.63E-07
	Up-regulated by Sulfur and SLIM1 (AT1G73730) (54)	LIT	5	2.96E-06	0.000296
	Upregulated genes in <i>ago1-25</i> (AT1G48410) (943)	LIT	24	1.15E-11	4.08E-09
	Upregulated in <i>arf2</i> (AT5G62000) (553)	LIT	23	1.43E-15	1.09E-12
	Downregulated in <i>arf2</i> (AT5G62000) (342)	LIT	7	0.000583	0.0237
	GO:0031669 cellular response to nutrient levels (314)	GO_BP	7	0.000353	0.0286
	GO:0071456 cellular response to hypoxia (24)	GO_BP	6	5.84E-10	2.17E-06
	GO:0009723 response to ethylene stimulus (353)	GO_BP	12	4.71E-08	0.0000418
	GO:0071395 cellular response to jasmonic acid stimulus (282)	GO_BP	8	0.0000264	0.00427
	GO:0009751 response to salicylic acid stimulus (470)	GO_BP	9	0.000173	0.0189
	GO:0043450 alkene biosynthetic process (133)	GO_BP	5	0.000229	0.0209
	GO:0006633 fatty acid biosynthetic process (303)	GO_BP	10	3.83E-06	0.000762
	GO:0009695 jasmonic acid biosynthetic process (135)	GO_BP	7	1.68E-06	0.000564
	GO:0009693 ethylene biosynthetic process (131)	GO_BP	5	0.000214	0.0208
	GO:0048574 long-day photoperiodism (24)	GO_BP	3	0.000124	0.016
Up-regulated in IZS 288	Cold Up-regulated CBF3 & CBF2 Target Genes Whose Expression is Affected by <i>ice1</i> (AT3G26744) (15)	LIT	4	1.13E-07	0.0000576
	Expressed 3-fold higher in <i>pk1</i> (AT2G25170) mutants versus wild-type plants (91)	LIT	4	0.000184	0.0394
	Upregulated genes in <i>sol2</i> (AT5G13290) mutant (75)	LIT	9	2.94E-12	4.48E-09
	GO:0032993 protein-DNA complex (66)	GO_CC	4	0.0000528	0.00565
	GO:0000786 nucleosome (60)	GO_CC	4	0.0000362	0.00565
	GO:0000785 chromatin (90)	GO_CC	4	0.000176	0.0126

Among the overlapping genes of IZS 288 and the gene sets representing different biological processes, glutaredoxin-C9/ROXY19/GRX480 (AT1G28480) and WRKY transcription factor 40 (AT1G80840) showed the highest frequency of occurrence among the gene sets (Tab. 3.11). Glutaredoxin-C9/ROXY19/GRX480 is a member of the glutaredoxin family that regulates protein redox state and its expression level is responsive to different phytohormones and stress conditions. It is speculated to be involved in the cross-talk between the salicylic acid (SA) signaling pathway and the jasmonic acid signaling pathway (Zander et. al., 2012). WRKY40 is involved in resistance to a variety of pathogens through a complex interaction with other WRKY transcription factors. It has also been shown that WRKY40 serves as a repressor of ABA signaling and serves as a regulator of stress responses of mitochondrial proteins (van Aken et. al., 2013).

Results

Table 3.11. List of overlapping genes between differential expressed genes in IZS 288 roots and different gene sets representing various biological process (gene ontology terms) hosted on the 'PlantGSEA' platform ([www.http://structuralbiology.cau.edu.cn/PlantGSEA](http://structuralbiology.cau.edu.cn/PlantGSEA)). Turquoise color represents the presence of the gene in the gene set.

Gene ID	Gene symbol	Description	CELLULAR_RESPONSE_TO_HYPOXIA	RESPONSE_TO_ETHYLENE_STIMULUS	RESPONSE_TO_JA_STIMULUS	OXYLIPIN_BIOSYNTHETIC_PROCESS	FATTY_ACID_BIOSYNTHETIC_PROCESS	JASMONIC_ACID_BIOSYNTHETIC_PROCESS	RESPONSE_TO_ABSENCE_OF_LIGHT	CELLULAR_RESPONSE_TO_SA_STIMULUS	CELLULAR_RESPONSE_TO_NUTRIENT_LEVEL	ALKENE_BIOSYNTHETIC_PROCESS	ETHYLENE_BIOSYNTHETIC_PROCESS	LONG-DAY_PHOTOPERIODISM
AT1G01480	ACS2	1-aminocyclopropane-1-carboxylate synthase 2												
AT1G09090	RBOHB	Respiratory burst oxidase-B												
AT1G14290	SBH2	sphingoid base hydroxylase 2												
AT1G14540		peroxidase 4												
AT1G14550		peroxidase 5												
AT1G14560	COAC1	mitochondrial CoA transporter.												
AT1G26380		FAD-binding and BBE domain-containing protein												
AT1G28480	GRX480	glutaredoxin-C9												
AT1G30135	JAZ8	protein TIFY 5A												
AT1G73010	PS2	phosphate starvation-induced protein 2												
AT1G76600		hypothetical protein												
AT1G80840	WRKY40	putative WRKY transcription factor 40												
AT2G22630	AGL17	agamous-like MADS-box protein AGL17												
AT2G26400	ARD3	1,2-dihydroxy-3-keto-5-methylthiopentene dioxygenase 1												
AT2G26530	AR781	hypothetical protein												
AT2G26560	PLA2A	phospholipase A 2A												
AT3G09600		myb family transcription factor												
AT3G15500	NAC3	NAC domain-containing protein 55												
AT3G23250	MYB15	myb domain protein 15												
AT3G27150		F-box/kelch-repeat protein												
AT3G47380		invertase/pectin methylesterase inhibitor domain-containing protein												
AT3G48850	PHT3;2	phosphate transporter 3;2												
AT3G55790		hypothetical protein												
AT3G55840		Hs1pro-1 protein												
AT3G56980	BHLH039	transcription factor ORG3												
AT4G26200	ACS7	1-aminocyclopropane-1-carboxylate synthase 7												
AT4G33950	OST1	serine/threonine-protein kinase SRK2E												
AT4G35770	SEN1	senescence-associated protein DIN1												
AT4G37370	CYP81D8	cytochrome P450, family81 subfamilyD polypeptide8												
AT4G37710		VQ motif-containing protein												
AT5G13080	WRKY75	putative WRKY transcription factor 75												
AT5G20230	BCB	blue copper protein												
AT5G37260	RVE2	REVEILLE 2 / DNA binding / transcription factor												
AT5G48000	CYP708A2	cytochrome P450 708A2												
AT5G48850	ATSDI1	tetratricopeptide repeat domain-containing protein												
AT5G59820	RHL41	C2H2-type zinc finger protein												

Results

Focusing more on the overlap between IZS 288 gene set and Fe deficiency responsive genes (Dinneny et al., 2008), 87% of the overlapping genes including transcription factor BHLH039 (AT3G56980) and ethylene-responsive transcription factor ERF071 (AT2G47520) showed opposite expression pattern. The only genes that showed similar expression pattern (i.e. induction) in both gene sets were phloem protein 2-like A6 (AT5G45070), phloem protein 2-like A8 (AT5G45080), pectinesterase 41 (AT4G02330) and non-specific lipid-transfer protein 5 (AT3G51600). Similarly, 76% of the overlapping genes between selenium (Se) responsive gene set and IZS 288 gene set showed opposing pattern of expression. Among the genes that showed similar pattern of expression in both gene sets senescence-associated protein/ SEN1 (AT4G35770), transcription factor reveille 2 /RVE2 (AT5G37260) and E3 ubiquitin protein ligase /ATL23 (AT5G42200) showed repression, while CBF3/DREB1A (AT4G25480) and pectinesterase 41 (AT4G02330) showed induction. Uniquely, all of the overlapping genes (i.e. 6) between arsenic (As) responsive genes and IZS 288 gene set showed repression of expression (Tab.3.12).

Table 3.12. List of overlapping genes between differential expressed genes in IZS 288 roots and Fe, Se and As responsive gene sets hosted on the 'PlantGSEA' platform. Blue color stands for repression and yellow color represents induction of a gene. (www. <http://structuralbiology.cau.edu.cn/PlantGSEA>).

Gene ID	Gene symbol	Description	IZS 288	Fe deprivation 72H	Se exposure 40µM	As(v) exposure 100µM
AT1G01480	ACS2	1-aminocyclopropane-1-carboxylate synthase 2	Blue	Yellow		
AT1G02850	BGLU11	beta glucosidase 11	Blue	Yellow		
AT1G04770		male sterility MS5 family protein	Blue	Yellow		
AT1G09080	BIP3	Hsp70 protein BiP chaperone BIP-L	Blue	Yellow		
AT1G12740	CYP87A2	cytochrome P450, family87, subfamilyA, polypeptide2	Yellow	Blue		
AT1G14550		peroxidase 5	Blue		Yellow	
AT1G26380		FAD-binding and BBE domain-containing protein	Blue	Yellow		Blue
AT1G28480	GRX480	glutaredoxin-C9	Blue		Yellow	
AT1G30135	JAZ8	protein TIFY 5A	Blue		Yellow	
AT1G52820		putative 2-oxoglutarate-dependent dioxygenase	Blue		Blue	
AT1G56430	NAS4	nicotianamine synthase	Blue	Yellow		
AT1G60730		NAD(P)-linked oxidoreductase-like protein	Blue	Yellow		
AT1G60750		auxin-induced atb2-like protein	Blue	Yellow		
AT1G67100	LBD40	LOB domain-containing protein 40	Blue	Yellow		
AT1G69880	TH8	thioredoxin H8	Blue		Yellow	
AT1G73010	PS2	phosphate starvation-induced protein 2	Blue		Yellow	Blue
AT1G73490		RNA recognition motif-containing protein	Yellow			
AT1G76600		hypothetical protein	Blue		Yellow	
AT1G76800		vacuolar iron transporter-like protein	Yellow		Blue	
AT1G80840	WRKY40	putative WRKY transcription factor 40	Blue		Yellow	Blue
AT2G02000	GAD3	glutamate decarboxylase 3	Blue		Yellow	
AT2G02010	GAD4	glutamate decarboxylase 4	Blue		Yellow	
AT2G15960		hypothetical protein	Blue		Blue	
AT2G17640		serine acetyltransferase 2	Blue		Yellow	
AT2G21640		hypothetical protein	Blue	Yellow		
AT2G22880		VQ motif-containing protein	Blue		Yellow	Blue
AT2G26530	AR781	hypothetical protein	Blue		Yellow	
AT2G26560	PLA2A	phospholipase A 2A	Blue			Blue
AT2G41730		hypothetical protein	Blue	Yellow		
AT2G42250	CYP712A1	cytochrome P450, family712, subfamilyA, polypeptide1	Blue		Blue	
AT2G47520	HRE2	ethylene-responsive transcription factor ERF071	Blue	Yellow		
AT3G21720	ICL	isocitrate lyase	Blue	Yellow		
AT3G23250	MYB15	myb domain protein 15	Blue		Yellow	

Results

AT3G27150	F-box/kelch-repeat protein	Blue	Yellow	White	White
AT3G48450	RPM1-interacting protein 4 (RIN4)	Blue	Yellow	White	White
AT3G51600	LTP5 non-specific lipid-transfer protein 5	Yellow	Yellow	White	White
AT3G55840	Hs1pro-1 protein	Blue	White	Yellow	White
AT3G56980	BHLH039 transcription factor ORG3	Blue	Yellow	White	White
AT4G02330	ATPMEPCRB pectinesterase 41	Yellow	Yellow	White	White
AT4G02810	hypothetical protein	Blue	White	Blue	White
AT4G08620	SULTR1;1 sulfate transporter 1.1	Blue	White	Yellow	White
AT4G11650	OSM34 osmotin-like protein OSM34	Blue	Yellow	White	White
AT4G16370	OPT3 oligopeptide transporter	Blue	Yellow	White	White
AT4G21990	APR3 5'-adenylylsulfate reductase 3	Blue	White	Yellow	White
AT4G25480	DREB1A dehydration-responsive element-binding protein 1A	Yellow	White	White	White
AT4G26200	ACS7 1-aminocyclopropane-1-carboxylate synthase 7	Blue	Yellow	White	White
AT4G35770	SEN1 senescence-associated protein DIN1	Blue	White	Blue	Blue
AT4G37370	CYP81D8 cytochromeP450, family81, subfamilyD, polypeptide8	Blue	Yellow	Yellow	White
AT4G37710	VQ motif-containing protein	Blue	White	Yellow	White
AT5G05250	hypothetical protein	Blue	Yellow	White	White
AT5G06900	CYP93D1 cytochromeP450, family93, subfamilyD, polypeptide1	Blue	White	Blue	Blue
AT5G15960	KIN1 stress-induced protein KIN1	Yellow	White	Blue	Blue
AT5G15970	KIN2 stress-induced protein KIN2	Yellow	White	Blue	Blue
AT5G20230	BCB blue copper protein	Blue	White	Yellow	White
AT5G24660	LSU2 response to low sulfur 2	Blue	Yellow	White	White
AT5G37260	RVE2 REVEILLE 2 / DNA binding / transcription factor	Blue	White	Blue	Blue
AT5G42200	E3 ubiquitin-protein ligase ATL23	Blue	White	Blue	Blue
AT5G43580	Serine protease inhibitor	Yellow	Blue	White	White
AT5G43780	APS4 sulfate adenylyltransferase	Yellow	White	Blue	White
AT5G45070	PP2-A8 protein PHLOEM protein 2-LIKE A8	Yellow	White	White	White
AT5G45080	PP2-A6 protein PHLOEM protein 2-LIKE A6	Yellow	Yellow	White	White
AT5G48000	CYP708A2 cytochrome P450 708A2	Blue	Blue	White	White
AT5G48850	ATSDI1 tetratricopeptide repeat domain-containing protein	Blue	Yellow	White	White
AT5G51440	heat shock protein 23.5	Blue	Yellow	White	White
AT5G52310	LTI78 low-temperature-responsive protein 78	Yellow	White	Blue	Blue
AT5G58120	TIR-NBS-LRR class disease resistance protein	Blue	White	Yellow	White
AT5G59820	RHL41 C2H2-type zinc finger protein	Blue	Yellow	Yellow	White

Furthermore, additional overlaps were observed between IZS 288 gene set and gene sets of various established mutant lines. Particularly, the mutant lines with defective ARGONAUTE1 /AGO1 (AT1G48410) and AUXIN RESPONSE FACTOR2 /ARF2 (At5g62000) showed the highest number of overlapping genes (Tab. 3.13). ARGONAUTE1 is one of the 10 argonaute proteins in *Arabidopsis* that are involved in posttranscriptional gene silencing (Kurihara et. al., 2009). The overlapping genes of *ago1-25* and IZS 288 showed contrasting pattern of expression (i.e. they were induced in *ago1-25* but showed repression in IZS 288). In case of ARF2, one of the 22 auxin response factor gene family in *Arabidopsis* is presumed to have a repressor role on auxin induced genes (Vert et. al., 2008). Here also the majority of the overlapping genes (77%) showed contrasting expression pattern (i.e. they were induced in the loss-of-function *arf2* but showed repression in IZS 288). Among the remaining 23% of genes that showed similar pattern of expression (i.e. repressed in both gene sets) are sulfur deficiency induced 1/ ATSDI1 (AT5G48850) and 5'-adenylylsulfate reductase 3/ APR3 (AT4G21990) genes. Interestingly, four genes up-regulated in *inducer of CBF expression 1 /ice1* (AT3G26744), a mutant defective in an upstream transcription factor required for chilling tolerance, also showed up-regulation in IZS 288 (Lee et. al., 2005).

Results

Table 3.13. List of overlapping genes between differential expressed genes in IZS 288 roots and gene sets representing *ago1*, *camata3*, *arf2*, *sol2*, *pkl*, *ice1* and *slim1* mutants hosted on the 'PlantGSEA' platform ([www.http://structuralbiology.cau.edu.cn/PlantGSEA](http://structuralbiology.cau.edu.cn/PlantGSEA)). Blue color stands for repression and yellow color represents induction of a gene.

Gene ID	Gene symbol	Description	IZS 288	ago1	camta3	arf2	sol2	pkl	ice1	slim1
AT1G01480	ACS2	1-aminocyclopropane-1-carboxylate synthase 2	Blue			Yellow				
AT1G02850	BGLU11	beta glucosidase 11	Blue			Yellow				
AT1G04770		male sterility MS5 family protein	Blue	Yellow		Blue				Yellow
AT1G09090	RBOHB	Respiratory burst oxidase-B	Blue	Yellow						
AT1G09350	GolS3	galactinol synthase 3	Blue						Yellow	
AT1G14540		peroxidase 4	Blue			Yellow				
AT1G14550		peroxidase 5	Blue			Yellow				
AT1G15790		hypothetical protein	Blue					Yellow		
AT1G21680		DPP6 N-terminal domain-like protein	Blue			Yellow				
AT1G23960		hypothetical protein	Blue				Yellow			
AT1G24420		HXXXD-type acyl-transferase-like protein	Blue	Yellow						
AT1G26380		FAD-binding and BBE domain-containing protein	Blue	Yellow						
AT1G26380		FAD-binding and BBE domain-containing protein	Blue			Yellow				
AT1G52790		oxidoreductase, 2OG-Fe(II) oxygenase family protein	Blue	Yellow						
AT1G52820		putative 2-oxoglutarate-dependent dioxygenase	Blue	Yellow						
AT1G60730		NAD(P)-linked oxidoreductase-like protein	Blue	Yellow						
AT1G67100	LBD40	LOB domain-containing protein 40	Blue			Blue				
AT1G67980	CCOAMT	caffeoyl-CoA 3-O-methyltransferase	Blue	Yellow		Yellow				
AT1G68450		VQ motif-containing protein	Blue	Yellow						
AT1G69880	TH8	thioredoxin H8	Blue	Yellow						
AT1G69920	GSTU12	glutathione S-transferase TAU 12	Blue			Yellow				
AT1G76600		hypothetical protein	Blue		Yellow					
AT1G77450	NAC032	NAC domain containing protein 32	Blue			Yellow				
AT1G80320		2-oxoglutarate (2OG) and Fe(II)-dependent oxygenase-like protein	Blue	Yellow						
AT1G80840	WRKY40	putative WRKY transcription factor 40	Blue		Yellow	Yellow				
AT2G17640		serine acetyltransferase 2	Blue							Yellow
AT2G22880		VQ motif-containing protein	Blue			Yellow				
AT2G26530	AR781	hypothetical protein	Blue		Yellow					
AT2G26560	PLA2A	phospholipase A 2A	Blue	Yellow						
AT2G38870		serine protease inhibitor, potato inhibitor I-type protein	Blue			Yellow				
AT2G41730		hypothetical protein	Blue			Yellow				
AT2G42250	CYP712A1	cytochrome P450, family 712, subfamilyA, polypeptide1	Blue	Yellow						
AT3G14660	CYP72A13	cytochrome P450, family72, subfamilyA, polypeptide13	Blue			Yellow				
AT3G21720	ICL	isocitrate lyase	Blue	Yellow		Yellow				
AT3G27150		F-box/kelch-repeat protein	Blue	Yellow						
AT3G27200		plastocyanin-like domain-containing protein	Blue				Yellow			
AT3G27360		histone H3	Blue				Yellow			
AT3G29970		B12D protein	Blue			Blue				
AT3G30720	QQS	qua-quine starch	Blue					Yellow		
AT3G44400		TIR-NBS-LRR class disease resistance protein	Blue				Yellow			
AT3G45130	LAS1	lanosterol synthase 1	Blue	Yellow						
AT3G47680		DNA binding protein	Blue				Yellow			
AT3G50970	LT130	dehydrin Xero 2	Blue					Yellow	Yellow	
AT4G02540		cysteine/histidine-rich C1 domain-containing protein	Blue				Yellow			
AT4G08110		pseudo	Blue				Yellow			
AT4G08620	SULTR1;1	sulfate transporter 1.1	Blue							Yellow
AT4G11650	OSM34	osmotin-like protein OSM34	Blue	Yellow						
AT4G16370	OPT3	oligopeptide transporter	Blue	Yellow						
AT4G21990	APR3	5'-adenylylsulfate reductase 3	Blue	Yellow		Blue				

Results

AT4G37370	CYP81D8	cytochrome P450, family81, subfamilyD, polypeptide8	Blue	Yellow					
AT5G06900	CYP93D1	cytochrome P450, family93, subfamilyD, polypeptide1	Blue	Yellow					
AT5G15960	KIN1	stress-induced protein KIN1	Yellow					Yellow	
AT5G20230	BCB	blue copper protein	Blue	Yellow	Yellow	Yellow			
AT5G37260	RVE2	protein REVEILLE 2 / DNA binding / transcription factor	Blue		Yellow	Blue			
AT5G43030		cysteine/histidine-rich C1 domain-containing protein	Yellow				Yellow		
AT5G43040		cysteine/histidine-rich C1 domain-containing protein	Yellow				Yellow		
AT5G43580		Serine protease inhibitor,	Yellow					Yellow	
AT5G48000	CYP708A2	cytochrome P450 708A2	Blue			Blue			Yellow
AT5G48850	ATSDI1	tetratricopeptide repeat domain-containing protein	Blue	Yellow		Blue			Yellow
AT5G51440		heat shock protein 23.5	Blue			Yellow			
AT5G52310	LTI78	low-temperature-responsive protein 78	Yellow						Yellow
AT5G58120		TIR-NBS-LRR class disease resistance protein	Blue				Yellow		
AT5G59820	RHL41	C2H2-type zinc finger protein	Blue	Yellow	Yellow				
AT5G64510		hypothetical protein	Blue	Yellow	Yellow	Yellow			

Finally, quantitative real-time PCR (qRT-PCR) was used to confirm the results of the microarray analysis for selected representative genes. The transcript level of six genes, i.e. QUA-QUINE STARCH /QQS (AT3G30720), nicotianamine synthase 4 /NAS4 (AT1G56430), metal tolerance protein A1/MTPA1 (AT3G61940), C-repeat-binding-factor 3 CBF3/ DREB1A (AT4G25480), RPM1-interacting protein 4 /RIN4 (AT3G48450) and the WD40 domain containing protein (i.e. the mutated gene in IZS 288), were analyzed in triplicate samples and the relative transcript levels (RTL) were determined. Except for CBF3 that showed larger difference in qRT-PCR, the differences in transcript values observed between the two genotypes (WT and IZS 288) and stress condition (at optimal condition and after chilling stress) were more or less equivalent in both qRT-PCR and microarray read outs (Fig. 3.14).

Table 3.14. A) Relative transcript levels (RTL) of six different genes determined by qRT-PCR and unlogged expression values from the microarray experiment. RTL values were expressed relative to EF1 α and are arithmetic means \pm SD of three independent experiments. B) Fold differences in transcript levels between the two genotypes and stress conditions determined by qRT-PCR and microarray analysis.

A)

	qRT-PCR				microarray			
	Col	IZS-288	Col-4°	IZS-288 4°	Col	IZS-288	Col-4°	IZS-288 4°
QQS	1.26	12.00	0.20	1.07	77.57	605.16	37.58	131.24
CBF3	2.34	6.22	65.49	95.36	103.29	242.92	2523.72	2856.18
MTPa1	5.16	1.14	1.00	1.40	136.49	36.04	29.95	33.62
NAS4	6.03	1.94	7.74	5.22	437.71	126.12	320.14	268.41
WD40	15.81	12.57	8.60	13.32	352.33	365.92	287.56	337.37
RIN4	345.79	58.55	46.94	36.25	3020.75	465.76	444.87	500.23

B)

	qRT-PCR				microarray			
	Col	IZS-288	Col-4°	IZS-288 4°	Col	IZS-288	Col-4°	IZS-288 4°
QQS	1.00	9.50	0.16	0.85	1.00	7.80	0.48	1.69
CBF3	1.00	2.66	27.96	40.71	1.00	2.35	24.43	27.65
MTPa1	1.00	0.22	0.19	0.27	1.00	0.26	0.22	0.25
NAS4	1.00	0.32	1.28	0.86	1.00	0.29	0.73	0.61
WD40	1.00	0.80	0.54	0.84	1.00	1.04	0.82	0.96
RIN4	1.00	0.17	0.14	0.10	1.00	0.15	0.15	0.17

3.3 Understanding the link between flavonoids and heavy metal ions

The root length of the five *tt* mutants on the specified media without the inclusion of heavy metal ions (Fig 3.53-55) were more or less comparable to that of the wild type (Ler-0) root length. However, *tt7* showed wide range of variation among seedlings grown in the same experimental condition as well as between experimental replicates. When it comes to tolerance towards heavy metal stress, the *tt* mutants demonstrated different levels of tolerance.

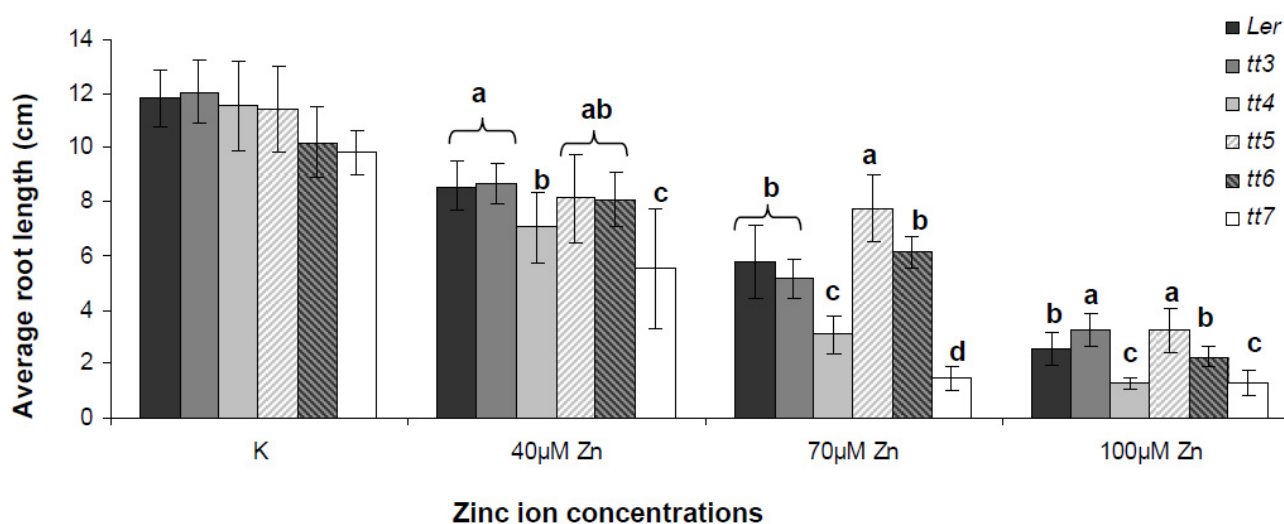


Figure 3.53. Zn hypersensitivity response of *tt* mutants. Vertical bars represent the average root length of 30 three weeks old seedlings grown on vertical agar plates treated with 40, 70 and 100 µM ZnSO₄. At control condition (K) root length was comparable for all different lines. However, at higher zinc concentration *tt4* and *tt7* showed reduction in root length. (Different letters represent significantly different means)

The *tt4* (Chalcone synthase deficient line) and *tt7* (Flavonoid 3-hydroxylase deficient line) mutant lines showed a strong dose dependent sensitivity towards Zn (Fig 3.53). The strongest reduction was observed in *tt7* at 70µM Zn concentration, where *tt7* seedlings root length measured only 25% of the average root length of the wild type (Ler-0). However, *tt3*, *tt5* and *tt6* showed no apparent hypersensitivity phenotype in response to the Zn ion concentration present in the media. Rather, at higher Zn concentrations *tt3* and *tt5* showed comparatively longer average root length than the wild type, which could be indicative of their tolerance towards Zn stress.

In the case of Cd stress, a minimum root length reduction was observed on all *tt* lines except for *tt5*. Similar to that of the response to Zn stress, *tt5* showed slightly better tolerance towards Cd stress as well (Fig 3.54).

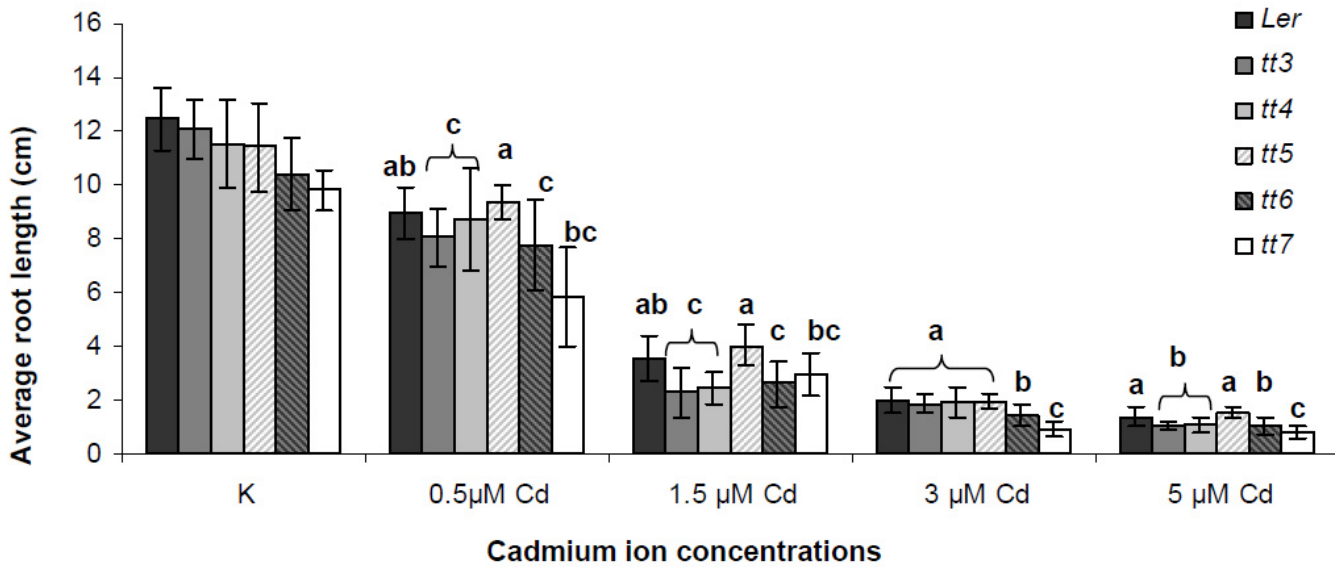


Figure 3.54. Cadmium (Cd) hypersensitivity response of *tt* mutants. Vertical bars represent the average root length of three weeks old seedlings grown on vertical agar plates treated with 0.5, 1.25, 3 and 5 μM CdCl₂. K represents control, media untreated with heavy metal ions. (Different letters represent significantly different means).

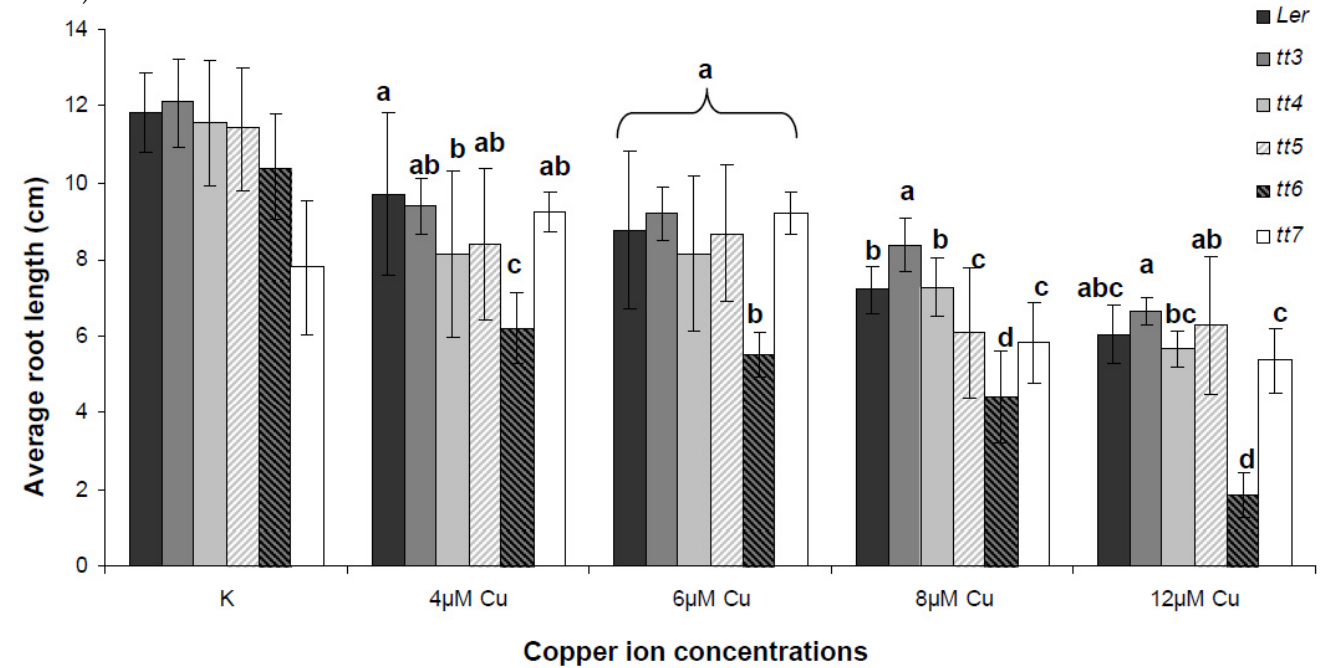


Figure 3.55. Copper (Cu) hypersensitivity response of *tt* mutants. Vertical bars represent the average root length of three weeks old seedlings grown on vertical agar plates treated with 4, 6, 8, and 12 μM CuCl₂. At control condition (K) root length was comparable for all different lines except for *tt7*. At the given experimental condition *tt7* showed slightly reduced root length even under normal (without Cu stress) growing condition. However, the effect of Cu stress was the strongest on mutant line *tt6*. (Different alphabets represent significantly different means)

On the other hand, the only mutant that showed hypersensitivity response to Cu stress is *tt6*. Particularly, at the highest concentration tested (12 μM of CuCl₂) *tt6* showed approximately a 70% root length reduction (Fig. 3.55). Another interesting observation in this experiment was that *tt7* (that showed strong hypersensitivity towards zinc and slight hypersensitivity towards cadmium) showed moderate growth improvement at lower Cu concentrations. This

Results

effect is more visible on figure 3.56 that depicts a picture of sample of seedlings grown at different Cu^{2+} concentration.

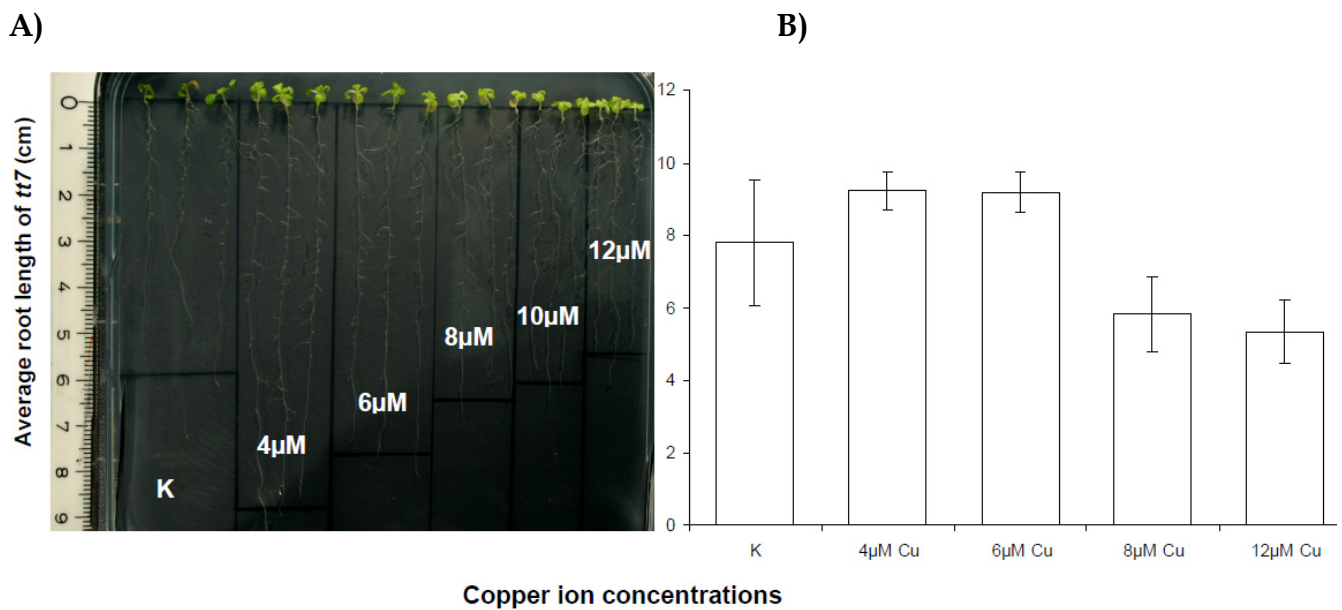


Figure 3.56. A) Picture of a vertical agar plates with seedlings of *tt7* grown at different Cu concentrations. B) A graph representing the average root length of *tt7* at 4, 6, 8, and 12 μM CuCl_2 .

Since *tt7* showed the most interesting phenotype (i.e. sensitivity towards cadmium and zinc and tolerance towards copper) further investigation was carried out on *tt7*. To begin with, its metal content was determined and compared to that of wild type (Ler-0), whereby *tt7* showed significantly higher content of zinc in both leaves and roots and higher content of cadmium in leaves (Fig 3.57). Moreover, *tt7* had a general trend to have higher content of metals in both leaves and roots, but, since there is large variation in metal content between seedlings within the same genotypes, the observed difference between genotypes is not large enough to be statistically significant.

Meanwhile, the impact of heavy metal stress on the metal content of *tt* mutants was investigated by measuring the metal content of *tt7* and wild type (Ler-0) after 7 days of Cu stress at different levels of ion concentration. In which case, the two genotypes (i.e. *tt7* and Ler-0) reacted differently to copper stress by showing significant difference in their Zn, Mn and Cd content of both leaves and roots (Fig. 3.58). Similarly, their Mo, Fe and Ni content in leaves and their Cu content in roots are significantly different between the two genotypes under Cu stress (Tab. 3.15). Additionally, the strength of the Cu ion stress had a significant effect on the Cu (incremental effect in both leaves and roots), Fe (reduction in leaves and an increase in roots) as well as Mo (reduction in both leaves and roots) content of both genotypes. In addition, the Mn content of leaves and the Cd content of roots also showed

Results

significant reduction because of the Cu stress in both genotypes. However, interaction between genotype and concentration of Cu stress was only observed in roots Cd content, where Cd content of Ler-0 roots increase significantly with the level of Cu stress up until the highest (8 μ M) level of stress, but in case of *tt7* roots a significant increase in Cd content was only observed at the highest level of Cu stress (Tab. 3.15) implying different degrees of response between the two genotypes.

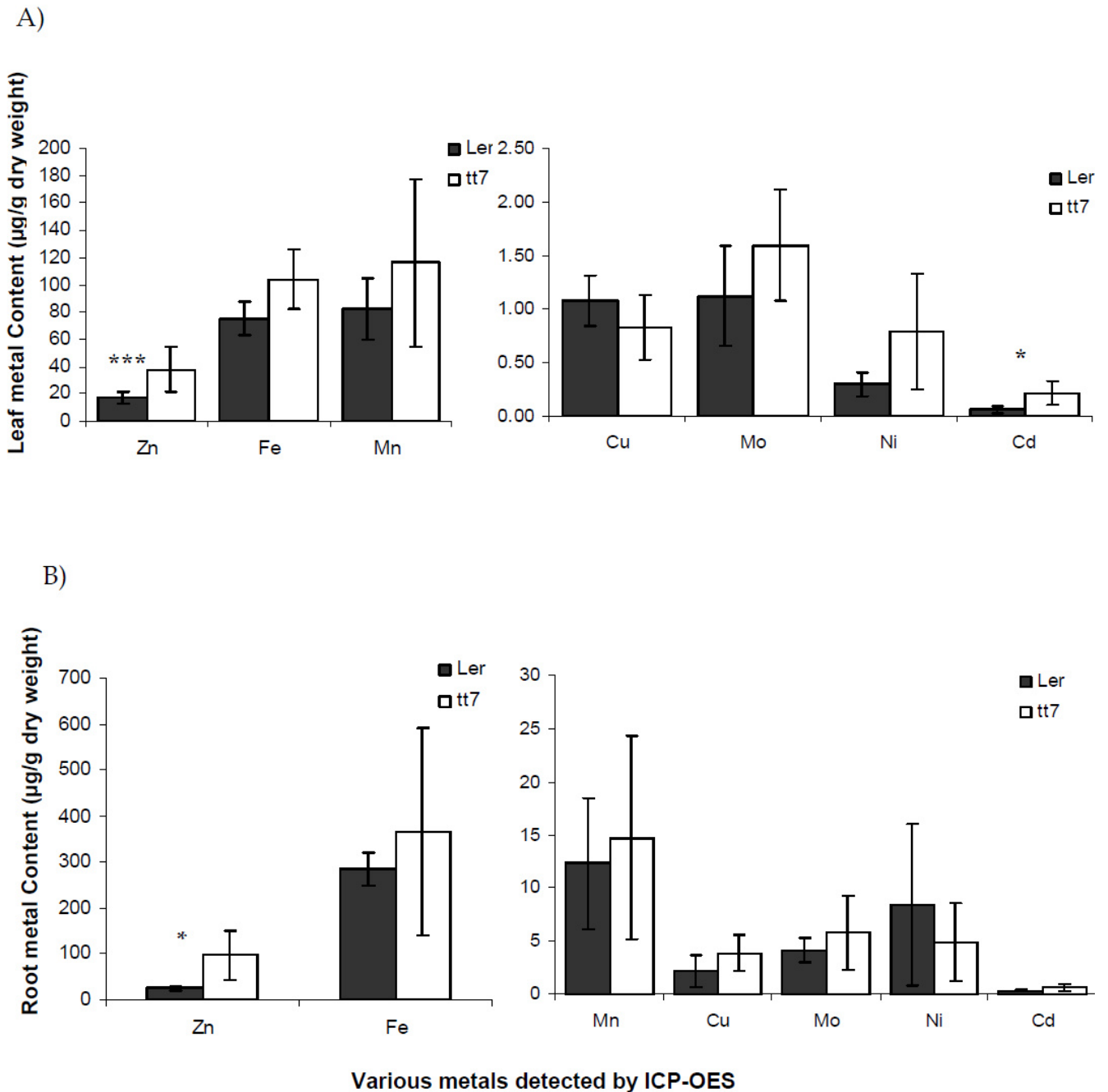


Figure 3.57. Metal content of A) leaves and B) roots of *tt7* and wild type grown on 1/10 Hoagland media hydroponically for three weeks. (‘****’ for 0.001, ‘***’ for 0.01 and ‘*’ for 0.05 significance level).

Results

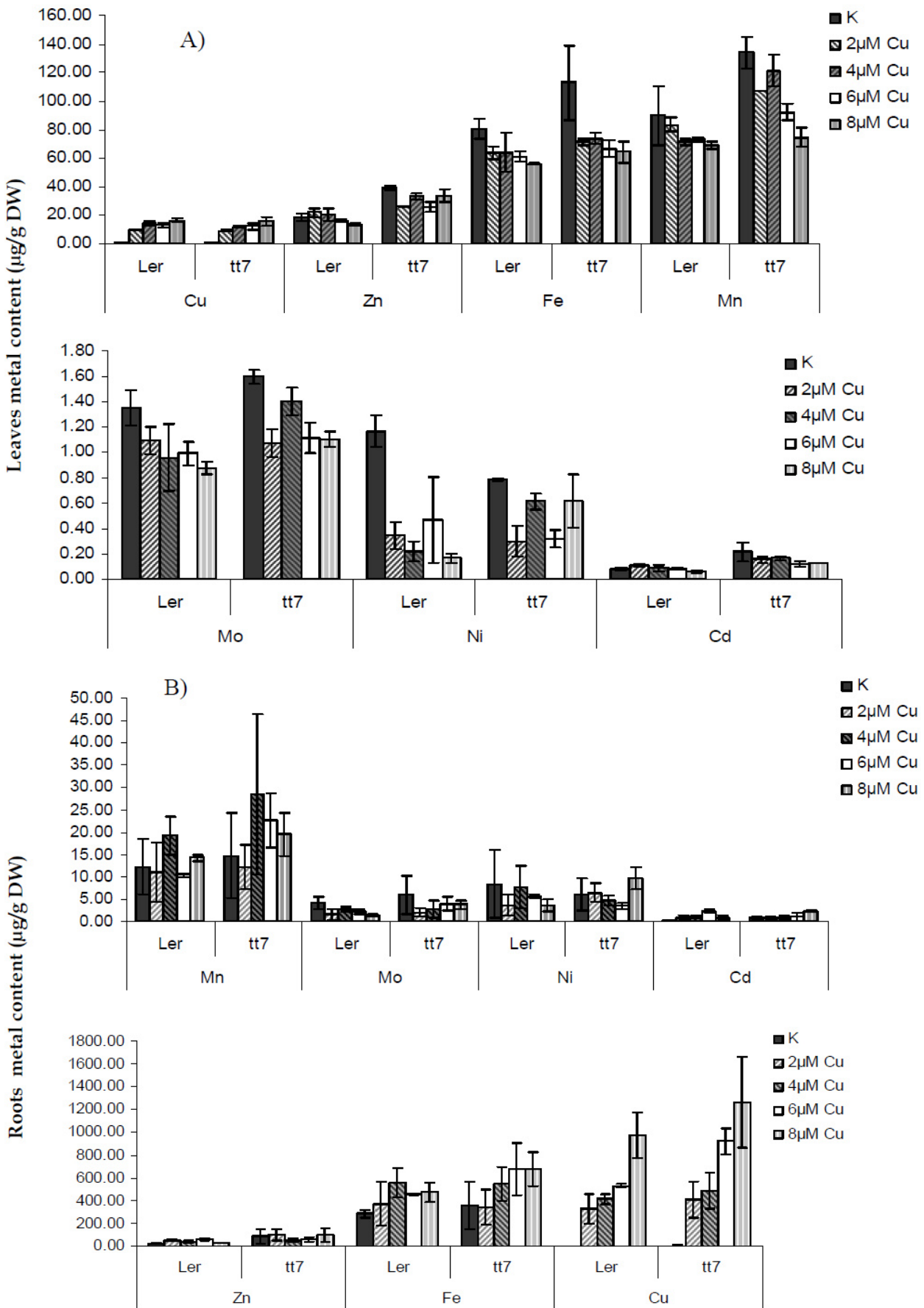


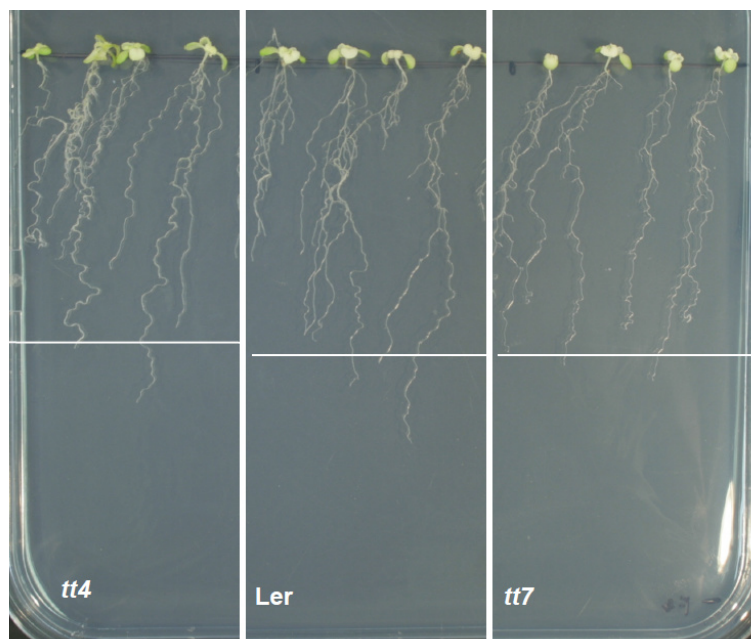
Figure 3.58. Metal content of A) leaves and B) roots of *tt7* and wild type grown on 1/10 Hoagland media hydroponically and exposed to different level of Cu stress (2µM, 4µM, 6µM and 8µM) for 7 days.

Table 3.15. Significant impact of Cu stress on metal content of *tt7* and wild type (Ler-0 and the possible interaction of the two factors (genotype and stress intensity)

<i>Metals</i>	<i>Plant part</i>	<i>Genotype</i>	<i>Cu concentration</i>	<i>Interaction</i>
Zinc	Leaves	***	-	-
	Roots	**	-	-
Iron	Leaves	**	*	-
	Roots	-	*	-
Copper	Leaves		***	-
	Roots	*	***	-
Manganese	Leaves	***	*	-
	Roots	*	-	-
Molybdenum	Leaves	**	**	-
	Roots	-	*	-
Nickel	Leaves	*	-	-
	Roots	-	-	-
Cadmium	Leaves	*	-	-
	Roots	*	**	*

(**** for 0.001, *** for 0.01 and ** for 0.05 significance level)

In a different approach, to check for the contribution of flavonoid-metal complexes as means of storage of metal ions, *tt4* and *tt7* were tested for iron deficiency symptoms by growing them side by side with Ler-0 on an iron deficient media. As seen on figure 3.59, even if leaf chlorosis is visible as a sign of iron deficiency, neither *tt4* (deficient in flavonoids) nor *tt7* (with excess kaempferol) showed deviating phenotype from the wild type.

**Figure 3.59.** A picture of a root growth assay depicting *tt4*, Ler-0 and *tt7* on vertical agar plate, where iron was omitted from the 1/10 Hoagland media. No difference in phenotype between the genotypes was observed.

4. Discussion and conclusion

4.1 The quest for new genes involved in zinc homeostasis

In comparison to the number of putative IZS mutants described, the small number of confirmed mutants (i.e. 255 putative/28 confirmed) gives the impression of the majority of the putative mutants turn out to be false positives. However, the reason behind this huge discrepancy between the number of putative and confirmed IZS mutants is that the confirmation step of the genetic screen is not yet complete. Only about 100 putative IZS mutants have been tested for the genuineness of the phenotype, the rest of the putative IZS mutants are awaiting the confirmation step. Therefore, in the near future there is still a potential for the number of IZS mutants to increase.

Among the five IZS mutants under investigation, four showed a combination of phenotypes. These mutants could be instrumental for the investigation of the interaction of different physiological process as well as homeostasis mechanisms of heavy metal ions like Zn, Cu and Mn. There are existing reports regarding shared detoxification strategies of toxic metal ions like Cd and toxic level of essential heavy metal ions like Zn, such as the induction of the synthesis of phytochelatins (Tennstedt et al., 2009). Similarly, there are transporter proteins like IRT1 and IRT2 that are implicated in the transport process of various metal ions like Fe, Zn, Mn and Cd (Hall and Williams, 2003). Therefore, identification of such mutants like IZS 377, 389, 390 and 394 that show hypersensitivity to a wide range of metal ions create new opportunity for the identification of multifunctional genes taking part in nonspecific metal uptake systems, synthesis of nonspecific metal chelating ligands and efflux process.

Particularly, the mutated gene in IZS 394 (since it shows salt hypersensitivity) appears to be a multifunctional gene with broader activity rather than specific role in metal homeostasis. However, before making a conclusive statement more tests should be carried out on additional abiotic stress, testing compounds such as mannitol, paraquat, low temperature etc.

Moreover IZS 479, which showed a specific Zn hypersensitivity phenotype, was demonstrated to carry a missense mutation in the sixth transmembrane domain of the MTP1 gene. *Arabidopsis thaliana*'s MTP1 gene was the first identified CDF protein family shown to be involved in Zn transport to the vacuole. The role of MTP1 in Zn transport has been

demonstrated through series of experiments following different leads and approaches. Ectopic overexpression of AtMTP1 under the control of a cauliflower mosaic virus (CaMV) 35S promoter resulted in the enhancement of Zn tolerance as well as a slight increase in Zn accumulation in the roots (van der Zaal et al., 1999). Later on, AtMTP1 was shown to localize in the vacuole and was able to complement the Zn hypersensitivity of yeast *zrc1cot1* double mutant. Moreover, T-DNA insertion knockout mutants as well as RNAi knockdown mutant lines were shown to have Zn hypersensitive phenotype and accumulate less Zn than wild type plants (Kobae et al., 2004; Desbrosses-Fonrouge et al., 2005). Very recently, Kawachi and colleagues (2012) using site-directed mutagenesis determined a number of amino acid residues within AtMTP1 gene required for Zn transport as well as Zn²⁺ ion specificity. Based on the impact of different point mutations on the function of AtMTP1 in Zn tolerance complementation assays in yeast *zrc1cot1* double mutant, 9 amino acids substitutions have been identified to cause a complete loss of the Zn tolerance that was conferred by the intact AtMTP1. Among these 9 amino acid residues with crucial role in the Zn transport of MTP1 belongs the aspartic acid at the 293rd position. Therefore, the strong Zn hypersensitivity phenotype observed in IZS 479 is likely to arise due to the EMS induced substitution of 293rd aspartic acid (D) by asparagine (N). A potential explanation for this effect is the location of the substituted amino acid within the protein. The 3D structural model of ATMP1 suggests that Asp293 is located in the opening of the cavity towards the vacuole. This residue may well be involved in the translocation of H⁺ and/or Zn²⁺ across the membrane (Kawachi et al., 2012). Similar reports have been published about the corresponding amino acid in the PtdMTP1 of the hybrid Poplar (*Populus trichocarpa* X *Populus deltoids*) and in the EcZitB of *Escherichia coli* (Lee et al., 2002, Blaudez et al., 2005). However, the lack of complementation assays using MTP1 gene on IZS 479 weakens the credibility of the final conclusion. Meanwhile, among the IZS mutants identified in the first round of screening, IZS 101 (OZS 1) carried the exact point mutation in the MTP1 gene and complementation assay using the genomic fragment of MTP1 was able to rescue the Zn hypersensitivity phenotype of IZS 101 (Weber et al., 2013). Hence, the probability for the identified point mutation to be the cause of the Zn hypersensitivity in IZS 479 is quite high.

In summary, 28 new IZS mutants have been identified that would hopefully in the future contribute in the process of deciphering the Zn homeostasis mechanism. Among these 28 newly identified mutants, five have been further characterized that led to the identification of

one mutant (IZS 479) with Zn specific phenotype. IZS 479 carried a point mutation in its MTP1 gene, which might have caused the Zn hypersensitivity. The fact that the Zn hypersensitivity screen identified a mutant affected in a gene with a known function in the Zn homeostasis mechanism by itself can serve as verification for the capacity of the screen.

A)

Arabidopsis thaliana
Arabidopsis lyrata
Ricinus communis
Populus trichocarpa
Drosophila melanogaster
Oryza sativa
Zea mays
Xenopus laevis
Homo sapiens

```

YLHVLGDSIQSVGMIGGAI I WYNPEWKIVDLICTLAFSVIVLGTTINMI
YLHVLGDSIQSVGMIGGAI I WYNPEWKIVDLICTLVFSVIVLGTTINMI
YLHVLGDSIQSIGVMIGGGI I WYKPEWKIVDLICTLIFS VVVLGTTIRML
YIHVLGDSIQSIGVMIGGAI V WYKPEWKIVDVICTLFFSVIVLGTTIKML
YLHVLGDSIQSIGVMIGGAI I WYKPEWKIIDLICTLIFS VIVLFTTIKML
YLHVLGDSIQSIGVMIGGAI I WYKPEWKIIDLICTLIFS VIVLFTTIKML
YLHVLGDSVQSVGMVGGAI I WYKPEWKVIDLICTLVFS VVVLFTTIKML
FIHVVGDLLQSVGLIAAYV I IYKPEYKIIDP ICTFLF SVLVLITTLTIL
FIHVIGDFMQSMGVLVAAY I ILYFKPEYKYVDP ICTFVFS I LVLGTTLTIL
::**:* * : **:* * : . . . : : : : **:* * : * ** : **:* * * : : :
    
```



B)

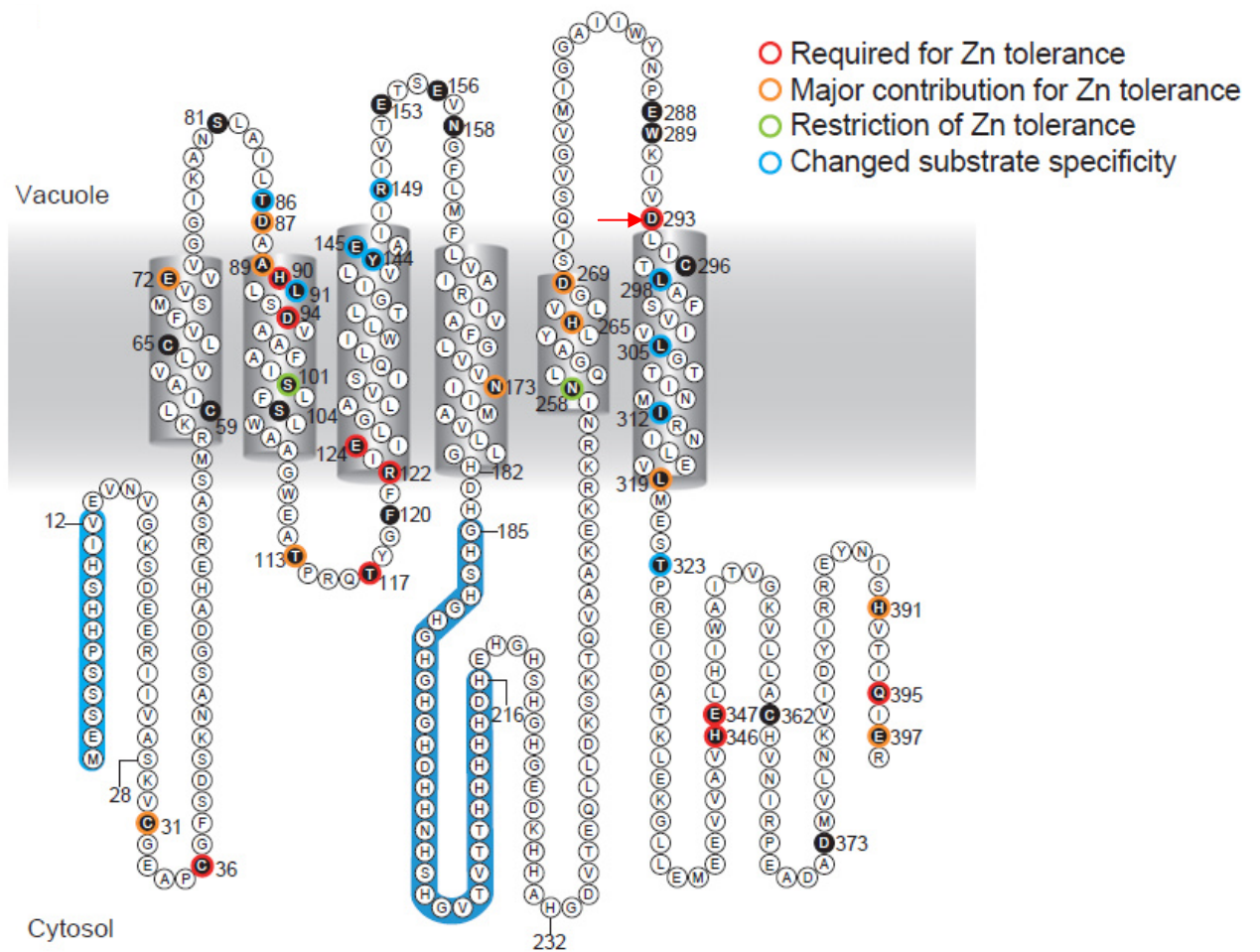


Figure 4.1. A) Multiple sequence alignment of homologues genes of MTP1, the red arrow indicates the conserved aspartic acid that got replaced by asparagine in IZS 479. B) Putative membrane topology model of MTP1 showing residues involved in the ability of AtMTP1 to confer tolerance to Zn in yeast. The red arrow indicates the location of the point mutation in IZS 479. This figure is adapted from Kawachi et al., (2012).

4.2 Mapping and characterization of IZS 288

4.2.1 Pleiotropic effects of the IZS 288 mutation

Among the Increased Zn Sensitive (IZS) mutants identified in the previous round of screening, IZS 288 showed extreme Zn hypersensitivity. IZS 288 in addition to its Zn hypersensitivity also showed pleiotropic effects like shorter primary root, earlier flower induction under short day condition, chilling hypersensitivity, alteration in leaf shapes, increased number of trichomes on the upper surface of leaves and accumulation of anthocyanins on the lower surface of leaves. Furthermore, IZS 288 has longer petioles, longer root hairs, and increased number of lateral roots, shorter hypocotyls and smaller cotyledons. The response of IZS 288 to exogenous auxin and auxin antagonists like PCIB and TIBA was also attenuated, which signifies the distortion of the auxin response spectrum of IZS 288. In the literature there have been reports about different auxin signaling and transport mutants showing a combination of various defects in root development (both in primary and lateral root growth), leaf structure alterations (including cotyledon size and petiole length), and variations in hypocotyl length and root hair density. For example, similar to IZS 288, the *arx3-1* (AUX/IAA 17) mutant shows a reduction in the elongation of the primary root and dark grown hypocotyl. It also shows an increase in the density of lateral roots and leaves have dark green hues. Interestingly, these phenotypes are partially rescued by the application of exogenous cytokinin (Leyser et al., 1996). In IZS 288 exogenous cytokinin application rescued the reduction of the primary root elongation and reduced the lateral root formation, too. The second example is the *yucca* mutant (auxin biosynthesis mutant with elevated amount of free auxin) that shows similar phenotypes like that of IZS 288 (i.e. shorter primary root and dark grown hypocotyl, increased number of lateral roots, longer root hairs and narrow leaves with extended petioles). In this mutant line, it has been shown that the phenotypes are caused by elevated levels of free auxin (Zhao et al., 2001). Additional interesting point between *yucca* and IZS 288 was observed in the microarray analysis of the *yucca* mutant that showed significantly lower transcript level of At2g20330 (i.e. the mutated gene in IZS 288) than in WT (Nemhauser et al., 2004). However, no significant association was detected between the IZS 288 gene set and gene sets representing auxin biosynthesis and/or signaling that are available in the PlantGSEA platform (Yi et. al., 2013). Taking into consideration these similarities and the moderate response of IZS 288 towards exogenous auxin and the primary root growth rescuing effect of exogenous cytokinin, it is tempting to assume IZS 288 might have a role in auxin related physiological processes and the transcript level of At2g20330 (the

mutated gene in IZS 288) is responsive to the amount of free auxin in the plant, hence the mutation in IZS 288 disrupted this process and caused the respective phenotypes. Following this line of argument an attempt was made to detect any possible difference in auxin response maxima between IZS 288 and WT using DR5::GUS marker, and under optimal condition no difference was observed. However, since IZS 288 is less responsive towards exogenous auxin, if there would be a variation between IZS 288 and WT, it is more likely for this difference to be apparent in the presence of exogenous auxin. Therefore it would be curtail to undertake the test in the presence of exogenous auxin.

Likewise, ethylene signaling defective mutant *eto1-1* (ethylene over producing mutant) showed a phenotype similar to that of IZS 288 (reduction in primary root elongation, increased number of lateral roots, shortened petiole and hypocotyl when grown in dark) (Guzman and Ecker, 1990). Furthermore, five genes (namely ASC2, ACS7, JAZ8, GRX480, and HS1^{pro-1}) involved in ethylene biosynthesis and 12 ethylene responsive genes showed lower transcript abundance in IZS 288, which could be an indicator of a disruption in the ethylene biosynthesis and/or signaling pathway. Therefore, further experiments testing for the classic ethylene triple response of IZS 288 as well as the impact of common ethylene inhibitors such as silver nitrate would be vital in order to identify the potential impact of the IZS 288 mutation on the ethylene signaling cascade.

Focusing more on the short root phenotype of IZS 288, under optimal growing condition the pronounced shortening of the elongation zone plus when exposed to Zn stress the reduction of the meristematic zone seems to be the reasons behind the root growth defects of IZS 288. The observed reduction of the meristematic region in the presence of Zn stress is further supported by the drop in the number of mitotically active cells of IZS 288 (as seen in the CycB1;1::GUS reporter lines). In WT roots also similar effects of Zn stress was observed; however, the extent of reduction of the meristematic zone was much more severe in IZS 288 roots. Likewise, in *mtp1* (a mutant line lacking vacuolar membrane Zn²⁺/H⁺ antiporter) Zn stress caused severe inhibition of root growth that occurred as result of suppression of cell division and elongation (Kawachi et al.,2009). In maize roots Zn stress was reported to inhibit root growth through a decrease in the number of meristematic cells and a reduction in the length of the fully elongated cells (Seregin et al., 2011). In sugar cane also as Zn stress has

been reported to cause a decline in mitotic activity of roots and total biomass (Jain et al., 2010).

Cytokinin is another factor involved in determining the size of the root meristem and its maintenance. It has been shown that mutants with reduced level of endogenous cytokinin like in the case of *Arabidopsis* histidine kinase 3 (*ahk3*), cytokinin oxidase-dehydrogenase1 (*AtCKX1*) and triple mutant of isopentenyltransferases (*ipt3, ipt5, ipt7*) exhibited increased root meristem size plus longer primary roots. Similarly, application of exogenous cytokinin has a reducing effect on the size of the root meristem as well as the root length in general (Dello Ioio et al., 2007). Furthermore, it has been observed that until the fourth day after germination the root meristem undergoes a gradual increase in size, but after the fifth day onwards a balance between cell division and cell differentiation is set, and this stage of the root meristem development is determined by cytokinin perception and cytokinin-mediated cell differentiation via the AHK3/ARR1 and AHK3/ARR12 two component signaling pathway (Dello Ioio et al., 2007). In a similar note, IZS 288 also maintained equivalent root length to the WT until the fourth day of germination. The reduction in root growth rate of IZS 288 was observed only after the fourth day of germination, which could be an indication of an alteration in the cytokinin signaling pathway. An alternative explanation could be a malfunction in the crosstalk between cytokinin and auxin in the maintenance of the root meristem. Since cytokinin promotes cell differentiation by increasing the abundance of short hypocotyl 2 (*SHY2/IAA3*) that represses the expression of auxin-efflux carrier proteins (*PIN1*, *PIN3* and *PIN7*) at the boundary between the meristematic zone and the root elongation zone. In contrast, auxin facilitates the degradation of *SHY2/IAA3* and promotes cell division (Dello Ioio et al., 2008). Hence, cytokinin and auxin interact antagonistically to control the balance of cell division and differentiation in the transition zone of the root tip (Su et al., 2010). Therefore, alteration in either auxin or cytokinin biosynthesis and signaling could be the reason behind the short root phenotype of IZS 288. Further investigation could be tailored to identify possible alteration in cytokinin signaling by using the cytokinin reporter line *ARR5::GUS*.

Meanwhile, under optimal growing condition IZS 288 had more lateral roots per unit root length as well as the incidence of secondary and tertiary lateral roots were higher than that of the WT. A recent report (Richard et al., 2011) has indicated the involvement of Zn in the

development of lateral roots in *A. thaliana*, whereby moderate Zn treatment (50 μ M) has resulted in an increase in the number of lateral roots of some *Arabidopsis* ecotypes. Even though, in this report the ecotype Colombia was not listed as an ecotype showing Zn related increase in the number of lateral roots, in our experimental setup Colombia also showed Zn induced lateral root number increase, but IZS 288 did not. In IZS 288 the highest number of lateral roots was observed on plates without Zn. One possible explanation for this observation is that the increased frequency of lateral roots in IZS 288 is directly linked to the irregularity in the Zn homeostasis mechanism. Thus, in WT roots Zn application activated a process that led to an increase in the number of lateral roots but in case of IZS 288, since the Zn homeostasis mechanism is distorted, increased number of lateral roots was observed without the application of Zn. The other possible explanation is that Zn influences lateral root development rather indirectly by manipulating the level of auxin or its signaling. As it has been previously described IZS 288 showed decreased response to exogenous auxin and many auxin insensitive mutants also display alteration in the number of lateral roots; hence, the alteration of root morphology in IZS 288 could be a result of distorted auxin biosynthesis, transport or signaling. One observation that supports this hypothesis is that a long term Zn exposure in IZS 288 caused a lateral root abortion (i.e. lateral roots remain as a balls of undifferentiated cells) which is similar to the phenotype observed in Aberrant Lateral Root Formation 3 mutant (*alf3*). It has been suggested that *alf3* affects a locus involved in either transport or biosynthesis of auxin in the developing lateral root and it can be rescued by exogenous application of indole-3-acetic acid (IAA) (Celenza et al., 1995). The second observation made in favor of the hypothesis that Zn interacts with auxin signaling in determining the development of lateral roots is the detection of Zn hypersensitivity phenotype in the auxin influx deficient mutant (*aux-1*). This further strengthens the involvement of auxin in Zn homeostasis mechanism or vice versa. The interconnection between the role of Zn and auxin in plant development has been first reported, when Zn deficient plants were shown to have lower level of indole-3-acetic acid (Skoog, 1940). Later on, the meristematic regions at leaf bases and root tips were shown to accumulate Zn and at the same time have high concentration of auxin, implying the interaction of auxin and zinc in the regulation of plant growth (Haslett et al., 2001). Similarly, enhancement of the auxin-induced growth of callus by zinc treatment was reported suggesting that zinc is an important factor in auxin-mediated plant growth (Oguchi et al., 2004).

The other observed irregularity in IZS 288 root is the increased number of cells at the side of the root cap (Lateral Root Cap cells, LRC). The root cap forms a protective cell layer that continually sloughs off as the root tip explores new territory and also serves as a sensor for environmental signals such as gravity, light and touch. The root cap is mainly composed of two types of cells: the columella cells which are the site for gravity sensing and the lateral root cap cells (LRC) (Ottenschlager et al., 2003). LRC divide periclinally to form new layers of LRC and anticlinally to produce a daughter cell that will differentiate into epidermal tissue (Petricka et al., 2012). Disorganization as well as physical and genetic ablation of the root cap has been reported to change the root architecture by inhibiting root meristematic activity and by stimulating lateral root initiation (Ottenschlager et al., 2003). Therefore, it is likely for the increased number of LRC to be related to the reduction in primary root length and increased number of lateral roots in IZS 288.

4.2.2 Chilling hypersensitivity of the IZS 288

Considering the fact that at optimum growing condition IZS 288 already showed transcriptional misregulation of 74 genes that were chilling responsive in WT roots, the chilling hypersensitivity phenotype of IZS 288 could be a secondary effect of the mutation. Among the 74 misregulated genes 65 of them showed similar pattern of expression in both IZS 288 roots at optimum growing condition and in the chilling exposed WT roots. Particularly, two transcription factors: WRKY transcription factor 75/ WRKY7 (AT5G13080) and MYB-like transcription factor /RVE8 (AT3G09600) that showed suppressed expression were part of this group. In *Arabidopsis* WRKY75 transcription factor is involved in regulating the phosphate starvation response. It has also been shown that in RNAi lines with suppressed expression of WRKY75 lateral root length and number, as well as root hair number, were significantly increased (Devaiah et al., 2007) which is also true in case of IZS 288. The second transcription factor, REV8, is a Myb-like transcription factor that shows high sequence similarity to CIRCADIAN CLOCK-ASSOCIATED1 (CCA1) and ELONGATED HYPOCOTYL (LHY), which are essential regulators of the *Arabidopsis* circadian clock (Rawat et al., 2011). Loss of RVE8 causes a delay and reduction in levels of evening-phased clock gene transcripts and significant lengthening of circadian clock pace (Hsu et al., 2013). Similarly, among the remaining 9 misregulated genes that showed opposing pattern of expression was found REV2/CIR1 (AT5G37260) another MYB family transcription factor involved in circadian regulation in *Arabidopsis* (Zhang et al., 2007). REV2 was up-regulated in

WT roots after chilling stress however it was down-regulated in IZS 288 roots under optimal growing condition.

Interestingly, four sulfur nutrition related genes (i.e. sulfate transporter 1.1 (AT4G08620), 5'-adenylsulfate reductase 3/APR3 (AT4G21990), response to low sulfur 2 (AT5G24660) and glutathione S-transferase U17(AT1G10370)) that showed up-regulation in WT roots after chilling stress were repressed in IZS 288 roots at optimum growing condition. In literature there are reports where inhibition of glutathione (GSH) synthesis and reduced glutathione reductase activity has led to reduced chilling tolerance in maize (*Zea mays*) (Kocsy et al., 2000). In *Chorispora bungeana* (an alpine plant) low-temperature induced GSH conferred chilling tolerance by maintaining high enzymatic activity and the fluid state of plasma membrane via increasing unsaturated fatty acids composition of the membrane (Wu et al., 2008). In contrast, increasing glutathione content through application of safeners (herbicide) in a chilling-sensitive maize inbred line increased protection against chilling-induced injury (Kocsy et al., 2001). Hence, in IZS 288 misregulation of the expression of sulfur uptake and assimilation genes could possibly lead to a reduction in GSH pool, which compromises their ability to degrade the high level of H₂O₂ created during chilling stress making them more susceptible to chilling stress. As a follow up one can verify this possibility by applying exogenous cysteine or γ -glutamylcysteine and increase the amount of GSH and investigate its impact in improving the chilling hypersensitivity of IZS 288.

Chilling stress induced profound transcriptional changes in IZS 288 influencing 11% of the genome while affecting 8% in the WT. In literature there are reports stating that 4%-20% of the *Arabidopsis* transcriptome are cold responsive (Chinnusamy et al., 2007). The regulation of 70% of the cold responsive genes was similar between IZS 288 and the WT, therefore the key to IZS 288 chilling hypersensitivity is hypothesized to lie in few of the differences observed between the two genotypes. One of such differences is the transcript level of cold response genes (like CBF3/DREB1A, LIT30, LIT78 and KIN1) not showing the same level of transcriptional induction after chilling stress in IZS 288. These genes showed two three fold up-regulation at optimum temperature in IZS 288 but after chilling stress they showed up to 20 fold lower transcript levels than in WT. One possible explanation for this variation could be the low transcript abundance of ICE1 (inducer of CBF expression1) in IZS 288 after chilling stress. ICE1 is a constitutive transcription factor that can bind to MYC recognition cis-

elements (CANNTG) in the promoter of CBF3/DREB1A and induce the expression of CBF3/DREB1A and its regulons during cold acclimation (Lee et al., 2005). In our case after chilling stress ICE1 showed a two fold up-regulation in WT facilitating the higher induction of CBF3 but in case of IZS 288 such effect was not observed. In further support for this notion, MYB15, an upstream transcription factor that negatively regulates the transcription of CBF genes was five fold up-regulated in IZS 288 after chilling stress. Here again, ICE1 appears to negatively regulate the transcription of MYB15 (Agarwal et al., 2006). Therefore, the low level ICE1 transcript abundance in IZS 288 after chilling stress might have led to higher transcript level of MYB15 and consequently to the repression of CBF3 (Fig. 4.2). The second possible explanation would be, since *cbf2* null mutant showed increased expression level of CBF1/DREB1B and CBF3/DREB1A and demonstrated freezing tolerance, CBF2/ DREB1C is suggested to be a negative regulator of both CBF1/DREB1B and CBF3/DREB1A (Novillo et al., 2004). Thus the increased expression level of CBF2/ DREB1C in IZS 288 could also have caused the lack of strong induction in CBF3/DREB1A. It is worth mentioning here that two zinc finger stress-response proteins, ZAT12 (At5g59820) and ZAT10/STZ (At1g27730), also showed higher level of induction in IZS 288 after chilling stress. These two stress-response proteins have been implicated to have a central role in reactive oxygen and abiotic stress signaling in *Arabidopsis* (Davletova et al., 2005; Mittler et al., 2006).

The other variation observed in chilling response of IZS 288 was that early and transient cold response genes were still up- or down-regulated after the 24 hours chilling stress. Based on a comparison made between the chilling responsive gene set of IZS 288 (i.e. 2560 genes up or down regulated as a result of chilling stress) and the cold stress response gene sets of the AtGenExpress global stress expression data set (Kilian et al., 2007) 31 genes that showed differential expression particularly at earlier time points of chilling stress (i.e. at 30 minutes, 1, 3, 6 and 12 hours) were part of the IZS 288 chilling responsive gene set (which was identified after exposing the plants to chilling stress (4°C) for 24 hours); which could be indicative of the lack of proper regulation of the expression of chilling responsive genes. Among these 31 genes three ethylene responsive element binding factor (ERF13 (AT2G44840), ERF6 (AT4G17490) and ERF2 (AT5G47220)), two MYB transcription factors (MYB4 (AT4G38620) and MYB44 (AT5G67300)) and a potential calcium sensor (TCH2/CLM24 (AT5G37770)) were included (Appendix. list 6). A previous study reported that CLM24 shows 15 fold increase after 4 hours exposure to 4°C, whereas CML24-

underexpressing transgenic lines are resistant to ABA inhibition of germination and seedling growth, show late flowering and have enhanced tolerance to $MgCl_2$, $ZnSO_4$, $CoCl_2$. Consequently, it has been postulated CML24 may have a role in redox signaling, whereby altering the sensitivity to and/or production of reactive oxygen species (Delk et al., 2005). Therefore, the constitutive up-regulation of C ML24 together with other factors may have negative impact on the chilling tolerance of IZS 288.

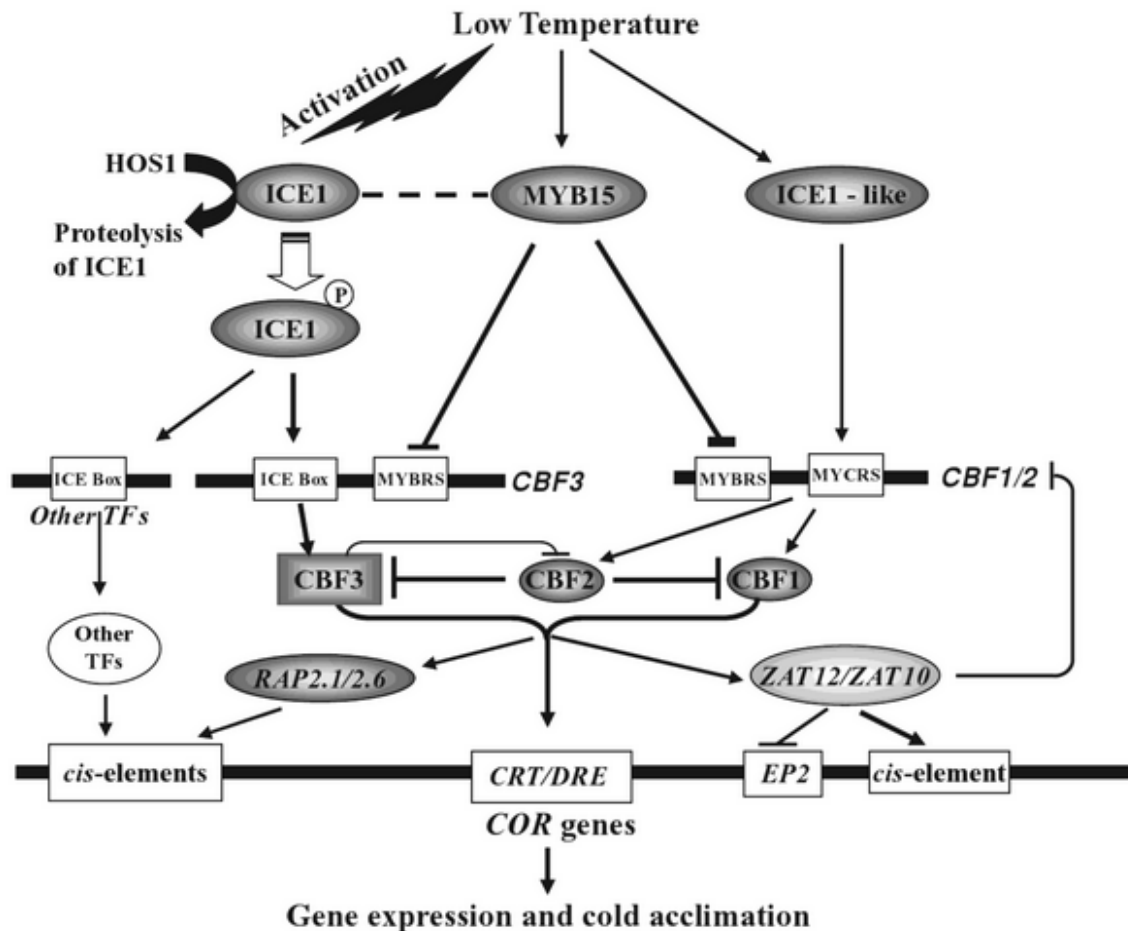


Figure 4.2. Schematic representation of the cold response pathway. Low temperature activates ICE1 and ICE1 like proteins that consequently induce the transcription of CBFs and at the same time block the transcription of MYB15. MYB15 when expressed negatively regulates the transcription of CBFs. This picture is adapted from Gong et al., 2009.

4.2.3 Zinc hypersensitivity of the IZS 288

Turning the focus to the Zn hypersensitivity phenotype of IZS 288, the microarray data analysis indicated that in IZS 288 the expression of Zn responsive genes were misregulated. Overlaps were observed in the comparison of IZS 288 gene set with that of Zn deficiency and excess Zn induced gene expression changes. It appears as if IZS 288 activated some of the Zn

deficiency and Zn toxicity response genes at the same time. On the other hand, few of the genes induced by Zn deficiency or excess Zn were showing expressional repression in IZS 288. MTP1A (AT3G61940) a member of Zn transporter (ZAT) family is one of the genes that showed repression in IZS 288. MTPA1/ATMTPA1 together with the homologous metal tolerance protein 1/MTP1 (AT2G46800) encodes functional proteins that mediate the detoxification of zinc in the cell vacuole (Drager et al., 2004; van de Mortel et al., 2006). In the hyperaccumulator *A. halleri* the expression of MTP1 in roots increased upon exposure to high zinc concentrations (Drager et al., 2004), however in *A. thaliana* the expression of MTPA1 showed an increase while being exposed to Zn deficiency (van de Mortel et al., 2006). In case of IZS 288 the basal expression level of MTP1A is lower than that of the WT, which might be a predisposing factor for the Zn stress hypersensitivity of IZS 288. Similar observations have been reported where mutants lacking functional MTP1 (the homolog of MTP1A) showing Zn hypersensitivity (Kobae et al., 2004; Desbrosses-Fonrouge et al., 2005; Kawachi et al., 2009).

Furthermore nicotianamine synthase 4 /NAS4 (AT1G56430) one of the four enzymes that synthesize nicotianamine also showed lower basal transcript level in IZS 288. In recent years, there has been an increasing amount of evidence supporting the role of nicotianamine (NA) in the intercellular and long-distance transport of Zn in plants (Klatte et al., 2009; Deinlein et al., 2012; Clemens et al., 2013). Particularly, Klatte et al. (2009) observed in quadruple NAS mutant line the Zn content of rosette leaves decreased by 38% implicating the direct role of NAS in Zn transport. Therefore, the low basal transcript level of NAS4 in IZS 288 can also contribute to its Zn hypersensitivity by hindering the Zn translocation towards rosette leaves. A third possible factor contributing to the Zn hypersensitivity phenotype of IZS 288 would be the BHLH transcription factor 39/ BHLH039 (AT3G56980) that also showed lower basal transcript level in IZS 288. It has been suggested that BHLH039 is involved in mediating signals related to Fe deficiency and/or Fe homeostasis. High Zn levels induce the expression of BHLH039 while lower Zn levels repressed its expression (Wang et al., 2007). Therefore, taking into account the expression of BHLH039 being Zn responsive, its reduced basal transcript level in IZS 288 might be one factor leading to Zn hypersensitivity.

However, all three cases of misregulation of Zn responsive genes in IZS 288 mentioned above could be the effects of altered Zn homeostasis mechanism rather than the causes of it.

Therefore, the Zn hypersensitivity of IZS 288 could also be one of the pleiotropic effects of a higher level signaling or metabolic pathways.

4.2.4 IZS 288 gene function

A map based cloning approach identified the mutated gene in IZS 288 to be a novel uncharacterized WD40 protein with homologs in a wide range of eukaryotic genomes. Interestingly, phylogenetic analysis identified only single-copy genes in each of the genomes with homologs of the IZS 288 gene. The diverse phenotypes observed in IZS 288 and the lethal or semi-lethal (sterile progeny) effect of the RNAi mediated knock-down of the *Drosophila melanogaster* homolog (CG5543) provides additional support for the single-copy gene per genome notion. If there were paralogs in either the *Arabidopsis* or the *Drosophila* genome, there would have been a redundancy in function and the occurrence of phenotypes by altering a single gene would have been less probable.

Based on the presence of a conserved 16 amino acid long motif within the WD40 domain that interacts with DDB1 (commonly known as DDB1-binding WD40 (DWD) motif) the IZS 288 gene is presumed to form a complex with cullin 4 RING ubiquitin E3 ligase (Lee et al., 2008). Cullin 4 ubiquitin E3 ligases are part of the ubiquitin proteasome pathway. The ubiquitin proteasome pathway is part of the mechanisms by which cells selectively discard defective or unwanted proteins as well as regulate the concentration of desirable proteins at a given time (Hershko and Ciechanover, 1998). The pathway entails a covalent attachment of the ubiquitin (Ub) protein (that serves as recognition signal for selective protein turnover) to target proteins using an ATP-dependent three-step conjugating cascade. The first step is the ATP dependent ubiquitin activation using the Ub-activating enzyme (E1). Then the ubiquitin is transferred to the ubiquitin conjugating enzyme (E2). Finally, the ubiquitin protein ligase (E3) delivers it to a substrate (Hershko and Ciechanover, 1998; Schwechheimer and Calderon-Villalobos, 2004; Smalle and Vierstra, 2004; Lee and Kim, 2011). Since the ubiquitin protein ligase (E3) determines the specificity of the entire pathway plants have numerous E3 ligases; the *Arabidopsis* genome contains more than 1300 genes that encode putative E3 subunits (Smalle and Vierstra, 2004). E3 ligases can either be monomeric proteins (like the HECT E3s and the RING E3s) or form multimeric complexes (i.e. cullin based E3 ligases) (Lee and Kim, 2011; Bedford et al., 2011). In cullin based E3 ligases the cullin proteins function as scaffolding subunits where the N-terminal region is capable of binding substrate adaptor

proteins and the C-terminal region of the cullin interacts with the catalytic module known as RING-finger protein (RBX1) that recruits E2 (Mazzucotelli et al., 2006; Biedermann and Hellmann, 2011; Lee and Kim, 2011). The *Arabidopsis* genome consists of five different cullins namely, cullin 1, cullin 2, cullin 3a, cullin 3b, and cullin 4, which form large array of substrate-specific E3 complexes (Lee and Kim, 2011). Among the E3 ligases the cullin-RING complexes comprise the largest known class of ubiquitin ligases (Petroski and Deshaies, 2005). The cullin 4 based E3 ligases use DNA damaged binding protein 1 (DDB1) as an adaptor to assemble the E3 ligase complex. In *Arabidopsis*, two closely related forms of DDB1 namely DDB1a and DDB1b are found (Schroeder et al., 2002). Genotypic and phenotypic analysis carried out on both genes indicated their essential function in CUL4 E3 ubiquitin ligases in *Arabidopsis* (Zhang, et. al., 2008). Most common substrate receptors of CUL4 that bind to DDB1 are composed of around seven WD40 domains, of which at least one ends in an aspartate-arginine motif (WDxR) (Lee et al., 2008; Biedermann and Hellmann, 2011; Lee and Kim, 2011). In the *Arabidopsis* genome 119 genes contain WDxR motif among which 85 contain a highly conserved 16-17 amino acid motif called the DWD box (DDB1 binding WD40). The mutated gene in IZS 288 (i.e. AT2G20330) is a member of these 85 member gene group. Lee and colleagues (2008) showed that using yeast two-hybrid assay and *in vivo* coimmunoprecipitation, 11 of the 85 *Arabidopsis* DWD proteins directly interact with DDB1 and thus may serve as substrate receptors for the DDB1- CUL4 E3 ubiquitin ligase complex. Hence, using similar approaches the direct interaction of AT2g20330 with DDB1 needs to be proven. Meanwhile, preliminary results from yeast two-hybrid and bimolecular fluorescence complementation (BiFC) assays indicated the presence of direct interaction between At2g20330 (the mutated gene in IZS 288) and DDB1 and the point mutation appears to disrupt this interaction (Prof. Stephan Clemens, personal communication, September 24, 2012).

In *Arabidopsis* RNAi mediated partial loss of function of cullin 4 resulted in a constitutive photomorphogenic (i.e. short hypocotyls and open and fully expanded cotyledons) phenotype (Chen et al., 2006). Similarly, Bernhardt and colleagues (2006) using T-DNA insertion and CUL4 antisense transgenic lines demonstrated reduced cullin 4 expression leads to a reduced number of lateral roots, abnormal vascular tissue and stomatal development. Therefore, the similar developmental defects observed in IZS 288 could have arisen as a result of partial reduction in the functionality of cullin 4 E3 ligase complex caused

by loss of a substrate receptor. Furthermore, several substrate receptors of cullin 4 E3 ligases have been discovered that take part in a range of developmental processes (Schroeder et al., 2002; Zhang et al., 2008; Lee et al., 2008; Biedermann and Hellmann, 2011). A recent study by Lee and colleagues (2010) identified two substrate receptors (DWA1 and DWA2) that are involved in the regulation of abscisic acid (ABA) signaling. Based on their observation of the increased accumulation of the leucine zipper transcription factor ABA INSENSITIVE 5 (ABI5) in DWA1 and DWA2 mutant lines they proposed DWA1 and DWA2 to be substrate receptors for ABI5. Later on, via coimmunoprecipitation they proved the physical association ABI5 with DWA1 and DWA2, which targets ABI5 for degradation. Following the same line of thought, on the bases of the findings of the microarray data it is possible to propose potential substrates of IZS 288. Hence, in the following paragraphs three potential substrates of IZS 288 are discussed in detail together with different strategies of proving them.

Based on the microarray findings IZS 288 appears to be involved in the regulation of jasmonic acid (JA) signaling. One observation that supports this hypothesis is the number of misregulated genes in IZS 288 that are JA stimulus responsive. Particularly, 6 transcription factors (namely ZAT12, MYB15, BHLH039, NAC3/ANAC055, WRKY40 and REV8) that regulate JA signaling response were among the misregulated genes in IZS 288 (Bu et al., 2008; Ivanov et al., 2011). Besides that, the JASMONATE ZIM-domain 8/JAZ8 (AT1G30135) showed low basal transcript level in IZS 288. JAZ8 is a member of the plant-specific transcriptional regulators that mediate repression of JA responses depending on the level of hormone in the cell (Shyu et al., 2012). Under optimal growing condition when the level of JA in a cell is low transcription factors (such as MYC2) that promote the expression of JA-responsive genes are repressed by members of the JAZ protein family. However, when JA accumulates in response to stress-related cues the bioactive form of the hormone stimulates the degradation of JAZ proteins via the ubiquitin 26S proteasome pathway releasing JAZ-bound transcription factors from repression, thereby allowing the expression of JA-responsive genes (Koo and Howe, 2012). The JA driven degradation of most of the 12 JAZ proteins occurs through binding to CORONATINE INSENSITIVE 1(COI1), which is the F-box protein component of the E3 ubiquitin ligase SCF^{COI1} (Shyu et al., 2012; Koo and Howe, 2012). However, very recently it was demonstrated that JAZ8 lacks the necessary motif to associate strongly with COI1 in the presence of the bioactive form of JA. Hence the mechanism by which it is removed from the cell remains unknown (Shyu et al., 2012).

Therefore, it is possible that JAZ8 is degraded by cullin 4 E3 ligase complex and IZS 288 serves as the receptor. Furthermore, the lower transcript level of JAZ8 in IZS 288 could be indicative of the presence of a negative feed back loop, where presumably excess accumulation of JAZ8 protein (due to lack of degradation) leads to the repression of JAZ8 expression. The first step to verify this hypothesis shall be testing the JA response of IZS 288, which could be easily demonstrated in the future using coronatine, a bacterial toxin that bears structural similarity to the bioavailable form of JA. Later on, the physical association of JAZ8 with IZS 288 could be investigated using yeast two hybrid or coimmunoprecipitation assays which are commonly used to detect protein-protein interactions. Furthermore the level of JAZ8 protein in WT and IZS 288 could be compared in order to show the mutation in IZS 288 has rendered malfunctioning in the degradation of JAZ8 leading to its accumulation. In the meantime, there is only circumstantial evidence supporting this notion, such as the down-regulation of sulfur uptake and assimilation genes which can serve as molecular markers for misregulation in JA signaling (i.e. sulfur deficiency leads to up-regulation of JA biosynthesis pathway (Nikiforova et al., 2003)).

In addition to being responsible for the turnover of proteins in eukaryotic cells, the ubiquitin 26S proteasome pathway is also involved in transcriptional regulation. One of the ways in which the 26S ubiquitin proteasome pathway influences transcription is through monoubiquitination of basal transcription factors or histone (Kodadek, 2009; Geng et al., 2012). Unlike the polyubiquitination of proteins that targets them for degradation, monoubiquitination provides signals for internalization of membrane proteins or for sorting newly synthesized proteins at the trans-Golgi network. It also regulates biological processes like histone modification, transcription and DNA repair (d'Azzo et al., 2005). The human steroid receptor coactivator-3 (SRC-3) is a good example for demonstrating this effect, where monoubiquitination leads to its activation but polyubiquitination beyond certain threshold targets it for degradation (Geng et al, 2012). On a similar note, in *Arabidopsis* the basal transcription factor complex (TFIIH) TTD-A subunit (AT1G12400) could be a potential substrate of IZS 288, which gets activated via monoubiquitination by the cullin 4 E3 ubiquitin ligase complex. The first observations that support this concept is a mutation in the human homologous gene of the basal transcription factor complex leads to a rare autosomal recessive disorder characterized by sulfur-deficient brittle hair and other neuroectodermal symptoms that commonly include mental and growth retardation (Hashimoto and Egly,

2009; Stefanini et al., 2010). Even if sulfur content was not determined experimentally, in IZS 288 a number of high affinity sulfur uptake and assimilation genes were repressed that might lead to alteration of the sulfur metabolism and that could be the result of malfunctioning of the basal transcription factor complex TTD-A subunit. Secondly, in IZS 288 the transcript level of the basal transcription factor complex TTD-A subunit was higher than in WT, which could also be an indication for its malfunctioning. Here again experimental set up demonstrating the interaction of the basal transcription factor complex (TFIIH) TTD-A subunit with IZS 288 is required in order to prove this notion. Following similar approaches as in case of JAZ8, yeast two hybrid assay or bimolecular fluorescence complementation (BiFC) assay could be set up, where IZS 288 is used as bait and its interaction with the basal transcription factor could be investigated.

The third potential substrates of IZS 288 are three core histone family proteins, namely histone 2B/ H2B (AT3G46030), histone 3.1/ H3.1 (AT3G27360) and the two paralogs of histone 4/H4 (AT3G45930 and AT3G46320) that showed higher basal transcript level in IZS 288. Chromatins are formed by chromosomal DNAs wrapping around histone octamers that consist of two sets of each of H2A/H2B and H3/H4 dimer. In all eukaryotes since most histones are encoded by multiple genes there is always a potential for generating excess histones (Singh et al., 2009; Singh et al., 2012). It has been reported that in yeast excess histone leads to chromosome instability and enhanced DNA damage (Takayama and Toda, 2010). Therefore, eukaryotic cells have acquired different mechanisms of strictly regulating their histone protein levels. One way of regulating histone levels is through post-transcriptional modifications such as ubiquitination (Singh et al., 2009). In mammals it has been demonstrated that H3 and H4 ubiquitination occur via cullin 4 ubiquitin E3 ligase complex, which also facilitates cellular response to DNA damage caused by UV irradiation (Wang et al., 2006). On a different note, ubiquitination of histones can also act non-proteolytically to control gene activity. Best studied examples for non-proteolytic control of gene activity by histone ubiquitination are H2A and H2B. The ubiquitination of H2A is typically associated with chromatin compaction and transcriptional repression, whereas H2B ubiquitination is associated with gene activation (Weake and Workman, 2008). Hence, it is possible for IZS 288 to be receptor of H2B, H3 and H4 and consequently the mutation might have stronger impact in regulation of transcription through chromatin remodeling. In IZS 288, the long list of pleiotropic effects and the overlaps between the differentially expressed genes set of IZS 288

and the Zn, Fe and sulfur response gene sets also suggest misregulation of transcription. Moreover, since both deficiency and toxicity induced genes appeared to be misregulated the defect seems to be in a general regulatory process rather than in a specific nutrient homeostasis process. However, the possibility for other explanations such as a cross talk between the different homeostasis processes can not be ruled out. Besides that, within this conceptual framework it would be possible to explain the observed Zn hypersensitivity of IZS 288. In literature there are reports showing the influence of Zn on histone expression and modification as well as on the ubiquitin 26S proteasome pathway. Such as in cultured hippocampal (brain) cells Zn induces polyubiquitination in a concentration- and time-dependent manner, may impair protein degradation pathway and may be a crucial factor mediating neuronal death following traumatic brain injury (Zhu et al., 2012). In *Drosophila* in addition to its essential role in the reprocessing of ubiquitin moieties from polyubiquitinated proteins, Zn can induce an extensive structural rearrangement of the 26S proteasome which could be part of the polyubiquitinated substrate identification system of the pathway (Kiss et al., 2005). Sadil and colleagues (2011) showed that Zn decreased the expression level of histone H3 and H4 in human neuronal cells and reduced histone H3 acetylation by altering the activity of histone de-acetylases. Therefore, in IZS 288 if the hypothesis holds true and the histone proteins are substrates, Zn could lead to even higher degree of misregulation of transcription by influencing the transcription and/or modification of histones.

There is also a large body of evidence linking histone modifications with chilling resistance (Stockinger et al., 2001; Benhamed et al., 2006, Sokol et al., 2007; Zhu et al., 2008; Kwon et al., 2009; Kumar and Wigge, 2010). Particularly in Kwon et al. (2009) work it has been shown that during exposure to cold stress the enrichment level of methylated histone 3 (H3K27me3) in two cold responsive genes, *COR15A* and *AtGOLS3*, decreased gradually. Zhu and colleagues (2008) showed HOS15, a histone H4 de-acetylase, is responsible for repressing gene expression in response to cold stress. Interestingly, in *Arabidopsis* the alternative histone H2A.Z has been identified as the sensor for ambient temperature. Genotypes deficient in incorporating H2A.Z into nucleosomes phenocopy warm grown plants, and show a striking constitutive warm temperature transcriptome (Kumar and Wigge, 2010). Hence, in IZS 288 the increased transcript level of *COR15A* and *AtGOLS3* at optimal temperature (without being exposed to chilling stress) could have been the result of a defect in histone occupancy

and/or modification that lead to the activation of stress induced genes without the exposure to the stress.

On a similar note, in *Arabidopsis* simultaneous knockout of two histone chaperons, NRP1 and NRP2, impaired postembryonic root growth. In the *nrp1-1 nrp2-1* double mutant, arrest of cell cycle progression at G2/M and disordered cellular organization occurred in root tips (Zhu et al., 2006). Surprisingly, the root structure of the *nrp1-1 nrp2-1* double mutant, with a very short primary root length and increased number of lateral roots, appears similar to that of the IZS 288 root morphology. Especially, the root tip structure, where the meristematic and elongation zones are reduced, shows similarity to the defects of IZS 288 root tip structure. Thus, the root architecture alteration of IZS 288 could also be a result of histone level imbalance caused by malfunctioning of a substrate receptor (i.e. IZS 288) of the ubiquitin mediated 26S proteasomal pathway. In future studies, the impact of the IZS 288 mutation on histone modifications could be investigated using Trichostatin A (TSA) an organic compound that inhibit a group of the histone deacetylase (HDAC) family of enzymes. Such a test will have a broad impact on both WT and IZS 288 plants; however if the mutation of IZS 288 has a direct effect on the process of histone modification, IZS 288 plants will show strong hypersensitivity than WT plants.

4.2.5 The IZS 288 mutation

Since the point mutation in IZS 288 has replaced the 377th threonine (a conserved amino acid across homologs genes) by isoleucine, the first assumption was the mutation might have caused a loss of phosphorylation site in the protein leading to malfunctioning of the protein. However, transgenic lines carrying alanine substitution for the 377th threonine, another non-phosphorylatable amino acid, did not exhibit IZS 288 like phenotypes (short root and zinc hypersensitivity), thus the mutation effects were not caused by loss of phosphorylation site. The alternative explanation for the effect of the point mutation in IZS 288 comes from comparing the amino acid property of threonine and the substitute amino acid isoleucine. The two amino acids differ both in their size as well as chemical property. As it can be seen on the Venn diagram illustrating the properties of amino acids (Fig 4.3) , threonine belongs to a group of amino acids that are slightly polar and small in size; but isoleucine belongs to the hydrophobic amino acid groups that have aliphatic side chains (Betts and Russell, 2003). Since the structure of the IZS 288 protein is not yet identified, demonstrating the impact of

the Thr/Ile substitution on the protein function is very difficult. However, based on the nature of the amino acids taking part in the substitution it is possible to infer the impact it might have on the protein structure. Threonine being slightly polar amino acid can reside on the surface of a protein and quite commonly situated in functional centers of proteins. On the other hand, Ile being hydrophobic amino acid prefers to be buried in protein hydrophobic cores and because of the non-reactive side chains are rarely directly involved in protein function. Hence substituting Thr by Ile may lead to destabilization of the protein structure inhibiting it from binding to cullin 4-DDB1 ubiquitin E3 ligase complex. An indirect supporting evidence for this supposition is both transgenic lines carrying alanine or serine substitution were able to complement the IZS 288 phenotype in planta. However, since the binding ability of IZS 288 construct carrying alanine/serine substations with DDB1 was not tested, the possibility for other explanations is not ruled out. In the future when information regarding the protein structure of IZS 288 or its homologs becomes available a better understanding of the effect of the point mutation on the protein structure can be achieved. In the mean time, there are reports in literature where substitution of threonine by isoleucine led to detrimental effect that could be considered as circumstantial evidences, like in the case of the S-opsin mutation that lead to Tritan color-vision deficiency (Blue-yellow color blindness) in human (Baraas et al., 2012) and GTPase gene (*SPG3A*) mutation that led to hereditary spastic paraplegia (muscle tightening in lower limbs) (Hedera et al., 2004).

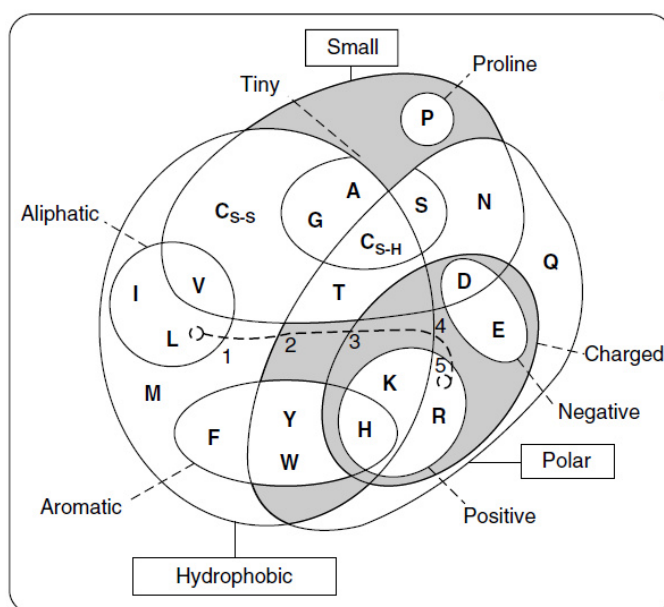


Figure 4.3. Venn diagram illustrating the properties of amino acids. This picture was adapted from Betts and Russell, 2003.

In summary, the IZS 288 mutant, in addition to being Zn hypersensitivity, also showed other pleiotropic effects like alteration of root morphology, early flowering and strong chilling hypersensitivity. This unique combination of phenotypes observed in IZS 288 could be useful later on to study the role of the Zn homeostasis mechanism in different developmental process as well as abiotic stress tolerance. The mapping and characterization of IZS 288 has lead to the identification of a novel gene with presumed function in the 26S ubiquitin proteasome pathway. The trail to identify a T-DNA mediated knockout line for IZS 288 was not successful. Based on the data at hand it is impossible to conclude if homozygous lines for the SALK_140479 T-DNA insertion line are lethal. Therefore, in the future it would be recommendable to set up a new cross between identified heterozygous lines of SALK_140479 and follow up the development of seeds in order to detect any possible defects in embryo development. Secondly, T-DNA insertion site should be verified by sequencing the neighboring genomic fragments up and down the insertion point. Despite the Zn hypersensitivity phenotype of IZS 288, no significant difference was observed in the elemental profile of both roots and shoots; however, future work is required to illustrate the impact of Zn stress on the elemental profile of IZS 288. The other open question that still requires further investigation is the influence of Zn on chilling tolerance of *Arabidopsis*. Since exposure to excess Zn under chilling temperature had drastic impact on the development of WT plants, it seems that Zn has a negative influence on the general process of chilling tolerance. Therefore, future studies should be directed in identifying the crosstalk between cold signaling and Zn homeostasis mechanism in *Arabidopsis thaliana*. On the other hand, even though the microarray data did not provide the necessary support, IZS 288 appeared to have auxin signaling related defects and a known auxin transport mutant (Aux1) showed Zn hypersensitivity; hence there is still room for further progress in determining the link between Zn and auxin signaling. Finally, among the outputs of the microarray analysis there were candidate genes with a potential to be substrates for the IZS 288 in the cullin 4 E3 ubiquitin ligase complex.

In the future, first the findings of the preliminary results regarding the interaction of the IZS 288 with that of DDB1, which was attained using yeast two hybrid interaction assay and bimolecular fluorescence complementation (BiFC) assays, should be further verified using different negative and positive controls in order to exclude the possibility of a false positive. In vivo coimmunoprecipitation (Co-IP) assay could also be performed as a third approach in

proving the interaction of IZS 288 with DDB1. One approach of attaining this would be, first to capture DDB1 from protein extract of *Arabidopsis* tissues using an antibody specific for DDB1 and then performing subsequent immunoblot assays using specific antibody for IZS 288 on the extract immunoprecipitated for DDB1. Furthermore, the effect of the point mutation in IZS 288 on its interaction with DDB1 should be further investigated by creating different constructs of IZS 288 carrying different amino acid substitutions at position presumed to have positive or negative impact on the interaction with DDB1. A starting point for this investigation could be the constructs carrying alanine or serine in the place of the 377th threonine. Since these two constructs were able to complement the phenotypes of IZS 288 it is possible that they maintained the interaction with DDB1. Secondly, the interaction of IZS 288 with the proposed candidate substrates should be tested. For this purpose IZS 288 could be used as bait in yeast two hybrids and its interaction with JAZ8, basal transcription factor complex (TFIIH) TTD-A subunit and the three histones families (i.e. H2B, H3.1 and H4) could be investigated. The principle behind a yeast two hybrid assay is the transcription factor, which is required for the activation of downstream reporter gene by binding onto an upstream activating sequence (UAS), is split into two separate fragments, known as the binding domain (BD) and the activating domain (AD). The construct containing the binding domain and protein of interest usually called the bait binds to the UAS, however for transcription of the reporter line to succeed a second construct called the prey carrying the activating domain and a potential interacting protein should interact with the bait. Hence, the activation of the reporter gene signifies an interaction between the protein of interest hosted in the bait construct and the potential interacting protein in the prey construct (Young, 1998). Alternatively, bimolecular fluorescence complementation (BiFC) assays could be used to validate the interaction of IZS 288 with the three potential substrates. The premise for the BiFC assay is the association of fluorescent protein fragments. The protein of interest and a potential interacting partner are fused to either the amine-terminus or carboxyl-terminus of unfolded complementary fragments of a fluorescent reporter protein and expressed in live cells. If and when these two proteins interact it allows the two fluorescent fragments to come to proximity leading to the re-formation of the reporter protein in its native three-dimensional structure and emit its fluorescent signal (Kerppola, 2008). Finally, positive interactions observed in the yeast two hybrid assays or BiFC assays could be confirmed using coimmunoprecipitation (Co-IP) technique.

4.3 Understanding the link between flavonoids and heavy metal ions

The potent capacity of metal-flavonoid complexes in scavenging radicals has been experimentally demonstrated (Kostyuk et al., 2001 and de Souza and de Giovani, 2004). Similarly, diversity in the metal chelating ability of flavonoids has been demonstrated. For example, Ren et al. (2008) report quercetin to have superior ability of chelating iron ions than kaempferol, and Mira et al. (2002) report a higher reducing capacity of flavonoids for copper ions than for iron ions.

On the other hand, the *tt* mutants have demonstrated a wide range of variation in tolerance response to different environmental cues. For instance, the impact of UV-B stress is higher on all three *tt* mutants tested so far (*tt4*, *tt5* and *tt6*) than wild type (Ler-0), but *tt5* and *tt6* suffered far more than *tt4*, which is attributed to diminished leaf sinapate esters content (Li et al., 1993). There are also reports showing distinction among *tt* lines morphological phenotypes. It has been reported that *tt4* shows quite low lateral root density whereas *tt5* and *tt6* have higher lateral root density than wild type. In addition *tt6* had longer hypocotyl and root hairs while *tt7* had shorter root hairs (Bauer and Djordjevic, 2009). Hence, it is possible that the reported developmental deference between the *tt* mutants could have contributed towards the difference in metal tolerance of the *tt* mutants.

Therefore, the observed variation among the *tt* mutants in their tolerance response to heavy metal ion stress could be a result of the presence and absence of different flavonoids as well as their efficiency in forming complexes with metal ions and the potential of this metal-flavonoid complexes in quenching the oxidative stress that might have arisen as a result of the excess metal ions. According to Koornneef et al. (1982) *tt4* is devoid of any detectable flavonoids; consequently, it's observed strong zinc and to a lesser extent cadmium hypersensitivity could be attributed to complete lack of flavonoids. However, even if the mutation in *tt5* renders accumulation of naringenin chalcone and deficiency in upstream flavonoid, *tt5* exhibited no apparent sensitivity towards the metal ions tested, rather it had slightly better root growth at moderate stress levels. This unexpected phenomenon could be due to spontaneous isomerization of naringenin chalcone (NC) to form naringenin (N) and subsequent flavonoids, and this excess accumulation of NC with that of N and subsequent flavonoids might provide an extra layer of protection from oxidative stress. Supporting the

hypothesis of spontaneous isomerization of naringenin chalcone to naringenin, previously conducted experiments on *tt5* have demonstrated naringenin chalcone accumulation plus an unidentified peak with a retention time equal to quercetin (Peer et al., 2001). Using thin-layer chromatography, Winkel-Shirley et al. (1995) had also detected kaempferol in seeds of *tt5*. Similarly, Pelletier et al. (1999) using HPLC showed flowers of *tt5* also contained kaempferol.

Similarly, the reason behind the lack of hypersensitivity response towards cadmium and zinc in *tt3* and *tt6* could be due to the accumulation of quercetin and kaempferol and N respectively (Bauer and Djordjevic, 2009). However, one possible explanation for the surprising hypersensitivity of *tt6* towards copper ions could be a weaker copper chelating potential of naringenin in comparison to kaempferol and quercetin. In order to test this, follow up experiments should be conducted that measure chelating potential of different flavonoids towards copper.

On the other hand, *tt7* showed no apparent hypersensitivity towards cadmium and copper, which is fitting to its kaempferol accumulating nature (Koornneef et al., 1982). However, a strong zinc hypersensitivity as well as higher content of zinc in both leaves and roots was observed in *tt7*. These characteristics of *tt7* are in line with phenotypes of AtHMA1 knock-out plants (i.e. a mutant line deficient in zinc detoxification mechanism) (Kim et al., 2009). Therefore, it is tempting to assume that lack of quercetin and/or the accumulation of kaempferol might have a negative impact on the zinc detoxification mechanisms of *Arabidopsis*. Nevertheless, since greater degree of variation has been observed among *tt7* seedlings as well as between different seed batches, additional experiments must be carried out in order to rule out the effect of extraneous factors.

Among all the effects observed in the *tt* mutant lines, the most prominent and consistent is the hypersensitivity phenotype observed in response to excess Zn. The mutant completely devoid of flavonoids (*tt4*) and the one that lacks quercetin (*tt7*) showed strong zinc hypersensitivity. The link between flavonoids and Zn hypersensitivity could arise from the induction of reactive oxygen species (ROS) by the presence of excess Zn in the medium (Kim et al. 1999) and the *tt* mutants' inability to deal with the extra amount of ROS generated. However, if excess ROS generation was the only reason behind the Zn sensitivity phenotype of *tt4* and *tt7* then one would expect them also to show Cu hypersensitivity. This was not the

case in both mutant lines. Therefore, there should be additional factors to it than only ROS generation. The second alternative explanation would be Zn may directly influence the phenylpropanoid pathway. Interestingly, it has been reported that in *Arabidopsis* PAL2 (which encodes a key enzyme in the early phenylpropanoid pathway) was among the genes up-regulated by exposure to excess Zn (van de Mortel et al., 2006). Thus, the induction of the phenylpropanoid pathway by excess Zn can be one indication in *Arabidopsis* for the recruitment of flavonoids in dealing with exposure to excess Zn. The means by which flavonoids offer protection against excess Zn could be either in a form of directly chelating away Zn ions or indirectly by influencing the Zn homeostasis mechanism. Moreover, only *tt4* and *tt7* showed Zn hypersensitivity, which could be indicative of preference for particular flavonoids in dealing with excess Zn. Particularly focusing on the *tt7* mutant, which accumulates kaempferol and lacks quercetin and still shows Zn hypersensitivity phenotype, it is tempting to speculate quercetin is more potent in dealing with excess Zn. In support of this idea, quercetin has three potential metal binding sites (Fig 4.4), while kaempferol has only two. Besides that, in kaempferol the two metal binding sites can not be used simultaneously (Hider et al., 2001). Therefore, quercetin may have a better Zn chelating potential than kaempferol. However, the reported developmental differences among the *tt* mutants can not be ruled out from being a possible explanation for the variation in Zn tolerance between the different *tt* mutants (Bauer and Djordjevic, 2009).

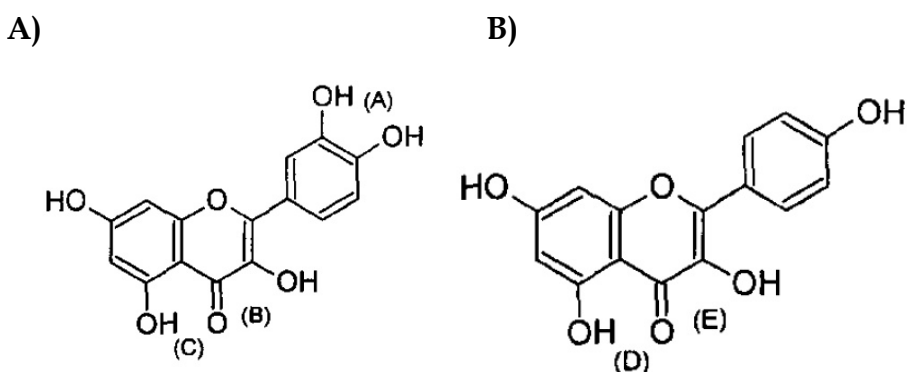


Figure 4.3. A) Potential metal binding sites of quercetin indicated by letters, the binding affinity of site (A) being greater than sites (B) and (C) at pH 7. B) Potential metal binding sites of kaempferol indicated by letters, but only (D) or (E) will be used for chelation; both can not be used simultaneously.

Additionally, independent of the copper stress effect, *tt7* contained more iron, manganese, molybdenum and cadmium and less nickel in its leaves than Ler-0. Nevertheless, copper stress caused similar effects on both genotypes except for cadmium content of roots, where *tt7* under the different copper stress levels was not able to accumulate cadmium to the same

extent as Ler-0. Meanwhile, an increase in copper content of both leaves and roots was observed, verifying the elevated concentration of available Cu ions in the different stress regimes. However, it had no impact on the zinc and nickel content of both organs. In spite of that, a significant reduction was detected in the iron, manganese and molybdenum content of leaves in both genotypes, and an increase in the root iron content, which could have arisen due to competition among different metal ions for shared transporters like *NRAMPs*, *IRT*, (Oomen et al., 2009, Hall and Williams, 2003) and chelators (Guo et al., 2008). The other possible explanation would be the interdependence of the different metal homeostasis mechanism on each other. For instance, a recent report has indicated that Cu deficiency affects the root-to-shoot Fe translocation of *Arabidopsis* (Bernal et al. 2012), which is in agreement to what has been observed here (i.e. elevated Cu availability caused a disruption in iron distribution by reducing the shoot iron content and at the same time increasing the root iron content).

Meanwhile, during the course of this project, Keilig and Ludwig-Müller, (2009) following similar experimental set up reported similar findings indicating the role of flavonoids in heavy metal stress tolerance. However, even if the final conclusion is similar, there are some major discrepancies in the details of these two experiments. According to Keilig and Ludwig-Müller, *tt5* showed hypersensitivity towards cadmium and zinc (even if a closer look at the graphs tells otherwise, like during cadmium stress the seedling weight of *tt5* and the root length of *tt7*) and the line *tt7* out performed *tt4* and *tt5* on cadmium treated plates. These variation might have arisen due to differences in the mediums used (i.e. MS and Hoagland) and the parameter considered to assess the impact of heavy metal stress (seedling weight). Especially, regarding the difference between the two media, the Ca^{2+} and Fe^{3+} content of full-strength MS (Murashige and Skoog) medium is tremendously higher than that of 1/10 Hoagland medium. Consequently to reach similar levels of Zn^{2+} and Cd^{2+} stress, up to 6-times higher amounts of metal solutions should be applied. Furthermore, the high content of cations in the medium plus vitamins and their interaction with the applied high concentration of metal salts can lead to additional factors influencing the growth of seedlings. Similar disparity between phenotypes observed in the two mediums has been reported in Tennstedt et al. (2009). While investigating stress factors with strong phenotype, the difference between the two mediums may not have a pronounced impact; but for experiments with subtle phenotypes such variations can have a significant effect with a

potential of masking important results. The second discrepancy between the two approaches was the traits considered to assess the impact of the stress (i.e. seedling fresh weight has been used as a main trait by Keilig and Ludwig-Müller, (2009) whereas in this project seedling root length was the main focus). Usually, diversified data sets have better chance in describing the physiological impact of a treatment. However, a particular trait selected based on previous observations and findings can also provide similar level of information. In this project seedling root length was used as a characteristic feature to measure the impact of heavy metal stress on plants because former findings have indicated root elongation to be far more sensitive than shoot growth to heavy metal stress (Cheung et al., 1989). Therefore, the *tt* mutants heavy metal sensitivity response observed as a change in their root elongation should be a better representative of the overall change caused by various metal ions stress.

In summary, based on the observation of these experiments, flavonoids seem to have some sort of interaction with heavy metal ions, particularly with zinc and copper ions and this interaction appears to be part of the heavy metal tolerance mechanism of *Arabidopsis thaliana* plants. Besides that, different flavonoids and intermediate compounds showed different capacity in shielding the effect of heavy metal stress. In contrast, the contribution of flavonoid-metal complexes in sequestration of metal ions particularly iron is very limited. In the future, determining the elemental profile of *tt4* mutant and investigating the effect of Zn stress on the elemental composition of both *tt4* and *tt7* might give a better understanding of the flavonoid metal interaction. Furthermore, in-depth analysis of the remaining *transparent testa* mutants like *tt1*, *tt2*, *tt8* and *ttg*, with mutations on transcriptional regulation of flavonoid biosynthesis genes might broaden the present perception about flavonoids and their role in heavy metal tolerance. The other approach could be testing the metal tolerance responses of progenies of crosses set up between the *tt* mutants that already showed hypersensitivity phenotype and other well established Zn hypersensitive mutants like MTP1. The results of such experiments can shed more light on the link between flavonoids and heavy metals like Zn.

4.4 Conclusion

This project was carried with the aim of identifying new components of the Zn homeostasis mechanism and deciphering the role of flavonoid towards heavy metal tolerance in plants.

The second round mutant screen on EMS mutagenized seeds was successful in identifying 28 new increased Zn sensitive (IZS) mutants. The steady increase in the number of the Zn sensitive mutant library will ensure in the future the identification of major stakeholders of the Zn homeostasis mechanism in plants, which will lead eventually to a better understanding of the Zn homeostasis mechanism. Having a broad and in-depth understanding of how the Zn homeostasis mechanism is governed in plants will arm the biofortification strategy with the necessary knowhow to improve the Zn content food items.

The mapping and functional characterization of IZS 288 has led to a discovery of a new gene family, the cullin 4 ubiquitin E3 ligases, that could be involved in Zn homeostasis process of *Arabidopsis*. It also gave a hint of a possible connection between Zn homeostasis and chilling stress tolerance mechanism of *Arabidopsis thaliana*. The comparative transcriptome of IZS 288 and WT identified candidate genes that are affected by the mutation in IZS 288; which could be substrates for IZS 288 and the cullin 4 ubiquitin E3 ligase complex in general. Future work in the verification of these candidate genes will illustrate either the interconnection of the Zn homeostasis mechanism with jasmonic acid signaling or identify the indirect effect of Zn on transcriptional regulation by regulating histone availability or modification.

Additionally, heavy metal stress tolerance test of five of the transparent testa (*tt*) mutants have verified the presence of metal and flavonoid interaction *in vivo*. It appears that the total lack of flavonoid synthesis (*tt4*) and/or the accumulation of quercetin (*tt7*) negatively influences Zn tolerance in *Arabidopsis thaliana*. Further studies investigating the impact of Zn stress on the overall elemental profile of *tt4* and *tt7* may identify a potential effect of flavonoids on the accumulation of Zn and other metals in *Arabidopsis thaliana*.

Overall, in the course of this project a novel WD40 gene from *Arabidopsis thaliana* that has homologs genes in wide range of eukaryotic organisms was identified. The function of this gene was still uncharacterized in almost all of the organisms with a homolog except for *Caenorhabditis elegans*. Therefore, the new knowledge acquired through this project would pave a way for functional characterization of many new genes in their respective genomes. In the future there are still several questions to be addressed such as proving the formation a complex between the WD40 protein of IZS 288 and the cullin 4 ubiquitin E3 ligase, verification of the candidate substrates, and clarifying the impact of the point mutation on

the function of the gene. Nevertheless, this project was successful in laying out the foundation for understanding the role of cullin 4 ubiquitin E3 ligases on the Zn homeostasis mechanisms of *Arabidopsis thaliana* plants.

5. Reference

1. van Acker, S.A., Tromp, M.N., Haenen, G.R., van der Vijgh, W.J. and Bast, A., (1995). Flavonoids as scavengers of nitric oxide radical. *Biochem Biophys Res Commun*, 214: 755–9.
2. Agarwal, M., Hao, Y., Kapoor, A., Dong, C.H., Fujii, H., Zheng, X. and Zhu, J.K., (2006). A R2R3 type MYB transcription factor is involved in the cold regulation of CBF genes and in acquired freezing tolerance. *J. Biol. Chem*, 281: 37636–37645.
3. van Aken, O., Zhang, B., Law, S., Narsai, R. and Whelan, J., (2013). AtWRKY40 and AtWRKY63 modulate the expression of stress-responsive nuclear genes encoding mitochondrial and chloroplast proteins. *Plant physiol*, 162: 254–271.
4. Alonso, J.M., Stepanova, A.N., Leisse, T.J., Kim, C.J., Chen, H., Shinn, P., Stevenson, D.K., Zimmerman, J., Barajas, P., Cheuk, R., Gadrinab, C., Heller, C., Jeske, A., Koesema, E., Meyers, C.C., Parker, H., Prednis, L., Ansari, Y., Choy, N., Deen, H., Geralt, M., Hazari, N., Hom, E., Karnes, M., Mulholland, C., Ndubaku, R., Schmidt, I., Guzman, P., Aguilar-Henonin, L., Schmid, M., Weigel, D., Carter, D.E., Marchand, T., Risseuw, E., Brogden, D., Zeko, A., Crosby, W.L., Berry, C.C. and Ecker, J. R., (2003). Genome-Wide Insertional Mutagenesis of *Arabidopsis thaliana*. *Science*, 301: 653-657.
5. Andreini, C., Banci, L., Bertini, I. and Rosato, A., (2006). Zinc through the three domains of life. *J Proteome Res*, 5: 3173–3178.
6. Andreini, C., Bertini, I., Cavallaro G., Holliday, G.L. and Thornton, J.M., (2008). Metal ions in biological catalysis: from enzyme databases to general principles. *J Biol Inorg Chem*, 13(8): 1205-1218.
7. Anthony, M.S., Clarkson, T.B., Hughs, C.L. Jr, Morgan, T.M. and Burke, G.L., (1996). Soybean isoflavones improve cardiovascular risk factors without affecting the reproductive system of peripubertal rhesus monkeys. *J Nutr*, 126: 43–50.
8. Arrivault, S., Senger, T. and Kramer, U., (2006). The *Arabidopsis* metal tolerance protein AtMTP3 maintains metal homeostasis by mediating Zn exclusion from the shoot under Fe and Zn oversupply. *Plant j*, 46: 861-879.
9. van Assche, F. and Clijsters, H., (1990). Effect of metals on enzyme activity in plants. *Plant Cell Environ*, 13: 195–206.
10. van Assche, F., Cardinaels, C. and Clijsters, H., (1988). Induction of enzyme capacity in plants as a result of heavy metal toxicity: dose response relation in *Phaseolus vulgaris* L., treated with zinc and cadmium. *Environ Pollut*, 52: 103-115.
11. Assunção, A.G.L., Herrero, E., Lin, Y.F., Huettel, B., Talukdar, S., Smaczniak, C., Immink, R.G.H., van Eldik, M., Fiers, M., Schat, H. and Aarts, M.G.M., (2010). *Arabidopsis thaliana* transcription factors bZIP19 and bZIP23 regulate the adaptation to zinc deficiency. *Proc. Natl. Acad. Sci*, 107 (22): 10296–10301.

12. Auld, D.S., (2001). Zinc coordination sphere in biochemical zinc sites. *Biometals*, 1: 271–313.
13. Baraas, R.C., Hagen, L.A., Dees, E.W. and Neitz, M., (2012). Substitution of isoleucine for threonine at position 190 of S-opsin causes S-cone-function abnormalities. *Vision Res*, 73: 1–9.
14. Barak, P. and Helmke, P.A., (1993). The chemistry of zinc. In: Robson, A.D., ed. Zinc in soil and plants. Kluwer Academic Publishers. Dordrecht, Netherlands, 1–13.
15. Barberon, M., Zelazny, E., Robert, S., Conéjéro, G., Curie, C., Friml, J. and Vert, G., (2011). Monoubiquitin- dependent endocytosis of the iron-regulated transporter 1 (IRT1) transporter controls iron uptake in plants, *Proc. Natl. Acad. Sci*, 108 (32): 450–458.
16. Baxter, I., (2010). Ionomics: The functional genomics of elements. *Brief Funct Genomics*, 9: 149–156.
17. Bedford, L., Lowe, J., Dick, L.R., Mayer, R.J. and Brownel, J.E., (2011). Ubiquitin-like protein conjugation and the ubiquitin-proteasome system as drug targets. *Nat Rev Drug Discov*, 10: 29–46.
18. Bell, C.J. and Ecker., J.R., (1994). Assignment of 30 microsatellite loci to the linkage map of *Arabidopsis*. *Genomics*, 19: 137–144.
19. Benhamed, M., Bertrand, C., Servet, C., and Zhou, D.X., (2006). *Arabidopsis* GCN5, HD1, and TAF1/HAF2 interact to regulate histone acetylation required for light responsive gene expression. *Plant Cell*, 18: 2893–2903.
20. Benjamini, Y., and Hochberg, Y., (1995). Controlling false discovery rate: A practical and powerful approach to multiple testing. *J. R. Stat. Soc. B*, 57: 289–300.
21. Benjamini, Y. and Yekutieli, D., (2001). The control of the false discovery rate in multiple testing under dependency. *Ann. Statist*, 29: 1165–1188.
22. Berg, J.M. and Shi, Y., (1996). The galvanization of biology: a growing appreciation for the roles of zinc. *Science*, 271: 1081–1085.
23. Bernal, M., Casero, D., Singh, V., Wilson, G.T., Grande, A., Yang, H., Dodani, S.C., Pellegrini, M., Huijser, P., Connolly, E.L., Merchant, S.S. and Krämer, U., (2012). Transcriptome Sequencing Identifies SPL7-Regulated Copper Acquisition Genes FRO4/FRO5 and the Copper Dependence of Iron Homeostasis in *Arabidopsis*. *Plant Cell*, 24(2): 738–761.
24. Bernhardt, A., Lechner, E., Hano, P., Schade, V., Dieterle, M., Anders, M., Dubin, M. J., Benvenuto, G., Bowler, C., Genschik, P. and Hellmann, H., (2006). CUL4 associates with DDB1 and DET1 and its down-regulation affects diverse aspects of development in *Arabidopsis thaliana*. *Plant J*, 47: 591–603.
25. Betts, M.J. and Russell, R.B., (2003). Amino acid properties and consequences of substitutions. In: Bioinformatics for Geneticists, M.R. Barnes, I.C. Gray eds, Wiley, England, 298–316.

26. Biedermann, S. and Hellmann, H., (2011). WD40 and CUL4-based E3 ligases: lubricating all aspects of life. *Trends Plant Sci*, 16: 38–46.
27. Blaudez, D., Kohler, A., Martin, F., Sanders, D. and Chalot, M., (2003). Poplar metal tolerance protein 1 confers zinc tolerance and is an oligomeric vacuolar zinc transporter with an essential leucine zipper motif. *Plant Cell*, 15: 2911–2928.
28. Bouis, H.E., (2003). Micronutrient fortification of plants through plant breeding: can it improve nutrition in man at low cost? *Proc Nutr Soc*, 62: 403–411.
29. Broadley, M.R., White, P.J., Hammond, J.P., Zelko, I. and Lux, A., (2007). Zinc in plants. *New Phytol*, 173: 677–702.
30. Brown, D.E., Rashotte, A.M., Murphy, A.S., Normanly, J., Tague, B.W., Peer, W.A., Taiz, L. and Muday, G.K., (2001). Flavonoids act as negative regulators of auxin transport in vivo in *Arabidopsis*. *Plant Physiol*, 126: 524–535.
31. Bu, Q., Jiang, H., Li, C.B., Zhai, Q., Zhang, J., Wu, X., Sun, J., Xie, Q. and Li, C., (2008). Role of the *Arabidopsis thaliana* NAC transcription factors ANAC019 and ANAC055 in regulating jasmonic acid-signaled defense responses. *Cell Research*, 18:756-767.
32. Buer C.S., Imin, N. and Djordjevic, M.A., (2010). Flavonoids: New Roles for Old Molecules. *J. Integr. Plant Biol*, 52(1): 98–111.
33. Buer, C.S. and Djordjevic, M.A., (2009). Architectural phenotypes in the transparent testa mutants of *Arabidopsis thaliana*. *J Exp Bot*, 60: 751–763.
34. Buer, C.S., Wasteneys, G.O. and Masle, J., (2003). Ethylene modulates root-wave responses in *Arabidopsis*. *Plant Physiol*, 132(2): 1085–96.
35. Burkhardt, P., Beyer, P., Wunn, J., Kloti, A., Armstrong, G., Schledz, M., von Lintig, J. and Potrykus, I., (1997). Transgenic rice (*Oryza sativa*) endosperm expressing daffodil (*Narcissus pseudonarcissus*) phytoene synthase accumulates phytoene, a key intermediate of provitamin A biosynthesis. *Plant J*, 11: 1071–1078.
36. Cakmak, I. and Marschner, H., (1986). Mechanism of phosphorus induced zinc deficiency in cotton: I. Zinc-deficiency enhanced uptake rate of phosphorus. *Physiol Plant*, 68: 483–490.
37. Cakmak, I., Gijiljt, K.Y., Marschner, H. and Graham, R.D., (1994). Effect of zinc and iron deficiency on phytosiderophore release in wheat genotypes differing in zinc efficiency. *J Plant Nutr*, 17: 1–17.
38. Cakmak, I., Yilmaz, A., Kalayci, M., Ekiz, H., Torun, B., Erenoglu, B. and Brown, H. J., (1996). Zinc deficiency as a critical problem in wheat production in central Anatolia. *Plant Soil*, 180: 165–172.
39. Callahan, D.L., Baker, A.J., Kolev, S.D. and Wedd, A.G., (2006). Metal ion ligands in hyperaccumulating plants. *J Biol Inorg Chem*, 11: 2–12.
40. Celenza, J.L., Grisafi, P.L. and Fink, G.R., (1995). A pathway for lateral root formation in *Arabidopsis thaliana*. *Genes Dev*, 9: 2131–2142.

41. Chaney, R.L., (1993). Zinc phytotoxicity. In: Robson, A.D., ed. Zinc in Soils and Plants. Kluwer Academic Publishers. Dordrecht, Netherlands, 135-150.
42. Chen, H., Shen, Y., Tang, X., Yu, L., Wang, J., Guo, L., Zhang, Y., Zhang, H., Feng, S., Strickland, E., Zheng, N. and Deng, X.W., (2006). *Arabidopsis* CULLIN4 forms an E3 ubiquitin ligase with RBX1 and the CDD complex in mediating light control of development. *Plant Cell*, 18: 1991-2004.
43. Cheung, Y.H., Wong, M.H. and Tam, N.F.Y., (1989). Root and shoot elongation as an assessment of heavy metal toxicity and 'Zn Equivalent Value' of edible crops. *Hydrobiologia*, 188(189): 377-383.
44. Chinnusamy, V., Zhu, J. and Zhu, J.K., (2007). Cold stress regulation of gene expression in plants. *Trends Plant Sci*, 12: 444-451.
45. Ciftci-Yilmaz, S. and Mittler, R., (2008). The zinc finger network of plants. *Cell Mol. Life Sci*, 65: 1150-1160.
46. Clemens, S., (2001). Molecular mechanisms of plant metal tolerance and homeostasis. *Planta*, 212: 475-486.
47. Clemens, S., (2006). Toxic metal accumulation, responses to exposure and mechanisms of tolerance in plants. *Biochimie*, 88: 1707-1719.
48. Clemens, S., (2010). Zn - A Versatile Player in Plant Cell Biology. In: Hell, R. and Mendel, R. R. eds. Cell Biology of Metals and Nutrients. Springer-Verlag, Heidelberg, 281-298.
49. Clemens, S., Deinlein, U., Ahmadi, H., Horeth, S. and Uraguchi, S., (2013). Nicotianamine is a major player in plant Zn homeostasis. *Biometals*, (in press).
50. Clough, S.J. and Bent, A.F., (1998). Floral dip: A simplified method for *Agrobacterium*-mediated transformation of *Arabidopsis thaliana*. *Plant J*, 16: 735-743.
51. Cobbett, C. and Goldsbrough, P., (2002). Phytochelatins and metallothioneins: roles in heavy metal detoxification and homeostasis. *Annu Rev Plant Physiol Plant Mol Biol*, 53: 159-182.
52. Colon-Carmona, A., You, R., Haimovitch-Gal, T. and Doerner, P., (1999). Technical advance: spatio-temporal analysis of mitotic activity with a labile cyclin-GUS fusion protein. *Plant J*, 20: 503-508.
53. Conway, G. and Toenniessen, G., (1999). Feeding the world in the twenty-first century. *Nature*, 402: c55-c58.
54. Curie, C., Cassin, G., Couch, D., Divol, F., Higuchi, K., Le Jean, M., Misson, J., Schikora, A., Czernic, P. and Mari, S., (2008). Metal movement within the plant: contribution of nicotianamine and yellow stripe 1-like transporters. *Ann. Bot*, 103 (1): 1-11.
55. Curtis, M.D. and Grossniklaus, U., (2003). A Gateway Cloning Vector Set for High-Throughput Functional Analysis of Genes in *Planta*. *Plant Physiology*, 133: 462-469.

56. d'Azzo, A., Bongiovanni, A. and Nastasi, T., (2005). E3 Ubiquitin ligases as regulators of membrane protein trafficking and degradation. *Traffic*, 6: 429-441.
57. Davletova, S., Schlauch, K., Coutu, J. and Mittler, R., (2005). The zinc-finger protein Zat12 plays a central role in reactive oxygen and abiotic stress signaling in *Arabidopsis*. *Plant Physiol*, 139: 847-856.
58. Deerfield II, D.W., Carter Jr., C.W. and Pedersen, L.G., (2001). Models for Protein-Zinc Ion Binding Sites. II. The Catalytic Sites. *Int. J. Quant. Chem.*, 83: 150-165.
59. Deinlein, U., Weber, M., Schmidt, H., Rensch, S., Trampczynska, A., Hansen, T.H., Husted, S., Schjoerring, J.K., Talke, Ina N., Krämer, U. and Clemens, S., (2012). Elevated Nicotianamine Levels in *Arabidopsis halleri* Roots Play a Key Role in Zinc Hyperaccumulation. *Plant Cell*, 24: 708-723.
60. Delk, N.A., Johnson, K.A., Chowdhury, N.I. and Braam, J., (2005). CML24, regulated in expression by diverse stimuli, encodes a potential Ca²⁺ sensor that functions in responses to abscisic acid, daylength, and ion stress. *Plant Physiol*, 139(1): 240-53.
61. Dello Ioio, R., Nakamura, K., Moubayidin, L., Perilli, S., Taniguchi, M., Morita, M.T., Aoyama, T., Costantino, P. and Sabatini, S., (2008). A genetic framework for the control of cell division and differentiation in the root meristem. *Science*, 322: 1380-1384.
62. Dello Ioio, R., Linhares, F.S., Scacchi, E., Casamitjana-Martinez, E., Heidstra, R., Costantino, P. and Sabatini, S., (2007). Cytokinins Determine *Arabidopsis* Root-Meristem Size by Controlling Cell Differentiation. *Curr Biol*, 17(8): 678-82.
63. Desbrosses-Fonrouge, A.G., Voigt, K., Schroder, A., Arrivault, S., Thomine, S. and Krämer U., (2005). *Arabidopsis thaliana* MTP1 is a Zn transporter in the vacuolar membrane which mediates Zn detoxification and drives leaf Zn accumulation. *FEBS Lett*, 579: 4165-4174.
64. Devaiah, B.N., Karthikeyan, A.S. and Raghothama, K.G., (2007). WRKY75 transcription factor is a modulator of phosphate acquisition and root development in *Arabidopsis*. *Plant Physiol*, 143(4): 1789-801.
65. Dietzl, G., Chen, D., Schnorrer, F., Su, K.C., Barinova, Y., Fellner, M., Gasser, B., Kinsey, K., Oettel, S., Scheiblauer, S., Couto, A., Marra, V., Keleman, K. and Dickson, B.J., (2007). A genome-wide transgenic RNAi library for conditional gene inactivation in *Drosophila*. *Nature*, 448: 151-156.
66. Dinneny, J.R., Long, T.A., Wang, J.Y., Jung, J.W., Mace, D., Pointer, S., Barron, C., Brady, S.M., Schiefelbein, J. and Benfey, P.N., (2008). Cell identity mediates the response of *Arabidopsis* roots to abiotic stress. *Science*, 320: 942-945.
67. Dixon, R. A. and Pasinetti, G. M., (2010). Flavonoids and isoflavonoids: from plant biology to agriculture and neuroscience. *Plant Physiol*, 154: 453-457.
68. Drager, D.B., Desbrosses-Fonrouge, A.G., Krach, C., Chardonnens, A.N., Meyer, R.C., Saumitou-Laprade, P. and Krämer, U., (2004). Two genes encoding *Arabidopsis*

- halleri* MTP1 metal transport proteins co-segregate with zinc tolerance and account for high MTP1 transcript levels. *Plant J*, 39(3): 425-39.
69. Dunand, C., Crèvecoeur, M. and Penel, C., (2007). Distribution of superoxide and hydrogen peroxide in *Arabidopsis* root and their influence on root development: possible interaction with peroxidases. *New Phytologist*, 174 : 332-341.
70. Eide, D., Broderius, M., Fett, J. and Guerinot, M. L., (1996). A novel iron regulated metal transporter from plants identified by functional expression in yeast. *Proc. Natl. Acad. Sci*, 93: 5624-5628.
71. Eide, D.J., (2006). Zinc transporters and the cellular trafficking of zinc. *Biochim. Biophys. Acta*, 1763: 711-722.
72. Elbaz, B., Shoshani-Knaani, N., David-Assael, O., Mizrachi-Dagri, T., Mizrahi, K., Saul, H., Brook, E., Berezin, I. and Shaul, O., (2006). High expression in leaves of the zinc hyperaccumulator *Arabidopsis halleri* of AhMHX, a homolog of an *Arabidopsis thaliana* vacuolar metal/proton exchanger. *Plant Cell Environ*, 29: 1179-1190.
73. Emery, L., Whelan, S., Hirschi, K. D. and Pittman, J. K., (2012). Protein phylogenetic analysis of Ca²⁺/cation antiporters and insights into their evolution in plants. *Frontiers in Plant Science*, 3: 1.
74. Errampalli, D., Patton, D., Castle, L., Mickelson, L., Hansen, K., Schnell, J., Feldmann, K. and Meinke, D., (1991). Embryonic lethals and T-DNA insertional mutagenesis in *Arabidopsis*. *Plant Cell*, 3:149-157.
75. Fan, T.W.M., Lane, A.N., Pedler, J., Crowley, D. and Higashi, R.M., (1997). Comprehensive analysis of organic ligands in whole root exudates using nuclear magnetic resonance and gas chromatography mass spectrometry. *Analytical Biochemistry*, 251: 57-68.
76. FAO, WFP and IFAD., (2012). The State of Food Insecurity in the World 2012: Economic growth is necessary but not sufficient to accelerate reduction of hunger and malnutrition. Rome, FAO.
77. Ferrali, M., Signorini, C., Caciotti, B., Sugherini, L., Ciccoli, L., Giachetti, D. and Comproti, M., (1997). Protection against oxidative damage of erythrocyte membrane by the flavonoid quercetin and its relation to iron chelating activity. *FEBS Lett*, 416: 123-129.
78. Ferrandiz, M. L. and Alcaraz, M. J., (1991). Anti-inflammatory activity and inhibition of arachidonic acid metabolism by flavonoids. *Agents Actions*, 32, 283-8.
79. Foley, J.A., Ramankutty, N., Brauman, K.A., Cassidy, E.S., Gerber, J.S., Johnston, M., Mueller, N.D., O'Connell, C., Ray, D.K., West, P.C., Balzer, C., Bennett, E.M., Carpenter, S.R., Hill, J., Monfreda, C., Polasky, S., Rockström, J., Sheehan, J., Siebert, S., Tilman, D. and Zaks, D.P., (2011). Solutions for a cultivated planet. *Nature*, 478: 337-342.

Reference

80. Fukao, Y., Ferjani, A., Tomioka, R., Nagasaki, N., Kurata, R., Nishimori, Y., Fujiwara, M. and Maeshima, M., (2011). iTRAQ Analysis Reveals Mechanisms of Growth Defects Due to Excess Zinc in *Arabidopsis*. *Plant Physiol*, 155: 1893–1907.
81. Gautier, L., Cope, L., Bolstad, B.M. and Irizarry, R.A., (2004). affy – Analysis of Affymetrix GeneChip data at the probe level. *Bioinformatics*, 20: 307–315.
82. Geng, F., Wenzel, S. and Tansey, W.P., (2012). Ubiquitin and Proteasomes in Transcription. *Annu. Rev. Biochem*, 81: 177–201.
83. Gentleman, R.C., Carey, V.J., Bates, D.M., Bolstad, B., Dettling, M., Dudoit, S., Ellis, B., Gautier, L., Ge, Y., Gentry, J., Hornik, K., Hothorn, T., Huber, W., Iacus, S., Irizarry, R., Leisch, F., Li, C., Maechler, M., Rossini, A.J., Sawitzki, G., Smith, C., Smyth, G., Tierney, L., Yang, J.Y. and Zhang, J., (2004). Bioconductor: Open software development for computational biology and bioinformatics. *Genome Biol*, 5: R80.
84. Gillis, J. and Pavlidis, P., (2011). The Impact of Multifunctional Genes on "Guilty by Association" Analysis. *PLoS ONE*, 6(2): 16.
85. Gitan, R.S. and Eide D.J., (2000). Zinc-regulated ubiquitin conjugation signals endocytosis of the yeast ZRT1 zinc transporter. *Biochem. J*, 346: 329–336.
86. Gong, Z., Chinnusamy, V. and Zhu, J.K., (2009). The molecular networks of abiotic stress signaling. In: Yang, Z., ed. *Intracellular Signaling in Plants*. Annual Plant Reviews. Blackwell, United Kingdom, 33: 388 – 416.
87. Goto, F., Yoshihara, T., Shigemoto, N., Toki, S. and Takaiwa, F., (1999). Iron fortification of rice seed by the soybean ferritin gene. *Nat. Biotechnol*, 17: 282–286.
88. Graham, R.D., (1991). Breeding wheat for tolerance to micronutrient deficient soils: present status and priorities. In: Saunders, D. A., ed. *Wheat for the non- Traditional Warm Areas*. CIMMYT. Mexico, 315–332.
89. de Groot, H., (1994). Reactive oxygen species in tissue injury. *Hepatology*, 41: 328–32.
90. Grotz, N., Fox, T., Connolly, E., Park, W., Guerinot, M.L. and Eide, D., (1998). Identification of a family of zinc transporter genes from *Arabidopsis* that respond to zinc deficiency. *Proc. Natl. Acad. Sci*, 95: 7220–7224.
91. Guerinot, M.L. and Eide, D., (1999). Zeroing in on zinc uptake in yeast and plants. *Curr. Opin. Plant Biol*, 2: 244–249.
92. Guerinot, M.L., (2000). The ZIP family of metal transporters. *Biochimica et Biophysica Acta*, 1465: 190–198.
93. Gunse, B., Poschenrieder, C. and Barcelo, J., (2000). The role of ethylene metabolism in the short-term responses to aluminium by roots of two maize cultivars different in Al-resistance. *Environ Exp Bot*, 43: 73–81.

94. Guo, W.J., Meetam, M. and Goldsbrough, P.B., (2008). Examining the Specific Contributions of Individual *Arabidopsis* Metallothioneins to Copper Distribution and Metal Tolerance. *Plant Physiol*, 146: 1697–1706.
95. Guzman, P. and Ecker, J.R., (1990). Exploiting the triple response of *Arabidopsis* to identify ethylene-related mutants. *Plant Cell*, 2: 513-523.
96. Hall, J.L. and Williams, L.E., (2003). Transition metal transporters in plants. *J Exp Bot*, 54(393): 2601-2613.
97. Hammond, J.P., Bowen, H.C., White, P.J., Mills, V., Pyke, K.A., Baker, A.J.M., Whiting, S.N., May, S.T. and Broadley, M.R., (2006). A comparison of the *Thlaspi caerulescens* and *Thlaspi arvense* shoot transcriptomes. *New Phytol*, 170: 239–260.
98. Hänsch, R. and Mendel, R., (2009). Physiological functions of mineral micronutrients (Cu, Zn, Mn, Fe, Ni, Mo, B, Cl). *Curr. Opin. Plant Biol*, 12: 259–266.
99. Hara, M., Kashima, D., Horiike, T. and Kuboi, T., (2010). Metal-binding characteristics of the protein which shows the highest histidine content in the *Arabidopsis* genome. *Plant Biotechnology*, 27: 475-480.
100. Hashimoto, S. and Egly, J.M., (2009). Trichothiodystrophy view from the molecular basis of DNA repair/transcription factor TFIIH. *Hum Mol Genet*, 18(R2): R224-30.
101. Haslett, B.S., Reid, R.J. and Rengel, Z., (2001). Zinc mobility in wheat: uptake and distribution of zinc applied to leaves or roots. *Ann Bot*, 87: 379–386.
102. Haydon M.J. and Cobbett, C.S., (2007). A Novel Major Facilitator Superfamily Protein at the Tonoplast Influences Zinc Tolerance and Accumulation in *Arabidopsis*. *Plant Physiol*, 143(4): 1705–1719.
103. Haydon, M.J., Kawachi, M., Wirtz, M., Stefan, H., Hell, R. and Krämer, U., (2012). Vacuolar nicotianamine has critical and distinct roles under iron deficiency and for zinc sequestration in *Arabidopsis*. *Plant Cell*, 24: 724–737.
104. Hedera, P., Fenichel, G.M., Blair, M. and Haines, J.L., (2004). Novel mutation in the SPG3A gene in an african american family with an early onset of hereditary spastic paraplegia. *Arch Neurol*, 61: 1600-1603.
105. Hegelund, J.N., Schiller, M., Kichey, T., Hansen, T.H., Pedas, P., Husted, S. and Schjoerring, J.K., (2012). Barley metallothioneins: MT3 and MT4 are localized in the grain aleurone layer and show differential zinc binding. *Plant Physiol*, 159(3):1125-37.
106. Herbiak, A., Koch, G., Mock, H. P., Dushkov, D., Czihal, A., Thielmann, J., Stephan, U.W. and Baeumlein, H., (1999). Isolation, characterization and cDNA cloning of nicotianamine synthase from barley: A key enzyme for iron homeostasis in plants. *Eur. J. Biochem*, 265: 231–239.
107. Hershko, A. and Ciechanover, A., (1998). The ubiquitin system. *Annu Rev Biochem*, 67: 425-479.

108. Hider, R.C., Liu, Z.D. and Khodr, H.H., (2001). Metal chelation of polyphenols. *Methods Enzymol*, 335: 190–203.
109. Hsu, P.Y., Devisetty, U.K. and Harmer, S.L., (2013). Accurate timekeeping is controlled by a cycling activator in *Arabidopsis*. *eLife*, 2: e00473.
110. Huang, C., Barker, S.J., Langridge, P., Smith, F.W. and Graham, R.D., (2000). Zinc deficiency up-regulates expression of high-affinity phosphate transporter genes in both phosphate- sufficient and -deficient barley roots. *Plant Physiol*, 124: 415–422.
111. Huffman, D.L. and O'Halloran, T.V., (2001). Function, structure, and mechanism of intracellular copper trafficking proteins. *Ann. Rev. Biochem*, 70: 677–701.
112. Hussain, D., Haydon, M.J., Wang, Y., Wong, E., Sherson, S.M., Young, J., Camakaris, J., Harper, J.F. and Cobbett, C.S., (2004). P-type ATPase heavy metal transporters with roles in essential zinc homeostasis in *Arabidopsis*. *Plant Cell*, 16: 1327–1339.
113. Irizarry, R.A., Bolstad, B.M., Collin, F., Cope, L.M., Hobbs, B. and Speed, T.P., (2003). Summaries of Affymetrix GeneChip probe level data. *Nucleic Acids Res*, 31: e15.
114. Ishimaru, Y., Masuda, H., Bashir, K., Inoue, H., Tsukamoto, T., Takahashi, M., Nakanishi, H., Aoki, N., Hirose, T., Ohsugi, R. and Nishizawa, N.K., (2010). Rice metal-nicotianamine transporter, OsYSL2, is required for the long-distance transport of iron and manganese. *Plant J*, 62: 379–390.
115. Ivanov, R., Brumbarova, T. and Bauer, P., (2011). Fitting into the harsh reality: regulation of iron deficiency responses in dicotyledonous plants. *Mol Plant*, 5(1): 27–42.
116. van Jaarsveld, P.J., Faber, M., Tanumihardjo, S.A., Nestel, P., Lombard, C.J. and Benadé, A.J., (2005). β -Carotene-rich orange-fleshed sweet potato improves the vitamin A status of primary school children assessed with the modified-relative-dose-response test. *Am J Clin Nutr*, 81(5): 1080-1087.
117. Jain, R., Srivastava, S., Solomon, S., Shrivastava, A.K. and Chandra, A., (2010). Impact of excess zinc on growth parameters, cell division, nutrient accumulation, photosynthetic pigments and oxidative stress of sugarcane (*Saccharum* spp.). *Acta Physiol. Plant*, 32: 979–986.
118. Kanehisa, M. and Goto, S., (2000). KEGG: Kyoto Encyclopedia of Genes and Genomes. *Nucleic Acids Res*, 28: 27-30.
119. Kawachi, M., Kobae, Y., Mori, H., Tomioka, R., Lee, Y. and Maeshima, M., (2009). A mutant strain *Arabidopsis thaliana* that lacks vacuolar membrane zinc transporter MTP1 revealed the latent tolerance to excessive zinc. *Plant Cell Physiol*, 50: 1156–1170.
120. Kawachi, M., Kobae, Y., Kogawa, S., Mimura, T., Krämer, U. and Maeshima, M., (2012). Amino acid screening based on structural modeling identifies critical residues for the function, ion selectivity and structure of *Arabidopsis* MTP1. *FEBS J*, 279(13): 2339-56.

121. Kawashima, I., Kennedy, T.D., Chino, M. and Lane, B.G., (1992). Wheat E_c metallothionein genes: like mammalian Zn^{2+} metallothionein genes, wheat Zn^{2+} metallothionein genes are conspicuously expressed during embryogenesis. *Eur. J. Biochem*, 209: 971–76.
122. Keilig, K. and Ludwig-Müller, J., (2009). Effect of flavonoids on heavy metal tolerance in *Arabidopsis thaliana* seedlings. *Botanical Studies*, 50: 311-318.
123. Keilin, D. and Mann, T., (1940). Carbonic anhydrase: Purification and nature of the enzyme. *Biochem. J*, 34: 1163-1176.
124. Kerppola, T.K., (2006). Design and implementation of bimolecular fluorescence complementation (BiFC) assays for the visualization of protein interactions in living cells. *Nat. Protoc*, 1: 1278–1286.
125. Kidd, P.S., Llugany, M., Poschenrieder, C., Gunsé, B. and Barcel, J., (2001). The role of root exudates in aluminium resistance and silicon-induced amelioration of aluminium toxicity in three variety of maize (*Zea mays* L.). *J Exp Bot*, 52: 1339-1352.
126. Kilian, J., Whitehead, D., Horak, J., Wanke, D., Weinl, S., Batistic, O., D'Angelo, C., Bornberg-Bauer, E., Kudla, J. and Harter, K., (2007). The AtGenExpress global stress expression data set: protocols, evaluation and model data analysis of UV-B light, drought and cold stress responses. *Plant J*, 50(2): 347-63.
127. Kim, E.Y., Koh, J.Y., Kim, Y.H., Sohn, S., Joe, E. and Gwag, B.J., (1999). Zn^{2+} entry produces oxidative neuronal necrosis in cortical cell cultures. *Eur. J. Neurosci*. 11: 327–334.
128. Kim Y.S., Schumaker, K.S. and Zhu, J.K., (2006). EMS Mutagenesis of *Arabidopsis*. In: Salinas, J. and Sanchez-Serrano, J.J., eds. *Methods in Molecular Biology*, Vol. 323: *Arabidopsis* Protocols, Second Edition. Humana Press Inc., Totowa, New Jersey.
129. Kim, B.E., Wang, F., Dufner-Beattie, J., Andrews, G.K., Eide, D.J. and Petris, M.J., (2004). Zn^{2+} -stimulated Endocytosis of the mZIP4 Zinc Transporter Regulates Its Location at the Plasma Membrane. *JBC*, 279(6): 4523–4530.
130. Kim, S.A. and Guerinot, M.L., (2007). Mining iron: iron uptake and transport in plants. *FEBS Lett*, 581: 2273–2280.
131. Kim, Y.Y., Choi, H., Segami, S., Cho, H.T., Martinoia, E., Maeshima, M. and Lee, Y., (2009). AtHMA1 contributes to the detoxification of excess Zn (II) in *Arabidopsis*. *Plant J*, 58: 737–753.
132. Kiss, P., Szabó, A., Hunyadi-Gulyás, E., Medzihradszky, K.F., Lipinszki, Z., Pál, M. and Udvardy, A., (2005). Zn^{2+} -induced reversible dissociation of subunit Rpn10/p54 of the *Drosophila* 26 S proteasome. *Biochem J*, 391: 301–310.
133. Klatte, M., Schuler, M., Wirtz, M., Fink-Straube, C., Hell, R. and Bauer, P., (2009). The analysis of *Arabidopsis* nicotianamine synthase mutants reveals functions for nicotianamine in seed iron loading and iron deficiency responses. *Plant Physiol*, 150: 257–271.

134. Klug, A. and Schwabe, J.W., (1995). Protein motifs 5. Zinc fingers. *FASEB J*, 9: 597-604.
135. Knight, J.K. and Wood, W.B., (1998). Gastrulation initiation in *Caenorhabditis elegans* requires the function of *gad-1*, which encodes a protein with WD repeats. *Dev Biol*, 198(2): 253-65.
136. Kobae, Y., Uemura, T., Sato, M.H., Ohnishi, M., Mimura, T., Nakagawa, T. and Maeshima, M., (2004). Zinc transporter of *Arabidopsis thaliana* AtMTP1 is localized to vacuolar membranes and implicated in zinc homeostasis. *Plant Cell Physiol*, 45: 1749-1758.
137. Kocsy, G., von Ballmoos, P., Rügsegger, A., Szalai, G., Galiba, G. and Brunold, C., (2001). Increasing the glutathione content in a chilling-sensitive maize genotype using safeners increased protection against chilling-induced injury. *Plant Physiol*, 127(3): 1147-56.
138. Kocsy, G., von Ballmoos, P., Suter, M., Rügsegger, A., Galli, U., Szalai, G., Galiba, G. and Brunold, C., (2000). Inhibition of glutathione synthesis reduces chilling tolerance in maize. *Planta*, 211(4): 528-36.
139. Kodadek, T., (2010). No Splicing, No Dicing: Non-proteolytic Roles of the Ubiquitin-Proteasome System in Transcription. *J Biol Chem*, 285(4): 2221-2226.
140. Koes, R.E., Quattrocchio, F. and Mol, J.N.M., (1994). The flavonoid biosynthetic pathway in plants: function and evolution. *BioEssays*, 16: 123-132.
141. Konieczny, A. and Ausubel, F.M., (1993). A procedure for mapping *Arabidopsis* mutations using co-dominant ecotype-specific PCR-based markers. *Plant J*, 4: 403-410.
142. Koo, A.J.K. and Howe, G.A., (2012). Catabolism and deactivation of the lipid-derived hormone jasmonoyl-isoleucine. *Front. Plant Sci*, 3:19.
143. Koornneef, M., (1990). Mutations affecting the testa color in *Arabidopsis*. *Arabidopsis Inf Serv*, 28: 1-4.
144. Koornneef, M., Luiten, W., de Vlaming, P. and Schram, A.W., (1982). A gene controlling flavonoid-3'-hydroxylation in *Arabidopsis*. *Arabidopsis Inf Serv*, 19: 113-115.
145. Korshunova, Y.O., Eide, D., Clark, W.G., Guerinot, M.L. and Pakrasi, H.B., (1999). The IRT1 protein from *Arabidopsis thaliana* is a metal transporter with broad specificity. *Plant Mol. Biol*, 40: 37-44.
146. Kostyuk, V.A., Potapovich, A.I., Vladykovskaya, E.N., Korkina, L.G. and Afanas'ev, I.B., (2001). Influence of metal ions on flavonoid protection against asbestos-induced cell injury. *Arch Biochem Biophys*, 385(1): 129-37.
147. Krämer, U. and Clemens, S., (2005). Functions and Homeostasis of Zinc, Copper and Nickel in plants. *Topics Curr. Genet*, 14: 215-271.

148. Krämer, U., Talke, I., Hanikenne, M., (2007). Transition metal transport. *FEBS Letters*, 581: 2263–2272.
149. Kumar, S.V. and Wigge, P.A., (2010). H2A.Z-containing nucleosomes mediate the thermosensory response in *Arabidopsis*. *Cell*, 140: 136–147.
150. Kunkel, T.A., (1985). Rapid and efficient site-specific mutagenesis without phenotypic selection. *Proc. Natl. Acad. Sci*, 82: 488–492.
151. Kupper, H., Kupper, F. and Spiller, M., (1996). Environmental relevance of heavy metal-substituted chlorophylls using the example of water plants. *J Exp Bot*, 47: 259–266.
152. Kurihara, Y., Kaminuma, E., Matsui, A., Kawashima, M., Tanaka, M., Morosawa, T., Ishida, J., Mochizuki, Y., Shinozaki, K., Toyoda, T. and Seki, M., (2009). Transcriptome analyses revealed diverse expression changes in ago1 and hyl1 *Arabidopsis* mutants. *Plant Cell Physiol*, 50: 1715–1720.
153. Kury, S., Dreno, B., Bezieau, S., Giraudet, S., Kharfi, M., Kamoun, R. and Moisan, J.P., (2002). Identification of SLC39A4, a gene involved in *Acrodermatitis enteropathica*. *Nat. Genet*, 31: 239–240.
154. Kwon, C.S., Lee, D., Choi, G., and Chung, W.I., (2009). Histone occupancy dependent and independent removal of H3K27 trimethylation at cold responsive genes in *Arabidopsis*. *Plant J*, 60: 112 - 121.
155. Lachman, J., Dudjak, J., Miholová, D., Kolihová, D. and Pivec, V., (2005). Effect of cadmium on flavonoid content in young barley (*Hordeum sativum* L.) plants. *Plant Soil Environ*, 51(11): 513–516.
156. Lanquar, V., Lelievre, F., Barbier-Brygoo, H., and Thomine, S., (2004). Regulation and function of AtNRAMP4 metal transporter protein. *Soil Science and Plant Nutrition*, 50: 1141–1150.
157. Lang, I. and Wernitznig, S., (2011). Sequestration at the cell wall and plasma membrane facilitates zinc tolerance in the moss *Pohlia drummondii*. *Environ. Exp Bot*, 74: 186–193.
158. Lee J.H. and Kim, W.T., (2011). Regulation of abiotic stress signal transduction by E3 ubiquitin ligases in *Arabidopsis*. *Mol Cells*, 31: 201– 208.
159. Lee, J.H., Terzaghi, W., Gusmaroli, G., Charron, J.B., Yoon, H.J., Chen, H., He, Y.J., Xiong, Y. and Deng, X.W., (2008). Characterization of *Arabidopsis* and rice DWD proteins and their roles as substrate receptors for CUL4–RING E3 ubiquitin ligases. *Plant Cell*, 20: 152–167.
160. Lee J.H., Yoon, H.J., Terzaghi, W., Martinez, C., Dai, M., Li, J., Byun, M.O. and Deng, X.W., (2010). DWA1 and DWA2, two *Arabidopsis* DWD protein components of CUL4-based E3 ligases, act together as negative regulators in ABA signal transduction. *Plant Cell*, 22: 1716–1732.

161. Lee, B.H., Henderson, D.A. and Zhu, J.K., (2005). The *Arabidopsis* Cold-responsive transcriptome and its regulation by ICE1. *Plant Cell*, 17: 3155–3175.
162. Lee, S., Jeon, U.S., Lee, S.J., Kim, Y.K., Persson, D.P., Husted, S., Schjorring, J.K., Kakei, Y., Masuda, H., Nishizawa, N.K. and An, G., (2009). Iron fortification of rice seeds through activation of the nicotianamine synthase gene. *Proc. Natl. Acad. Sci*, 106: 22014-22019.
163. Lee, S.M., Grass, G., Haney, C.J., Fan, B., Rosen, B.P., Anton, A., Nies, D.H. and Rensing, C., (2002). Functional analysis of the *Escherichia coli* zinc transporter ZitB. *FEMS Microbiol Lett*, 215: 273–278.
164. Lee, Y. and Lim, C., (2008). Physical Basis of Structural and Catalytic Zn-Binding Sites in Proteins. *J Mol Biol*, 379(3): 545-53.
165. Lekka, C.E., Ren, J., Meng, S. and Kaxiras, E., (2009). Structural, Electronic, and Optical Properties of Representative Cu-Flavonoid Complexes. *J Phys Chem B*, 113: 6478–6483.
166. Leyser, H.M.O., Pickett, B.F., Dharmasiri, S. and Estelle, M., (1996). Mutations in the *AXR3* gene of *Arabidopsis* result in altered auxin response including ectopic expression from the *SAUR-AC1* promoter. *Plant J*, 10:403–413.
167. Li, J., Ou-Lee, T.M., Raba, R., Amundson, R.G. and Last, R.L., (1993). *Arabidopsis* flavonoid mutants are hypersensitive to UV-B irradiation. *Plant Cell*, 5: 171-179.
168. Lin, J. K. and Weng, M. S., (2006). Flavonoids as nutraceuticals. In: Grotewold, E., ed. *The science of flavonoids*. Springer. Columbus, 213–238.
169. Magori, S., Tanaka, A. and Kawaguchi, M., (2010). Physically Induced Mutation: Ion Beam Mutagenesis. In: Meksem, K. and Kahl, G., eds. *The handbook of plant mutation screening*. Wiley-Vch. Weinheim, 3-16.
170. Maksymiec, W., (2007). Signaling responses in plants to heavy metal stress. *Acta Physiol Plant*, 29:177–187.
171. Manara, A., (2012). Plant Responses to Heavy Metal Toxicity. In: Furini, A. ed. *Plants and Heavy Metals*. Springer. Briefs in Molecular Science. Netherlands, 27-53
172. Marais, J.P.J., Deavours, B., Dixon, R.A and Ferreira, D., (2006). The Stereochemistry of Flavonoids. In: Grotewold, E., ed. *The science of flavonoids*. Springer. Columbus, 1-46.
173. Maret, W., and Sandstead, H.H., (2006). Zinc requirements and the risks and benefits of zinc supplementation. *J Trace Elem Med Biol*, 20 (1): 3–18.
174. Marschner, H., (1995). *Mineral nutrition of higher plants*. Academic Press. London, 889.
175. Matsubara, T., Hiurab, Y., Kawahitob, O., Yasuzawab, M. and Kawashirob, K., (2003). Selection of novel structural zinc sites from a random peptide library. *FEBS Letters*, 555: 317-321.

176. Mayer, J.E., Pfeiffer, W.H. and Beyer, P., (2008). Biofortified crops to alleviate micronutrient malnutrition. *Curr. Opin. Plant Biol*, 11: 166-170.
177. Mazzucotelli, E., Belloni, S., Marone, D., De Leonardis, A.M., Guerra, D., Di Fonzo, N, Cattivelli, L. and Mastrangelo, A.M., (2006). The E3 ubiquitin ligase gene family in plants: regulation by degradation. *Curr Gen*, 7: 509-522.
178. McCallum, C.M., Comai, L., Greene, E.A. and Henikoff, S., (2000). Targeted screening for induced mutations. *Nat. Biotech*, 18: 455-457.
179. Middleton, E.J., (1998). Effect of plant flavonoids on immune and inflammatory cell function. *Adv Exp Med Biol*, 439: 175-82.
180. Milliken, J.A., Waugh, D. and Kadish, M.E., (1963). Acute interstitial pulmonary fibrosis caused by a smoke bomb. *Can Med Ass J*, 88: 36 - 39.
181. Mills, R.F., Krijger, G.C., Baccharini, P.J., Hall, J.L. and Williams, L.E., (2003). Functional expression of AtHMA4, a P1B-type ATPase in the Zn/Co/Cd/Pb subclass. *Plant J*, 35: 164-175.
182. Mira, L., Fernandez, M.T., Santos, M., Rocha, R., Florêncio, M.H. and Jennings, K.R., (2002). Interactions of flavonoids with iron and copper ions: a mechanism for their antioxidant activity. *Free Radic Res*, 36(11):1199-208.
183. Mittler, R., Kim, Y., Song, L.H., Coutu, J., Coutu, A., Ciftci-Yilmaz, S., Lee, H., Stevenson, B., and Zhu, J.K., (2006). Gain- and loss-of-function mutations in Zat10 enhance the tolerance of plants to abiotic stress. *FEBS Lett*, 580: 6537-6542.
184. Morel, M., Crouzet, J., Gravot, A., Auroy, P., Leonhardt, N. , Vavasseur, A. and Richaud, P., (2008). AtHMA3, a P1B-ATPase allowing Cd/Zn/Co/Pb vacuolar storage in *Arabidopsis*. *Plant Physiol*, 149 (2): 894-904.
185. van de Mortel, J.E., Almar Villanueva, L., Schat, H., Kwekkeboom, J., Coughlan, S., Moerland, P.D., Ver Loren van Themaat, E., Koornneef, M. and Aarts, M.G.M., (2006). Large expression differences in genes for iron and zinc homeostasis, stress response, and lignin biosynthesis distinguish roots of *Arabidopsis thaliana* and the related metal hyperaccumulator *Thlaspi caerulescens*. *Plant Physiol*, 142: 1127-1147.
186. Nelbach, M., Pigiet, J.V.P., Gerhart, J.C. and Schachman, H.K., (1972). *Biochemistry*, 11: 315.
187. Nemhauser, J.L., Mockler, T.C. and Chory, J., (2004). Interdependency of brassinosteroid and auxin signaling in *Arabidopsis*. *PLoS Biol*, 2(9): E258.
188. Nijveldt, R.J., van Nood, E., van Hoorn, D.E.C., Boelens, P.G., van Norren, K. and van Leeuwen, P.A.M., (2001). Flavonoids: a review of probable mechanisms of action and potential applications. *Am J Clin Nutr*, 74: 418-25.
189. Nikiforova, V., Freitag, J., Kempa, S., Adamik, M., Hesse, H. and Hoefgen, R., (2003). Transcriptome analysis of sulfur depletion in *Arabidopsis thaliana*: interlacing of biosynthetic pathways provides response specificity. *Plant J*, 33: 633-650.

190. Novillo, F., Alonso, J.M., Ecker, J.R. and Salinas, J., (2004). CBF2/DREB1C is a negative regulator of CBF1/DREB1B and CBF3/DREB1A expression and plays a central role in stress tolerance in *Arabidopsis*. *Proc. Natl. Acad. Sci*, 101: 3985–3990.
191. Oguchi, K., Tanaka, N., Komatsu, S. and Akao, S., (2004). Characterization of NADPH-dependent oxireductase induced by auxin in rice. *Physiol Plant*, 121: 124–131.
192. Oomen, R.J.F.J., Wu, J., Lelièvre, F., Blanchet, S., Richaud, P., Barbier-Brygoo1, H., Aarts, M.G.M. and Thomine, S., (2009). Functional characterization of NRAMP3 and NRAMP4 from the metal hyperaccumulator *Thlaspi caerulescens*. *New Phytologist*, 181: 637–650.
193. Orlova, M.A, and Orlov, A.P., (2011). Role of Zinc in an Organism and Its Influence on Processes Leading to Apoptosis. *Br J Med Med Res*, 4: 239-305.
194. Ottenschlager, I., Wolff, P., Wolverson, C., Bhalerao, R.P., Sandberg, G., Ishikawa, H., Evans, M. and Palme, K., (2003). From the cover: gravity-regulated differential auxin transport from columella to lateral root cap cells. *Proc Natl Acad Sci*, 100: 2987–2991.
195. Palmer, C.M., and Guerinot, M.L., (2009). Facing the challenges of Cu, Fe and Zn homeostasis in plants. *Nat. Chem. Biol*, 5: 333–340.
196. Palmgren, M.G., Clemens, S., Williams, L.E., Krämer, U., Borg, S., Schjørring, J.K. and Sanders, D., (2008). Zinc biofortification of cereals: problems and solutions. *Trends Plant Sci*, 13 (9): 464–473.
197. Papadopoulos, J.S. and Agarwala, R., (2007). COBALT: constraint-based alignment tool for multiple protein sequences. *Bioinformatics*, 23(9): 1073-9.
198. Peer, W.A., Brown, D.E., Tague, B.W., Muday, G.K., Taiz, L. and Murphy, A.S., (2001). Flavonoid accumulation patterns of *transparent testa* mutants of *Arabidopsis*. *Plant Physiol*, 126: 536– 548.
199. Pelletier, M.K., Burbulis, I.E. and Winkel-Shirley, B., (1999). Disruption of specific flavonoid genes enhances the accumulation of flavonoid enzymes and end-products in *Arabidopsis* seedlings. *Plant Mol. Biol*, 40, 45–54.
200. Penkett, C.J., Morris, J.A., Wood, V. and Bähler, J., (2006). YOGY: a web-based, integrated database to retrieve protein orthologs and associated Gene Ontology terms. *Nucleic Acids Res*, 34: 330-334.
201. Petricka, J.J., Winter, C.M. and Benfey, P.N., (2012). Control of *Arabidopsis* root development. *Annu. Rev. Plant Biol*, 63: 563-590.
202. Petroski, M.D. and Deshaies, R.J., (2005). Function and regulation of cullin-RING ubiquitin ligases. *Nat. Rev. Mol. Cell Biol*, 6: 9–20.
203. Rawat, R., Takahashi, N., Hsu, P.Y., Jones, M.A., Schwartz, J., Salemi, M.R., Phinney, B.S. and Harmer, S.L., (2011). REVEILLE8 and PSEUDO-RESPONSE REGULATOR5 Form a Negative Feedback Loop within the *Arabidopsis* Circadian Clock. *PLoS Genet*, 7(3): e1001350.

204. Reichman, S.M., (2002). The Responses of Plants to Metal Toxicity: A Review Focusing on Copper, Manganese and Zinc. Australian Minerals & Energy Environment Foundation, Published as Occasional Paper No. 14. Accessed on: 12,08,2012. Available at: http://www.plantstress.com/Articles/toxicity_i/Metal_toxicity.pdf.
205. Ren, F., Liu, T., Liu, H. and Hu, B., (1993). Influence of zinc on the growth, distribution of elements and metabolism of one-year old American ginseng plants. *J. Plant Nut*, 16: 393-405.
206. Ren, J., Meng, S., Lekka, C.E. and Kaxiras, E., (2008). Complexation of flavonoids with iron: structure and optical signatures. *J Phys Chem B*, 112: 1845-1850.
207. Ren, Y., Liu, Y., Chen, H., Li, G., Zhang, X. and Zhao, J., (2011). Type 4 metallothionein genes are involved in regulating Zn ion accumulation in late embryo and in controlling early seedling growth in *Arabidopsis*. *Plant Cell Environ*, 35 (4): 770-789.
208. Rengel, Z., Remheld, V. and Marschner, H., (1998). Uptake of zinc and iron by wheat genotypes differing in tolerance to zinc deficiency. *Plant Physiol*, 152: 433-436.
209. Richard, O., Pineau, C., Loubet, S., Chalies, C., Vile, D., Marquès, L. and Berthomieu, P., (2011). Diversity analysis of the response to Zn within the *Arabidopsis thaliana* species revealed a low contribution of Zn translocation to Zn tolerance and a new role for Zn in lateral root development. *Plant, Cell and Environment*, 34: 1065-1078.
210. Robinson, N.J., Wilson, J.R. and Turner, J.S., (1996). Expression of the type 2 metallothionein-like gene MT2 from *Arabidopsis thaliana* in Zn²⁺-metallothionein-deficient *Synechococcus* PCC 7942: putative role for MT2 in Zn²⁺ metabolism. *Plant Mol. Biol*, 30: 1169-79.
211. Rogg, L.E., Lasswell, J., and Bartel, B., (2001). A Gain-of-Function Mutation in *IAA28* Suppresses Lateral Root Development. *Plant Cell*, 13: 465-480.
212. Rose, T.J., Impa, S.M., Rose, M.T., Pariasca-Tanaka, J., Mori, A., Heuer, S., Johnson-Beebout, S.E., Wissuwa, M., (2013). Enhancing phosphorus and zinc acquisition efficiency in rice: a critical review of root traits and their potential utility in rice breeding. *Ann Bot*, 112(2): 331-45.
213. Sadli, N., Ahmed, N., Ackland, M.L., Sinclair, A., Barrow, C.J. and Suphioglu, C., (2011). Effect of zinc and DHA on expression levels and post translational modifications of histones H3 and H4 in human neuronal cells, neurodegenerative diseases - processes, prevention, protection and monitoring. In: Raymond, C.C., ed. InTech, Available at: http://cdn.intechopen.com/pdfs/24868/InTech-Effect_of_zinc_and_dha_on_expression_levels_and_post_translational_modifications_of_histones_h3_and_h4_in_human_neuronal_cells.pdf. Accessed at: July 07.2013.
214. Salt, D.E., Prince, R.C., Baker, A.J.M., Raskin, I., Pickering, I.J., (1999). Zinc ligands in the metal hyperaccumulator *Thlaspi caerulescens* as determined using x-ray absorption spectroscopy. *Environ Sci Technol*, 33: 713-717.

215. Sandstead, H.H. and Klevay, L.M., (2000). History of Nutrition Symposium: Trace Element Nutrition and Human Health. *J. Nutr*, 130: 483–484
216. Sarret ,G., Saumitou-Laprade, P., Bert, V., Proux, O., Hazemann, J.L., Traverse, A., Marcus, M.A. and Manceau, A., (2002). Forms of zinc accumulated in the hyperaccumulator *Arabidopsis halleri*. *Plant Physiol*, 130, 1815–1826.
217. Saslowsky, D.E., Dana, C.D. and Winkel-Shirley, B., (2000). An allelic series for the chalcone synthase locus in *Arabidopsis*. *Gene*, 255: 127–138.
218. Schaaf, G., (2005). A putative function for the *Arabidopsis* Fe–phytosiderophore transporter homolog AtYSL2 in Fe and Zn homeostasis. *Plant Cell Physiol*, 46 (5): 762–774.
219. Schaaf, G., Ludewig, U., Erenoglu, B.E., Mori, S., Kitahara, T. and von Wirén, N., (2004). ZmYS1 functions as a proton-coupled symporter for phytosiderophore- and nicotianamine-chelated metals. *J. Biol. Chem*, 279 (10): 9091–9096.
220. Schmidhuber, J., and Tubiello, F.N., (2007). Global Food Security under Climate Change. *Proc. Natl. Acad. Sci*, 104 (50): 19703–19708.
221. Schroeder, D.F., Gahrtz, M., Maxwell, B.B., Cook, R.K., Kan, J.M., Alonso, J.M., Ecker, J.R. and Chory, J., (2002). De-etiolated 1 and damaged DNA binding protein 1 interact to regulate *Arabidopsis* photomorphogenesis. *Curr. Biol*, 12: 1462–1472.
222. Schwechheimer, C. and Calderon, Villalobos, LI., (2004). Cullin containing E3 ubiquitin ligases in plant development. *Curr. Opin. Plant Biol*, 7: 677-686.
223. Sen, A., (1982). Poverty and Famines: An Essay on Entitlement and Deprivation Oxford University Press, Oxford.
224. Seregin, I.V., Kozhevnikova, A.D., Gracheva, V.V., Bystrova, E.I. and Ivanov, V.B., (2011). Tissue zinc distribution in maize seedling roots and its action on growth. *Russian J. Plant Physiol.*, 58: 109-117.
225. Sharma, N., Cram, D., Huebert, T., Zhou, N. and Parkin, I.A., (2007). Exploiting the wild crucifer *Thlaspi arvense* to identify conserved and novel genes expressed during a plant's response to cold stress. *Plant Mol. Biol*, 63: 171–184.
226. Sharma, P.N., Kumar, N. and Bisht, S.S., (1994). Effect of zinc deficiency on chlorophyll content, photosynthesis and water relations of cauliflower plants. *Photosynthetica*, 30: 353–359.
227. Shaul, O., Hilgemann, D.W., de-Almeida-Engler, J., Van Montagu, M., Inze, D. and Galili, G., (1999). Cloning and characterization of a novel Mg²⁺/H⁺ exchanger. *EMBO J*, 18: 3973–3980.
228. Shimizu, H., Ross, R.K., Bernstein, L., Yatani, R., Henderson, B.E. and Mack, T.M., (1991). Cancers of the prostate and breast among Japanese and white immigrants in Los Angeles County. *Br J Cancer*, 63(6): 963–966.

229. Shiono, M., Matsugaki, N. and Takeda, K., (2005). Phytochemistry: structure of the blue cornflower pigment. *Nature*, 436: 791.
230. Shoji, K., Miki, N., Nakajima, N., Monomoi, K., Kato, C. and Yoshida, K., (2007). Perianth bottom-specific blue color development in tulip cv. Murasakizuisho requires ferric ions. *Plant Cell Physiol*, 48: 243–251
231. Shyu, C., Figueroa, P., DePew, C.L., Cooke, T.F., Sheard, L.B., Moreno, J., Katsir, L., Zheng, N., Browse, J. and Howe, G.A., (2012). JAZ8 lacks a canonical degron and has an EAR motif that mediates transcriptional repression of jasmonate responses in *Arabidopsis*. *Plant Cell*, 24: 536–550.
232. Sinclair, S.A. and Krämer, U., (2012). The zinc homeostasis network of land plants *Biochimica et Biophysica Acta*, 1823: 1553–1567.
233. Singh, R.K., Gonzalez, M., Kabbaj, H.M. and Gunjan, A., (2012). Novel E3 ubiquitin ligases that regulate histone protein levels in the budding yeast *saccharomyces cerevisiae*. *PLoS One*, 7(5): e36295.
234. Singh, R.K., Paik, J. and Gunjan, A., (2009). Generation and management of excess histones during the cell cycle. *Front Biosci*, 14: 3145–3158.
235. Sirtori, C.R. and Lovati, M.R., (2001). Soy proteins and cardiovascular disease. *Curr Atheroscler Rep*, 3: 47–53.
236. Skoog, F., (1940). Relationship between zinc and auxin in the growth of higher plants. *Am J Bot*, 27:939–950.
237. Smalle, J. and Vierstra, R.D., (2004). The ubiquitin 26S proteasome proteolytic pathway. *Annu. Rev. Plant Physiol*, 55: 555–590.
238. Smyth, G.K., (2004). Linear models and empirical Bayes methods for assessing differential expression in microarray experiments. *Stat. Appl. Genet. Mol. Biol*, 3: Article3.
239. Sokol, A., Kwiatkowska, A., Jerzmanowski, A. and Prymakowska-Bosak, M., (2007). Up-regulation of stress-inducible genes in tobacco and *Arabidopsis* cells in response to abiotic stresses and ABA treatment correlates with dynamic changes in histone H3 and H4 modifications. *Planta*, 227: 245-254.
240. Song, W.Y., Choi, K.S., Kim, D.Y., Geisler, M., Park, J., Vincenzetti, V., Schellenberg, M., Kim, S.H., Lim, Y.P., Noh, E.W., Lee, Y. and Martinoia, E., (2010). *Arabidopsis* PCR2 is a zinc exporter involved in both zinc extrusion and long-distance zinc transport. *Plant Cell*, 22 (7): 2237–2252.
241. de Souza, R.F. and de Giovani, W.F., (2004). Antioxidant properties of complexes of flavonoids with metal ions. *Redox Rep*, 9(2): 97-104.
242. Stefanini, M., Botta, E., Lanzafame, M. and Orioli, D., (2010). Trichothiodystrophy: From basic mechanisms to clinical implications. *DNA Repair*, 9: 2–10.

243. Stephan, U.W. and Scholz, G., (1993). Nicotianamine: Mediator of transport of iron and heavy metals in the phloem? *Physiol. Plant*, 88: 522–529.
244. Stockinger, E.J., Mao, Y., Regier, M.K., Triezenberg, S.J. and Thomashow, M.F., (2001). Transcriptional adaptor and histone acetyltransferase proteins in *Arabidopsis* and their interactions with CBF1, a transcriptional activator involved in cold-regulated gene expression. *Nucleic Acids Res*, 29: 1524-1533.
245. Stracke, R., Huep, G. and Weisshaar, B., (2010). Use of Mutants from T-DNA Insertion Populations Generated by High-Throughput Screening. Mutagenesis. In: Meksem, K. and Kahl, G., eds. The handbook of plant mutation screening. Wiley-Vch. Weinheim, 31-54.
246. Su, Y.H., Liu, Y.B. and Zhang, X.S., (2011). Auxin–Cytokinin Interaction Regulates Meristem Development. *Mol Plant*, 4(4): 616-25.
247. Sudhalakshmi, R.K. and Rajarajan, A., (2007). Influence of Zinc Deficiency on Shoot / Root Dry Weight Ratio of Rice Genotypes. *JABS*, 3(4): 295-298.
248. Suzuki, M., Takahashi, M., Tsukamoto, T., Watanabe, S., Matsushashi, S., Yazaki, J., Kishimoto, N., Kikuchi, S., Nakanishi, H., Mori, S. and Nishizawa, N.K., (2006). Biosynthesis and secretion of mugineic acid family phytosiderophores in zinc-deficient barley. *Plant J*, 48(1): 85-97.
249. Suzuki, M., Tsukamoto, T., Inoue, H., Watanabe, S., Matsushashi, S., Takahashi, M., Nakanishi, H., Mori, S. and Nishizawa, N.K., (2008). Deoxymugineic acid increases Zn translocation in Zn-deficient rice plants. *Plant Mol. Biol*, 66 (6): 609–617.
250. Swarup, R., Kramer, E.M., Perry, P., Knox, K., Leyser, H.M.O, Haseloff, J., Beemster, G.T.S., Bhalarao, R. and Bennett, M.J., (2005). Root gravitropism requires lateral root cap and epidermal cells for transport and response to a mobile auxin signal. *Nat Cell Biol*, 7: 1057–1065.
251. Tainer, J.A., Getzoff, E.D., Beem, K.M., Richardson, J.S. and Richardson, D.C., (1982). Determination and analysis of the 2 A structure of copper, zinc superoxide dismutase. *J. Mol. Biol*, 160: 181-217.
252. Takagi, S., Nomoto, K. and Takemoto, T., (1984). Physiological aspect of mugineic acid, a possible phytosiderophore of graminaceous plants. *J. Plant Nut*, 7: 469–477.
253. Takahashi, M., Terada, Y., Nakai, I., Nakanishi, H., Yoshimura, E., Mori, S. and Nishizawa, N.K., (2003). Role of nicotianamine in the intracellular delivery of metals and plant reproductive development. *Plant Cell*, 15: 1263–1280.
254. Takatsuji, H., (1998). Zinc-finger transcription factors in plants. *Cell. Mol. Life Sci*, 54: 582–596.
255. Takayama, Y. and Toda, T., (2010). Coupling histone homeostasis to centromere integrity via the ubiquitin-proteasome system. *Cell Division*, 5:18.
256. Talke, I.N., Hanikenne, M. and Krämer, U., (2006). Zinc-dependent global transcriptional control, transcriptional deregulation, and higher gene copy number

- for genes in metal homeostasis of the hyperaccumulator *Arabidopsis halleri*. *Plant Physiol*, 142: 148–167.
257. Tennstedt, P., Peisker, D., Bottcher, C., Trampczynska, A. and Clemens, S., (2009). Phytochelatin synthesis is essential for the detoxification of excess zinc and contributes significantly to the accumulation of zinc. *Plant Physiol*, 149: 938–948.
258. Thomine, S., Lelievre, F., Debarbieux, E., Schroeder, J.I. and Barbier-Brygoo, H., (2003). AtNRAMP3, a multispecific vacuolar metal transporter involved in plant responses to iron deficiency. *Plant J*, 34: 685–695.
259. Trampczynska, A., Küpper, H., Meyer-Klaucke, W., Schmidt, H. and Clemens, S., (2010). Nicotianamine forms complexes with Zn(II) in vivo. *Metallomics*, 2: 57–66.
260. Tsimogiannis, D., Samiotaki, M., Panayotou, G. and Oreopoulou, V., (2007). Characterization of flavonoid subgroups and hydroxy substitution by HPLC-MS/MS. *Molecules*, 12: 593-606.
261. Uauy, C., Distelfeld, A., Fahima, T., Blechl, A. and Dubcovsky, J., (2006). A NAC gene regulating senescence improves grain protein, zinc and iron content in wheat. *Science*, 314: 1298–1301.
262. Ulmasov, T., Murfett, J., Hagen, G., and Guilfoyle, T.J., (1997). Aux/IAA proteins repress expression of reporter genes containing natural and highly active synthetic auxin response elements. *Plant Cell*, 9: 1963–71.
263. Vallee, B.L. and Auld, D.S., (1992). Active zinc binding sites of zinc metalloenzymes. In: Birkedal-Hansen, H., Werb, Z., Welgus, H. and Van Wart, H. eds. Matrix Metalloproteinases and Inhibitors. Stuttgart, Germany, Fischer, 5.
264. Vallee, B.L. and Falchuk, K.H., (1993). The biochemical basis of zinc physiology. *Physiological reviews*, 73(1): 79-118.
265. Verret, F., Gravot, A., Auroy, P., Leonhardt, N., David, P., Nussaume, L., Vavasseur, A. and Richaud, P., (2004). Overexpression of AtHMA4 enhances root-to-shoot translocation of zinc and cadmium and plant metal tolerance. *FEBS Lett.* 576: 306–312.
266. Vert, G., Walcher, C.L., Chory, J. and Nemhauser, J.L., (2008). Integration of auxin and brassinosteroid pathway by auxin response factor 2. *Proc Natl Acad Sci*, 105: 9829–9834.
267. Vinkenborg, J.L., (2010). Fluorescent sensor proteins for intracellular metal imaging. Ph.D. Thesis. Eindhoven University of Technology. Netherland.
268. Walther, U.I., Schulze, J. and Forth, W., (1995). Inhibition of RNA synthesis in cultured lung cells exposed to zinc chloride. *Arch Pharmacol*, 17(12): 661-667.
269. Wang, H., Zhai, L., Xu, J., Joo, H.Y., Jackson, S., Erdjument-Bromage, H., Tempst, P., Xiong, Y. and Zhang, Y., (2006). Histone H3 and H4 Ubiquitylation by the CUL4-DDB-ROC1 Ubiquitin Ligase Facilitates Cellular Response to DNA Damage. *Mol Cell*, 22: 383–394.

270. Wang, H.Y., Klatter, M., Jakoby, M., Bäumlein, H., Weisshaar, B. and Bauer, P., (2007). Iron deficiency-mediated stress regulation of four subgroup Ib bHLH genes in *Arabidopsis thaliana*. *Planta*, 226: 897–908.
271. Wang, J., Evangelou, B.P., Nielsen, M.T. and Wagner, G.J., (1992). Computer-simulated evaluation of possible mechanisms for sequestering metal ion activity in plant vacuoles: II. Zinc. *Plant Physiol*, 99: 621–626.
272. Wang, K., Zhou, B., Kuo, Y.M., Zemansky, J. and Gitschier, J., (2002). A novel member of a zinc transporter family is defective in Acrodermatitis enteropathica. *Am. J. Hum. Genet*, 71: 66–73.
273. Waters, B.M. and Pedersen, J.F., (2009). Sorghum germplasm profiling to assist breeding and gene identification for biofortification of grain mineral and protein concentrations. *The Proceedings of the International Plant Nutrition Colloquium XVI. Paper 1228*.
274. Weake, V.M. and Workman, J.L., (2008). Histone ubiquitination: triggering gene activity. *Mol. Cell*, 29: 653–63.
275. Weber, M., Deinlein, U., Fischer, S., Rogowski, M., Geimer, S., Tenhaken, R. and Clemens, S., (2013). A mutation in the *Arabidopsis thaliana* cell wall biosynthesis gene pectin methylesterase3 as well as its aberrant expression cause hypersensitivity specifically to Zn. *Plant J. (in press)*.
276. Weber, M., Harada, E., Vess, C., von Roepenack-Lahaye, E. and Clemens, S., (2004). Comparative microarray analysis of *Arabidopsis thaliana* and *Arabidopsis halleri* roots identifies nicotianamine synthase, a ZIP transporter and other genes as potential metal hyperaccumulation factors. *Plant J*, 37: 269–281.
277. Welch, R.M., (1995). Micronutrient nutrition of plants. *Crit Rev Plant Sci*, 14: 49-82.
278. Welch, R.M., Hart, J.J., Norvell, W.A., Sullivan, L.A. and Kochian, L.V., (1999). Effects of nutrient solution zinc activity on net uptake, translocation, and root export of cadmium and zinc by separated sections of intact durum wheat (*Triticum turgidum* L-var durum) seedling roots. *Plant and Soil*, 208: 243-250.
279. White, P.J. and Broadley, M.R., (2011). Physiological limits to zinc biofortification of edible crops. *Front Plant Sci*, 2: 80.
280. WHO, (2005). Comparative Quantification of Health Risks: Global and Regional Burden of Diseases Attributable to Selected Major Risk Factors. Vol. 1–3.
281. WHO, (2009). Global health risks: mortality and burden of disease attributable to selected major risks. Geneva.
282. Williams, L.E., Pittman, J.K. and Hall, J.L., (2000). Emerging mechanisms for heavy metal transport in plants. *Biochimica et Biophysica Acta*, 1465: 104-126.
283. Williams, R.J.P., (1982). Metals ions in biological catalysts. *Pure Appl.Chem*, 54 (10): 1889-1904.

284. Winkel, B.S.J., (2006). The Biosynthesis of Flavonoids. In: Grotewold, E., ed. The science of flavonoids. Springer. Columbus, 71-96.
285. Winkel-Shirley, B., (2002). Biosynthesis of flavonoids and effects of stress. *Curr Opin Plant Biol*, 5: 218-223
286. Winkel-Shirley, B., Kubasek, W.L., Storz, G., Bruggeman, E., Koornneef, M., Ausubel, F.M. and Goodman, H.M., (1995). Analysis of *Arabidopsis* mutants deficient in flavonoid biosynthesis. *Plant J*, 8: 659-671.
287. Wintz, H., Fox, T., Wu, Y.Y., Feng, V., Chen, W.Q., Chang, H.S., Zhu, T. and Vulpe, C., (2003). Expression profiles of *Arabidopsis thaliana* in mineral deficiencies reveal novel transporters involved in metal homeostasis. *J Biol Chem*, 278: 47644-47653.
288. von Wirén, N., Marschner, H. and Romheld, V., (1996). Roots of iron-efficient maize also absorb phytosiderophore-chelated zinc. *Plant Physiol*, 111 (4): 1119-1125.
289. Wirth, J., Poletti, S., Aeschlimann, B., Yakandawala, N., Drosse, B., Osorio, S., Tohge, T., Fernie, A., Günther, D., Gruissem, W. and Sautter, C., (2009). Rice endosperm iron biofortification by targeted and synergistic action of nicotianamine synthase and ferritin. *Plant Biotechnol. J*, 7(7): 631-644.
290. Wiseman, H., (2006). Isoflavonoids and human health. In: Andersen, Ø. M. and Markham, K. R. eds. Flavonoids chemistry, biochemistry and applications. CRC Press, Taylor & Francis Group, New Your, 371-396.
291. Woolhouse, H.W., (1983). Responses to the Chemical and Biological Environment. In: Lange, O. L., Nobel, P. S., Osmond, C. B. and Ziegler, H., eds. Encyclopedia of Plant Physiology. New Series Vol. 12, Springer Verlag, Berlin.
292. Wu, J., Zhao, Z., An, L., Liu, Y., Xu, S., Gao, D. and Zhang, Y., (2008). Inhibition of glutathione synthesis decreases chilling tolerance in *Chorisporabungeana* callus. *Cryobiology*, 57(1): 9-17.
293. Ye, S., Dhillon, S., Ke, X., Collins, A.R., and Day, I.N., (2001). An efficient procedure for genotyping single nucleotide polymorphisms. *Nucleic Acids Res*, 29: e88.
294. Yi, X., Du, Z. and Su, Z., (2013). PlantGSEA: a gene set enrichment analysis toolkit for plant community. *Nucleic Acids Res*, 41(Web Server issue):W98-W103.
295. Yoshida, K., Kitahara, S., Ito, D. and Kondo, T., (2006). Ferric ions involved in the flower color development of the Himalayan blue poppy. *Meconopsis grandis*. *Phytochemistry*, 67: 992-998.
296. Yoshida, K., Toyama-Kato, Y., Kameda, K. and Kondo, T., (2003). Sepal color variation of *Hydrangea macrophylla* and vacuolar pH measured with a proton-selective microelectrode. *Plant Cell Physiol*, 44: 262-268.
297. Young, K., (1998). Yeast two-hybrid: so many interactions, (in) so little time. *Biol Reprod*, 58 (2): 302-11.

298. Yurekli, F. and Porgali Z.B., (2006). The effects of excessive exposure to copper in bean plants. *Acta Biologica Cracoviensia Series Botanica*, 48 (2): 7-13.
299. van der Zaal, B.J., Neuteboom, L.W., Pinas, J.E., Chardonnens, A.N., Schat, H., Verkleij, J.A.C. and Hooykaas, P.J.J., (1999). Overexpression of a novel *Arabidopsis* gene related to putative zinc-transporter genes from animals can lead to enhanced zinc resistance and accumulation. *Plant Physiol*, 119: 1047-1055.
300. Zander, M., Chen, S., Imkampe, J., Thurow, C. and Gatz, C., (2012). Repression of the *Arabidopsis thaliana* jasmonic acid/ethylene-induced defense pathway by TGA-interacting glutaredoxins depends on their C-terminal ALWL motif. *Mol Plant*, 5(4): 831-40.
301. Zhang, X., Chen, Y., Wang, Z.Y., Chen, Z., Gu, H. and Qu, L.J., (2007). Constitutive expression of CIR1 (RVE2) affects several circadian-regulated processes and seed germination in *Arabidopsis*. *Plant J*, 51(3): 512-25.
302. Zhang, Y., Feng, S., Chen, F., Chen, H., Wang, J., McCall, C., Xiong, Y. and Deng, X.W., (2008). *Arabidopsis* DDB1-CUL4 ASSOCIATED FACTOR1 forms a nuclear E3 ubiquitin ligase with DDB1 and CUL4 that is involved in multiple plant developmental processes. *Plant Cell*, 20: 1437-1455.
303. Zhao, Y., Christensen, S.K., Fankhauser, C., Cashman, J.R., Cohen, J.D., Weigel, D. and Chory, J., (2001). A role for flavin monooxygenase-like enzymes in auxin biosynthesis. *Science*, 291: 306-309.
304. Zheng, Q. and Wang, X.J., (2008). GOEAST: a web-based software toolkit for Gene Ontology enrichment analysis. *Nucleic Acids Res*, 36 (Web Server issue), W358-W363.
305. Zhu, J., Jeong, J.C., Zhu, Y., Sokolchik, I., Miyazaki, S., Zhu, J.K., Hasegawa, P.M., Bohnert, H.J., Shi, H., Yun, D.J. and Bressan, R.A., (2008). Involvement of *Arabidopsis* HOS15 in histone deacetylation and cold tolerance. *Proc Natl Acad Sci*, 105: 4945-4950.
306. Zhu, L., Ji, X.J., Wang, H.D., Pan, H., Chen, M. and Lu, T.J., (2012). Zinc neurotoxicity to hippocampal neurons in vitro induces ubiquitin conjugation that requires p38 activation. *Brain research*, 1438: 1-7.
307. Zhu, Y., Dong, A., Meyer, D., Pichon, O., Renou, J.P., Cao, K. and Shen, W.H., (2006). *Arabidopsis* NRP1 and NRP2 encode histone chaperones and are required for maintaining postembryonic root growth. *Plant Cell*, 18: 2879-2892.

Appendix

Appendix list-1

Hoagland medium recipe

10X Stock solution concentration

200 μ M MgSO₄
 100 μ M HPO₄(NH₄)₂
 280 μ M Ca(NO₃)₂
 600 μ M KNO₃
 5 μ M Fe-HBED
 Adjust to 1L by milli q water

for 2L 10X Stock solution

5.6 mL 1M MgSO₄
 2ml 1M HPO₄(NH₄)₂
 4ml 1M Ca(NO₃)₂
 12ml 1M KNO₃
 10ml 10mM Fe-HBED

Agar plates Hoagland medium composition

10ml 10X-stock solution
 10g sucrose
 975mg MES buffer
 10 g TypA agar
 Adjust to 1L by milli q water and set pH to 5.7 by adding KOH

Hydroponic solution Hoagland medium composition

1M (NH₄)₂SO₄
 1M KNO₃
 1M MgSO₄
 1M Ca(NO₃)₂

for 25L Hydroponic solution

5ml 1M (NH₄)₂SO₄
 5ml 1M KNO₃
 5ml 1M MgSO₄
 5ml 1M Ca(NO₃)₂
 5ml Microelement mix
 12.5 ml 10mM Fe-HBED
 Adjust to 25L by milli q water
 Set pH to 5.7 with 1/5 85% H₃PO₄

Components of the Microelement mix

4.6 μ M H₃BO₃
 32 nM CuSO₄
 0.9 μ M MnCl₂
 11 nM MoO₃
 77 nM ZnSO₄

for 1L Microelement mix

1.43g H₃BO₃
 40mg CuSO₄ × 5H₂O
 905mg MnCl₂ × 4H₂O
 20ml 0.4mg/l at pH-11 MoO₃ solution
 110mg ZnSO₄ × 7H₂O

Recipe for 1L 10mMFe-HBED

4.25g HBED
 30ml 1M KOH
 2.7g FeCl₃ × 6H₂O
 800 ml milli q water
 Set pH to 5.7

Appendix list-2

Mapping primers

Name		Sequence	Annaeling temperature	Restriction enzyme
Perl222	Frw	ACCAGTAAGAGATTCTACAGAAGTATCC	56	RsaI
	Rev	GATGATCAGCATCGTCGAAAC		
MASC909	Frw	TGTTCTGGTCTGCATGTCGAG	58	RsaI
	Rev	AGTAGCCTCTTCTGCGGAAAT		
Perl457	Frw	TGGTCTAACTTCGGTTCTAC	54.5	Tail(MaeII)(65°C)
	Rev	TGACTCGCTATGICTACATCC		
Perl100	Inner Frw	ACGATGAGATAGTCAGCAGCCTC	64	
	Inner Rev	ATGGATACACTCTTCAAACCTCCGTC		
	Outer Frw	TTGAAAGCCCATTTCGTTCTTC		
	Outer Rev	ATCTTGCTCTTCGTTAAACCAGC		
Perl785	Inner Frw	TGGTTTGCAATTCGAGGAC	57	
	Inner Rev	ATAGACCCTTCCACAATTTACGGA		
	Outer Frw	AAGGTGAAAGATGCACACATCAC		
	Outer Rev	AAATCCGAACGATCAGTCCAG		
SNP8909	Inner Frw	AATCTCGCATATGATGCGATG	59.6	
	Inner Rev	TCCTTAGATGTTACCACCTATCCG		
	Outer Frw	GTCTCTCAAACCATCAAGCC		
	Outer Rev	GAAGAAGCTGGTCCGCTTC		
Perl617	Inner Frw	AACTCTGGGATTATCAATCCGCA	67	
	Inner Rev	AGGGAATGTCCTAACGTTATCG		
	Outer Frw	TTTGCTGGCTACACTGTTGAAGTIG		
	Outer Rev	TGTACCAATCATGACCATATCCAC		
Perl03	Inner Frw	CGCTAGGTGCAACTGCGAGG	63.4	
	Inner Rev	TTCCGGATGTGCCCGGAGG		
	Outer Frw	TCGTCCATGCCGATATGGTGGTAC		
	Outer Rev	TAAGTCCCCTCCAATTCGTGTTACC		
Perl907	Inner Frw	TATTGAGGCATGCGTAAAGAGC	64	
	Inner Rev	ACGGACGTTGATCACATCACTAC		
	Outer Frw	TCGAGGGAGATTCCCTCAGTG		
	Outer Rev	AGGTGATCCAAAACTAAAGCAGAC		
Perl738	Inner Frw	TCCCAGACTTCATTTCGGCT	64	
	Inner Rev	CCTTCTCAATACCTGGACAGACC		
	Outer Frw	TTCATGTAGGCGTCACATGC		
	Outer Rev	TCACCTTCCATCTGACTACCCTAG		
SNP8985	Inner Frw	TCAAAGTAGAACCCCTGGTCCCAATCA	60.6	
	Inner Rev	AAATGGAGTGCATGGAAATGCAACGC		
	Outer Frw	AACTAGCATGTGCACGCTCTCAC		
	Outer Rev	TTGGACAGTTGCTTCTCTGTGGT		
Perl1797	Inner Frw	CTGATCGCATGTTCTTTACGCAG	60.6	
	Inner Rev	AGCATTGACGGTGAAAGCAACTG		
	Outer Frw	TCTACTGAAGTTGTTTGGTTCCG		
	Outer Rev	ATCAACATTGAGCATCTTCGATATGG		
Perl953	Inner Frw	ATGGAGCCTATACTAATGAGACGC	61	
	Inner Rev	CAGTAACCATCTCTATGGACTGCAT		
	Outer Frw	AGAAAGGAGTTAGGAGTTCTTCCGG		
	Outer Rev	AATTGTCICTCGGACGAAAGAAGTG		
Perl9811	Outer fwr	AGGAAGAAGGTGACCAGAACGAGTC	64.6	
	Iner(ler)fwr	TGCTTGAGTTATCGGTCTCCTCGAC		
	Outer rev	TGAGGACTGACGATGACATGCAGC		
Perl9577	Outer fwr	AGGCAGCGTGCCATCTTCTAG	61.3	
	Iner(ler)fwr	ACCTGAATGTCAACCAGATGTTGCA		
	Outer rev	CTTGAACAGTGGTCTGATGAATCC		
BKN331	Outer fwr	TGTTCCAAGGGTTTCTATGAGG	58.9	
	Iner(ler)fwr	TGGAGCTGTTTATCAATGTTGCC		
	Outer rev	AAGGGTCACTCTTGTTGCTAC		
Perl339	Outer fwr	TGGCGTGGTGTGAGCAATCTGC	63.9	
	Iner(ler)fwr	TGAAGGAGCCAGCGTCACTCTC		
	Outer rev	AAGGTAGCACAAACCTGTGGCTC		
SNP8965	Outer fwr	TTAAGGCCAGTTTTAGGTCAC	58.3	
	Iner(ler)fwr	AGACAACCTTCTCAGACTCAGCA		
	Outer rev	ACCTTCAAGAACACCATGC		
Perl143	Outer fwr	TCGGACCAAGTGTAGTTCACGG	61.9	
	Iner(ler)fwr	ACCTGACGAGCCGCTTGTAGTC		
	Outer rev	TGCTGTTTGTGACAGACAGTGGTG		

Appendix list

Sequencing primers

<i>Candidate gene</i>	<i>Primer name</i>		<i>Sequence</i>	<i>Annealing temperature</i>
AT2G20208	AT2G20208a	Frw	TCTGAAATTGGTCACCTCACA	58
		Rev	ATGACCCGTAGATAGTTCCTA	
AT2G20230	AT2G20230a	Frw	AGCATCAGATAAGAGCGAAACAA	55.5
		Rev	AGACCAAGCTTGAGGTGAAC	
	AT2G20230b	Frw	GATAAACGTGGGTTTTGTTTCTGG	54.5
		Rev	TGAATTACCTGGACTGCTACCA	
	AT2G20230c	Frw	AGGGCTTTCATTGAAGAAAACATCG	57.5
		Rev	TGCTAACTCAAACCTGTTACAGGA	
AT2G20280	AT2G20280a	Frw	ACTAGTTCCTTGATGAGGCCA	54
		Rev	AGCTAAGAACGACCGTATGAG	
	AT2G20280b	Frw	AGAGTCACACTGGAGATGGAT	56
		Rev	TTTCTGCGCACTTGGTTCAT	
	AT2G20280c	Frw	TGATTAGACTAACATCACCA	53
		Rev	TTGGTGATGTATCTTGGCA	
	AT2G20280d	Frw	TTGACACTGCCCGCCTTGAA	57
		Rev	GAGAACCTTCCATCGGATCCGTGTACA	
AT2G20330	AT2G20330a	Frw	TTCAATAGACATGCTGCATAGTATCT	55.5
		Rev	GGAAGAAATCTGTAGATGATTACCAAC	
	AT2G20330b	Frw	TCTCTGAACAATGGTAATGCA	53
		Rev	TCGATCAAGATTGGAGTCTC	
	AT2G20330c	Frw	TCCAACGTATATATCTGGTCGGCT	59.5
		Rev	TCCAAGGGATGAATTCGAGACTACAGT	
	AT2G20330d	Frw	TCCCTCAGATGGCTCTATCTGTCT	59.5
		Rev	TTGTCGCCGGTAAACAGCAAC	
AT2G20340	AT2G20340a	Frw	GAGATATCCACTCCCCTGAAACC	58
		Rev	TCATACTTGCGCAAAACAGGCT	
	AT2G20340b	Frw	AGCTTTTGCCTGATTCTGCACC	59
		Rev	TGGCAAGCCTTCTGTAAAGCTGA	
	AT2G20340c	Frw	GCTTGAGAAGCTCGTTGTCTACT	58
		Rev	TGAGGAACCATTTGTGAGCATTCA	
	AT2G20340d	Frw	AGAGTATCGGCAATACATTGACGGTG	60
		Rev	TTCTTCGTCTTTCACAGGCACGAG	
	AT2G20340e	Frw	TCTTGTTTGCAGATTGTCACAC	55
		Rev	TCGCATGGTATAAAAATACGTCTAACA	
AT2G20350	AT2G20350a	Frw	ACTTCTCAGTGACCGTGAGCAAC	62
Rev	TGAAGCAAGTAAGATGCCTCTTCCT			
AT2G20360	AT2G20360a	Frw	TGCTTGTATCCTCGAGGCAG	57.8
		Rev	ACATAACACGGCAAGAACATTCTC	
	AT2G20360b	Frw	AGTGAACITTTCTCGAGAGCT	55
		Rev	ATTGATAACGACATTAGCCTTGG	
	AT2G20360c	Frw	TTGATCCAAGAGATGAAGACTCGA	57.4
		Rev	TACGGTTTTCCCAGTTCTGCA	
	AT2G20360d	Frw	TCGGTACACATAACTCTCTCTG	55
		Rev	ATTGCCTGGAACAGATTGTG	
	AT2G20360e	Frw	CACTGTCCATGGAAGAAACTC	55
		Rev	TCTTGACCATGTAAGGAAACTTC	
AT2G20362	AT2G20362a	Frw	ATCTCTGGAGAGACAGGATAGACTCA	57
Rev	GTCGTTTGTCCCCTAGACTACTACA			
AT2G20370	AT2G20370a	Frw	AACAGCTCCAATTGCAACCTAG	56.7
		Rev	ACCTTCATCAGAGAAGACACCTTC	
	AT2G20370b	Frw	ACCAGTAGCCAATTCTAGTCCAC	58
		Rev	CATTGCTCTCCCCAAAATCGCA	
	AT2G20370c	Frw	TGTCGAAACTCAAATGTTGGC	58
		Rev	AACATAGGCACTGCTTCAGT	

Appendix list

AT2G20380	AT2G20380a	Frw	AGTGA CTGCAGATCATATTTATAAGCG	55
		Rev	AGACACTCAA ACTTGGATTCCCTG	
	AT2G20380b	Frw	AGCATTCC TTTTCATATGTTGGAGT	55
		Rev	AGGTTTCCGATT TGTCTGATCTC	
AT2G20390	AT2G20390a	Frw	TTGATGCA ATTAGGACTTGAATGCT	57
		Rev	TGAGAAAGGGCC ATGGTACA	
	AT2G20390b	Frw	ACAGGGAATGAACAAGACTG	55
		Rev	CTGATAGTTGAATTGTGAATCGATTCCG	
	AT2G20390c	Frw	TGTCCAAACGAGTCTCTTGCT	57
		Rev	AACCCAGAACCCTACAGATCATC	
AT2G20410	AT2G20410a	Frw	CTCAACCGCCAATCGAATAGTA	57.5
		Rev	CCAAGCAAAATCAGGTCTTGCT	
	AT2G20410b	Frw	TGGTATCGTTGTTACTAATCTCC	54.5
		Rev	GGTAACTGCTTTGAATCAAGTTC	
	AT2G20410c	Frw	TCTATTCCTGTACAATGCAAGAG	54.5
		Rev	ACAGTCTACTCAAAACTCATTGC	
AT2G20420	AT2G20420a	Frw	TAAATGAGCCGCGACATAG	55.8
		Rev	AAGACCACTCTTGAATGTTCCA	
	AT2G20420b	Frw	TCGTGTGATACAGTTGGTTGT	55.6
		Rev	CCTACGCAAAACCATGACTTG	
	AT2G20420c	Frw	CTGAGATTCTTTCTCATGCGGGT	58
		Rev	AGAAAGAAGGTTCTTTTACCTGGT	
	AT2G20420d	Frw	ACGTTGGTGGAAATGCTTCTG	57.8
		Rev	TTGTTTCAGTGACAGCTATAGTGTTG	
AT2G20430	AT2G20430a	Frw	AGCCATTGGAGCTAGCAGCAAAG	61
		Rev	TAATGCCACCGCACCAAGCT	
	AT2G20430b	Frw	TCACATCCATCCAAATATGCGTAGGA	58
		Rev	GCAACTCACAATGTCAAGCTCCA	
	AT2G20430c	Frw	AATGTATCGGAGCCCTTCA	55
		Rev	ATACGCTCTCAACCCATCA	
AT2G20440	AT2G20440a	Frw	TGTATGTCTCTATGTCATTTGCT	52.5
		Rev	TCACTCGTTTCTCTCAAAGC	
	AT2G20440b	Frw	GCAATGTCTCCTAGTATCTGCATAC	56.5
		Rev	CACAGGTCATTAAGACAGTGGATC	
	AT2G20440c	Frw	ACTCTTACCTAGATGTTGATGGAGACG	58
		Rev	TACGTCACAATGGCAGTCGTTT	
	AT2G20440d	Frw	CTGTAACAGTGTTTTTACGATCCA	56.5
		Rev	TTGTCAGGCTGGAAAGACTCT	
	AT2G20440e	Frw	ATGGCCATCTTCAGTAAAGGCAGC	61
		Rev	CTGAAGATTCCGGCTGTTAGGATCTCA	

IZS 288 gene Cloning primers

<i>Use</i>	<i>Primer name</i>	<i>Sequence</i>	<i>Annealing temperature</i>
Prmomotor-GUS line	P330-1fw	tgctttctctcctctcag	53
	P330-1rev	gagtttccatcatatttccaaacatag	
Genomic fragment	GF330fw	tacgcagagagagagaggtgatg	57
	GF330rev	tccaaaacagaacgtgagtttccatc	
35S:At2g20330-GFP tag	35S330Tfw	tgacgaagaagaaggtgacactaaaaa	55
	35S330Trev	tagacctccaattcgtcctccat	
35S:377 th Ser	wd-40 Ser fw	cactgatgatataagctctgtaaag	52.8
	wd-40 Ser rev	ctttacagagcttatatcatcagtg	
35S:377 th Al	wd-40 Ala fw	cactgatgatataagctctgtaaag	54.4
	wd-40 Ala rev	ctttacagaggcttatatcatcagtg	
35S:Xenopus-WDR70	Xenopus-wdr 70 fw	atgggcttctctggatttgg	51.8
	Xenopus-wdr 70 rev	tcagatcttgcgctcttcc	

T-DNA lines confirmation primers

<i>SALK-line</i>		<i>Primer name</i>	<i>Sequence</i>	<i>Annealing temperature</i>
SALK_038590	Self made	T-DNA-038590 rev	gcgactatcgagcttgagaacg	57.1
		WT-038590 fw	ctctcagaccagcctaagacca	
	Salk-primer	SALK_038590LP	gtgcaccaaggaagaaatctg	52.4
		SALK_038590RP	agctttgagaacgggagtctc	54.4
SALK_140479	Self made	T-DNA-140479 rev	gattcggaccggaacacttc	55.7
		WT-140479 fw	gcattccccttagttgaaagtca	
	Salk-primer	SALK_140479LP	caaatatgcaaaaccaatgcc	48.5
		SALK_140479RP	atccccctcatcatcagaatc	52.4
SALK_065643	Self made	T-DNA-065643 rev	attcggaccggaacacttcg	56.3
		WT-065643 fw	ccgagagaaatcacaattgcaccg	
	Salk-primer	SALK_065643LP	atgccacaaaactccacatag	52.4
		SALK_065643RP	tggtgatatccgacgaaactc	52.4

qRT-PCR primers used for confirmation of microarray

<i>Use</i>	<i>Primer name</i>	<i>Sequence</i>
QQS (AT3G30720)	qpcr-QQS-3-fw	AGCTTCAAACCAAACAATTCAAC
	qpcr-QQS-3-rev	CATTTTGAGCCTTGCGACAC
CBF3/ DREB1A (AT4G25480)	qpcr-CBF3-3-fw	GCGCTAAGGACATCCAAAAG
	qpcr-CBF3-3-rev	GTCGTCGCATCACACATCTC
RIN4 (AT3G48450)	qpcr-RPM1-2-fw	ATGGGATGCGACTAATCCTG
	qpcr-RPM1-2-rev	ACAGCGGTTTTTCATCGTCTT
MTPA1 (AT3G61940)	qpcr-mtpa1-3-fw	AATGGAGAGCACACCGAGAG
	qpcr-mtpa1-3-rev	CCACAACCTTCCTCAATTTCCA
NAS4 (AT1G56430)	AhNAS4-fw	TGGACCTAGAGCGTTTCTCTATCCC
	AhNAS4-rev	ACCGATAAAACTTGAAACCTTGG
IZS 288 (AT2G20330)	WD40RT-fw-1	CTTCAATGCTTTCTCTTTTCTCG
	WD40RT-rev-1	GCATGAGGATTGTGTACTACTGGT

Appendix list-3

LB Medium recipe (1L)

10 g Bacto-tryptone
5 g yeast extract
5 g NaCl
* for Agar plates: 15 g Agar

YEP Medium recipe (1L)

10 g Peptone
5 g Yeast extract
5 g NaCl
* for Agar plates: 15 g Agar

Concentration of antibiotics for selection

Rifampicin	50 µg/ml
Gentamycin	25 µg/ml
Kanamycin	50 µg/ml
Spectinomycin	50 µg/ml

Stock solution of antibiotics

10 mg/ml Rifampicin
50mg/ml Gentamycin
50mg/ml Kanamycin
50mg/ml Spectinomycin

Appendix list-4

Highly enriched gene ontology terms in 1992 genes that were chilling responsive in WT roots after 24 hours of chilling stress and clustered into five groups by K-mean algorithm using the Pearson correlation coefficient as a distance metrics. The enrichment analysis was carried out using the Gene Ontology Enrichment Analysis Software Toolkit (GOEAST) (Zheng and Wang, 2008). The header 'level' represents the longest path connecting back to the root of the GO hierarchical tree and adjusted p value or false discovery rate (FDR) was calculated using Benjamini Yekutieli (2001) method. Cluster -1 is made up of genes that were constitutively up-regulated at optimal growing conditions only in WT, Cluster-2 contains genes that showed similar chilling induced transcriptional repression in both WT and IZS 288, Cluster-3 contains genes that showed chilling stress induced expression in both genotypes, Cluster-4 contains genes that showed strong induction of expression as a result of chilling stress only in IZS 288 roots and Cluster-5 is composed of genes that showed strong induction of expression as a result of chilling stress only in WT roots.

<i>Cluster-1 (279 genes)</i>	<i>Level</i>	<i>No. Genes associated to GO-ID</i>	<i>No. genes in common</i>	<i>p value</i>
response to reactive oxygen species	4	163	12	0.0101
AT5G12030 heat shock protein 17.6A				
AT1G14540 peroxidase 4				
AT1G51400 Photosystem II 5 kD protein				
AT2G32120 heat-shock protein 70T-2				
AT4G32320 L-ascorbate peroxidase				
AT1G54050 HSP20-like chaperone				
AT1G74310 heat shock protein 101				
AT5G27600 long-chain acyl-CoA synthetase 7				
AT5G37670 heat shock protein 15.7				
AT2G26150 heat stress transcription factor A-2				
AT5G64110 peroxidase 70				
AT5G64120 peroxidase 71				
response to hydrogen peroxide	5	119	9	0.0098
AT5G64110 peroxidase 70				
AT5G12030 heat shock protein 17.6A				
AT4G32320 L-ascorbate peroxidase				
AT1G74310 heat shock protein 101				
AT1G14540 peroxidase 4				
AT1G54050 HSP20-like chaperone				
AT2G32120 heat-shock protein 70T-2				
AT2G26150 heat stress transcription factor A-2				
AT5G64120 peroxidase 71				
response to heat	4	144	17	5E-09
AT5G52640 heat shock protein 81-1				
AT5G51440 heat shock protein 23.5				
AT5G37670 heat shock protein 15.7				
AT5G12020 heat shock protein 17.6-II				
AT3G46230 heat shock protein 17.4				
AT3G24500 multiprotein-bridging factor 1c				
AT1G74310 heat shock protein 101				
AT1G13080 cytochrome P450 71B2				
AT1G59860 HSP20-like chaperone				
AT1G54050 HSP20-like chaperone				
AT5G12030 heat shock protein 17.6A				
AT4G25200 small heat shock protein 23.6				
AT1G53540 HSP20-like chaperone				
AT1G07400 class I heat shock protein				
Cluster-2 (792 genes)				
photosynthesis, light reaction	4	71	11	0.0432
AT5G66570 oxygen-evolving enhancer protein 1-1				
AT5G64040 photosystem I reaction center subunit N				
AT5G01530 chlorophyll a-b binding protein CP29.1				
AT3G60370 FKBP-type peptidyl-prolyl cis-trans isomerase 6				
AT3G54890 light-harvesting complex I chlorophyll a/b binding protein 1				
AT3G47470 chlorophyll a-b binding protein 4				
AT4G27800 protein phosphatase 2C 57				

Appendix list

AT4G22890 PGR5-like protein 1A
 AT2G34420 light-harvesting complex II chlorophyll a/b binding protein 1
 AT4G11960 PGR5-like protein 1B
 AT3G08940 chlorophyll a-b binding protein CP29.2
 AT2G34430 light-harvesting complex II chlorophyll a/b binding protein 1

Cluster-3 (493 genes)

phenylpropanoid biosynthetic process	5	125	13	0.0025
AT2G47460 transcription factor MYB12 Disease resistance-responsive (dirigent-like protein) family protein				
AT1G58170 protein				
AT5G41040 omega-hydroxypalmitate O-feruloyl transferase				
AT5G23190 cytochrome P450 86B1				
AT5G08640 flavonol synthase/flavanone 3-hydroxylase				
AT3G53260 phenylalanine ammonia-lyase 2				
AT4G25310 protein SRG1				
AT1G06000 UDP-glycosyltransferase-like protein Disease resistance-responsive (dirigent-like protein) family protein				
AT1G64160 protein				
AT1G78600 light-regulated zinc finger protein 1 disease resistance-responsive, dirigent domain-containing protein				
AT2G21100 protein				
AT1G04220 3-ketoacyl-CoA synthase 17				
AT2G02990 ribonuclease 1				
AT4G25300 protein SRG1				
response to cold	4	264	26	4E-07
AT4G17090 beta-amylase 3				
AT1G46768 ethylene-responsive transcription factor RAP2-1				
AT5G15960 stress-induced protein KIN1				
AT5G15970 stress-induced protein KIN2				
AT5G58670 phosphoinositide phospholipase C 1 low-temperature-responsive protein 78/desiccation-responsive protein 29A				
AT5G52310 protein				
AT3G50970 dehydrin Xero 2				
AT4G30650 putative low temperature and salt responsive protein				
AT4G26080 protein phosphatase 2C 56				
AT4G25480 dehydration-responsive element-binding protein 1A				
AT4G24960 HVA22-like protein d RNA recognition motif and CCHC-type zinc finger domain-containing protein				
AT3G26420 protein				
AT3G26430 GDSL esterase/lipase				
AT3G26744 transcription factor ICE1				
AT3G22840 chlorophyll A-B binding, early light-inducible protein				
AT3G03050 cellulose synthase-like protein D3				
AT1G20450 dehydrin ERD10				
AT1G29390 cold regulated 314 thylakoid membrane 2				
AT1G10760 alpha-glucan water dikinase 1				
AT2G16500 arginine decarboxylase 1				
AT2G21660 glycine-rich RNA-binding protein 7				
AT1G09350 galactinol synthase 3				
AT1G05260 peroxidase 3 2,3-bisphosphoglycerate-independent phosphoglycerate mutase 1				
AT1G09780 protein				
AT2G15970 cold regulated 413 plasma membrane 1				
AT2G28900 outer plastid envelope protein 16-1				
AT1G20440 dehydrin COR47				
AT1G29395 cold regulated 314 inner membrane 1				
response to water deprivation	5	195	16	0.0039
AT1G46768 ethylene-responsive transcription factor RAP2-1				
AT5G15960 stress-induced protein KIN1				
AT5G15970 stress-induced protein KIN2				
AT5G58670 phosphoinositide phospholipase C 1 low-temperature-responsive protein 78/desiccation-responsive protein 29A				
AT5G52310 protein				
AT5G40390 putative galactinol--sucrose galactosyltransferase 5				
AT3G61890 homeobox-leucine zipper protein ATHB-12				
AT3G50970 dehydrin Xero 2				
AT4G25480 dehydration-responsive element-binding protein 1A				
AT4G24960 HVA22-like protein d				
AT1G15690 Pyrophosphate-energized vacuolar membrane proton pump 1				
AT1G20450 dehydrin ERD10				
AT1G29395 cold regulated 314 inner membrane 1				
AT2G21620 adenine nucleotide alpha hydrolases-like protein				
AT1G05260 peroxidase 3				
AT2G15970 cold regulated 413 plasma membrane 1				
AT1G20440 dehydrin COR47				

Appendix list

rRNA processing	9	57	10	0.0004
AT1G48920	nucleolin			
AT5G66540	hypothetical protein			
AT5G63120	DEAD-box ATP-dependent RNA helicase 30			
AT5G55920	S-adenosyl-L-methionine-dependent methyltransferase-like protein			
AT4G25730	FtsJ-like methyltransferase family protein			
AT4G04940	transducin/WD40 domain-containing protein			
AT4G02400	U3 ribonucleoprotein-like protein			
AT3G21540	transducin/WD40 domain-containing protein			
AT2G47990	transducin family protein / WD-40 repeat family protein			
AT4G26600	S-adenosyl-L-methionine-dependent methyltransferase-like protein			
Cluster-4 (243 genes)				
oligosaccharide biosynthetic process	6	43	5	0.0494
AT1G25150	F-box family protein			
AT1G24881	F-box protein			
AT1G24800	F-box protein			
AT1G25055	F-box protein			
AT1G25211	F-box protein			
AT4G39770	haloacid dehalogenase-like hydrolase domain-containing protein			
AT4G22590	haloacid dehalogenase-like hydrolase domain-containing protein			
AT4G22592	uncharacterized protein			
AT4G12430	haloacid dehalogenase-like hydrolase domain-containing protein			
AT4G12432	uncharacterized protein			
AT1G35910	haloacid dehalogenase-like hydrolase domain-containing protein			
carbohydrate biosynthetic process	5	228	10	0.0494
AT1G24881	F-box protein			
AT5G48300	glucose-1-phosphate adenylyltransferase small subunit			
AT3G50760	putative galacturonosyltransferase-like 2			
AT4G39770	haloacid dehalogenase-like hydrolase domain-containing protein			
AT4G22592	uncharacterized protein			
AT4G12430	haloacid dehalogenase-like hydrolase domain-containing protein			
AT4G12432	uncharacterized protein			
AT1G71100	ribose 5-phosphate isomerase A			
AT1G06780	alpha-1,4-galacturonosyltransferase			
AT1G60470	galactinol synthase 4			
AT1G25211	F-box protein			
AT4G22590	haloacid dehalogenase-like hydrolase domain-containing protein			
AT1G35910	haloacid dehalogenase-like hydrolase domain-containing protein			
AT1G25150	F-box family protein			
AT1G25055	F-box family protein			
AT1G24800	F-box family protein			
response to high light intensity	6	49	5	0.0494
AT5G59720	heat shock protein 18.2			
AT5G57050	protein phosphatase 2C 77			
AT1G01470	putative desiccation-related protein LEA14			
AT1G27730	zinc finger protein STZ/ZAT10			
AT2G17840	senescence/dehydration related protein			
response to cold	4	264	11	0.0438
AT5G57560	xyloglucan endotransglucosylase/hydrolase protein 22			
AT5G54470	B-box type zinc finger-containing protein			
AT5G42900	cold regulated protein 27			
AT3G61190	BON1-associated protein 1			
AT4G34710	arginine decarboxylase 2			
AT4G25490	dehydration-responsive element-binding protein 1B			
AT1G27730	zinc finger protein STZ/ZAT10			
AT2G42530	cold-regulated protein 15b			
AT2G42540	cold-regulated protein 15a			
AT2G17840	senescence/dehydration related protein			
AT4G25470	dehydration-responsive element-binding protein 1C, CBF2			

Appendix list

response to water deprivation	5	195	9	0.0584
AT5G57050	protein phosphatase 2C 77			
AT4G27410	NAC domain-containing protein 72			
AT4G25490	dehydration-responsive element-binding protein 1B			
AT3G11020	dehydration-responsive element-binding protein 2B			
AT1G01470	putative desiccation-related protein LEA14			
AT1G27730	zinc finger protein STZ/ZAT10			
AT1G08920	sugar transporter ERD6-like 3			
AT2G17840	senescence/dehydration related protein			
AT2G05520	glycine-rich protein 3			
response to abscisic acid stimulus	5	285	11	0.0584
AT5G57050	protein phosphatase 2C 77			
AT5G37260	protein REVEILLE 2 / DNA binding / transcription factor			
AT3G59220	pirin			
AT4G34710	arginine decarboxylase 2			
AT4G27410	NAC domain-containing protein 72			
AT4G18010	Type I inositol-1,4,5-trisphosphate 5-phosphatase 2			
AT3G28580	AAA-type ATPase family protein			
AT1G69260	Ninja-family protein AFP1			
AT1G27730	zinc finger protein STZ/ZAT10			
AT1G08920	sugar transporter ERD6-like 3			
AT2G05520	glycine-rich protein 3			
trehalose biosynthetic process	8	21	4	0.0322
AT4G39770	haloacid dehalogenase-like hydrolase domain-containing protein			
AT4G22592	uncharacterized protein			
AT4G12430	haloacid dehalogenase-like hydrolase domain-containing protein			
AT4G12432	uncharacterized protein			
AT4G22590	haloacid dehalogenase-like hydrolase domain-containing protein			
AT1G35910	haloacid dehalogenase-like hydrolase domain-containing protein			
Cluster-5 (185 genes)				
oxidation-reduction process	3	1315	27	0.0038
AT5G12270	oxidoreductase, 2OG-Fe(II) oxygenase family protein			
AT5G58910	laccase 16			
AT5G50590	hydroxysteroid dehydrogenase 4			
AT5G48880	3-ketoacyl-CoA thiolase 5			
AT5G47990	cytochrome P450 705A5			
AT5G48000	cytochrome P450 708A2			
AT5G06730	peroxidase 54			
AT5G05600	oxidoreductase, 2OG-Fe(II) oxygenase family protein			
AT5G01050	laccase-9			
AT3G52970	cytochrome P450, family 76, subfamily G, polypeptide 1			
AT3G51240	Naringenin,2-oxoglutarate 3-dioxygenase			
AT4G39950	tryptophan N-hydroxylase 1			
AT4G37430	cytochrome P450 81F1			
AT4G33010	glycine dehydrogenase [decarboxylating] 2			
AT4G31500	cytochrome P450 83B1			
AT4G21990	5'-adenylsulfate reductase 3			
AT4G18360	(S)-2-hydroxy-acid oxidase			
AT1G18140	laccase 1			
AT2G34060	peroxidase 19			
AT3G14690	cytochrome P450, family 72, subfamily A, polypeptide 15			
AT1G78570	UDP-glucose 4,6-dehydratase			
AT1G23800	aldehyde dehydrogenase 2B7			
AT2G05620	protein PROTON GRADIENT REGULATION 5			
AT2G25450	putative 2-oxoacid dependent dioxygenase			
AT5G50690	hydroxysteroid dehydrogenase 7			
AT5G06720	peroxidase 53			
AT5G01040	laccase 8			
AT4G37410	cytochrome P450, family 81, subfamily F, polypeptide 4			
AT4G37400	cytochrome P450, family 81 subfamily F polypeptide 3			
sulfur compound metabolic process	3	178	8	0.0223
AT4G14030	putative selenium-binding protein			
AT4G14040	selenium-binding protein 2, SBP2			

Appendix list

AT5G63980	inositol polyphosphate 1-phosphatase				
AT4G39950	tryptophan N-hydroxylase 1				
AT4G31500	cytochrome P450 83B1				
AT4G21990	5'-adenylylsulfate reductase 3				
AT1G74100	sulfotransferase 16				
AT2G36880	S-adenosylmethionine synthase 3				
AT2G25450	putative 2-oxoacid dependent dioxygenase				
response to temperature stimulus		3	392	14	0.0023
AT5G63980	inositol polyphosphate 1-phosphatase				
AT5G56000	molecular chaperone HtpG				
AT5G49910	heat shock protein 70-2				
AT5G37500	Potassium channel GORK				
AT5G10230	annexin D7				
AT5G02490	heat shock protein 70				
AT4G30660	putative low temperature and salt responsive protein				
AT4G26850	GDP-L-galactose phosphorylase				
AT3G09440	protein heat shock protein 70-3				
AT2G47180	galactinol synthase 1				
AT1G43160	ethylene-responsive transcription factor RAP2-6				
AT1G55490	RuBisCO large subunit-binding protein subunit beta				
AT2G38750	annexin D4				
AT5G56010	heat shock protein 81-3, HSP81-3				
AT5G56030	heat shock protein 81-2, HSP8-2				
phenylpropanoid metabolic process		4	163	12	1E-05
AT5G58910	laccase 16				
AT5G13930	chalcone synthase				
AT5G05270	chalcone-flavanone isomerase-like proetin				
AT5G01050	laccase-9				
AT3G55120	chalcone--flavonone isomerase 1				
AT3G51240	Naringenin,2-oxoglutarate 3-dioxygenase				
AT4G25640	detoxifying efflux carrier 35				
AT1G18140	laccase 1				
AT1G66800	Rossmann-fold NAD(P)-binding domain-containing protein				
AT1G78570	UDP-glucose 4,6-dehydratase				
AT2G36880	S-adenosylmethionine synthase 3				
AT2G23910	Rossmann-fold NAD(P)-binding domain-containing protein				
AT5G01040	laccase 8, LAC8				
lignin metabolic process		5	64	6	0.005
AT5G58910	laccase 16				
AT5G01050	laccase-9				
AT1G18140	laccase 1				
AT1G66800	Rossmann-fold NAD(P)-binding domain-containing protein				
AT2G36880	S-adenosylmethionine synthase 3				
AT2G23910	Rossmann-fold NAD(P)-binding domain-containing protein				
AT5G01040	laccase 8, LAC8				
phenylpropanoid catabolic process		5	16	3	0.0432
AT5G58910	laccase 16				
AT5G01050	laccase-9				
AT5G01040	laccase 8				
AT1G18140	laccase 1				
lignin catabolic process		6	16	3	0.0432
AT5G58910	laccase 16				
AT5G01050	laccase-9				
AT5G01040	laccase 8				
AT1G18140	laccase 1				
triterpenoid metabolic process		7	15	3	0.0374
AT5G47990	cytochrome P450 705A5				
AT5G48000	cytochrome P450 708A2				
AT5G48010	thalianol synthase 1				
flavonoid biosynthetic process		6	50	5	0.0135
AT5G13930	chalcone synthase				
AT5G05270	chalcone-flavanone isomerase-like proetin				
AT3G55120	chalcone--flavonone isomerase 1				
AT3G51240	Naringenin,2-oxoglutarate 3-dioxygenase				
AT1G78570	UDP-glucose 4,6-dehydratase				

Appendix list

auxin transport	6	46	4	0.0693
AT5G13930 chalcone synthase				
AT3G14370 protein kinase WAG2				
AT1G77690 auxin transporter-like protein 3				
AT1G78570 UDP-glucose 4,6-dehydratase				
tryptophan metabolic process	9	22	3	0.0796
AT4G39950 tryptophan N-hydroxylase 1				
AT4G31500 cytochrome P450 83B1				
AT2G29690 anthranilate synthase component I-2				
defense response by cell wall thickening	7	17	3	0.0487
AT4G39950 tryptophan N-hydroxylase 1				
AT4G31500 cytochrome P450 83B1				
AT4G26850 GDP-L-galactose phosphorylase				
callose deposition in cell wall	7	19	3	0.0624
AT4G39950 tryptophan N-hydroxylase 1				
AT4G31500 cytochrome P450 83B1				
AT4G26850 GDP-L-galactose phosphorylase				

Appendix list-5

Highly enriched gene ontology terms in 2560 genes that were chilling responsive in IZS 288 roots after 24 hours of chilling stress and clustered into five groups by K-mean algorithm using the Pearson correlation coefficient as a distance metrics. The enrichment analysis was carried out using the Gene Ontology Enrichment Analysis Software Toolkit (GOEAST) (Zheng and Wang, 2008). The header 'level' represents the longest path connecting back to the root of the GO hierarchical tree and adjusted p value or false discovery rate (FDR) was calculated using Benjamini Yekutieli (2001) method. Cluster -1 is made up of genes that were constitutively up-regulated at optimal growing conditions only in IZS 288, Cluster-2 contains genes that showed strong induction of expression as a result of chilling stress only in IZS 288 roots, Cluster-3 contains genes that showed chilling induced transcriptional repression in both genotypes, chilling stress induced expression in both genotypes, Cluster-4 contains genes that showed strong induction of expression as a result of chilling stress only in IZS 288 roots and Cluster-5 is composed of genes that showed strong induction of expression as a result of chilling stress only in WT roots.

	<i>No. Genes</i>	<i>No.</i>	<i>No.</i>	
	<i>associated</i>	<i>genes in</i>	<i>genes in</i>	
<i>Cluster-1 (571 genes)</i>	<i>Level</i>	<i>to GO-ID</i>	<i>common</i>	<i>p value</i>
No GO Terms were found significantly enriched				
Cluster-2 (250 genes)				
regulation of transcription, DNA-dependent	8	940	29	0.0789
at2g47520 ethylene-responsive transcription factor ERF071				
at4g17785 transcription factor MYB39				
at5g51190 ethylene-responsive transcription factor ERF105				
at3g56400 putative WRKY transcription factor 70				
at3g50260 ethylene-responsive transcription factor ERF011				
at4g37610 BTB and TAZ domain protein 5				
at4g28140 ethylene-responsive transcription factor ERF054				
at4g28110 myb domain protein 41				
at1g13600 basic leucine-zipper 58				
at1g05690 BTB and TAZ domain protein 3				
at3g23250 myb domain protein 15				
at1g42990 bZIP transcription factor 60				
at1g64380 ethylene-responsive transcription factor ERF061				
at2g47260 WRKY DNA-binding protein 23				
at2g40340 dehydration-responsive element-binding protein 2C				
at1g10170 NF-X1-type zinc finger protein NFXL1				
at2g44840 ethylene-responsive transcription factor 13				
at2g38340 dehydration-responsive element-binding protein 2E				
at2g38470 putative WRKY transcription factor 33				
at2g23760 BEL1-like homeodomain 4				
at4g17490 ethylene-responsive transcription factor 6				
at2g40350 putative dehydration-responsive element-binding protein 2H				

Appendix list

regulation of RNA biosynthetic process	7	940	29	0.0002
at2g47520 ethylene-responsive transcription factor ERF071				
at4g17785 transcription factor MYB39				
at5g51190 ethylene-responsive transcription factor ERF105				
at3g56400 putative WRKY transcription factor 70				
at3g50260 ethylene-responsive transcription factor ERF011				
at4g37610 BTB and TAZ domain protein 5				
at4g31800 WRKY transcription factor 18				
at4g28140 ethylene-responsive transcription factor ERF054				
at4g28110 myb domain protein 41				
at4g25490 dehydration-responsive element-binding protein 1B				
at1g13600 basic leucine-zipper 58				
at1g05690 BTB and TAZ domain protein 3				
at1g59530 basic leucine-zipper 4				
at3g23250 myb domain protein 15				
at3g22830 heat stress transcription factor A-6b				
at1g42990 bZIP transcription factor 60				
at1g64380 ethylene-responsive transcription factor ERF061				
at2g47260 WRKY DNA-binding protein 23				
at1g44830 ethylene-responsive transcription factor ERF014				
at2g46400 putative WRKY transcription factor 46				
at2g40340 dehydration-responsive element-binding protein 2C				
at1g10170 NF-X1-type zinc finger protein NFXL1				
at2g44840 ethylene-responsive transcription factor 13				
at2g38340 dehydration-responsive element-binding protein 2E				
at2g38470 putative WRKY transcription factor 33				
at2g23760 BEL1-like homeodomain 4				
at4g17490 ethylene-responsive transcription factor 6				
at5g49520 putative WRKY transcription factor 48				
at1g21910 ethylene-responsive transcription factor ERF012				
at2g40350 putative dehydration-responsive element-binding protein 2H				
phosphorelay signal transduction system	5	206	9	0.0877
at2g47520 ethylene-responsive transcription factor ERF071				
at5g51190 ethylene-responsive transcription factor ERF105				
at3g50260 ethylene-responsive transcription factor ERF011				
at4g28140 ethylene-responsive transcription factor ERF054				
at1g64380 ethylene-responsive transcription factor ERF061				
at1g21910 ethylene-responsive transcription factor ERF012				
at2g44840 ethylene-responsive transcription factor 13				
at4g17490 ethylene-responsive transcription factor 6				
at1g44830 ethylene-responsive transcription factor ERF014				
response to ethylene stimulus	5	235	11	0.0134
at2g47520 ethylene-responsive transcription factor ERF071				
at5g51190 ethylene-responsive transcription factor ERF105				
at3g50260 ethylene-responsive transcription factor ERF011				
at4g28140 ethylene-responsive transcription factor ERF054				
at3g23250 myb domain protein 15				
at1g64380 ethylene-responsive transcription factor ERF061				
at1g68765 protein IDA				
at1g21910 ethylene-responsive transcription factor ERF012				
at2g44840 ethylene-responsive transcription factor 13				
at4g17490 ethylene-responsive transcription factor 6				
at1g44830 ethylene-responsive transcription factor ERF014				
ethylene mediated signaling pathway	8	155	9	0.0125
at2g47520 ethylene-responsive transcription factor ERF071				
at5g51190 ethylene-responsive transcription factor ERF105				
at3g50260 ethylene-responsive transcription factor ERF011				
at4g28140 ethylene-responsive transcription factor ERF054				
at1g64380 ethylene-responsive transcription factor ERF061				
at1g21910 ethylene-responsive transcription factor ERF012				
at2g44840 ethylene-responsive transcription factor 13				
at4g17490 ethylene-responsive transcription factor 6				
at1g44830 ethylene-responsive transcription factor ERF014				
response to chitin	5	24	120	2E-20
at5g66070 NEP1-interacting protein-like 1				
at5g59820 C2H2-type zinc finger protein				
at5g51190 ethylene-responsive transcription factor ERF105				
at5g49520 putative WRKY transcription factor 48				
at5g09800 U-box domain-containing protein 28				
at3g56400 putative WRKY transcription factor 70				
at3g50260 ethylene-responsive transcription factor ERF011				
at3g49530 NAC domain-containing protein 62				
at4g37610 BTB and TAZ domain protein 5				
at4g31800 WRKY transcription factor 18				
at4g28140 ethylene-responsive transcription factor ERF054				

Appendix list

at4g28110	myb domain protein 41				
at1g66160	U-box domain-containing protein 20				
at3g28210	zinc finger AN1 domain-containing stress-associated protein 12				
at3g23250	myb domain protein 15				
at1g42990	bZIP transcription factor 60				
at1g64380	ethylene-responsive transcription factor ERF061				
at2g40140	zinc finger CCCH domain-containing protein 29				
at2g46400	putative WRKY transcription factor 46				
at2g37430	C2H2 and C2HC zinc finger domain-containing protein				
at2g44840	ethylene-responsive transcription factor 13				
at2g38470	putative WRKY transcription factor 33				
at4g17490	ethylene-responsive transcription factor 6				
at5g64660	U-box domain-containing protein 27				
response to temperature stimulus		4	12	264	0.0245
at5g59820	C2H2-type zinc finger protein				
at5g59720	heat shock protein 18.2				
at5g57560	xyloglucan endotransglucosylase/hydrolase protein 22				
at5g50720	HVA22-like protein e				
at5g43760	3-ketoacyl-CoA synthase 19				
at3g50260	ethylene-responsive transcription factor ERF011				
at3g49530	NAC domain-containing protein 62				
at4g34150	calcium-dependent lipid-binding domain-containing protein				
at4g25490	dehydration-responsive element-binding protein 1B				
at4g03430	pre-mRNA-processing factor 6				
at3g22370	alternative oxidase 1A				
at2g40140	zinc finger CCCH domain-containing protein 29				
at2g40340	dehydration-responsive element-binding protein 2C				
at2g38470	putative WRKY transcription factor 33				
at2g40350	putative dehydration-responsive element-binding protein 2H				
response to cold		4	264	12	0.0094
at5g59820	C2H2-type zinc finger protein				
at5g57560	xyloglucan endotransglucosylase/hydrolase protein 22				
at5g50720	HVA22-like protein e				
at5g43760	3-ketoacyl-CoA synthase 19				
at3g50260	ethylene-responsive transcription factor ERF011				
at3g49530	NAC domain-containing protein 62				
at4g34150	calcium-dependent lipid-binding domain-containing protein				
at4g25490	dehydration-responsive element-binding protein 1B				
at4g03430	pre-mRNA-processing factor 6				
at3g22370	alternative oxidase 1A				
at2g40140	zinc finger CCCH domain-containing protein 29				
at2g38470	putative WRKY transcription factor 33				
Cluster-3 (873 genes)					
response to high light intensity		6	49	11	0.0082
at2g47450	signal recognition particle 43 kDa protein				
at5g66570	oxygen-evolving enhancer protein 1-1				
at3g51910	heat stress transcription factor A-7a				
at4g12400	putative stress-inducible protein				
at1g74310	heat shock protein 101				
at1g52560	HSP20-like chaperone				
at1g54050	HSP20-like chaperone				
at2a32120	heat-shock protein 70T-2				
at2g29500	HSP20 family protein				
at2g46240	BCL-2-associated athanogene 6				
at2g19310	HSP20-like chaperone				
response to heat		4	144	19	0.0092
at5g52640	heat shock protein 81-1				
at5g37670	heat shock protein 15.7				
at3g51910	heat stress transcription factor A-7a				
at4g25200	small heat shock protein 23.6				
at4g12400	putative stress-inducible protein				
at3g24500	multiprotein-bridging factor 1c				
at1g74310	heat shock protein 101				

Appendix list

at1g48050 ATP-dependent DNA helicase 2 subunit KU80
 at1g16030 heat shock protein 70B
 at1g52560 HSP20-like chaperone
 at1g13080 cytochrome P450 71B2
 at1g59860 HSP20-like chaperone
 at1g54050 HSP20-like chaperone
 at1g09090 Respiratory burst oxidase-B
 at1g09080 Hsp70 protein BiP chaperone BIP-L
 at2g32120 heat-shock protein 70T-2
 at2g46240 BCL-2-associated athanogene 6
 at2g19310 HSP20-like chaperone
 at1g07400 HSP20 family protein
 at2g29500 class I heat shock protein

Cluster-4 (514 genes)

carbohydrate metabolic process 3 873 47 7E-05

at4g17090 beta-amylase 3
 at5g11110 sucrose phosphate synthase 2F
 at5g56630 6-phosphofructokinase 7
 at5g56350 pyruvate kinase
 at5g55180 O-Glycosyl hydrolases family 17 protein
 at5g51830 fructokinase
 at5g40390 putative galactinol--sucrose galactosyltransferase 5
 at5g18670 inactive beta-amylase 9
 at3g62720 xyloglucan 6-xylosyltransferase
 at3g60120 beta glucosidase 27
 at3g58790 alpha-1,4-galacturonosyltransferase
 at3g57520 putative galactinol--sucrose galactosyltransferase 2
 at3g50760 putative galacturonosyltransferase-like 2
 at3g44990 xyloglucan:xyloglucosyl transferase
 at4g39770 haloacid dehalogenase-like hydrolase domain-containing protein
 at4g34480 glucan endo-1,3-beta-glucosidase 7
 at4g33440 glycoside hydrolase family 28 protein / polygalacturonase (pectinase)
 family protein
 at4g30290 xyloglucan:xyloglucosyl transferase
 at4g28320 mannan endo-1,4-beta-mannosidase 5
 at4g23920 UDP-D-glucose/UDP-D-galactose 4-epimerase 2
 at4g22592 uncharacterized protein

 at4g19810 Glycosyl hydrolase family protein with chitinase insertion domain
 at4g18010 Type I inositol-1,4,5-trisphosphate 5-phosphatase 2
 at4g12430 haloacid dehalogenase-like hydrolase domain-containing protein
 at4g12432 uncharacterized protein
 at1g22170 phosphoglycerate mutase-like protein
 at1g36770 pseudo
 at3g28530 UDP-glucose 4-epimerase
 at3g23820 UDP-D-glucuronate 4-epimerase 6
 at3g02570 mannose-6-phosphate isomerase
 at3g03050 cellulose synthase-like protein D3
 at1g71100 ribose 5-phosphate isomerase A
 at1g30080 glycosyl hydrolases family 17 domain-containing protein
 at1g06780 alpha-1,4-galacturonosyltransferase
 at1g02460 Pectin lyase-like protein
 at1g32860 glucan endo-1,3-beta-glucosidase 11
 at1g10640 Pectin lyase-like protein
 at1g10760 alpha-glucan water dikinase 1
 at1g14720 xyloglucan:xyloglucosyl transferase
 at1g09350 galactinol synthase 3
 at1g60470 galactinol synthase 4
 at2g20370 xyloglucan galactosyltransferase KATAMARI1
 at2g27500 glucan endo-1,3-beta-glucosidase 14

 at2g35710 nucleotide-diphospho-sugar transferase domain-containing protein
 at2g34850 UDP-arabinose 4-epimerase
 at4g22590 haloacid dehalogenase-like hydrolase domain-containing protein
 at4g18340 glycosyl hydrolase family 17 protein
 at1g35910 haloacid dehalogenase-like hydrolase domain-containing protein
 at2g36870 xyloglucan:xyloglucosyl transferase
 at5g10100 haloacid dehalogenase-like hydrolase domain-containing protein

Appendix list

disaccharide metabolic process	6	44	8	0.004
at4g17090	beta-amylase 3			
at5g11110	sucrose phosphate synthase 2F			
at5g40390	putative galactinol--sucrose galactosyltransferase 5			
at4g39770	haloacid dehalogenase-like hydrolase domain-containing protein			
at4g22592	uncharacterized protein			
at4g12430	haloacid dehalogenase-like hydrolase domain-containing protein			
at4g12432	uncharacterized protein			
at4g22590	haloacid dehalogenase-like hydrolase domain-containing protein			
at1g35910	haloacid dehalogenase-like hydrolase domain-containing protein			
at5g10100	haloacid dehalogenase-like hydrolase domain-containing protein			
response to temperature stimulus	3	392	26	0.0012
at4g17090	beta-amylase 3			
at5g57050	protein phosphatase 2C 77			
at5g54470	B-box type zinc finger-containing protein low-temperature-responsive protein 78/desiccation-responsive protein			
at5g52310	29A			
at5g47230	ethylene-responsive transcription factor 5			
at5g42900	cold regulated protein 27			
at5g37770	calcium-binding protein CML24			
at3g61190	BON1-associated protein 1			
at4g38580	farnesylated protein 6			
at4g37910	molecular chaperone DnaK			
at4g34710	arginine decarboxylase 2			
at4g25480	dehydration-responsive element-binding protein 1A			
at4g24960	HVA22-like protein d			
at3g11020	dehydration-responsive element-binding protein 2B			
at3g03050	cellulose synthase-like protein D3			
at1g27730	zinc finger protein STZ/ZAT10			
at1g80820	cinnamoyl-CoA reductase			
at1g10760	alpha-glucan water dikinase 1			
at2g42530	cold-regulated protein 15b			
at2g42540	cold-regulated protein 15a			
at1g09350	galactinol synthase 3			
at1g05260	peroxidase 3			
at2g17840	senescence/dehydration related protein			
at2g41100	calmodulin-like protein 12			
at4g26080	protein phosphatase 2C 56			
at4g25470	dehydration-responsive element-binding protein 1C			
response to cold	4	264	21	0.0008
at4g17090	beta-amylase 3			
at5g54470	B-box type zinc finger-containing protein low-temperature-responsive protein 78/desiccation-responsive protein			
at5g52310	29A			
at5g47230	ethylene-responsive transcription factor 5			
at5g42900	cold regulated protein 27			
at5g37770	calcium-binding protein CML24			
at3g61190	BON1-associated protein 1			
at4g34710	arginine decarboxylase 2			
at4g26080	protein phosphatase 2C 56			
at4g25480	dehydration-responsive element-binding protein 1A			
at4g24960	HVA22-like protein d			
at3g03050	cellulose synthase-like protein D3			
at1g27730	zinc finger protein STZ/ZAT10			
at1g80820	cinnamoyl-CoA reductase			
at1g10760	alpha-glucan water dikinase 1			
at2g42530	cold-regulated protein 15b			
at2g42540	cold-regulated protein 15a			
at1g09350	galactinol synthase 3			
at1g05260	peroxidase 3			
at2g17840	senescence/dehydration related protein			
at4g25470	dehydration-responsive element-binding protein 1C, CBF2			
response to ethylene stimulus	5	235	16	0.0298
at5g67300	transcription factor MYB44			
at5g59430	Telomere repeat-binding protein 1			
at5g47230	ethylene-responsive transcription factor 5			
at5g37260	protein REVEILLE 2 / DNA binding / transcription factor			
at5g13330	ethylene-responsive transcription factor ERF113			
at5g10510	AP2-like ethylene-responsive transcription factor AIL6			
at3g54990	AP2-like ethylene-responsive transcription factor SMZ			
at4g11280	1-aminocyclopropane-1-carboxylate synthase 6			
at3g25730	AP2/ERF and B3 domain-containing transcription factor ARF14			
at3g06490	myb domain protein 108			

Appendix list

at1g28370	ethylene-responsive transcription factor 11				
at2g28550	ethylene-responsive transcription factor RAP2-7				
at1g62300	WRKY transcription factor 6				
at2g05520	glycine-rich protein 3				
at2g46830	protein CCA1				
at2g33710	ethylene-responsive transcription factor ERF112				
response to abscisic acid stimulus		5	285	19	0.0124
at5g67300	transcription factor MYB44				
at5g57050	protein phosphatase 2C 77 low-temperature-responsive protein 78/desiccation-responsive protein				
at5g52310	29A				
at5g37770	calcium-binding protein CML24				
at5g37260	protein REVEILLE 2 / DNA binding / transcription factor				
at5g01810	CBL-interacting serine/threonine-protein kinase 15				
at3g61890	homeobox-leucine zipper protein ATHB-12				
at3g59220	pirin, PRN1				
at4g34710	arginine decarboxylase 2				
at4g27410	NAC domain-containing protein 72				
at4g24960	HVA22-like protein d				
at4g18010	Type I inositol-1,4,5-trisphosphate 5-phosphatase 2				
at3g06490	myb domain protein 108				
at1g69260	Ninja-family protein AFP1				
at1g27730	zinc finger protein STZ/ZAT10				
at1g08920	sugar transporter ERD6-like 3				
at2g05520	glycine-rich protein 3				
at2g46830	protein CCA1				
at4g26080	protein phosphatase 2C 56, ABI1				
response to lipid		4	413	22	0.0548
at5g67300	transcription factor MYB44				
at5g67480	BTB and TAZ domain protein 4				
at5g59430	Telomere repeat-binding protein 1				
at5g57050	protein phosphatase 2C 77 low-temperature-responsive protein 78/desiccation-responsive protein				
at5g52310	29A				
at5g37770	calcium-binding protein CML24				
at5g37260	protein REVEILLE 2 / DNA binding / transcription factor				
at5g01810	CBL-interacting serine/threonine-protein kinase 15				
at3g61890	homeobox-leucine zipper protein ATHB-12				
at3g59220	pirin				
at4g34710	arginine decarboxylase 2				
at4g27410	NAC domain-containing protein 72				
at4g24960	HVA22-like protein d				
at4g18010	Type I inositol-1,4,5-trisphosphate 5-phosphatase 2				
at4g08950	Phosphate-responsive 1 family protein				
at3g06490	myb domain protein 108				
at1g69260	Ninja-family protein AFP1				
at1g27730	zinc finger protein STZ/ZAT10				
at1g08920	sugar transporter ERD6-like 3				
at2g05520	glycine-rich protein 3				
at2g46830	protein CCA1				
at4g26080	protein phosphatase 2C 56, ABI1				
trehalose biosynthetic process		8	21	5	0.0283
at4g39770	haloacid dehalogenase-like hydrolase domain-containing protein				
at4g22592	uncharacterized protein				
at4g12430	haloacid dehalogenase-like hydrolase domain-containing protein				
at4g12432	uncharacterized protein				
at4g22590	haloacid dehalogenase-like hydrolase domain-containing protein				
at1g35910	haloacid dehalogenase-like hydrolase domain-containing protein				
at5g10100	haloacid dehalogenase-like hydrolase domain-containing protein				
Cluster-5 (352 genes)					
phenylpropanoid biosynthetic process		5	125	14	1E-05
at2g47460	transcription factor MYB12				
at1g58170	Disease resistance-responsive (dirigent-like protein) family protein				
at5g41040	omega-hydroxypalmitate O-feruloyl transferase				
at5g23190	cytochrome P450 86B1				
at5g13930	chalcone synthase				
at5g08640	flavonol synthase/flavanone 3-hydroxylase				
at5g05270	chalcone-flavanone isomerase-like protein				

Appendix list

at3g51240	Naringenin,2-oxoglutarate 3-dioxygenase				
at4g34230	cinnamyl alcohol dehydrogenase 5				
at1g06000	UDP-glycosyltransferase-like protein				
at1g64160	Disease resistance-responsive (dirigent-like protein) family protein				
at2g37040	phenylalanine ammonia-lyase 1				
at2g23910	Rossmann-fold NAD(P)-binding domain-containing protein				
flavonoid biosynthetic process		6	50	7	0.0055
at2g47460	transcription factor MYB12				
at5g13930	chalcone synthase				
at5g08640	flavonol synthase/flavanone 3-hydroxylase				
at5g05270	chalcone-flavanone isomerase-like proetin				
at3g55120	chalcone--flavonone isomerase 1				
at3g51240	Naringenin,2-oxoglutarate 3-dioxygenase				
at1g06000	UDP-glycosyltransferase-like protein				
ketone biosynthetic process		5	68	9	0.0006
at2g47460	transcription factor MYB12				
at5g13930	chalcone synthase				
at5g08640	flavonol synthase/flavanone 3-hydroxylase				
at5g05270	chalcone-flavanone isomerase-like proetin				
at3g55120	chalcone--flavonone isomerase 1				
at3g51240	Naringenin,2-oxoglutarate 3-dioxygenase				
at1g06000	UDP-glycosyltransferase-like protein				
at1g17050	solaneyl diphosphate synthase 2				
at1g78510	solaneyl diphosphate synthase 1, SPS1				
response to light stimulus		4	476	20	0.0248
at4g14690	early light-inducible protein 2				
at5g15960	stress-induced protein KIN1				
at5g15970	stress-induced protein KIN2				
at5g58760	DNA damage-binding protein 2				
at5g13930	chalcone synthase				
at3g55120	chalcone--flavonone isomerase 1				
at3g51240	Naringenin,2-oxoglutarate 3-dioxygenase				
at3g47340	asparagine synthetase [glutamine-hydrolyzing]				
at4g37580	hookless 1 / N-acetyltransferase				
at1g69530	expansin A1				
at3g17609	transcription factor HY5-like protein				
at1g60950	ferredoxin-2				
at1g06040	Salt tolerance protein				
at1g01060	protein late elongated hypocotyl				
at1g65060	4-coumarate--CoA ligase 3				
at2g47180	galactinol synthase 1				
at2g05620	protein PROTON GRADIENT REGULATION 5				
at2g37970	SOUL heme-binding-like protein				
at2g46670	CCT motif family protein				
at2g02950	phytochrome kinase substrate 1				
at2g40080	hypothetical protein				
at2g46790	two-component response regulator-like APRR9				
response to red or far red light		5	171	10	0.0753
at4g14690	early light-inducible protein 2				
at5g15960	stress-induced protein KIN1				
at5g15970	stress-induced protein KIN2				
at4g37580	hookless 1 / N-acetyltransferase				
at1g69530	expansin A1				
at3g17609	transcription factor HY5-like protein				
at1g06040	Salt tolerance protein				
at2g37970	SOUL heme-binding-like protein				
at2g46790	two-component response regulator-like APRR9				
at2g02950	phytochrome kinase substrate 1				
at2g40080	hypothetical protein				
at2g46670	CCT motif family protein				
response to temperature stimulus		3	392	24	1E-05
at5g15960	stress-induced protein KIN1				
at5g15970	stress-induced protein KIN2				
at5g63770	diacylglycerol kinase 2				
at5g58670	phosphoinositide phospholipase C 1				
at5g56030	heat shock protein 81-2				
at5g49910	heat shock protein 70-2				
at5g10230	annexin D7				
at5g09590	mitochondrial HSO70 2				
at5g02490	heat shock protein 70				
at3g50970	dehydrin Xero 2				

Appendix list

at4g30650	putative low temperature and salt responsive protein RNA recognition motif and CCHC-type zinc finger domain-containing				
at3g26420	protein				
at3g26430	GDSL esterase/lipase				
at3g22840	chlorophyll A-B binding, early light-inducible protein				
at3g09440	protein heat shock protein 70-3				
at1g20450	dehydrin ERD10				
at1g29390	cold regulated 314 thylakoid membrane 2				
at2g16500	arginine decarboxylase 1				
at2g47180	galactinol synthase 1				
at2g21660	glycine-rich RNA-binding protein 7				
at1g43160	ethylene-responsive transcription factor RAP2-6				
at2g15970	cold regulated 413 plasma membrane 1				
at2g28900	outer plastid envelope protein 16-1				
at2g46670	CCT motif family protein				
at1g20440	dehydrin COR47				
at1g29395	cold regulated 314 inner membrane 1				
at2g46790	two-component response regulator-like APRR9				
response to cold		4	264	17	0.0006
at5g15960	stress-induced protein KIN1				
at5g15970	stress-induced protein KIN2				
at5g63770	diacylglycerol kinase 2				
at5g58670	phosphoinositide phospholipase C 1				
at5g10230	annexin D7				
at3g50970	dehydrin Xero 2				
at4g30650	putative low temperature and salt responsive protein RNA recognition motif and CCHC-type zinc finger domain-containing				
at3g26420	protein				
at3g26430	GDSL esterase/lipase				
at3g22840	chlorophyll A-B binding, early light-inducible protein				
at1g20450	dehydrin ERD10				
at1g29390	cold regulated 314 thylakoid membrane 2				
at2g16500	arginine decarboxylase 1				
at2g21660	glycine-rich RNA-binding protein 7				
at1g43160	ethylene-responsive transcription factor RAP2-6				
at2g15970	cold regulated 413 plasma membrane 1				
at2g28900	outer plastid envelope protein 16-1				
at1g20440	dehydrin COR47				
at1g29395	cold regulated 314 inner membrane 1				
response to water deprivation		5	195	11	0.0564
at5g15960	stress-induced protein KIN1				
at5g15970	stress-induced protein KIN2				
at5g58670	phosphoinositide phospholipase C 1				
at5g56030	heat shock protein 81-2				
at5g10230	annexin D7				
at3g50970	dehydrin Xero 2				
at1g20450	dehydrin ERD10				
at1g29395	cold regulated 314 inner membrane 1				
at2g15970	cold regulated 413 plasma membrane 1				
at2g05620	protein PROTON GRADIENT REGULATION 5				
at2g47800	ABC transporter C family member 4				
at1g20440	dehydrin COR47				
cold acclimation		5	22	8	1E-06
at5g15960	stress-induced protein KIN1				
at5g15970	stress-induced protein KIN2				
at3g50970	dehydrin Xero 2 RNA recognition motif and CCHC-type zinc finger domain-containing				
at3g26420	protein				
at3g26430	GDSL esterase/lipase				
at1g20450	dehydrin ERD10				
at1g29390	cold regulated 314 thylakoid membrane 2				
at2g15970	cold regulated 413 plasma membrane 1				
at1g20440	dehydrin COR47				
at1g29395	cold regulated 314 inner membrane 1				

Appendix list-6

List of transient cold responsive gens in 288

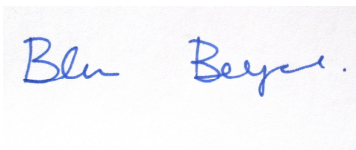
<i>Gene ID</i>	<i>Gene Symbol</i>	<i>Description</i>
AT1G18010		Major facilitator superfamily protein
AT1G18000		Major facilitator superfamily protein
AT1G19380		hypothetical protein
AT1G28480	GRX480	glutaredoxin-GRX480
AT1G65390	PP2-A5	protein PHLOEM protein 2-LIKE A5
AT1G72940		Toll-Interleukin-Resistance domain-containing protein
AT1G73805		protein SAR Deficient 1
AT1G77530		O-methyltransferase family protein
AT1G77520		O-methyltransferase family protein
AT2G16900		phospholipase-like protein (PEARLI 4) family
AT2G44840	ERF13	ethylene-responsive transcription factor 13
AT3G19030		hypothetical protein
AT3G44260		putative CCR4-associated factor 1
AT3G45660		probable nitrate excretion transporter 2
AT3G45650	NAXT1	nitrate excretion transporter1
AT5G59570		protein BROTHER OF LUX ARRHYTHMO
AT3G46640	PCL1	protein phyto clock 1
AT4G08950	EXO	phosphate-responsive 1 family protein
AT4G17490	ERF6	ethylene responsive element binding factor 6
AT4G38620	MYB4	transcription repressor MYB4
AT5G37770	TCH2	calcium-binding protein CML24
AT5G38350		TIR-NBS-LRR class disease resistance protein
AT5G38700		hypothetical protein
AT5G43890	YUC5	probable indole-3-pyruvate monooxygenase YUCCA5
AT5G47220	ERF2	ethylene-responsive transcription factor 2
AT5G58650	PSY1	tyrosine-sulfated glycopeptide 1
AT5G64850		hypothetical protein
AT5G64940	ATH13	putative ABC transporter
AT5G67300	MYBR1	transcription factor MYB44
AT5G52790		CBS domain-containing protein-related
COX1		cytochrome c oxidase subunit 1

Erklärung

Hiermit erkläre ich, dass ich die Arbeit selbstständig verfasst und keine anderen als die von mir angegebenen Quellen und Hilfsmittel benutzt habe.

Ferner erkläre ich, dass ich anderweitig mit oder ohne Erfolg nicht versucht habe, diese Dissertation einzureichen. Ich habe keine gleichartige Doktorprüfung an einer anderen Hochschule endgültig nicht bestanden.

Bayreuth, 07. August 2013

A handwritten signature in blue ink on a light-colored background. The signature reads "Blen Beyene Chichaibelu" in a cursive script.

Blen Beyene Chichaibelu